To the Graduate Council:

I am submitting herewith a thesis written by Fredrick Scott Dibrell entitled "Annealing Behavior of Crosslinked Polyolefins." I have examined the final copy of this thesis for form and content and recommend it be accepted in partial fulfillment of the requirements for the degree of Master of Science, with a major in Polymer Engineering.

Paul J. Phillips, Major Professor

We have read this thesis
and recommend its acceptance:

Accepted for the Council:

Vice Provost
and Dean of The Graduate School

ANNEALING BEHAVIOR OF CROSSLINKED POLYOLEFINS

A Thesis

Presented for the

Master of Science

Degree

The University of Tennessee

Fredrick Scott Dibrell

December 1990

A thesis begins in delight and ends in wisdom,
the picture is the same for love.

Robert Frost ?

Dedicated to my family

ACKNOWLEDGEMENTS

The author wishes to sincerely thank his advisor, Dr. Paul Phillips, for his guidance and support throughout this work. It has really been a very broadening experience as well as an honor to perform research under his supervision, and I will always be indebted to him. I also would like to express an appreciation to my committe members, Dr. Spruiell and Dr. Benson for their help throughout my time in graduate school.

The author also extends his gratitude to EPRI for providing the funding for this research.

I would also like to thank my family (Mom, Dad, Uncle Doc, and Aunt Inez) for their continuing support throughout my extended education.

Work on this level would be very hard to imagine performing without the support and guidance of one's peers. There are several of the senior students who have contributed greatly to my knowledge of polymers as well as my general well being by offering their freindship freely. I am very greatful to these people and I will never forget them. They include Scott "Moonstruck Puppy Dog" Lambert, Andy Campbell, Trishna Ray (T-Ray) Chauduri, Russell Wong, Rajen Patel and Dr. Y.D. Lee. I am also indebted to my fellow classmates whom I have been in contact with for making things more enjoyable and fun. These people include Aaron "Roachman" Greso, Aki Fukada, Ken "Coach" Monar, Francisco "Semental" Medellin, Steve, Paul, Ahmed Hammai, Nejib, and Xin Lee.

I would also like to acknowledge the undergraduate research assistants who helped me with this research as well. These people are Herbert "Dano-Wiz" Thomas with his Malaysian Guayule Rubber Destructo Ball, Eric Murrel, and Jolomi "with the Salami" Omatete.

I also give thanks to God for giving me what so many others never have in life..... a chance.

ABSTRACT

A technique has been developed using differential scanning calorimetry (DSC) to study the annealing behavior of semicrystalline polyolefins. Using software available on the DSC, an annealed endotherm can be subtracted from an unannealed endotherm to generate a subtraction curve. The position of the loss peak on the subtraction curve, Td, yields an estimation of the annealing temperature, and the temperature at which the gain peak occurs, Tp, follows a logarithmic annealing time dependence from which the kinetics of annealing can be followed.

The annealing behavior of crosslinked low density polyethylene (XLPE), ethylene propylene copolymer (EPR) and terpolymer (EPDM) as well as crosslinked EPR and crosslinked EPDM, materials typically used in the composition of nuclear control cable insulation, were studied using this subtraction technique. Several actual insulation formulations were studied as well. The results indicated that the annealing process is ubiquitous and can generally be described by an equation of the form:

$$Tp = A + B\mathrm{Log}(t)$$

where A is a parameter dependent upon the annealing temperature and B is a parameter dependent only upon the material for annealing temperatures between approximately 45 to 70 °C.

Once the annealing parameter B is known for a material, the thermal history (i.e. time and temperature of annealing) can be estimated using this general annealing equation. Estimations of the thermal history of several aged cable samples were determined using this technique.

TABLE OF CONTENTS

SECTION Page

1. INTRODUCTION 1

2. REVIEW OF THEORETICAL BACKGROUND AND LITERATURE 3

2.1. Polymer Crystallization 3
2.1.1 Crystal Structure 4
2.1.2 Factors Effecting Crystallinity 4

2.2. Morphology 7
2.2.1 Single Crystals 7
2.2.2 Spherulites 7
2.2.3 Axialites 8
2.2.4 Cable Morphology 8

2.3. Crystallization Models 9
2.3.1 Arguments Concerning the Nature of the Fold Surface 11

2.4. Crystallization Theory 14
2.4.1 Melting 19

2.5. Annealing 20
2.5.1 Annealing Observations 20
2.5.2 Mechanisms of Annealing 22
2.5.3 Crystal Imperfections 28

2.6. Treeing 31
2.6.1 Environmental Factors 32
2.6.2 Intrinsic Defects 33

SECTION PAGE

2.6.3 Electrical Trees 33
2.6.4 Water Trees 34

2.7. Insulation Stabilization 35
2.7.1 Tree Retardants 35
2.7.2 Flame Retardants 37
2.7.3 Anti-Oxidants 39
2.7.4 Ozone Cracking Prevention 41
2.7.5 UV Stabilization 41
2.7.6 Formulation of a Control Cable 42

3. EXPERIMENTAL PROCEDURES 44

3.1. Materials 44

3.2. Preparation of Crosslinked Polymers 44
3.2.1 Powdering of EPR and EPDM 46
3.2.2 Addition of Dicumyl Peroxide 46
3.2.3 Crosslinking Procedure 46
3.2.4 Extraction 47

3.3. Differential Scanning Calorimetry 47
3.3.1 Generation of Subtraction Curve 49

3.4. Sample Preparation for Annealing Studies 50

4. RESULTS 52

4.1. Effects of Annealing 52

4.2. General Features of the Subtraction Technique 53

SECTION PAGE

4.3. Annealing Studies of Reference Materials 60
4.3.1 Crosslinked Low Density Polyethylene (XLPE) 60
4.3.2 Ethylene Propylene Copolymer (ERP) 62
4.3.3 Ethylene Propylene Terpolymer (EPDM) 66
4.3.4 Crosslinked Ethylene Propylene Copolymer (XEPR) ... 71
4.3.5 Crosslinked Ethylene Propylene Terpolymer (XEPDM) 78

4.4. Control Cables 78
4.4.1 Cable A1 [Eaton (Samuel Moore)] 84
4.4.2 Cables A2 and A3 [Eaton (Samuel Moore)] 91
4.4.3 Cable C1 [BIW] 96
4.4.5 Cable D1 [Anaconda] 104
4.4.6 Cable B1 [Rockbestos] 115

4.5. Factors Effecting the Subtraction Curve 126
4.5.1 Multiple Annealing 126
4.5.2 Cycling 135
4.5.3 Effects of Nonisothermal Crystallization upon the Subtraction Curve 135

4.6. Aged Samples 140
4.6.1 Cable 246-155-RP 140
4.6.2 Cable 246-155-RW 146

5. DISCUSSION 158

5.1. Reference Materials 158
5.1.1 Crosslinked Low Density Polyethylene (XLPE) 158
5.1.2 Ethylene Propylene Coploymer (EPR) 161
5.1.3 Ethylene Propylene Terpolymer (EPDM) 161

SECTION PAGE

5.1.4 Crosslinked EPR (XEPR) 165
5.1.5 Crosslinked EPDM (XEPDM) 165

5.2. Control Cables 169
5.2.1 Cable A1 [Eaton (Samuel Moore)] 169
5.2.2 Cable A3 [Eaton (Samuel Moore)] 169
5.2.3 Cable C1 [BIW] 174
5.2.4 Cable D1 [Anaconda] 174
5.2.5 Cable B1 [Rockbestos] 177

5.3. Data Analysis 182

5.4. Estimating Thermal History 182
5.4.1 Development of a Calibration Curve 185
5.4.2 Development of the General Annealing Equation 187

5.5. Multiple Annealing and Cycling Studies 192

5.6. Aged Samples 194
5.6.1 Cable 246-155-RW 194
5.6.2 Cable 246-155-RP 200

5.7. Sources of Error 203
5.7.1 Constant Versus Fluctuating Temperatures 203
5.7.2 Multiple and High Temperature Annealing 204
5.7.3 Radiation Exposure 205

6. CONCLUSIONS 206

6.1. Annealing Behavior of "Reference" Polyolefins 206

6.2 Control Cables 207

SECTION PAGE

6.3. Determination of Thermal History 207

7. FUTURE WORK 209

7.1. Multiple Annealing 209

7.2. High Temperature Annealing 209

7.3. Radiation Effects 209

7.4. Temperature Fluctuations 209

7.5. General Annealing Studies 210

LIST OF REFERENCES 211

VITA 215

LIST OF FIGURES

FIGURE Page

2.1: Schematic of the unit cell of polyethylene..... 5

2.2: Polmer crystallization models: a) Fringed-micelle b) Adjacent reentry c) switchboard..... 10

2.3: Idealized schematic model for lamellar crystal growth (Hoffman et al. 1976)..... 16

2.4: Schematic diagram of a molecular kink as a mechanism for thickening..... 23

2.5: Schematic representation of a possible thickening mechanism proposed by Dreyfuss and Keller (1970)..... 24

2.6: Omega defect: a) Structures allowing formation of omega defects in chain folded systems (Hoffman 1985) b) Possible omega defect mechanism (Phillips and Rensch 1989)..... 26

2.7: Schematic of a point defect in the form of a chain end..... 29

2.8: a) A stacking fault in **polyethylene;** b) Schematic representation of an edge and a screw dislocation showing the dislocation line vector **d** and the Burgers vector **b**..... 30

4.1: Manifestation of annealing upon XLPE: a) 70 C annealing; b) quenched endotherm..... 54

FIGURE PAGE

4.2: General features of the subtraction curve: a) quenched endotherm; b) annealed endotherm; c) subtraction curve..... 55

4.3: Distortions in the baseline of the subtraction curve: a) XLPE; b) Anaconda insulation (D2); c) Eaton Corp. insulation (A3); d) Anaconda insulation (D1)..... 57

4.4: Determination of peak positions: a) subtraction curve of XEPR annealed at 60 C for 12 hours; b) derivative of subtraction curve..... 59

4.5: Effects of annealing at various temperatures upon the endotherms of XLPE..... 61

4.6: Tp versus time for XLPE..... 64

4.7: Annealing effects upon the endotherms of EPR..... 65

4.8: Typical subtraction curve of EPR annealed for 12 hours at 60 C..... 67

4.9: Tp versus time for EPR..... 69

4.10: Annealing effects upon the endotherms of EPDM..... 70

4.11: Typical subtraction curve of EPDM showing 60 C annealing..... 72

4.12: Tp versus time for EPDM..... 74

4.13: Annealing effects upon the endotherms of XEPR..... 75

FIGURE PAGE

4.14: Typical subtraction curve of XEPR showing 70 C annealing..... 76

4.15: Tp versus time for XEPR..... 79

4.16: Annealing effects upon the endotherms of XEPDM..... 80

4.17: Typical subtraction curve for XEPDM showing 50 C annealing..... 81

4.18: Tp versus time for XEPDM..... 83

4.19: DSC endotherms for cable A1: a) original; b) quenched..... 85

4.20: Original subtraction curve for A1..... 86

4.21: Annealing effects upon the "history erased" endotherms of cable A1..... 87

4.22: Typical Subtraction curve of cable A1 showing 70 C annealing..... 88

4.23: Tp versus time for cable A1..... 90

4.24: Original A1 cable annealed at 70 C: a) annealed endotherm; b)subtraction curve..... 92

4.25: Tp versus time for original and history erased cable A1..... 93

4.26: Original endotherms for cable A2 and A3: a) cable A2; b) cable A3..... 94

FIGURE PAGE

4.27: Subtraction curve for original cable A3 95

4.28: Annealing effects upon the "history erased" endotherms of cable A3 97

4.29: Typical subtraction curve for A3 showing 50 C annealing 98

4.30: Tp versus time for cable A3 100

4.31: Original cable A3 annealed for 97 hours at 70 C: a) endotherm; b) subtraction curve 101

4.32: Tp versus time for original and "history erased" samples of cable A3 annealed at 70 C 102

4.33: DSC endotherms for cable C1: a) original; b) quenched 103

4.34: Original subtraction curve for cable C1 105

4.35: Annealing effects upon the "history erased" samples of cable C1 106

4.36: Typical subtraction curve for cable C1 107

4.37: Tp versus time for cable C1 109

4.38: DSC endotherms for cable D1: a) original; b) quenched 110

4.39: Subtraction curve for original cable D1 111

FIGURE PAGE

4.40: Annealing effects upon the history erased samples of cable D1 112

4.41: Typical subtraction curve for cable D1 showing 50 C annealing 113

4.42: Tp versus time for cable D1 116

4.43: DSC endotherms for cable B1: a) original; b) quenched 117

4.44: Original subtraction curve of cable B1 118

4.45: Low temperature annealing effects upon the melting behavior of cable B1 119

4.46: High temperature annealing effects upon the melting behavior of cable B1 121

4.47: Typical subtraction curve for B1 showing 70 C annealing 122

4.48: Subtraction curves for high temperature annealing of cable B1 123

4.49: Tp versus time for cable B1 125

4.50: Original cable B1 annealed at 70 C: annealed endotherm; b) subtraction curve 127

4.51: Tp versus time for 70 C annealing of original and "history erased" samples of cable B1 128

FIGURE PAGE

4.52: Effects of annealing at 98 C followed by 70 or 80 C annealing upon the original endotherms of cable B1..... 129

4.53: Tp versus time for original cable B1 annealed at 98 C followed by 70 or 80 C annealing..... 130

4.54: DSC endotherm and subtraction curve for multiple annealing of XLPE at 70, 60, 50, and 35 C: a) endotherm; b) subtraction curve..... 132

4.55: DSC endotherm and subtraction curve for multiple annealing of XLPE at 70 and 50 C: a) endotherm; b) subtraction curve..... 133

4.56: DSC endotherm and subtraction curve for multiple annealing of EPDM at 70, 50, and 25 C: a) endotherm; b) subtraction curve..... 134

4.57 DSC endotherm and subtraction curve for multiple annealing of EPDM at 70 and 35 C: a) endotherm; b) subtraction curve..... 136

4.58: Non-isothermal cooling rate effects upon the subtraction curves for XLPE: a) 40 - 2 C/min; b) 40 - 400 C/min; c) 2- 40 C/min; d) 2 - 400 c/min..... 138

4.59: Endotherms of XLPE showing the effect of different non-isothermal cooling rates: a) 400 C/min; b) 2 C/min..... 139

4.60: DSC endotherms for cable 246-155-RP; a) RP-3; b) RP-5; c) RP-control..... 141

FIGURE PAGE

4.61: Subtraction curve for RP-control..... 143

4.62: Subtraction curves for RP-3 generated from the subtraction of the quenched from the aged endotherms..... 144

4.63: Subtraction curve for RP-3 generated from the subtraction of the control from the original endotherm..... 145

4.64: Subtraction curves for RP-5 generated from the subtraction of the quenched from the aged endotherms..... 147

4.65: Inconsistencies in the high temperature melting behavior of RP-5..... 148

4.66: Subtraction curve for RP-5 generated from the subtraction of the control from the original endotherm..... 149

4.67: DSC endotherms for cable 246-155-RW: a) RW-4; b) RW-2; c) RW-1; d) RW-control..... 150

4.68: Subtraction curves for RW-1 generated from the subtraction of the quenched from the aged endotherms..... 151

4.69: Subtraction curve for RW-1 generated from the subtraction of the control from the original endotherm..... 152

4.70: Subtraction curves for RW-2 generated from the subtraction of the quenched from the aged endotherms..... 154

4.71: Subtraction curve for RW-2 generated from the subtraction of the control from the original endotherm..... 155

FIGURE PAGE

4.72: Subtraction curves for RW-2 generated from the subtraction of the quenched from the aged endotherms..... 156

4.73 Subtraction curve for RW-4 generated from the subtraction of the control from the original endotherm..... 157

5.1: Tp versus logarithmic time for XLPE..... 159

5.2: Tp versus logarithmic time for EPR..... 162

5.3: Tp versus logarithmic time for EPDM..... 164

5.4: Tp versus logarithmic time for XEPR..... 166

5.5: Tp versus logarithmic time for XEPDM..... 167

5.6: Tp versus logarithmic time for cable A1..... 170

5.7: Tp versus logarithmic time for original and history erased samples of cable A1..... 171

5.8: Tp versus logarithmic time for cable A3..... 172

5.9 Tp versus logarithmic time for original and history erased samples of cable A3..... 173

5.10: Tp versus logarithmic time for cable C1..... 175

5.11: Tp versus logarithmic time for cable D1..... 176

5.12: Tp versus logarithmic time for low temperature annealing of cable B1..... 178

FIGURE PAGE

5.13: Tp versus logarithmic time for high temperature annealing of cable B1 179

5.14: Tp versus logarithmic time for original and history erased samples of cable B1 180

5.15: Tp versus time for 98 C annealing followed by 70 or 80 C annealing of original cable B1 181

5.16: Y-intercepts of annealing equations plotted against annealing temperatures for EPRs and EPDMs 190

5.17: Y-intercepts of annealing equations plotted against annealing temperatures for XLPE, B1, and A3 191

5.18: Y-intercepts of annealing equations plotted against annealing temperatures for high temperature annealing of cable B1 196

LIST OF TABLES

TABLE PAGE

2.1: Examples of Commercial Flame Retardants [Mark et al. 1975] 38
2.2: Nuclear Control Cable Formulation [Markezich 1989] 43
3.1: Classification of the Supplied Nuclear Control Cables 45
4.1: Data from 45 °C annealing of XLPE 58
4.2: Annealing Data for XLPE 63
4.3: Annealing Data for EPR 68
4.4: Annealing Data for EPDM 73
4.5: Annealing Data for XEPR 77
4.6: Annealing Data for XEPDM 82
4.7: Annealing Data for Cable A1 89
4.8: Annealing Data for Cable A3 99
4.9: Annealing Data for Cable C1 108
4.10: Annealing Data for Cable D1 114
4.11: Annealing Data for Cable B1 124
5.1: Annealing parameters 163
5.2: Data from statistical analysis of annealing results 183
5.3: Examples of typical time estimation errors 184
5.4: Characteristic parameters for the various materials 188
5.5: Summary of multiple annealing and cycling experiments 193
5.6: Predictions for cable 246-155-RW 195
5.7: Annealing data for cable B1 annealed at 98 °C and 80 °C 198
5.8: Predictions for cable 246-155-RP 201

1. INTRODUCTION

Many of the electrical insulating materials in use today consist of blends of various semicrystalline polyolefins. Crosslinked low density polyethylene (XLPE) is one such polyolefin which is commonly used in high voltage applications. Ethylene propylene copolymers (EPR) or terpolymers (EPDM) are often blended with low density polyethylene (LDPE) and crosslinked to yield an insulating thermoset which is used in control and lower voltage cable formulations. Crosslinked blends of LPE, EPR, and high density polyethylene (HDPE) are also common in lower voltage cables as well.

When these materials are subjected to operating temperatures below their melting points, the crystalline structure changes. This phenomenon is referred to as annealing, or, in other words, heat treatment without complete melting. The process of annealing results in the melting and recrystallization of a portion of the lower melting material as well as lamellar thickening of the higher melting crystals.

The manner in which these materials thermally age is an important phenomenon to understand and quantify. Elevated temperatures which produce annealing effects in semicrystalline polyolefins essentially result in the accelerated aging of the insulation. In the nuclear industry, where stringent regulations require frequent testing and requalification of control cables, a method which allows one to estimate the thermal history of insulations, and thus their effective lifetimes, would be extremely useful. Such an estimation technique has been developed using differential scanning calorimetry (DSC).

Annealing is manifest in the form of a shoulder slightly above the annealing temperature on the DSC endotherm. This shoulder represents the melting point of the new crystals which were recrystallized at the annealing temperature. The temperature at which this shoulder appears will increase slightly with increasing annealing time. By taking advantage of software available on the

DSC which allows the subtraction of endotherms, a curve which allows the estimation of the thermal history can be generatated by subtracting the endotherm representing the unannealed sample from the endotherm corresponding to the annealed sample. The position of what is termed the loss peak on this subtraction curve, Td, allows the estimation of the annealing temperature. The position of what is know as the gain peak, Tp, follows a logarithmic time dependence and can be used to estimate the annealing time.

The annealing behavior of XLPE, EPR, EPDM, crosslinked EPR, and crosslinked EPDM were studied at annealing temperatures ranging from 45 to 70 °C and various annealing times up to 1000 hours. Equations were obtained of the form:

$$Tp = A + B\mathrm{Log}(t)$$

where the parameter A was found be dependent upon annealing temperature alone and the parameter B was independent of the annealing temperature over the range of 44 to 70 °C and was representative of the material.

From the annealing studies of these standard materials, a general annealing equation was developed for EPRs and XLPEs which allows the estimation of thermal history over the spectrum of annealing temperatures studied.

Various nuclear control cable samples were studied in detail and were found to behave in a similar manner to the standard materials.

The subtraction technique was also applied to actual aged samples from power plants in order to gain an understanding of the applicability of the technique to realistic situations.

2. REVIEW OF THEORETICAL BACKGROUND AND LITERATURE

This thesis presents a method to determine the thermal history of polyolefin electrical cable insulation using Differential Scanning Calorimetry (DSC) analysis. The technique involves the subtraction of two DSC endotherms from one another to generate a third curve termed a subtraction curve. Information can be obtained from the subtraction curve to give clues to the time and temperature of annealing as well as the rate of cooling from the melt. It is a straightforward and easy to use technique which in principle requires no extensive knowledge of the physics of the polymer materials composing the insulation. However, there are many complicated processes occurring within the insulation both during manufacture and operation, and these processes are manifest partially through this technique. Interpreting the results of this technique without a basic understanding of the principles involved can and probably will lead to poor analysis and predictions. Therefore this review will present the basic and relevant theories of polymer crystallization and annealing, as well as principles involved in polyolefin compounding and failure.

2.1. Polymer Crystallization

The ability of many polymers to crystallize is truly an amazing phenomenon. One can imagine having a pound of cooked spaghetti and having to arrange this spaghetti such that it has order. One would first have to disentangle each piece then lay it down to order it. In a real polymer system the molecules are many times longer than the spaghetti and are able to order themselves and crystallize within seconds. Much of the cable insulation manufactured today is composed of polyolefins which possess some crystallinity and it is this crystallinity which enables the prediction of thermal history. So an understanding of some of the basic physics can be quite useful in

understanding how this technique works.

2.1.1 Crystal Structure

If a system is said to be crystalline then the molecules or atoms within the system are arranged in a manner such that there is a definite order and repeat structure. This repeat structure is referred to as the unit cell, of which there are seven basic types. The unit cell can consist of several atoms or molecules, or, in the case of polymers, a particular sequence of the molecule. The manner in which the the molecules are arranged within the unit cell and the symmetry which is characteristic of a particular packing allows for the categorization of the crystal structure further by the assignment of one of 230 space groups. For example with polyethylene, a polymer which in cross-linked form comprises much of the high voltage insulation in use today, there are five molecules in each unit cell, the corner molecules being shared by adjacent cells, with a repeat of two carbons such that the unit cell is orthorhombic and the space group is Pnam (Figure 2.1).

Crystal structure determinations are achieved through the science of x-ray diffraction. Crystallography is in itself a totally different discipline as well as an art form, and the understanding of which is not necessary to the basic concepts of polymer crystallization dealt with in this work.

2.1.2 Factors Effecting Crystallinity

There are several factors which affect the ability of a polymer to crystallize. The chemical structure, or configuration, is perhaps the most important controlling factor. A polymer molecule must have a certain length of crystallizable units in order to generate crystallinity within the system as a whole. Referring back to Figure (2.1), if we randomly replaced the hydrogen atoms along the main chain with

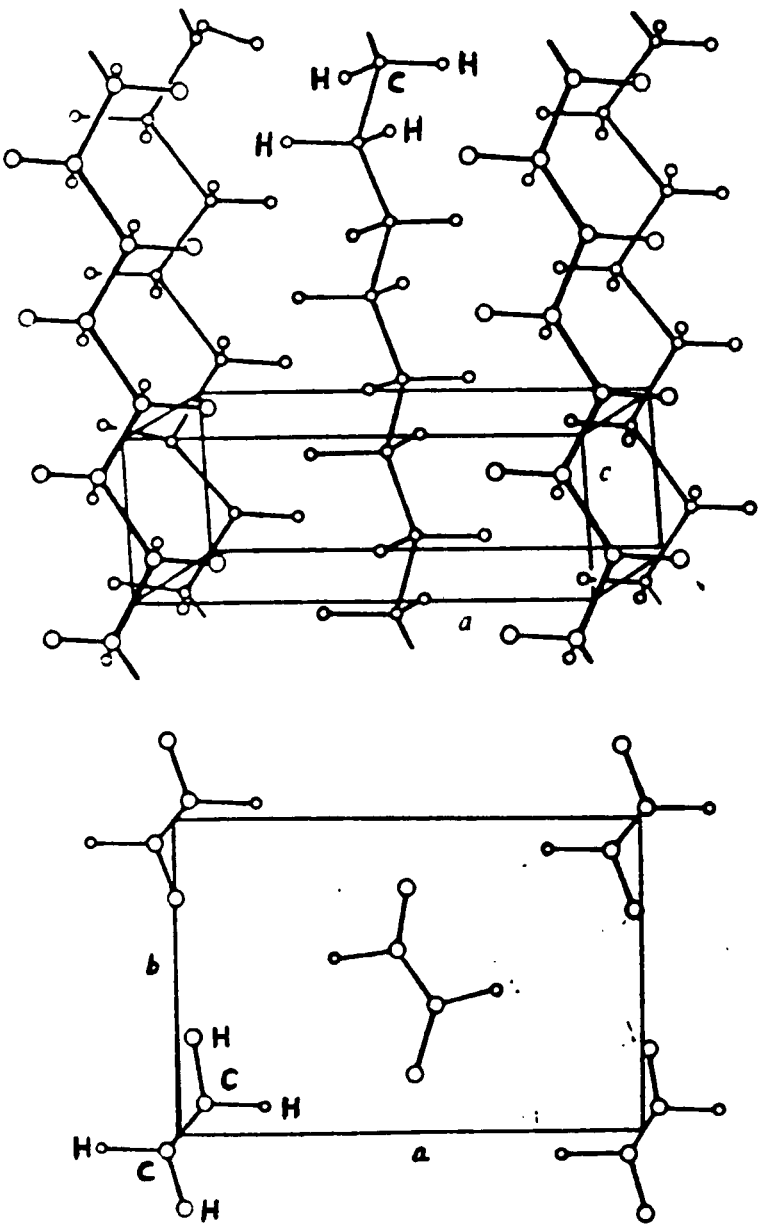


Figure 2.1. Schematic of the unit cell of polyethylene.

another bulky constituent we would disrupt the ability of the polyethylene to crystallize because the constituent would not pack into the unit cell. Eventually, if we replaced enough of the hydrogens randomly, one would prevent the polymer from crystallizing. While in practice different types of polyethylenes do contain branches and crosslinks which are unable to be incorporated within the crystal structure, there are still enough crystallizable units in sequence to give rise to some crystallinity.

Constituents on the main chain do not necessarily dictate whether a material will possess crystallinity. If the constituents are arranged in a non-random manner the polymer is said to be either isotactic or syndiotactic. Tacticity relates to the arrangement of stereoisomers along the backbone of the molecule. If the repeating monomer is arranged in such a manner that the main chain consists of either totally right or left handed stereoisomers the polymer is referred to as isotactic. If the chain consists of alternating left and right handed stereoisomers it is termed syndiotactic, and if they are randomly distributed, atactic. Both isotactic and syndiotactic polymers usually posses some crystallinity.

There are other factors which can affect the crystallinty of a polymer system. Mobility of the main chain constituents also may limit the ability of the polymer to crystallize under certain conditions. A rigid polymer such as PET can be manufactured such that the final product is totally amorphous. This is achieved by quenching from the melt. However, upon annealing at a temperature above Tg, the material will crystallize.

In general, the slower the cooling of a polymer which is able to crystallize the more crystallinity it will possess. The fact that different crystallinities can be produced from different cooling rates may make it possible to infer the type of cooling experienced by a sample of insulation.

2.2. Morphology

2.2.1 Single Crystals

Single crystals are generally formed by crystallization from dilute polymer solutions. A single crystal consists of one lamella on which polymer molecules nucleate and crystallize from the solution. The first polyethylene single crystals were reported by Jaccodine (1955), and since that time single crystals of most other polymers have been produced as well. The study of single crystals led the early attempts at understanding the nature of crystallinity, melting, and annealing of semi-crystalline polymer systems.

Single crystals are generally small, only on the order of 100 A in thickness and several micrometers across. The final thickness depends upon the crystallization temperature as well as further annealing treatments after crystallization is complete. They usually appear as rhomboids or in the form of hollow pyramids which often collapse upon drying. The simplest crystals are obtained from dilute solution, with more complicated morphologies such as twins, dendritic crystals, and spiral growths being formed as the concentration of the polymer is increased. Eventually crystalline aggregates and spherulites are formed if the concentration is increased enough.

2.2.2 Spherulites

Polymers crystallized from more concentrated solutions and the melt often exhibit spherulitic morphologies. Spherulites consist of lamella radiating from a central point such as to form a sphere until impingement with another spherulite occurs. Impingement results in a polyhedral shape as opposed to a true sphere. Spherulites from polymers always exhibit a "maltese cross" under crossed-polars due to reorientation of the polarization by the symmetry and orientation of the crystals. In some cases the spherulites exhibit what is called

banding. This banding takes the form of concentric rings in optical extinction patterns within the spherulite and is thought to be due to the regular twisting of the lamella. Spherulites vary in size according to the polymer system and the crystallization temperature, with larger spherulites being formed at higher crystallization temperatures.

2.2.3 Axialites

Axialites encompass a variety of morphologies intermediate between single crystals and spherulites, being crystalline aggregates composed of numerous lamellae. Axialites exhibit a splaying of lamellae which yields a less compact structure than that of a spherulite. Often they are in the form of polyhedral structures termed hedrites. Hedrites often exhibit extinction patterns resembling the maltese cross typical of spherulitic morphologies when viewed along one axis. However, they show little birefringence when viewed normal to their basal plane. Work with hedrites by Niegisch (1959) revealed that radially oriented fibrous lamella can form what are called ovoids. These lamellae can also crystallize in a spirally oriented manner creating what are termed spiral ovoids [Rabek 1980)].

2.2.4 Cable Morphology

Electron microscopy studies performed by Phillips and Vantansever (1988) on several crosslinked low density polyethylene high voltage cables revealed that the insulation is composed primarily of nonbanded-sheaf like structures made up of linear lamellae separated by areas of randomly oriented wormlike lamellae. Occasionally banded sheaves were observed as well.

Lee and Phillips (1989) performed optical microscopy upon regions in which electrical breakdown had occurred in crosslinked low density polyethylene typically used in insulation and discovered

the presence of small banded spherulites with average diameters of 15 μm. This is indicative of the high temperature developed at the region due to electrical breakdown, which facilitated separation of the extractable portion of the polyethylene from the crosslinked gel portion.

2.3. Crystallization Models

During the early years of polymer science very little was known about how polymers crystallized. X-ray line broadening studies revealed the size of polymer crystals to be small and the unit cell had been determined from diffraction studies, but how the molecules arranged themselves to give rise to crystallinity had yet to be elucidated. Even today there is a great deal of controversy over the matter and several schools of thought exist.

One of the first models was put forth by Herman, et al (1930) and was based upon the knowledge of polymer crystals existing at that time. This model, known as the Fringed-Micelle model, postulates that polymer molecules contain regions of order and disorder (Figure 2.2a). The model was able to account for both the small crystal size and the fact that the crystal dimensions are much smaller than the actual molecular length, and the mechanical behavior exhibited by many semi-crystalline polymers. However with the discovery in the 1940's of spherulitic morphologies, the Fringed-Micelle model was proven to be wrong.

Not until the mid to late 1950's did a better understanding begin to develop. The main breakthroughs came from the study of polyethylene single crystals. Some of the first work was performed by Jaccodine (1955) who obtained rhombic shaped crystals of a fairly low molecular weight (10,000) polyethylene from dilute solutions of benzene and xylene. Keller (1957), Fischer (1957), and Till (1957)

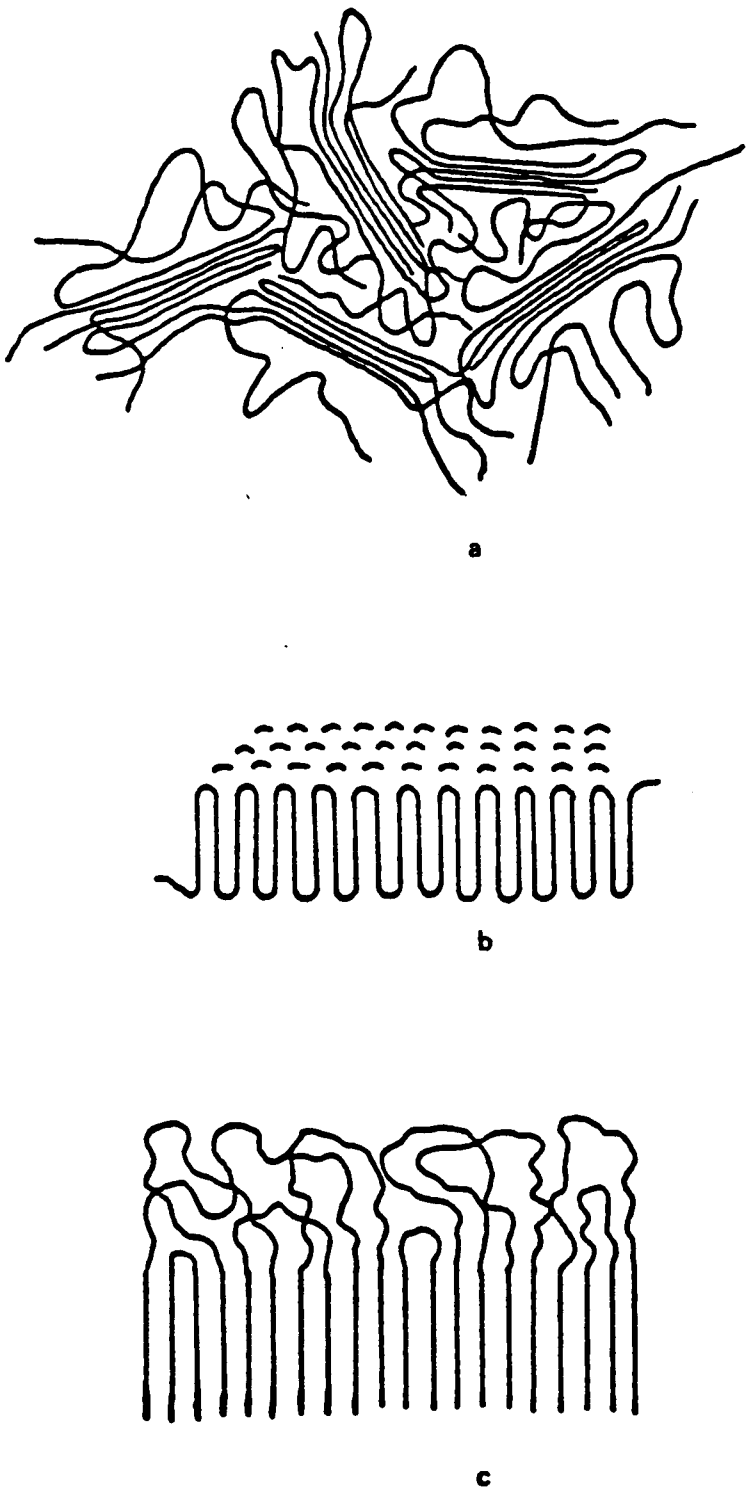


Figure 2.2. Polymer crystallization models: a) Fringed micelle b) Adjacent reentry c) switchboard reentry.

later expanded upon this work with linear polyethylene, and used both their electron microscopy and electron diffraction results to conclude that the polyethylene molecules lay with their lengths perpendicular to the crystal surface. From this they were able to postulate that the molecules could fold back on themselves after exiting the crystal surface and reenter the crystal. This led to the adjacent reentry model proposed by Keller (1957) which basically postulates that once the polymer molecule exits the crystal it folds back upon itself and lays down on the crystal surface adjacent to the last crystallized segment from which it folded (Figure 2.2b). The folds are thought to be relatively tight, consisting of only five methylene groups. The model explains the small lamellar thickness, surface packing density, molecular orientation, as well as the lack of much amorphous material within the single crystal, as shown by sharp electron diffraction spots from the crystals.

The counterpart of the adjacent reentry theory is the model of Flory (1962) known as the switchboard reentry model (Figure 2.2c), which consists of longer folds which reenter the crystal in a non-adjacent manner. Flory bases this theory upon discrepancies between crystalline densities obtained from unit cell calculations and the experimentally determined densities. According to Flory, the lower experimental densities are due to the amorphous zone arising from non-adjacent reentry. However, the lower density can be as easily explained as due to surface roughness and a few loose folds and tie molecules in the adjacent reentry model.

A similar model to that of Flory's is the interzonal model of Mandelkern (1975). This model proposes that the molecules form an ordered amorphous region as they leave the crystal and turn into a true disordered state some distance from the actual crystal surface.

2.3.1 Arguments Concerning the Nature of the Fold Surface

The nature of the fold surface has been the center of controversy in polymer physics for some time. Many of the arguments arise over

the crystallization of polymers from the melt. While the basic physics behind the crystallization is the same for both single crystals and melt crystallized morphologies, the environment from which each crystallizes is drastically different. In the case of single crystals from dilute solution, the polymer molecules are surrounded by solvent molecules and do not become intimate with other polymer molecules until they attach themselves to the crystal substrate. Thus, for low concentrations, they are free from entanglements with other polymer molecules in the uncrystallized state. In the melt there is no solvent so the polymer molecules will be entangled with each other thus inhibiting the ability of the molecules to diffuse to the crystal growth front. One can easily envisage how the situation would be greatly different from that of dilute solution.

Another problem arising with melt crystallized polymers is the ability to study the lamellae. Polymers crystallized from the melt do not crystallize in the form of single crystals but crystalline aggregates composed of many lamellae. Therefore, it is much harder to study the lamella of a melt crystallized polymer as one would study a single crystal grown from solution.

However, with the refinement of the technique of neutron scattering, much information has been gained about the behavior of the molecules crystallized from the melt. Neutron scattering is based upon similar principles as light scattering, the difference being that neutron scattering enables one to study systems other than those of dilute solutions. Deuterium is used to label the polymers since its scattering length is different from that of hydrogen. Information can therefore be obtained concerning the size, shape, and trajectory of the labeled polymers in the melt and crystallized states within a system containing both labeled and hydrogenated polymer molecules. Results of neutron scattering on melt grown crystals have shown that the radius of gyration of the deuterated molecules decreases by about ten percent upon incorporation into the crystal. The radius of gyration is defined as the root mean square distance of the elements of the chain from its center of gravity, and therefore is

a measure of the effective size of a polymer molecule.

Since the radius of gyration only decreases by a slight amount, supporters of the switchboard model have claimed that adjacent reentry is mostly absent from the stems that are in the crystal [Flory and Yoon 1978]. However, Hoffman (1979) explains the liquid-like radius of gyration to be the result of tie molecules and multiple nucleation at distant points within the same lamella, the primary mode of folding remaining adjacent reentry.

Other arguments have been made concerning the ability of the molecules to disentangle themselves at a rate high enough such to effectively yield adjacent reentry. Yoon and Flory (1979) claim that the polymer molecules' rate of disentanglement is far below that required to fit experimental crystallization kinetics, therefore eliminating the possibility of adjacent reentry.

This argument is countered by proponents of adjacent reentry by taking into the effect of reptation given by DeGennes (1971,1976), which can be invisioned as sucking a piece of spaghetti from a bowl of entangled pasta. If this concept is used, the rates of disentanglement will be increased such that at least short sequences of adjacent reentry are possible [DiMarzio et al. 1979].

One last important point which needs to be addressed are the conclusions which can be drawn from single crystal studies. Considering the highly structured and symetrical features of single crystals grown from solution, it seems more conceivable that the geometries produced are the result of adjacent reentry folding. In a conceptual sense, it seems highly unlikely that such morphologies can be consistently produced through a random switchboard reentry type of folding. Studies performed with mixtures of deuterated and hydrogenated polyethylene using infrared spectroscopy have produced results indicating that solution grown single crystals are produced predominantly by adjacent reentry folding [Cheam and Krimm 1981]. The same conclusions were drawn from neutron scattering studies performed by Spells et al. 1980.

Therefore, it seems likely that the molecules in the melt would

exhibit the same tendencies to fold in an adjacently reentered manner, but to an extent is dictated by the chain microstructure and degree of supercooling (i.e. crystallization temperature). While it is conceivable that some adjacent reentry could take place, there has been no experimental evidence produced thus far to prove conclusively that adjacent reentry is not the primary mode of folding.

2.4. Crystallization Theory

Crystallization can be considered as a series of steps consisting of primary nucleation, growth, and secondary crystallization. Primary nucleation involves the initial formation of a crystalline or ordered entity from which the molecules start crystalline growth, usually termed a nucleus.

There are two types of primary nucleation, homogeneous and heterogenous. Homogenous nucleation involves the formation of nuclei randomly throughout the melt without any preexisting surfaces on which to nucleate. The second type of primary nucleation is called heterogenous nucleation and involves the formation of the nucleus upon impurities within the melt. Heterogenous nucleation occurs instantaneously and usually is the predominant form of nucleation in most processed polymers, including cable insulation. Often certain impurities, known as nucleating agents, are added in processing to attain different mechanical properties.

The driving force for the formation of the nuclei is a lowering of enthalpy as the polymer molecules crystallize. The governing thermodynamic equation is known as the Gibb's free energy equation after an American theoretician of the 19th century:

$$\Delta G = \Delta H - T\Delta S \qquad 2.1$$

In order for a spontaneous change to occur, such as crystallization,

the amount of free energy (G) available must decrease.

Upon crystallization many things happen. Initially there is an increase in the Gibbs free energy due to the creation of a crystal surface. After the nucleus reaches a certain critical size the rise in free energy is offset by the lowering of the enthalpy (H) due to the incorporation of the polymer molecules into the crystal, and the nucleus is said to be stable.

Entropy (S) is another competing factor as well. Entropy is the measure of the amount of disorder in a system, so as the molecules crystallize they gain order and the entropy decreases giving rise to an increase in the free energy. However, this entropy loss is also offset by the decrease in enthalpy.

Once the primary nucleus is formed, eventually an additional part of the molecule will nucleate upon the growth face. This process is known as secondary nucleation. Crystal growth continues through a cycle of secondary nucleation followed by the laying down of the molecule which nucleated upon the existing crystal face, preferentially through adjacent reentry. The speed at which the growth occurs is dependent upon such factors as the temperature, molecular weight, pressure, and chain mobility and microstructure.

Lauritzen and Hoffman (1973) developed a theory assuming adjacent reentry which leads to some equations which have been instructive toward understanding polymer crystallization, as well as predicting actual crystallization kinetics. An idealized model is shown in Figure 2.3. The surface nucleus grows in the "g" direction with the measured growth in the "G" direction. The change of free energy as a result of laying down ν molecular strands with ν -1 folds and length l will be (ignoring chain end effects):

$$\varphi_S = 2bl\sigma_S + 2(\nu - 1)ab\sigma_e \qquad 2.2$$

This is due to the creation of three new surfaces for each new stem which lays down and the replacement of one surface by an identical one. For each new stem there is the formation of a new surface in

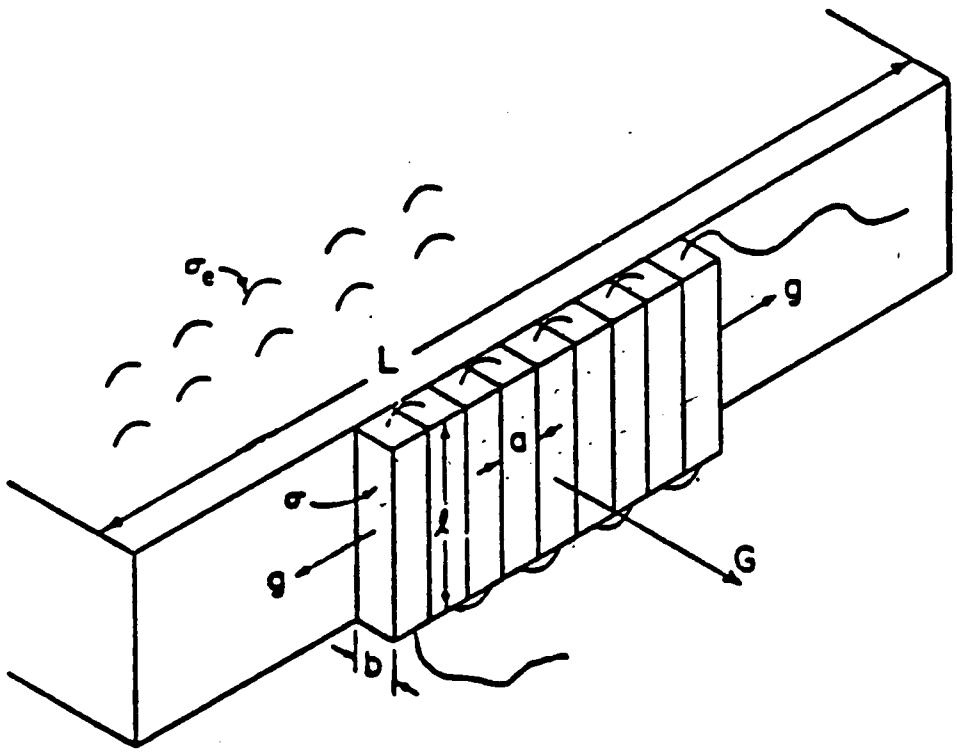


Figure 2.3 Idealized schematic model for lamellar crystal growth (Hoffman et al. 1976).

the direction of "g" ($2bl\sigma_s$) and then two identical new surfaces at the fold ($2ab\sigma_e$). If the next stem laid down upon the crystal surface in a non-adjacent reentered manner, the increase in free energy would be $3bl\sigma_s + 2ab\sigma_e$ due to the creation of five new surfaces as opposed to only three with adjacent reentry. Thus, adjacent reentry is thermodynamically favored over non-adjacent reentry in an idealized situation.

The reduction in free energy due to the incorporation of strands will be given by:

$$\varphi_c = - \nu\, abl\Delta f \qquad 2.3$$

Combining the two equations we have an expression for the total change in free energy:

$$\Delta G_v = 2bl\sigma_s + 2(\nu - 1)ab\sigma_e - \nu abl\Delta f \qquad 2.4$$

Assuming a large number of stems the $-2ab\sigma_e$ term is negligible and upon rearrangement:

$$\Delta G_v = 2bl\sigma_s + \nu\, ab(2\sigma_e - l\Delta f) \qquad 2.5$$

The creation of a secondary nucleus initially leads to an increase in the free energy and at the point of creation there is a chance of either the nucleus detaching from the surface or growing by the addition of new stems. As the nucleus grows it eventually approaches a region of stability where there is no longer a chance of the molecules detaching. It is interesting to note that Hoffman et al (1976) assumed a single stem nucleus. Kinetic studies performed recently by Lambert and Phillips (1990) with crosslinked high-density polyethylene has yielded evidence suggestive of a three stem nucleus.

If the unit volume of a crystal is considered at a temperature (Tm^o) at which it would melt if it had infinite dimensions, then the

following expression can be obtained:

$$\Delta f = \Delta h_f - Tm^o \Delta S_v \qquad 2.6$$

where Δh_f and ΔS_v are the enthalpy and entropy per unit volume, respectively. Tm^o can be obtained experimentally by extrapolating a plot of the crystallization temperature (Tc) versus the melting temperature (Tm) to a line of Tm=Tc. The point of intersection is Tm^o. At Tm^o the melt is in equilibrium with the crystalline state and so $\Delta f = 0$. This leads to the following equation:

$$\Delta S_v = \Delta h_f / Tm^o \qquad 2.7$$

However at a temperature below Tm^o, Δf will be finite. Assuming that ΔS_v is not temperature dependent, one can substitute 2.7 into 2.6 to obtain:

$$\Delta f = \Delta h_f - T\Delta h_f / Tm^o \qquad 2.8$$

When the nucleus reaches a size such that it is stable, ΔG_v will be zero, and assuming that the surface free energy will be small compared to the fold surface energy, an expression for the critical length of a strand can be obtained by substitution of 2.8 into 2.5, :

$$l^o = 2\sigma_e Tm^o / \Delta h_f [Tm^o - T] \qquad 2.9$$

It is important to note that l^o is the initial lamellar thickness of the critical nucleus and much thickening occurs during isothermal crystallization. However, the equation is useful in conceptualizing the effect of supercooling and the heat of fusion upon lamellar thickness.

The complete theory of Lauritzen and Hoffman involves several other considerations not mentioned here and allows for fairly accurate modeling of kinetic isothermal crystallization behavior. The

theory predicts the existence of three regimes of growth. The first regime occurs when the rate of lateral spreading (g) is much greater than the nucleation rate. In the second regime, the two rates are equal, and in the third regime, first suggested by Phillips (1979), the rate of surface nucleation greatly exceeds that of lateral spreading.

2.4.1 Melting

The same thermodynamics can be used to predict melting behavior also. Considering a lamellar crystal of lateral dimensions a and b, thickness l, and with fold surface energy σ_e and lateral surface energy σ_s, melting will cause a decrease of $2al\sigma_s + 2bl\sigma_s + 2ab\sigma_e$ in the free energy. However the incorporation of molecules into the melt will cause an increase in the free energy by $abl\Delta f$. The overall free energy change is thus:

$$\Delta G = 2(a+b)l\sigma_s + 2ab\sigma_e - abl\Delta f \qquad 2.10$$

Assuming that the crystal is fairly large such that the fold surfaces are much greater than those of the lateral surfaces, the term $2(a+b)\, l\sigma_s$ can be considered negligible. At the melting point the system is in equilibrium and the change in the free energy is equal to zero. Using the expression obtained earlier for the heat of fusion, we can obtain the final working equation:

$$Tm = Tm^o - 2\sigma_e Tm^o/l\Delta h_f \qquad 2.11$$

This equation is useful in seeing the effect of lamellar thickness and the heat of fusion upon the melting behavior. Also, a plot of Tm versus 1/l will have a slope of $-2\sigma_e Tm^o/\Delta h_f$ and an intercept of Tm^o.

2.5. Annealing

The heat treatment of a system which does not result in large scale melting is generally referred to as annealing. In metal systems where crystals have been plastically deformed, annealing generally results in atoms moving to form a more perfect and less strained array in the form of smaller and less distorted grains. This will act to improve ductility in the system. The annealing of a polymeric system results in morphological changes also, but on a much smaller scale than occurs in metals. If a semi-crystalline polymer system is annealed at a fairly low temperature in relation to its crystallization temperature, the result will often be in the form of crystal perfection. Lamellae can also thicken in the solid state by drawing in molecular strands from other regions of the crystal or the amorphous regions. At higher temperatures crystals which are thinner and less perfect will tend to melt out completely while the bulk of the crystalline portion of the polymer remains in the solid state. Over a period of time the material which melted will recrystallize in the form of thicker lamellae crystals. As the time of annealing is increased it is possible that the newly crystallized material will perfect as well, further increasing its melting point. This recrystallization and perfection will manifest itself on a DSC trace as a shoulder or smaller peak at a temperature above the annealing temperature. The subtraction technique allows one to study the position of various shoulders and peaks generated by annealing in a more detailed fashion than possible by simply examining the DSC endotherm.

2.5.1 Annealing Observations

Some of the first most revealing studies of the mechanisms of annealing were performed by Keller and O'Conner (1950). They showed that the small angle long spacing of single crystal mats increased from 120 angstroms to between 200 and 300 angstroms.

The long spacing is the distance from the top of a lamella through the lamella and also through the intervening amorphous region down to the top of the next lamella.

Statton and Geil (1960) expanded on this work and confirmed the increase in long spacing with annealing. Their electron microscopy on single crystals which had been annealed near the melting point produced pictures of lamellae with holes in them. This is often termed a "swiss cheese" or "amoeba-like" morphology. Regions of the lamellae were thickening at the expense of others (i.e. drawing molecules in from other less perfect areas) and hence producing holes. Holland (1964) was able to produce a "picture frame" morphology upon annealing single crystals of polyethylene. He postulated that this resulted from the inner material dissolving and recrystallizing along the edges with increased thickness.

The increase in small angle long spacing was found to have a logarithmic time dependence as well. This was shown by Fisher and Schmidt (1962), among others, in work with linear polyethylene. They found that the long period increased with annealing time and temperature, the rate of increase being greater for higher annealing temperatures.

Petermann and Gleiter (1976) used the defocus imaging technique with transmission electron microscopy to observe the migration of the amorphous regions parallel to the [002] direction in bulk polyethylene samples, resulting in solid state crystal growth. They also interpreted some of their micrographs as resulting from melting of thinner lamellae and subsequent recrystallization.

Transmission electron microscopy studies performed later by Petermann and Gohil (1976) on isotactic polystyrene crystals revealed that slow heating of the material favored solid-state thickening, while faster heating rates tended to yield melting and recrystallization. They were also able to observe the growth of thicker lamellae at the expense of both thinner and bent lamella.

In a more applied study Kapur and Rogers (1972) examined the effects of room temperature (25 ^{o}C) annealing upon polypropylene

crystallized by quenching from the melt. They found no changes in the crystallinity, crystal structure, or crystal size, but observed a sixteen percent increase in the yield stress, a 150 percent increase in the draw stress, and a 185 percent increase in the modulus. They contributed these results as due to the relaxation of residual stresses caused by quenching. They also considered that chain mobility could be decreased due to secondary crystallization and that microvoids could collapse upon annealing as well.

2.5.2 Mechanisms of Annealing

There have been several mechanisms suggested to explain experimental observations of annealing and crystal thickening. One can envision molecules pulling themselves through the lattice in order to generate a thicker lamella at the expense of lamellar width. However, this seems hard to conceive considering it must occur for all molecules within the crystal at a considerable expenditure of energy. Reneker (1962) postulated that point dislocations in the form of molecular kinks, which result in extra $-CH_2-$ units incorporated within the crystal, could be a possible source of thickening (Figure 2.4). He was able to calculate that there could exist two defects per molecule in a typical crystal of polyethylene. Upon annealing these kinks could straighten out and hence lead to lamellar thickening.

Dreyfuss and Keller (1970) suggested that thickening could occur by a mutual rearrangement within a chain folded molecule without coordinated displacement of the molecule as a whole (Figure 2.5).

Peterlin (1964) put forth a more extensive theory based upon thermodynamic, molecular weight, and diffusion considerations. In order to explain the temperature dependence of the long period growth rate Peterlin postulated that the material needed must be transported from the free ends toward the center of the

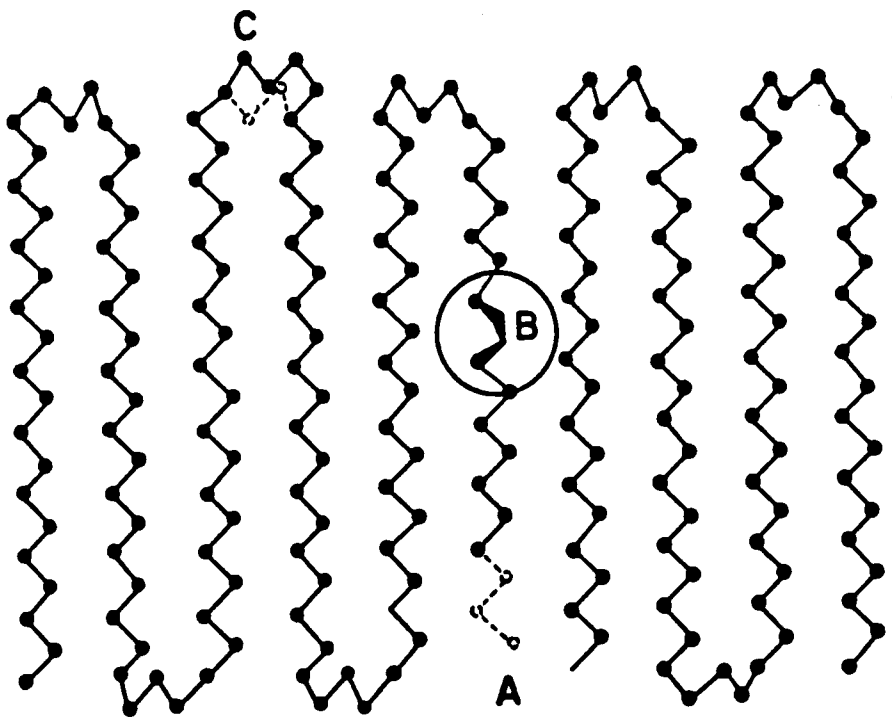


Figure 2.4. Schematic diagram of a molecular kink as a mechanism for thickening.

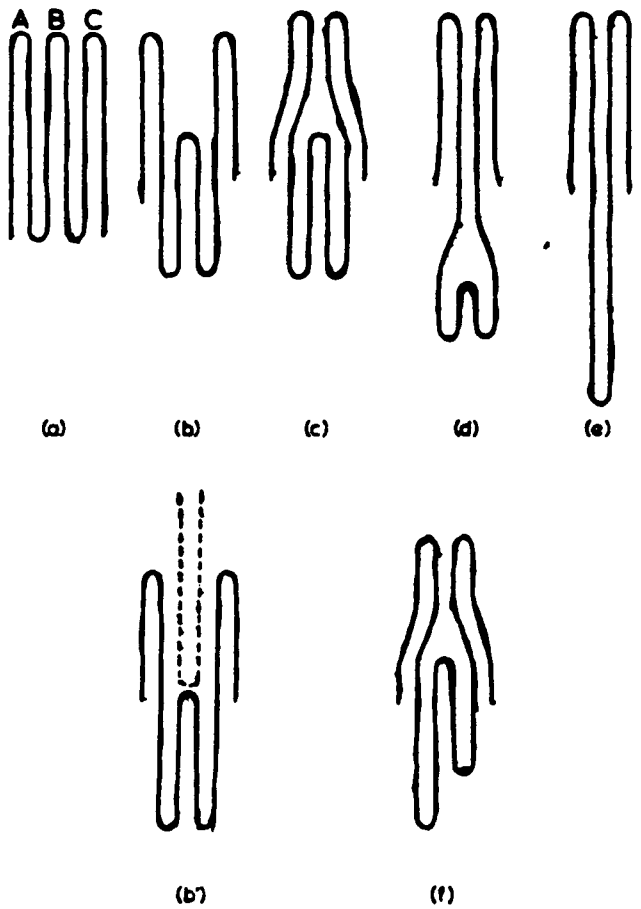


Figure 2.5. Schematic representation of a possible thickening mechanism proposed by Dreyfuss and Keller (1970).

macromolecule, and hence has to proceed by collective jumps of all monomers of one straight chain section between the fold surfaces.

Sanchez et. al (1973, 1974) put forth the most thorough mathematical theory to date to explain crystal thickening. They base their equations upon thermodynamic considerations, namely that the fold surface energy is approximately ten times that of the lateral surface energy and hence the reduction of surface free energy serves as the driving force for crystal thickening. Assuming it is an irreversible process, the rate of crystal thickening can be taken to be proportional to the surface free energy gradient:

$$x^2 dl/dt = -k d\sigma_e/dl \qquad 2.12$$

where x is the lateral dimension of the crystal and l is the thickness. This equation can then be integrated with only a few assumptions and yields an expression for the lamellar thickness as a function of time.

Phillips and Rensch (1989) analyzed the lamellar thickening behavior of poly(ε–caprolactone) using the Sanchez-Eby theory of thickening. They were able to develop a "master" isothermal thickening curve for different molecular weights as well as calculate an activation energy from the shift factors obtained. They were able to conclude that the active unit involved in thickening is approximately one stem. Phillips and Rensch also suggested that thickening could occur through an "omega defect", first put forth by Hoffman (1985) to explain the physical origin of the substrate length in regime theory. The defect can be visualized by considering a compressed inch worm, which resembles an omega. The arched back of the worm constitutes a fold in the molecule along the lateral surface. This is shown in Figure 2.6, and could result in a one stem thickening unit.

Premelting of surface layers of lamellae has been postulated by Fischer (1969) and Zachmann (1967) to explain the change in small angle x-ray scattering intensity with temperature. Premelting is

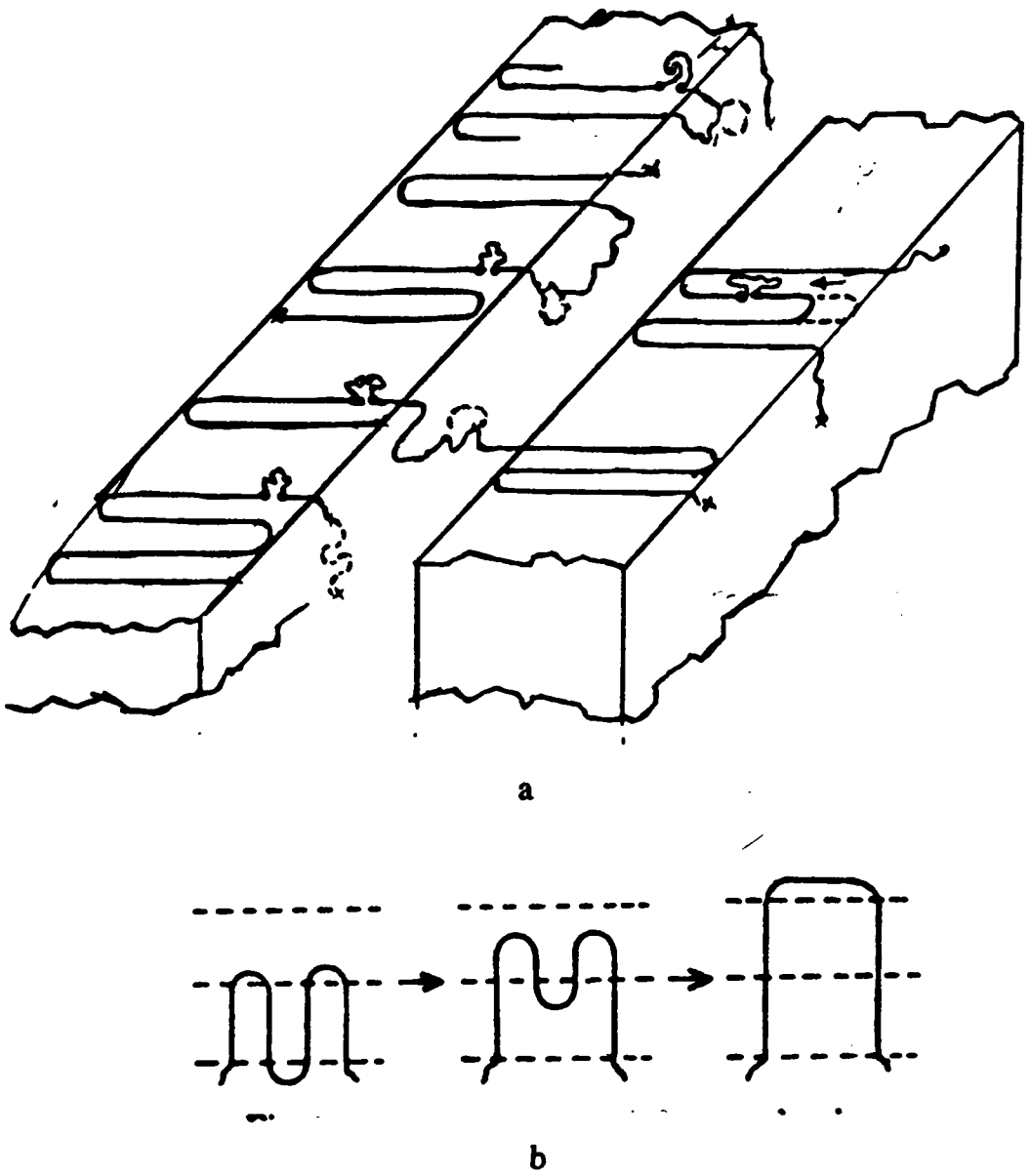


Figure 2.6. Omega defect: a) Structures allowing formation of omega defects in chain folded systems (Hoffman 1985) b) Possible omega defect mechanism (Phillips and Rensch 1989).

considered as a homogenous process which effects all lamellae uniformly.

Fischer (1969) also suggested a chain refolding scheme as an extension of his premelting models. The crystal core thickness is presumed to remain constant as the surface melts by material drawn in from the surroundings. This is thought to produce an increase in the amorphous interlamellar region determined by a temperature dependent equilibrium between the two states.

Killian (1969) and Flory (1955) have suggested another mechanism which consists of the selective melting of lamellae with different thickness and impurity content. The less stable lamella, i.e. thinner and imperfect, will tend to melt first and recrystallize in the form of thicker lamella.

Pope and Keller (1976) and Pope (1976) used differential scanning calorimetry and small angle x-ray scattering to study the effects of annealing upon low density polyethylene. They identified three types of endotherms, a high temperature one attributed to melting of primary lamella, a second intermediate one due to melting of the products of reorganization of the scan, and a third lower endotherm attributed to melting of material crystallized upon cooling from the annealing temperature. Pope and Keller (1976) also use the selective mechanism to explain temperature induced reversible changes in long spacing. They argue that there is a wide range of lattice spacings due to many different lamellar thicknesses . Therefore removal of the thinnest of these during annealing should result in the observed increase in the overall periodicity (long period).

However, Strobl et al. (1980) found that in the temperature range where melting and crystallization is accompanied by a drastic change in long period the change in the mean crystal thickness is negligible. They postulate that the changes in the distribution function for the amorphous layer thickness and not the lamellar layer thickness were responsible for the shift in long period. They suggested that the amorphous layer thus governs the ability of a crystal to thicken.

2.5.3 Crystal Imperfections

There is a wide variety of imperfections which can be present within a polymer crystal lattice. Molecular kinks, chain ends, branch points, impurities, and folds which may be incorporated within the lattice constitute what are called point defects. A point defect created by a chain end is shown in Figure 2.7.

The second type of imperfection is often referred to as a dislocation or line defect. A dislocation is basically a line array of motifs which show a deviation from the regular arrangement of motifs within the crystal structure. A motif is the characteristic repeat unit in a crystal lattice. An example is shown in Figure 2. a. Dislocations can be classified as either edge or screw dislocations, depending upon the position of the vector **d** running along the edge of the extra plane of motifs in relation to the vector **b** (Burgers vector) measuring the size of the dislocation. If the two are parallel the dislocation is called a screw dislocation and if the two are perpendicular it is referred to as an edge dislocation (Figure 2. b).

Dislocations are generally studied using electron microscopy through what are called Moire patterns, which are produced by double diffraction of the electron beam when two crystals are slightly misaligned. Crystalline defects, both line and point, will also produce broadening in the x-ray diffraction maxima as well giving rise to the concentric rings as opposed to sharp spots typical of metals and highly perfected crystalline material.

There are several other possible sources of defects. Some of these include the nature of the folds, such as the length of the fold and the presence of a branch or crosslink on the fold. Boundaries between twins, different phases, and regions of different stacking or orientation can also be considered as defects as well. However, these

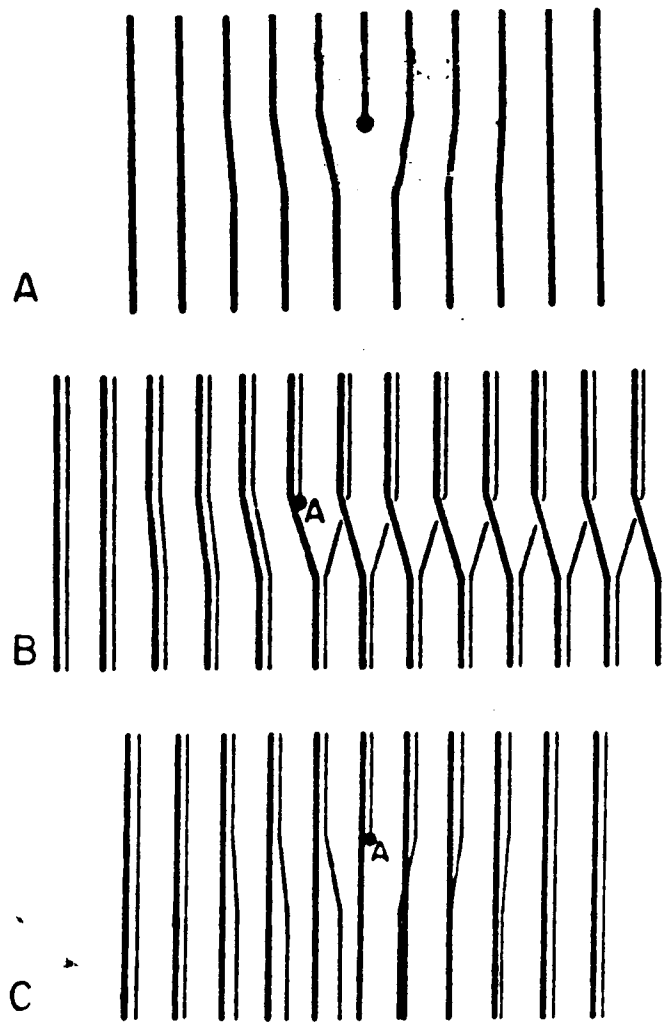
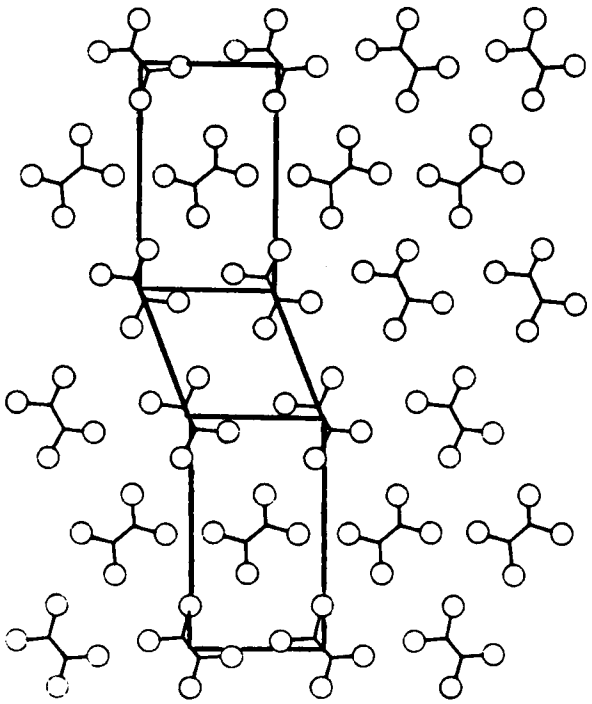
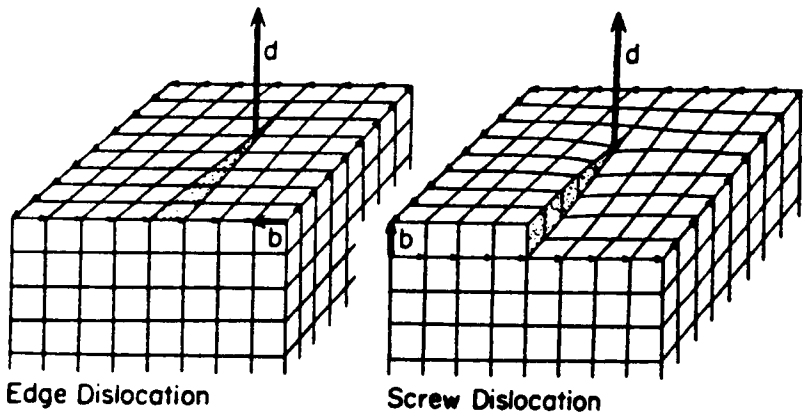


Figure 2.7. Schematic of a point defect in the form of a chain end.



a



b

Figure 2.8. a) A stacking fault in polyethylene; b) Schematic representation of an edge and a screw dislocation showing the dislocation line vector **d** and the Burgers vector **b**.

types of defects are much harder to quantify and do not relate readily to annealing effects.

Crystalline defects act to lower the heat of fusion of a crystal by interfering with the attractive forces (van der Waals, ionic, or hydrogen bonding) of the molecules for each other in the crystalline array. This in turn lowers the melting point of a particular region or lamella where defects are present (Eq. 2.11) making that particular lamella more susceptible to melting and subsequent recrystallization.

Defects can also be a source of stress within the lattice as well. The study by Pertermann and Gohil (1976), mentioned earlier, yielded photographic evidence that bent lamella, i.e. regions containing stress, tend to melt out first. Thus defect areas will also be more susceptible to annealing than other more perfect regions or lamella.

When a lamella is subjected to annealing these defects can also "anneal out" toward the intercrystalline regions. This will raise the heat of fusion of the crystal resulting in a slightly higher melting temperature.

2.6. Treeing

Since this thesis deals primarily with polyolefin cable insulation, it seems only fitting to provide a brief review of some of the factors contributing to the failure of insulation. The cables which have been studied in this work are mainly control cables which are not generally exposed to high voltages. The mode of failure for these types of insulation is mechanical in nature. Exposure to radiation and heat from external sources act over extended periods of time to cause degradation which often leads to loss of the mechanical properties. This leads to cracking in the outer jackets and insulation. For the higher voltage transmission and distribution cables, failure is largely due to high electrical stresses created within the insulation. Some of the principles and contributing factors involved with electrical breakdown in high voltage cables will be briefly reviewed.

We can consider two basic groups of factors, those due to environmental factors and those due to intrinsic flaws within the insulation. Environmental factors consist of the effect of temperature, exposure to water, air or sunlight, and the magnitude of the current flowing within the conductor. Intrinsic defects within the insulation are in the form of voids, gel particles, protrusions form the conductor or insulation shield as well as contaminants such as dust particles [Kiss 1979]. In practice, the combination of these two groups leads to the failure of the insulation, usually in the form of what are called "trees".

Trees are channels which form over an extended period of time within the high voltage insulation and act to reduce the effective thickness of the insulation such that electrical breakdown occurs. A tree is classified as a water tree if it grows in the presence of moisture and an electrical tree if moisture is absent. They can also be subclassified as vented or non-vented trees, according to the availability of air and water. Vented trees tend to initiate at interfaces, such as between the insulation and conductor jacket or insulation shield and hence have a good source of air or water from which to propagate and grow. Non-vented trees initiate within the insulation at voids or defects and usually do not grow to the extent of vented trees.

2.6.1 Environmental Factors

Often the life of a cable can be greatly affected by the environment in which the cable is used. Exposure of the unshielded insulation to air or sunlight can act to degrade the polymer over an extended period of time and reduce the effectiveness of the insulation. Another factor is the voltage developed within the conductor. Higher voltages will result in greater electrical stresses being developed within the insulation, particularly around defects, which act as stress concentrators. Also, if a cable is used in an environment which contains moisture, such as with underground

transmission lines, water can be drawn into the cable and eventually lead to water treeing.

2.6.2 Intrinsic Defects

The purity of cable insulation is a very important variable which has to be controlled during manufacture, particularly for the higher voltage rated cables. Impurities act as electrical stress concentrators which can eventually lead to treeing and failure.

Probably the most common type of imperfection is voids within the insulation. These voids can be generated by gas evolution during the peroxide crosslinking process, improper die settings, and shrinkage upon cooling. These voids are thought to become critical at sizes larger than 50 um in diameter and are less prevalent in dry cured as opposed to steam cured cables [Tanaka 1983]. Other imperfections can be in the form of rough edges or protrusions on the conductor or insulation shield or the presence of foreign particles. It is also possible to have polymeric contamination in the form of gel particles or prematurely crosslinked polymer [Kiss 1979]. All of these contaminants affect the insulation adversely by acting as electrical stress concentrators.

2.6.3 Electrical Trees

Electrical trees can be characterized as permanent hollow channels which take the form of tree-like structures within the insulation. They are known to occur at higher electrical stresses in the absence of moisture.

Electrical trees are thought to be initiated by interfacial injection and extraction of electrons by AC current from a sharp point or conductor edge which projects into the insulation [Eichhorn 1983]. It is postulated that this injection and extraction may create the situation where the electron can be accelerated through a high field such that it can accumulate enough energy (10ev) to ionize a small

portion of the insulation, resulting in decomposition. Once this occurs to generate a cavity, creating an electrical stress concentrator, growth will occur by partial discharge through the weaker areas of the insulation or, if the tree is vented to air, by oxidative attack as well.

It has also been proposed that high AC electrical stress exerted over a small cavity could create sufficient periodic Maxwell stress to lead to fatigue failure of the polymer around the cavity and initiate the tree [Eichhorn 1983].

Another theory relates to thermal effects, either by Joule heating or the conversion of discharge energy into heat. Both of these thermal effects could act to thermally decompose localized portions of the insulation [Mason 1959].

2.6.4 Water Trees

As mentioned before, water trees are thought to propagate and grow in the presence of moisture. While electrical trees tend to form under high electrical fields, water trees tend to form at much lower levels of electrical stress which are experienced during normal operation. They are also considered as an aging phenomena which can contribute to the eventual failure of the insulation. In appearance water trees tend to be fairly diffuse structures which often resemble a bush, bow-tie, or a string of beads and all forms will disappear upon drying.

It is thought that water is drawn into the insulation by dielectrophoresis. Dielectrophoresis considers the movement of polarizable molecules in a divergent field [Tanaka 1983]. Once the water has penetrated the insulation and either filled or generated voids, the initiation of water trees occurs by one of several proposed mechanisms. It has been postulated that partial discharge occurs in air filled regions in voids filled with water or around particles in the insulation [Nitta 1974]. This theory also involves the chemical decomposition of water into hydrogen and oxygen, which can act to oxidize the polymer in the region of discharge. After this, water

penetrates the newly damaged region and discharge eventually occurs again.

Another mechanism which has been proposed involves the expansion of water within cavities due to Joule heating. It is thought that this expansion can lead to larger more spherical cavities which in turn leads to tensile and compressive forces being developed. This is thought to cause the formation of other voids in regions of tension (perpendicular to the conductor). Once these smaller voids occur, water can leach into them and eventually another sphere is formed, hence the "string of beads" appearance of many water trees [Tanaka et al. 1974].

2.7. Insulation Stabilization

As mentioned earlier, there are many factors which contribute to the premature failure and degradation of polymeric insulation. However, many of these harmful factors can be neutralized by different additives. Tree retardants, anti-oxidants, UV stabilizers, fillers, and flame retardants all play a very important part in the effective design of safe and long lasting insulating materials for both high and low voltage applications.

2.7.1 Tree Retardants

There are a number of ways to limit the formation of trees within insulation. As discussed earlier, the major source of tree initiation is the presence of voids and protrusions in the insulation which act as electrical concentrators and also allow partial discharge to occur. The most straight forward means of correcting this is by limiting void formation during processing. It has been shown that steam cured cables contain more voids than gas cured, so switching from steam to gas curing is the best way to achieve low void content during manufacture [Kiss 1979].

The replacement of impregnated conductive tapes by an extruded

conductive shield composed of a semi-conducting polymer has proven useful in eliminating protrusions into the insulation [Fugisawa 1968].

However, even preventive measures during manufacture will not prevent the presence of some voids within the insulation. Tree retardants in the form of chemical additives and fillers are added to reduce tree initiation and improve insulation lifetime.

There are several principles which can be followed in designing a tree retardant. The first, and perhaps most obvious, is to simply fill the voids. This can be achieved in the form of eletronegative gases such as nitrogen (N_2) and sulfur hexaflouride (SF_6) which help to prevent partial discharges [Eichhorn 1983]. Other fillers act by providing a semiconducting coating to the inside of the cavities as well as physically filling the voids. Additives such as silicon oils, polybutene, paraffin oil, cumyl alcohol, and dimethylglycol fall under this category. Inorganic fillers such as calcinated clays, talc, silica, mica, and magnesia are used to relax locally intensified electrical stresses, and hence inhibit tree formation [Tanaka 1983].

Other additives, termed voltage stabilizers, act by "scavenging" high energy electrons injected into the insulation through the process of resonance trapping. Resonance trapping basically involves the injection of a high energy electron into a conjugated system where it is then reduced in energy by resonance stabilization and released as a low energy electron. Compounds typical of this mode of inhibition usually contain at least one electron acceptor group in the form of an unsaturated radical containing a π bond such as $-NO_2$, -CN, =CO, phenol, or polycylic aromatic [Eichhorn 1983]. They also typically contain an electron donor group such as amino and lower alkyl radicals which contain a transferable proton such as $-N(CH_3)_2$, $-NH_2$, or $-CH_3$. A typical formulation for a voltage stabilizer system patented in the 1960's by Simplex Wire and Cable is given as 1.5 percent o-nitotouluene, .25 percent 2,4 dinitrotoluene, .25 percent diphenylamine [Eichhorn 1983].

2.7.2 Flame Retardants

Given the number of fires caused by faulty wiring in both homes and industry, it should be easy to realize the importance of flame retardation in insulators. The ability of an insulator to resist combustion can be of importance in the nuclear industry where many of the lower voltage cables are used for control and safety equipment.

Combustion begins with the thermal-oxidative degradation of the insulation, which can occur over a fairly wide range of temperatures. If exposed to air at temperatures below about 80 ^{o}C, the primary mode is simple oxidation which usually occurs at a slow rate. Much of the insulation is tightly jacketed thus limiting the availability of oxygen. However, at higher temperatures the rate of oxidation increases and the formation of hydroperoxyl groups (-O-OH) on the carbons of the main chain begins to occur. They can then disassociate into free radicals [Mark et al.1975]:

$$\text{-C-O-OH} \text{ ---- } \text{-C}\bullet + \bullet\text{O-OH} + \text{-C-O}\bullet + \text{HO}\bullet$$

These free radicals will then nucleate chain reactions which can facilitate the decomposition of the main chain. This is the first step to combustion. To offset this effect chemicals are added which act as "targets" for the free radicals, and hence reduce the amount of attack upon the main chain. These additives are termed as chain transfer agents. Some of the best chain transfer agents are electron rich molecules, such as amines and phenols. However, these chemicals are often quite expensive and will become volatile at higher temperatures. In practice, halogenated compounds are used instead because of reduced cost and better stability. A few examples of some commercial flame retardant chain transfer agents are given in Table 2.1.

Table 2.1: Examples of Commercial Flame Retardants [Mark et al. 1975]

Trade Name	Composition	Supplier
I) *Halogen-Rich Flame Retardants*		
Chloro wax	Chloriated parrafin	Diamond Shamrock
DER	Brominated epoxy resin	Dow Chemical
Tribromophenol	$C_6H_2Br_3OH$	Great Lakes Chemicals
Phosphorous tribromide	PBr_3	Great Lakes Chemicals
Polytribromstyrol	$-CH(C_6H_2Br_3)CH_2-$	Kalk
HET	Chlorenic acid	Hooker Chemicals
Firemaster 5BT	Pentabromotoluene	Michigan Chemicals
Firemaster BP4A	Tetrabromobisphenol A	Michigan Chemicals
BP-10	Decabromobiphenyl	Michigan Chemicals
Aroclor 5442	Chlorinated triphenyl	Monsanto Chemical
Hexabromobenzene	C_6Br_6	Michigan Chemicls
Dechlorane Plus	$(C_5Cl_6)_2$	Occidental Chemical
EB-80	Pentabromoethylbenzene	Great Lakes Chemicals
II) *Char-Forming Flame Retardants*		
Aerotex NDC	Mixture of phosphates	American Cyanamid
CZC	Chrominated zinc chloride	DuPont
Firemaster HHP	Sb_2O_3	Michigan Chemical
Oncor 23A	Sb_2O_3-$(SiO_2)_n$	National Lead Co.
F 1309	Sb_2O_3-tricresylphosphate	Podell Ind. Inc.
III) *Glass-Forming Flame Retardants*		
Aerotex	Mix. of borates & phosphates	American Cyanamid
Arko-AS	Mix. of borates & phosphates	Arkansa Co.
IV) *Miscellaneous Flame Retardants*		
Diammonium phosphate	$(NH_4)_2HPO_4$	Stauffer Chemical
Firebrake ZB	$2ZNO(B_2O_3)_3(H_2O)_{3.5}$	U.S. Borax
Zinc Borate	$ZN(BO_2)_2$	Kraft Chemical
C-30 BF	$Al_2O_3 3H_2O$	Alcoa
Ammonium bromide	NH_4Br	Allied & Dow Chemicals
Molybdenum oxide	MoO_3	Climax Molybdenum
Fyrol 32-B	$(BrCH_2CH_2BrCH_2O)_3PO$	Stauffer Chemical
TPP	Triphenylphosphite	Weston
TPPO	$OP(C_6H_5)_3$	M&T
Thiourea	$(NH_2)_2C=S$	Allied Chemical

If the temperature is increased further, between 120 and 250 °C, the chain transfer agents will no longer be able to offset the chain scission reactions and degradation will occur. At temperatures in excess of 200 °C the halogen flame retardants will often become volatile as well, further enhancing chain scission. Once this happens, chemical decomposition begins to occur producing volatile products such as carbon monoxide, monomers, hydrogen, and smaller hydrocarbons. For this stage of combustion, compounds are added which decompose to form non-combustible gases like carbon dioxide, water, and ammonia. A typical formulation is a mixture of $(NH_4)_2$ and NH_4Br which reacts at 200 °C to produce HBr, which acts as a radical chain terminator, as well as the non-combustible products CO_2, H_2O, and NH_3 [Mark et al. 1975].

Additives in the form of inorganic powders can act to increase the thermal conductivity of the system, hence slowing the rate of temperature increase. Examples of these types of fillers are carbon black, silica, and alumina. Other additives, such as $(NH_4)_3BO_3$, $(NH_4)_4B_2O_5$, $(NH_4)_3PO_4$, $(Na)_3BO_3$, and $(Na)_3PO_4$ act to produce glassy coatings around a decomposing area [Mark et al. 1975]. This lowers both the accessibly of oxygen and the volatility of the decomposition products.

Other fillers in the form of antimony oxides and zinc salts act to form char which inhibits flammability. The antimony oxides also act synergistically with the halogenated compounds discussed earlier by binding to them at elevated temperatures. This, in turn, will lower their volatility and increase their residence time within the insulation at higher temperatures.

2.7.3 Anti-Oxidants

The long-term degradation at low temperatures due to oxidation can greatly reduce the effective life of an insulator. The electronegative carbonyl groups created by oxidation act to reduce

the insulating properties of the polymer by raising both the conductivity and dielectric constant. While PVC jackets are used to limit the exposure to both oxygen and UV radiation, anti-oxidants in a variety of forms are used to ensure that the insulation is guarded against oxidation, particularly around areas where the cable may be spliced.

Oxidation in polymer systems is a free radical chain reaction which proceeds primarily within the amorphous regions. There are two main groups of anti-oxidants which are distinguished according to their mode of action. The first group is referred to as chain breaking or primary anti-oxidants. These anti-oxidants work by interfering with the chain propagating steps by forming stable free radicals when they react with free radicals present on the chain (RO_2 or RO). Phenoxy radicals, stable radicals of naphthols and aromatic amines, quinones and conjugated molecules, such as anthracene are all examples of primary antioxidants [Kelen, 1983].

Another type of chain terminating anti-oxidant acts as a hydrogen donor, thus stabilizing the chain as well as competing with the polymer for peroxy radicals. The most effective types of hydrogen donors are generally hindered phenols and secondary aryl amines containing O-H and N-H bonds, respectively. A widely used antioxidant of this type is butylated hydroxytoluene manufactured by ICI, Shell, and Uniroyal [Kelen 1983].

The second group of antioxidants are termed preventive or secondary anti-oxidants and act by counteracting the formation of free radicals. UV stabilizers and light absorbers can be classified as preventive anti-oxidants since they act to absorb radiation which could initiate the formation of free radicals. Systems which are in contact with metals, such as cable insulation, often employ metal-ion deactivators which deactivate the metal by chelation. Bishydrazone is an example of this type of anti-oxidant. Other preventive antioxidants contain phosphorus or sulphur and are able to destroy hydroperoxides without the formation of free radicals. The inorganic phosphites and sulfites are able to react with the hydroperoxides to

form alcohols, phosphates, and sulfates. These types of compounds are generally termed as hydroperoxide decomposing anti-oxidants, and include compounds such as zinc dibutyldithiocarbamate and hindered piperdine derivatives as well [Kelen 1983].

Carbon black is an anti-oxidant, with its effectiveness inversely proportional to particle size and directly proportional to bound oxygen and sulfur content [Winslow 1979]. The sulfurized blacks tend to form sulfur dioxide which can act as a hydroperoxide decomposer.

2.7.4 Ozone Cracking Prevention

Ozone acts to decompose rubbers by cleaving π bonds and forming aldehyde, ketone, or carboxylic acid groups where the chain was broken. EPR rubbers used in nuclear control cables have a fairly high resistance to attack from ozone, but additives are often included in the insulation formulations to ensure even further protection. Rubbers which are particularly vulnerable to ozone are styrene-butadiene rubber and polyisoprene, the effects of which are manifest as cracks or, in old rubber boots, leaks.

Paraffin wax is often used in conjunction with an alkylated p-phenylenediamine derivative to protect against ozone degradation. The wax protects the rubber by diffusing to the surface forming a protective coating and the diamine reacts with ozone through its π bonds at the surface adding a further protective coat [Winslow 1979].

2.7.5 UV Stabilization

Ultraviolet radiation acts to degrade polymers by creating radicals and causing chain scission. Protection against UV radiation can often be accomplished by coating a polymer with a component which will reflect sunlight. Pigments such as carbon black, zinc oxide, and colored dyes such as phthalocyanine blues and greens are quite effective at limiting the penetration of UV radiation into the

insulation. Other UV stabilizers act to dissipate the energy of UV radiation by being sent into an excited state. The molecule then loses its excess energy by vibrational relaxation and emission [Kelen 1983]. 2-Hydroxybenzophenone, 2-hydroxyphenylbenzotriazole and their derivatives are examples of this type of UV absorbers, the benzophenones being more effective in polyolefin applications.

2.7.6 Formulation of a Control Cable

The cables used in this study are primarily the lower voltage rated cables typically used for control and safety equipment in nuclear power plants. A typical formulation is given for this type of insulation in Table 2.2. The insulating dielectric material is ethylene propylene diene rubber (EPDM) and low density polyethylene. Dechlorane Plus is a halogenated flame retardant compound which acts as a chain transfer agent to scavenge free radicals produced in the early stages of combustion. Antimony oxide is another form of flame retardant which binds to the dechlorane at elevated temperatures, thus increasing the halogenated flame retardant's lifetime within the insulation at the higher temperatures. It also acts as a char producer during combustion as well. Calcined clay is a typical filler which acts to fill voids and retard tree formation as well as enhance the mechanical properties. Zinc oxide is a additive which acts as a photostabilizer by preventing the penetration of UV radiation into the cable. The paraffin wax is another filler which is typically used for protection against ozone and surface oxidation. Lead oxide is most likely a heat stabilizer. Carbon black serves as a multi-purpose additive in the form of an antioxidant, filler, and UV stabilizer as well as a mild flame retardant. Agerite Resin D is a patented anti-oxidant. Vinyl silane is a silicon containing compound which is presumably a surface treatment for the clay to make it bond to the polymer. Luperox is a peroxide crosslinking agent which will be depleted after curing.

Table 2.2: Nuclear Control Cable Formulation [Markezich 1989]

FORMULATION	PARTS
EPDM	90
Low Density Polyethylene	20
Dechlorane Plus	33
Antimony Oxide	12
Calcinated Clay	60
Zinc Oxide	5
Paraffin Wax	5
Lead Oxide	5
Agerite Resin D	2
Vinyl Silane A-172	1
Carbon Black	2
Luperox 500-R	3

3. EXPERIMENTAL PROCEDURES

3.1. Materials

Crosslinked low-density polyethylene was prepared in the laboratory by compression molding using Union Carbide grade HFDE 4201 low density polyethylene pellets premixed with two percent dicumylperoxide for crosslinking.

The ethylene propylene copolymer (EPR) and the ethylene propylene terpolymer (EPDM) were both kindly supplied by Dr. D.J. Lohse at Exxon Research and Engineering, Annandale, New Jersey. The EPR is Exxon Vistalon 707 (CAS # 9010-79-1) with a Mooney viscosity of 22 (Mw of 150,000 to 200,000). The EPR contains 66 wt% ethylene. The ethylene propylene terpolymer is Exxon MDV 8731 (CAS # 25038-36-2) produced by polymerization of 3 wt% ethylidene norborene with ethylene and propylene. Its ethylene content is 74 wt% and its Mooney viscosity is 24. Both EPDM and EPR were mixed with DCP and crosslinked in the laboratory.

The cables which have been investigated consist of the lower voltage rated cables typical of those used in the nuclear industry for control and safety equipment. The cables are classified in Table 3.1. The cables were given a provisional designation according to the order of investigation and later indentified in a more formal manner according to manufacturer. The formal identification will be used throughout the remainder of this work.

3.2. Preparation of Crosslinked Polymers

As mentioned earlier, the LDPE was supplied premixed with DCP for croslinking purposes. However, the EPR and EPDM had to be mixed in the laboratory with the crosslinking agent. This relatively simple procedure is outlined in the following sections.

Table 3.1: Classification of the Supplied Nuclear Control Cables.

Cable Identification Number	Provisional Number	Manufacturer	Description
A1	(#1)	Eaton Corp. (Samuel Moore)	Dekoron Polyset P/N 015800-n
A2	(#6)	Eaton Corp. (Samuel Moore)	Dekoron 2/C 600V 0815182-8
A3	(#9)	Eaton Corp. (Samuel Moore)	Dekoron 2/CD 600V 015601-1
B1	(#2)	Rockbestos	3/C 600V Firewall III Type TC
C1	(#3)	BIW	600V 2/C EPR/HYP 021866
C2	(#11)	BIW	Tefzel
D1	(#4)	Anaconda	Flame Guard 1KV
D2	(#5)	Anaconda	M Durasheath EP 600V
E1	(#7)	Okonite	PLT Okolon C T use 600V
E2	(#8)	Okonite	EPR Okoprene 2000V
E3	(#10)	Okonite	FMR

3.2.1 Powdering of EPR and EPDM

Both the EPR and EPDM were first transformed into powder to better facilitate homogenous mixing of the peroxide. This was done by dissolving about 5 grams of polymer into 100 ml of hot xylene (110 oC). Once dissolution was complete the solution was added dropwise into a beaker containing roughly 800 ml of cold methanol (cooled with solid CO_2). This procedure resulted in precipitation of the polymer in the form of fine powder which was then washed with cold methanol under suction and dried in a vacuum oven at a temperature of 40 oC for 48 hours to evaporate any residual xylene or methanol.

3.2.2 Addition of Dicumyl Peroxide

In order to mix the polymer and peroxide, 2 wt% DCP (0.1 g) was dissolved in 50 ml of methanol at 35 oC after which 5 grams of polymer powder was added to form a slurry. This slurry was stirred with a magnetic stirrer until most of the solvent had evaporated. The wet powder was then placed in the vacuum oven and dried for 48 hours to remove the solvent.

3.2.3 Crosslinking Procedure

The melting and curing process for the EPR, EPDM, and XLPE was performed with a Wabash Hydraulic Press Model 12-12-2TMB capable of exerting 24,000 tons of force upon a four inch ram with temperature control of the platens. The crosslinking procedure was identical for all materials.

The polymer was first melted in the press at a temperature of 135 ^{o}C for eight to ten minutes, then 10 tons of pressure was applied for about four minutes. The polymer was then removed and allowed to cool while the press was heated to the curing temperature of 200

°C. When the temperature of the press had stabilized the polymer was placed back in the press and cured for three to five minutes at full pressure. The crosslinked polymer was then cooled to room temperature by cold water which is able to circulate through the heating platens.

3.2.4 Extraction

The boiling xylene method was used to determine the amount of extractable material present in the crosslinked polymers. This method consists of placing pre-weighed rectangular samples (10 x 30 x 3 mm) of the crosslinked polymer into small "cages", which prevent the samples from tearing apart, and boiling them for 72 hours in xylene. The samples were then placed into a jar of xylene and held at a temperature of 110 oC for 24 hours after which the samples were placed into a vacuum oven and dried for 72 hours. The percent extractables were determined by subtracting the weight obtained for the dried gel from the weight of the original sample and then dividing by the weight of the original sample.

3.3. Differential Scanning Calorimetry

A DSC is basically a device which is used to study the thermal behavior of materials over a programmed temperature range and rate of heating or cooling. DSCs contain an analysis chamber where a nitrogen environment is provided. Within the chamber are two holders with separate heaters to control the temperature. The environment of the holders can be changed to any desired purge gas such as air or oxygen, but nitrogen is typically used for melting and crystallization studies. One of the holders is for the sample and the other for the reference. Samples are prepared by pressing them into aluminum pans, so in order to account for thermal effects upon the aluminum, the reference holder contains an empty pan and lid.

DSCs measure the power supplied to the heater for the sample

holder relative to that of the reference holder as a function of temperature or time in order to keep the sample and reference at the same temperature. The power required is usually measured in mW and recorded as the ordinate while the temperature or time is recorded as the abscissa.

If one places two empty pans of the same weight in each holder and heats them up, theoretically a straight horizontal line will be obtained because the power supplied to the heaters to keep the sample the same as the reference will be the same. Let us suppose we place a crystalline material, for example ice, in the sample holder and program the DSC to heat from -10 ^{o}C to 10 ^{o}C. From -10 ^{o}C to about -.5 ^{o}C the heat supplied to the sample holder will be used to raise the temperature of the ice, so the plot will appear as a straight line with perhaps a slight slope due to the difference in weight and the heat capacity of the ice. However, around 0 ^{o}C the heat supplied to the sample will no longer raise the temperature of the ice, but will be used to melt the ice. Therefore, the power required by the sample holder heater to keep the sample the same as the reference will be greatly increased and a sharp peak will be obtained until melting is finished. After melting is complete, the heat will once again be used to raise the temperature of the sample, which is now water.

The area under the peak produced is called the heat of fusion and is simply the amount of heat required to melt the given mass of the material. This process is said to be endothermic since it requires heat and the DSC plot generated is often termed an endotherm.

Upon cooling form 10 ^{o}C to -10 ^{o}C the reverse occurs since crystallization liberates heat and less power is required to keep the sample the same temperature as the reference. Therefore a peak will be obtained pointing in the opposite direction with negative area. This process is said to be exothermic and the corresponding DSC plot is often referred to as an endotherm.

The DSC which has been used in this research is a Perkin Elmer DSC 7 attached to a Perkin Elmer Professional Computer PE 7500

with a TAC-7 interface between the computer and the DSC. A Perkin Elmer Graphic Plotter 2 was used to plot the data.

Calibration was performed using the N.B.S. standard Indium which has a melting point of 156.56 °C and a heat of fusion of 28.45 J/g.

3.3.1 Generation of Subtraction Curve

The Perkin Elmer DSC-7, as well as many of the other newer DSCs manufactured by other companies, comes equipped with software which allows one to manipulate data in many ways. There is a prompt (optimize data) for the optimization of data which allows one to flatten the baseline if it is sloped or to rescale the plot in order to make it appear bigger or smaller. One can also change the abscissa from temperature to time if so desired. Another window, labelled select calculations, enables one to calculate the heat of fusion, temperature of onset, and the peak temperature for a particular thermal transition. It will also calculate the heat capacity and glass transition temperature if applicable. Contained within another window (change curvetype) is software which will smooth a rough or noisy curve. Within this same prompt is software which also calculates the derivative and allows one to subtract two curves from one another.

Each annealed sample was heated in the DSC from -20 °C to 150 °C at a rate of 10 °C/min and held in the melt for five minutes. The sample was then cooled at a rate of 40 °C/min to -20 °C and held at this temperature for five minutes, and then the sample was reheated to 150 °C with a heating rate of 10 °C/min. This procedure generates two endotherms and one exotherm. The first endotherm will be referred to as the annealed endotherm and the second endotherm will always be designated as the quenched endotherm. The exotherm is not used for any analysis.

In order to eliminate any noise in the subtraction curve, DSC endotherms were first smoothed before subtraction. The quenched

endotherm was always subtracted from the annealed endotherm.

The derivative of the subtraction curve was calculated and used to better estimate the peak locations on the subtraction curve. The temperature corresponding to the ordinate of zero indicates a peak position. Data was extracted from the subtraction and derivative curves by using the select calculations window which allows one to follow along the curve with a cursor and displays the position.

3.4. Sample Preparation for Annealing Studies

Samples were prepared by cutting cross-sections of the insulating materials. Sample weights were kept fairly constant for a particular cable sample and generally ranged from five to ten milligrams, depending upon the diameter of the insulation.

Endotherms labelled "History Erased" were produced by heating a sample of the insulation up to 150 ^{o}C in the DSC and holding it there for five minutes. The sample was then cooled to -20 ^{o}C at a cooling rate of 40 ^{o}C/min. The sample was then placed directly in an oil bath. This procedure assures that any thermal history due to manufacture or subsequent annealing will not be present in the insulation.

Samples labelled as "Original" were placed directly into an oil bath such that they contained all the previous thermal history as well as that administered in the laboratory. All samples were annealed only once and then discarded to reduce the chance of oxidation effecting the results.

Each sample was cut, weighed on a Mettler M3 capable of percision to one thousandth of a milligram, and then crimped into a Perkin Elmer # 0219-0041 aluminum sample pan. The pan was then covered in Saran wrap and wrapped tightly in aluminum foil to prevent water or oil exposure during annealing.

Haake L D8, Haake R N3 refrigerated bath, and a Neslab RTE-8 refrigerated circulating bath were used for the annealing experiments. Temperature was calibrated with a Omega Digital

Thermocouple Model 211 and a Fisher Scientific Model 14-985-5B thermometer as well as with the digital temperature reading on the Haake baths. All temperatures obtained from the different measuring devices corresponded within 0.3 ^{o}C of each other. The thermocouple was also stuffed into a DSC pan, wrapped in Saran and aluminum foil and then placed into a test tube to best duplicate the actual condition of the sample. There was no difference between this reading and that given on the bath temperature display.

4. RESULTS

4.1. Effects of Annealing

Often many of the bulk produced semi-crystalline polymers, such as LDPE, EPR, and EPDM used in cable insulation, contain fairly broad molecular weight distributions as well as fairly high branch contents. The result of this is the formation of lamellae with different thicknesses. The thicker lamellae tend to be formed from material which has the greatest distance along the main chain between branch points and the thinner lamellae are formed from lower molecular weight material and material which is high in branch content. Often during processing the material may be cooled at fairly high rates as well, which limits the ability of a polymer, especially one high in branch content, to crystallize to the extent which is possible under slow cooling conditions. This results in generally thinner and more imperfect lamellae.

Annealing such a system will allow some of the material to reach its full "crystalline potential". Initially when the system is subjected to the annealing temperature the thinner and imperfect lamellae will melt while the thicker material will remain unaffected. Over a period of time some of this material which melted is able to recrystallize in the form of thicker and more perfect lamellae with higher melting points than they had previously. Thus some of the material may obtain the most perfect and thickest lamellae which are possible for its molecular weight and branch content. Extended annealing time also can affect the higher melting crystals which did not melt initially upon annealing. These lamellae may tend to become more thermodynamically stable by reducing their surface free energies through thickening mechanisms. These crystals will show a slight increase in melting temperature as well, but the effect is not as pronounced as for the lamellae which totally melt and recrystallize.

In practice LDPE, EPR, and EPDM are often crosslinked creating

essentially what can be considered as a two phase system. The gel phase, which consists of the cross-linked network, and the soluble phase, which is composed of material which was not incorporated into the gel network. This basically limits the molecular weight distribution because the gel phase can be considered as one giant molecule and that of the soluble phase is generally narrow. However, the molecular weight between crosslinks and branch points within the gel phase will create a lamellar thickness distribution similar in nature to that of an uncrosslinked system such that the same basic principles of annealing discussed for a noncrosslinked system will hold.

The melting and recrystallization is manifest through thermal analysis in the form of a shoulder slightly above the annealing temperature on the endotherm if the annealing temperature is at least 15 °C below the major melting peak. This is shown in Figure 4.1 (a) for a sample of XLPE annealed at 70 °C for approximately twelve hours. The shoulder represents the melting point of the lamellae which were able to recrystallize at the annealing temperature. The DSC endotherm of the unannealed sample is shown for comparison in Figure 4.1 (b). One can observe that there is no shoulder present. By subtracting the unannealed endotherm from the endotherm of the annealed sample a subtraction curve is generated from which information can be obtained about the time and temperature of the heat treatment.

4.2. General Features of the Subtraction Curve

The curve generated from the subtraction of the quenched endotherm from the annealed endotherm of a particular sample contains several points which are related to the thermal history of the polymer. The basic features of the subtraction curve are shown in Figure 4.2 for a sample of cross-linked low density polyethylene (XLPE) annealed at 45 °C for approximately 474 hours. Both the annealed and quenched endotherms are shown as well as the curve

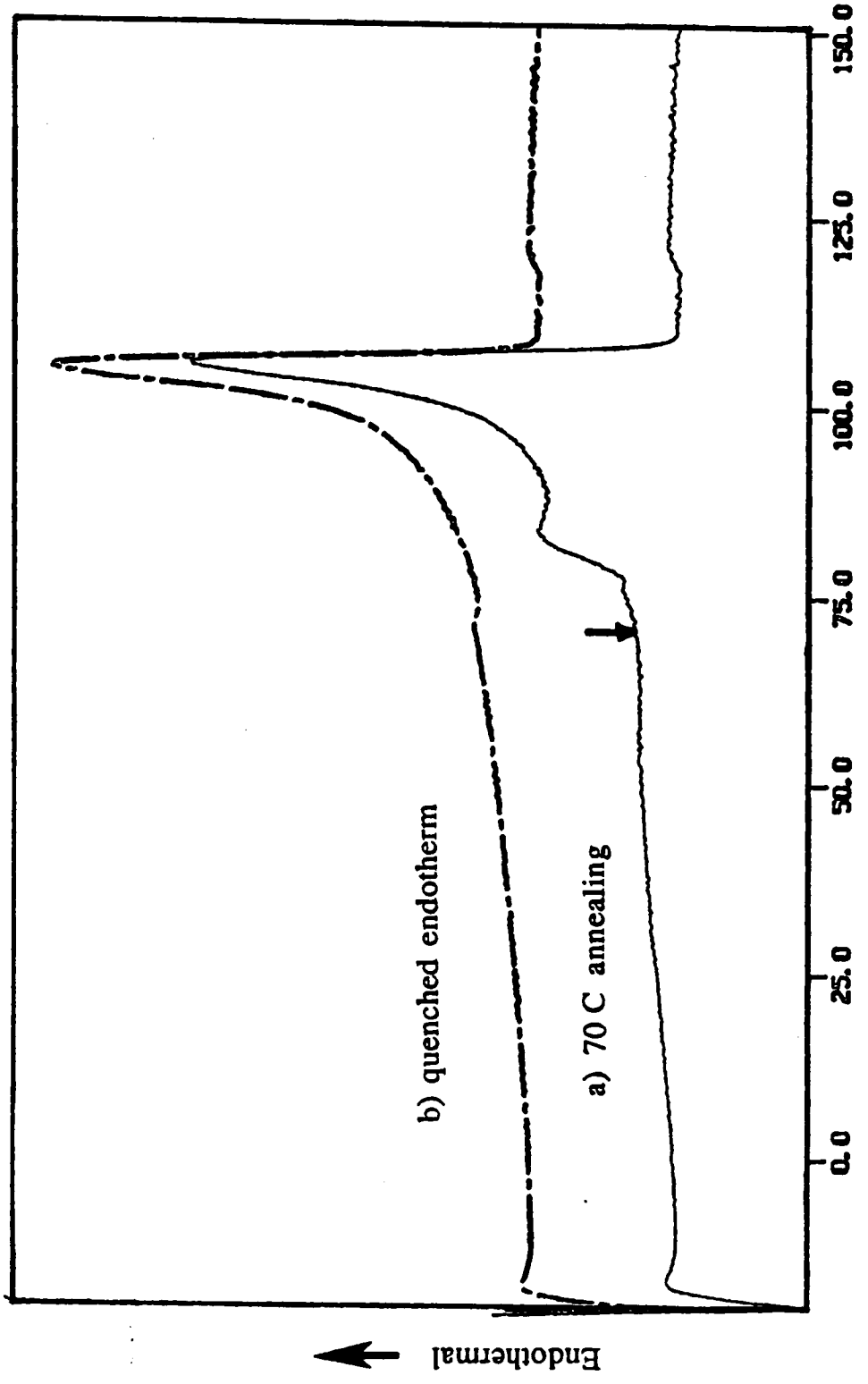


Figure 4.1: Manifestation of annealing upon XLPE: a) 70 C annealing; b) quenched endotherm.

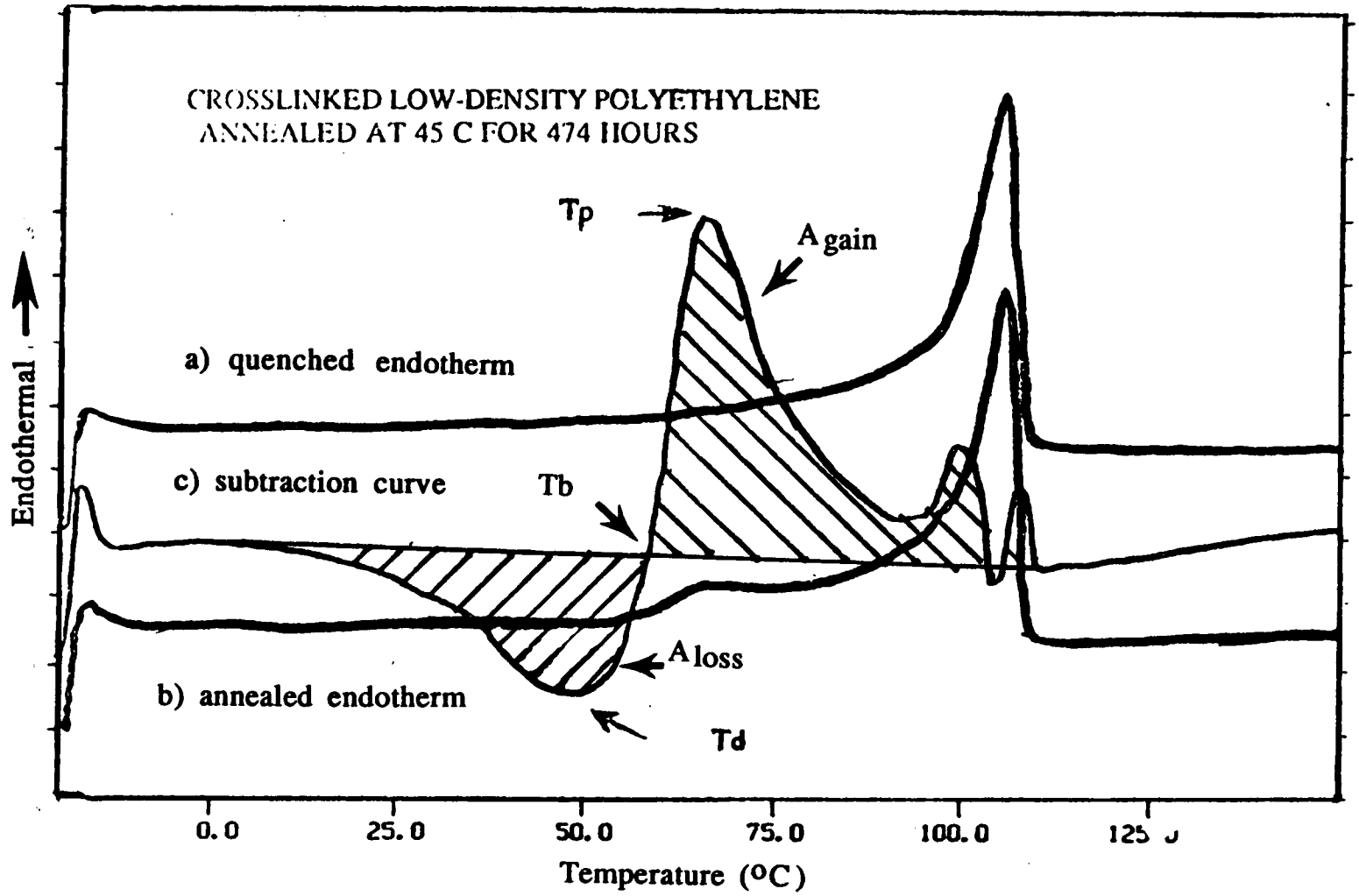


Figure 4.2: General features of the subtraction curve: a) quenched endotherm; b) annealed endotherm; c) subtraction curve.

obtained from the subtraction technique.

There are two points upon the subtraction curve which show a time dependence for a particular annealing temperature, the position of the gain peak and the point at which the baseline intersects the start of the gain peak. These two points are labelled as Tp (the peak temperature) and Tb (the baseline temperature), respectively. Both of these temperatures increase with annealing time. However, if a good baseline is not obtained, which is often the case, Tb can be a matter of guesswork. The subtraction curve baseline is usually worse for the case of insulation or polymer systems containing material with low crystallinities and melting points. These materials tend to anneal extensively at room temperature which generally causes massive distortions in the baseline at and below about 30 °C. Figure 4.3 shows some examples of poor baselines of the subtraction curves for several materials. Tp on the other hand is always discernable regardless of the condition of the baseline and seems to show the more consistent behavior. The position of the loss peak shows very little time dependence for all the materials examined and for all practical purposes can be considered a function of the annealing temperature alone. This point is labelled as Td (the depression temperature), and is generally within 5 °C of the actual annealing temperature. The area of both the loss and gain peaks show initial increases with annealing time for about 24 hours after which their values show no particular trend. The values of Tp, Tb, Td, A_{loss} (A1), and A_{gain} (A2) are shown for 45 °C annealing of XLPE in Table 4.1.

Tp, Tb, and Td were determined from the derivative of the subtraction curve. Since these points correspond to peak positions, the point corresponding to the ordinate value of zero on the derivative curve relative to the peak of interest upon the subtraction curve indicates the peak's location. An example of this is shown in Figure 4.4 for a subtraction curve corresponding to a sample of cross-linked ethylene propylene copolymer (XEPR) annealed at 60 °C for 13.1 hours.

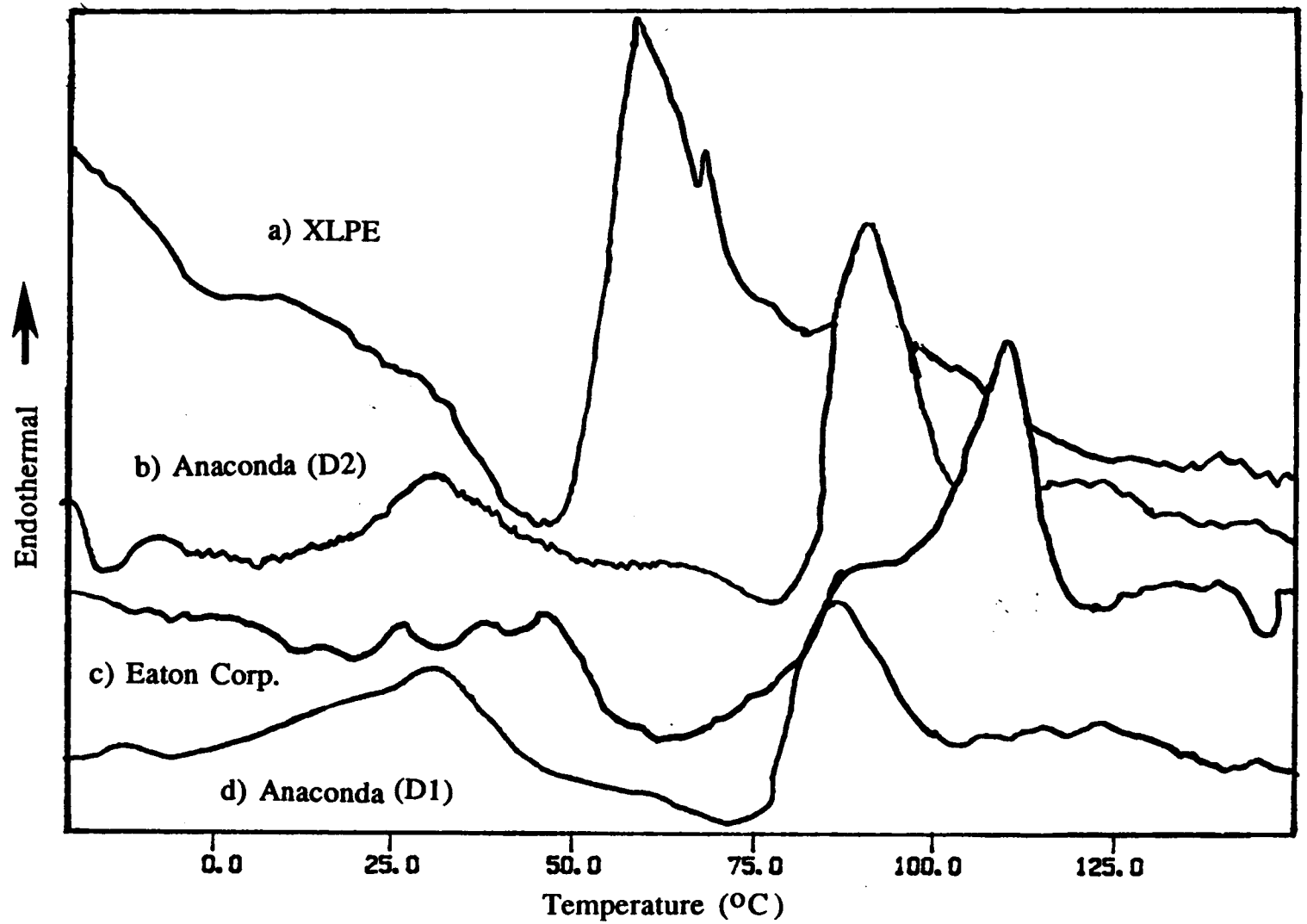


Figure 4.3: Distortions in the baseline of the subtraction curve: a) XLPE; b) Anaconda insulation (D2); c) Eaton Corp. insulation (A3); d) Anaconda insulation (D1).

Table 4.1: Data from 45 °C annealing of XLPE.

Time (hrs)	Tb (C)	Tp (C)	Td (C)	A1 (-mJ)	A2 (mJ)
3	48.7	56.3	43.6	1.01	3.51
11.2	52.0	58.9	44.8	3.69	9.82
25	52.6	59.6	43.6	6.79	9.42
48.6	53.8	61.2	44.8	7.63	8.56
73.2	54.1	62.7	44.5	7.89	12.76
145.1	53.7	62.8	44.8	6.65	12.90
162.1	55.9	63.2	46.9	14.04	20.56
210.2	55.8	63.6	44.8	10.74	15.78
255.3	56.3	64.0	46.2	13.98	30.75
474.3	57.1	65.3	47.5	14.11	18.67
546.2	56.2	65.3	46.3	9.72	19.23
1706	56.8	67.2	47.5	8.89	25.12
1713	58.4	67.1	49.7	16.26	16.93

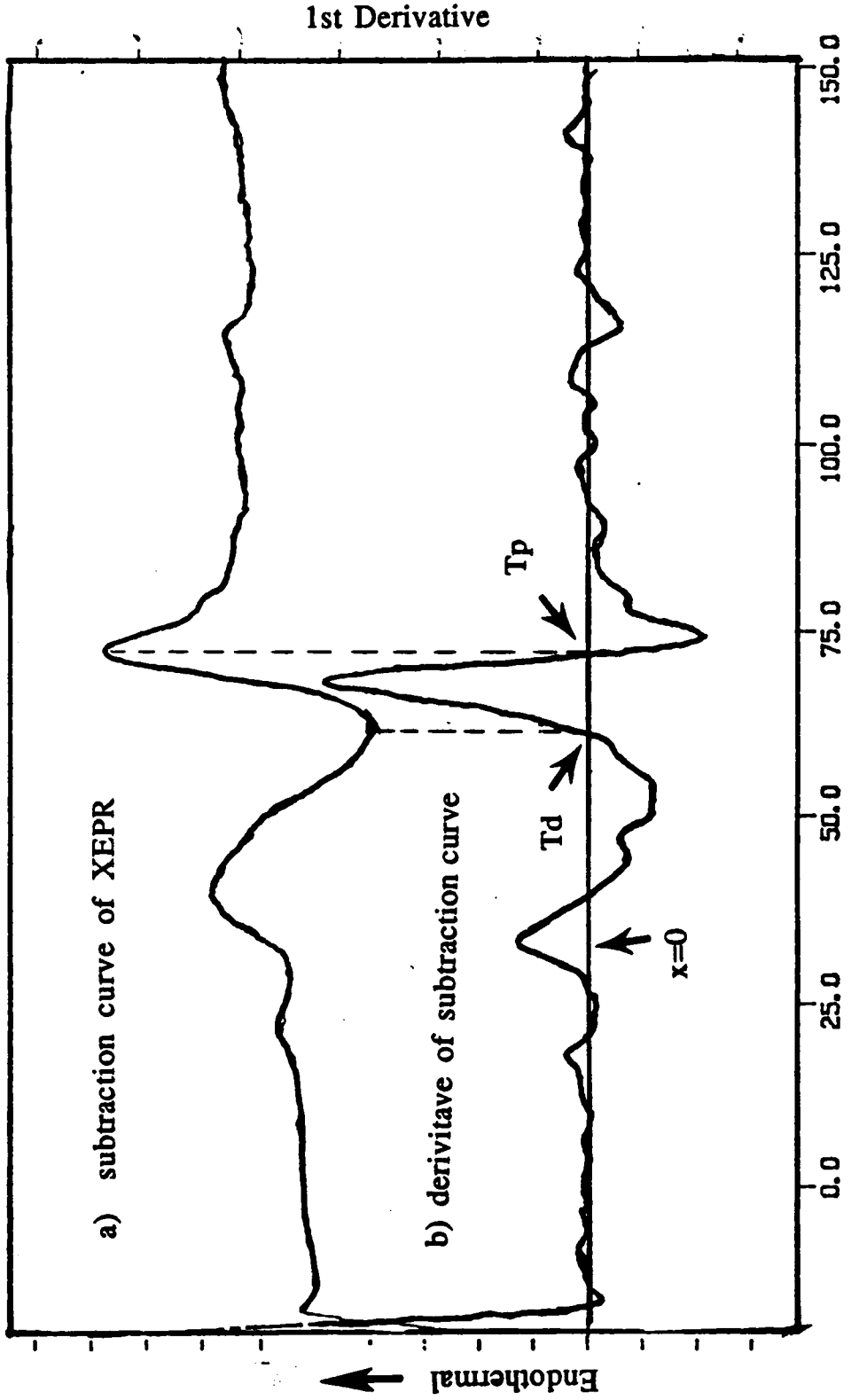


Figure 4.4: Determination of peak positions: a) subtraction curve of XEPR annealed at 60 C for 12 hours; b) derivative of subtraction curve.

4.3. Annealing Studies of Reference Materials

In order to gain a basic understanding of the manifestation of the kinetics of annealing through the subtraction technique, the annealing behavior of five "reference" materials was studied at various temperatures. These standards are XLPE, EPR, EPDM, XEPR, and XEPDM.

4.3.1 Crosslinked Low Density Polyethylene (XLPE)

The effects of annealing are manifest on a DSC endotherm in the form of a shoulder slightly above the annealing temperature. This shoulder is produced by what is thought to be the melting of thinner and imperfect lamellae and the subsequent recrystallization of the material in the form of thicker and more perfect lamellae. Hence the shoulder represents the melting point of the new crystals produced by annealing. Figure 4.5 shows the effect of annealing upon XLPE at various temperatures ranging from room temperature to 70 °C. The formation of the shoulder can be observed to occur with annealing at 20 °C and becomes more pronounced, shifting to higher temperatures as the annealing temperature is increased.

As the annealing time is increased the shoulder also shifts to higher temperatures, but the effect is generally slow and for annealing times above approximately five days the shift is generally well under 0.5 °C per 100 hours of annealing. A shift of this magnitude is not easily detected from the DSC endotherm. Also one can not distinguish from the DSC endotherm the difference between a sample which has been annealed at a lower temperature for a long period of time and a sample which has been annealed at a higher temperature for a shorter period of time. The advantage of the subtraction technique is that it enables one to distinguish between short and long term annealing.

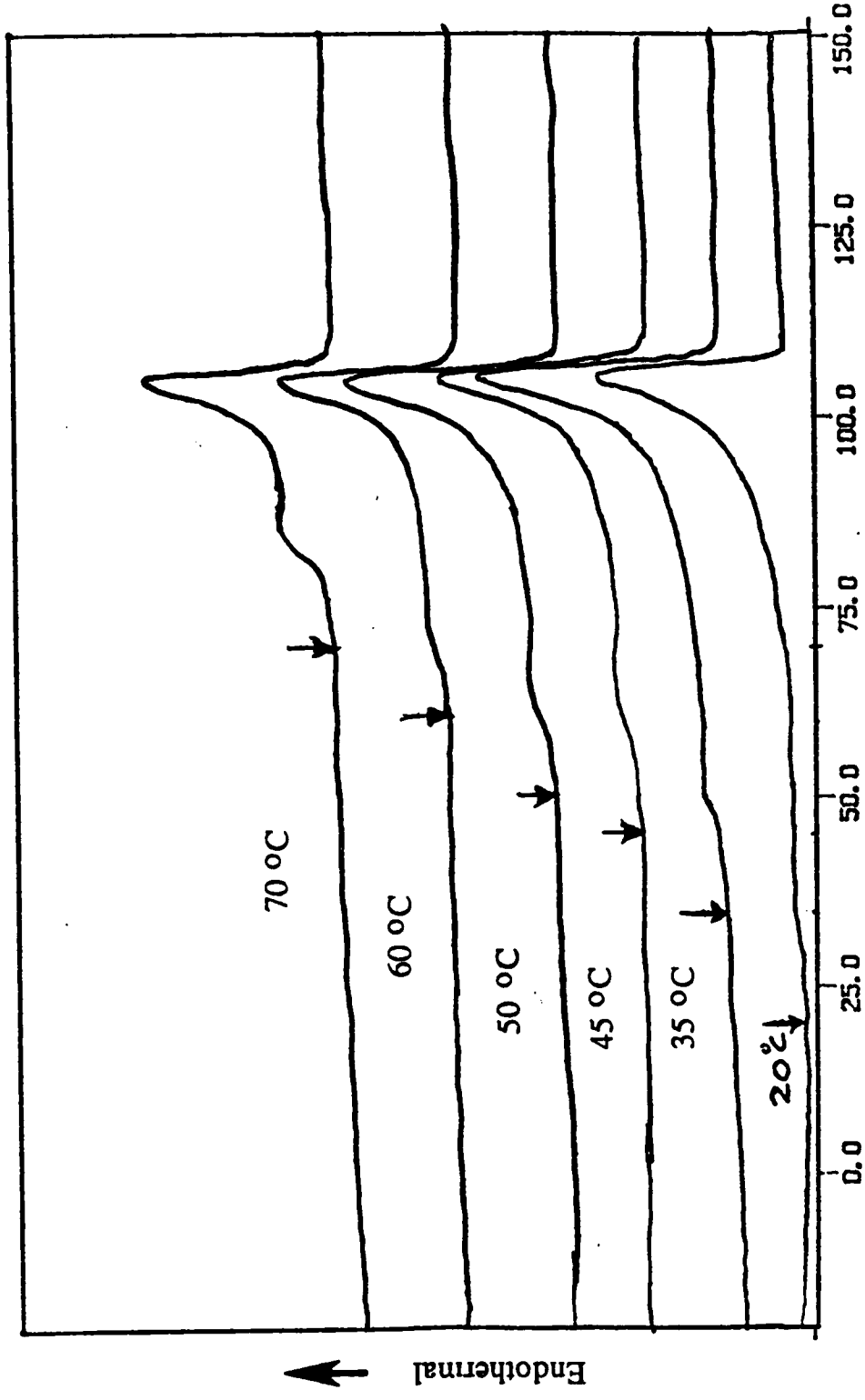


Figure 4.5: Effects of annealing at various temperatures upon the endotherm of XLPE.

The annealing behavior of XLPE was followed in detail for annealing temperatures of 35, 45, 60, and 70 °C at various annealing times ranging from one to over a 1000 hours. The data obtained for XLPE is shown in Table 4.2. For each annealing temperature the value of Td is within approximately 3 °C of the actual annealing temperature. The position of the gain peak, Tp, and the position where the baseline crosses the gain peak, Tb, both increase with annealing time. However, one can observe that the values for Tp show the more consistent behavior. Therefore, the position of the gain peak was used to study the kinetics of annealing. A plot of Tp versus annealing time is shown in Figure 4.6. One can notice that the curves are shifted upward with increasing annealing temperature. The position of the gain peak shows a logarithmic relation with annealing time for each of the annealing temperatures.

4.3.2 Ethylene Propylene Copolymer (EPR)

Annealing of XLPE at temperatures below 70 °C resulted in the formation of a shoulder on its DSC endotherm. For the case of EPR the situation is quite different. Figure 4.7 shows the effect of 50, 60, and 70 °C annealing upon the DSC endotherm of EPR. One can observe that annealing at these temperatures induces crystallization on a fairly large scale. The quenched endotherm shows very little crystallinity with the major melting point occurring at approximately 45 °C. Thus annealing essentially resulted in melting and recrystallization of most of the material. Another feature which is of interest is the "hump" located above 25 °C on each of the endotherms. One can observe that this hump increases in size as the annealing temperature is raised. Its presence is most likely due to the crystallization upon cooling from the annealing temperature of the material which was unable to recrystallize during annealing. As the annealing temperature is increased, more of the material is unable to recrystallize during annealing and therefore crystallizes

Table 4.2: Annealing data for XLPE.

	35 °C Annealing			45 °C Annealing			60 °C Annealing			70 °C Annealing		
Time	Tb	Tp	Td	Tb	Tp	Td	Tb	Tp	Td	Tb	Tp	Td
3	37.3	48.0	38.4	48.7	56.3	43.6	64.0	70.9	59.7	75.4	79.3	70.1
6							67.0	71.3	58.5			
12	37.0	51.35	38.0	52.0	58.9	44.8	67.4	72.2	59.8	77.3	81.8	71.2
24	38.6	51.75	37.9	52.6	59.6	43.6	67.6	73.4	60.2	77.0	81.3	70.1
48	40.4	52.35	37.0	53.8	61.2	44.8				77.8	83.0	69.6
72	40.9	53.35	35.5	54.1	62.7	44.5				78.4	83.9	71.6
100	44.8	53.6	36.1	55.3	61.9	46.3				78.1	84.0	71.9
150	45.4	53.9	36.4	53.7	63.2	46.9	69.5	76.1	60.1			
200							71.6	78.5	62.0			
250	40.7	53.95	37.0	56.3	64.0	46.2				79.0	85.1	73.0
360							71.1	78.7	61.3	80.4	85.7	73.7
400							71.4	78.7	63.8			
450				57.1	65.3	47.5	71.5	78.6	62.2			
550				56.2	65.3	46.3				80.5	85.3	74.0
1000	47.8	55.3	36.7	56.8	67.2	47.5						

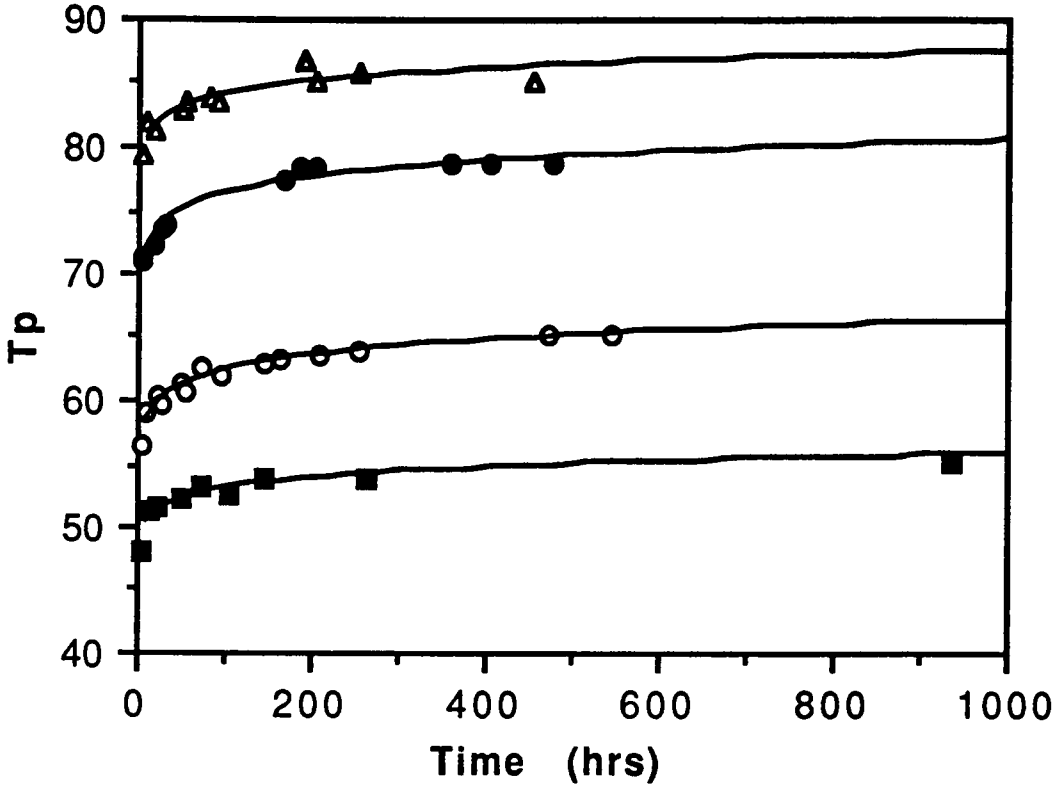


Figure 4.6: Tp versus time for XLPE. ■ 35 C annealing;
○ 45 C annealing; ● 60 C annealing;
▲ 70 C annealing.

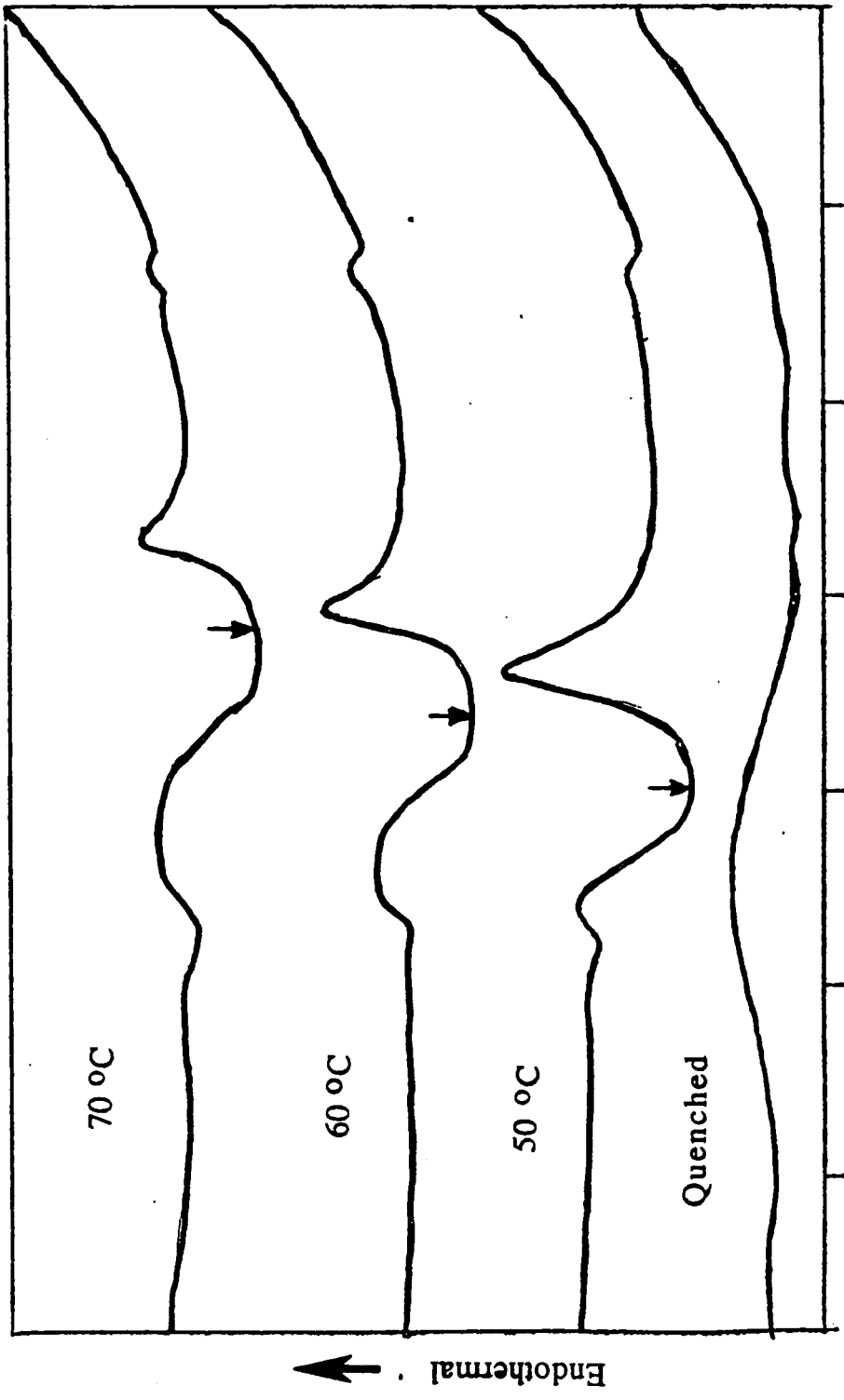


Figure 4.7: Annealing effects upon the endotherms of EPR.

upon cooling which results in the observed increase in the size of the hump with increasing annealing temperature. This lower melting material also appears to anneal at room temperature as shown by the shoulder present at 25 °C.

Figure 4.8 shows a typical subtraction curve for EPR. The same basic features are evident. The position of the loss peak (Td) indicates the annealing temperature and the position of the gain peak (Tp) can be followed as a function of logarithmic time. Evidence of room temperature annealing is manifest in the form of second less-pronounced loss and gain peaks around 30 °C. While the samples were taken directly from the annealing bath and placed into either the DSC or a refrigerator, the transfer time was sufficiently long for discernable effects to be generated.

The annealing behavior of EPR was studied at temperatures of 50, 60, and 70 °C. The annealing data are shown in Table 4.3. One can observe that the values of Td remain fairly constant with time and are consistently about 4 °C below the actual annealing temperatures for 60 and 70 °C annealing. For 50 °C annealing the values for Td are only about one degree below the actual annealing temperature. The values of Tp show the expected increase with annealing time. The values for Tb also show a general increase with annealing time, but the data is less consistent. The shift in the gain peak is plotted against annealing time for the three temperatures in Figure 4.9.

One can observe that the curves generated are similar to those of XLPE. They seem to show a logarithmic time dependence and are shifted upward with increasing annealing temperature.

4.3.3 Ethylene Propylene Terpolymer (EPDM)

EPDM shows remarkably similar behavior to that of EPR. The endotherms for samples annealed for 96 hours at 50, 60, and 70 °C are shown in Figure 4.10. Annealing at each of the temperatures induces crystallization to occur and increasing the annealing temperature results in an increase in the peak position. As observed

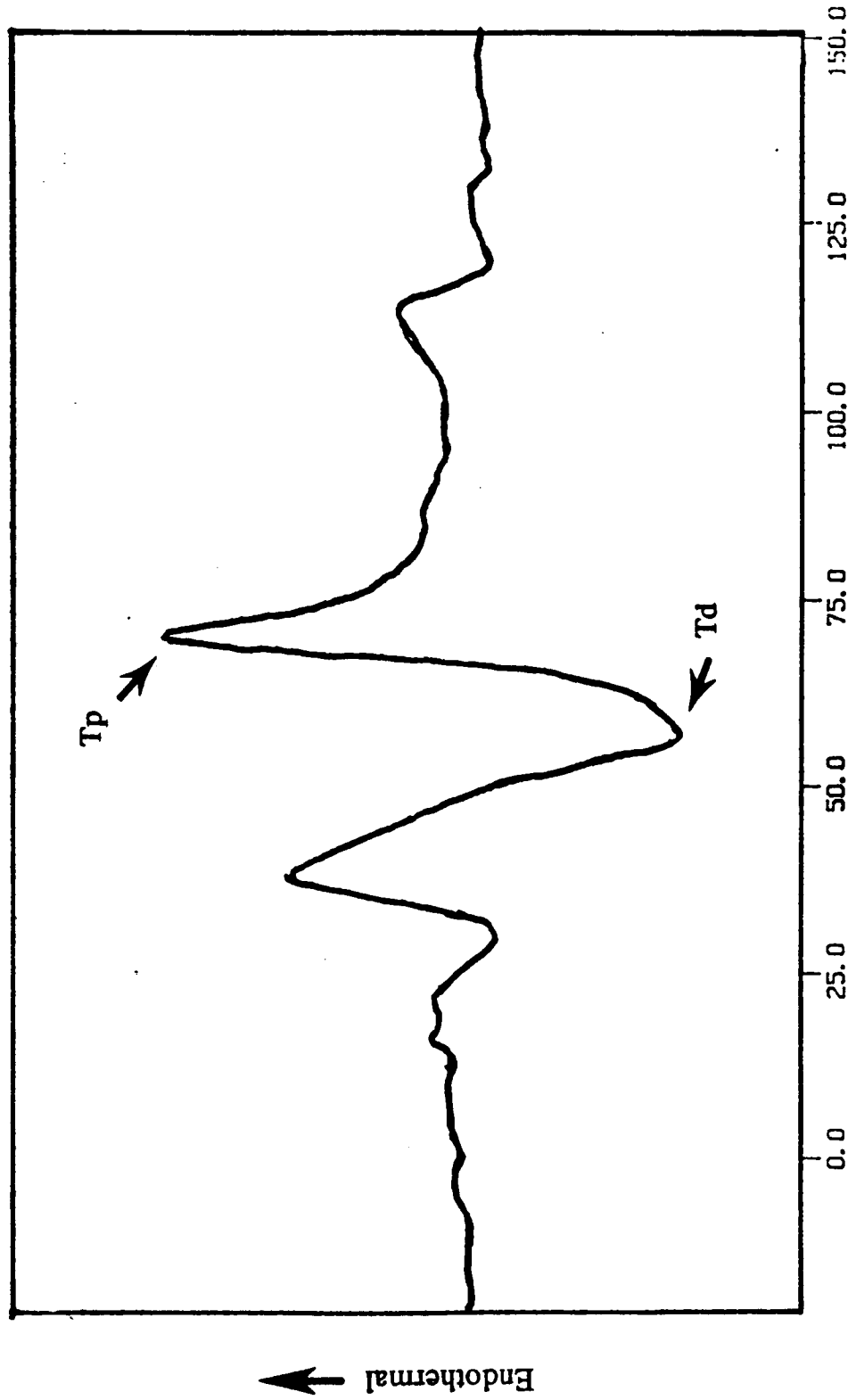


Figure 4.8: Typical subtraction curve of EPR annealed for 12 hours at 60 C.

Table 4.3: Annealing data for EPR.

	50 °C annealing			60 °C annealing			70 °C annealing		
Time	Td	Tp	Tb	Td	Tp	Tb	Td	Tp	Tb
3	49.5	61.45	57.1	58.0	69.75	65.8	66.4	78.45	75.5
6	49.0	62.15	57.4	57.2	70.15	66.4	66.2	78.85	75.7
12	49.5	63.65	57.0	57.2	70.50	66.8	67.0	80.25	76.8
24	50.2	64.35	59.2	58.5	72.05	68.5	65.6	80.35	76.9
96	48.7	64.95	60.5	57.8	73.45	69.4	65.6	82.40	78.4
236	48.8	66.20	60.5	57.0	73.85	69.7	65.5	83.20	79.3
332	48.8	66.30	60.9	55.4	73.90	69.8	64.1	83.25	77.6
433	51.5	66.90	61.9	56.2	74.45	70.3	64.9	83.75	78.1
790	50.2	67.50	62.0	56.4	75.18	71.0	66.0	83.87	

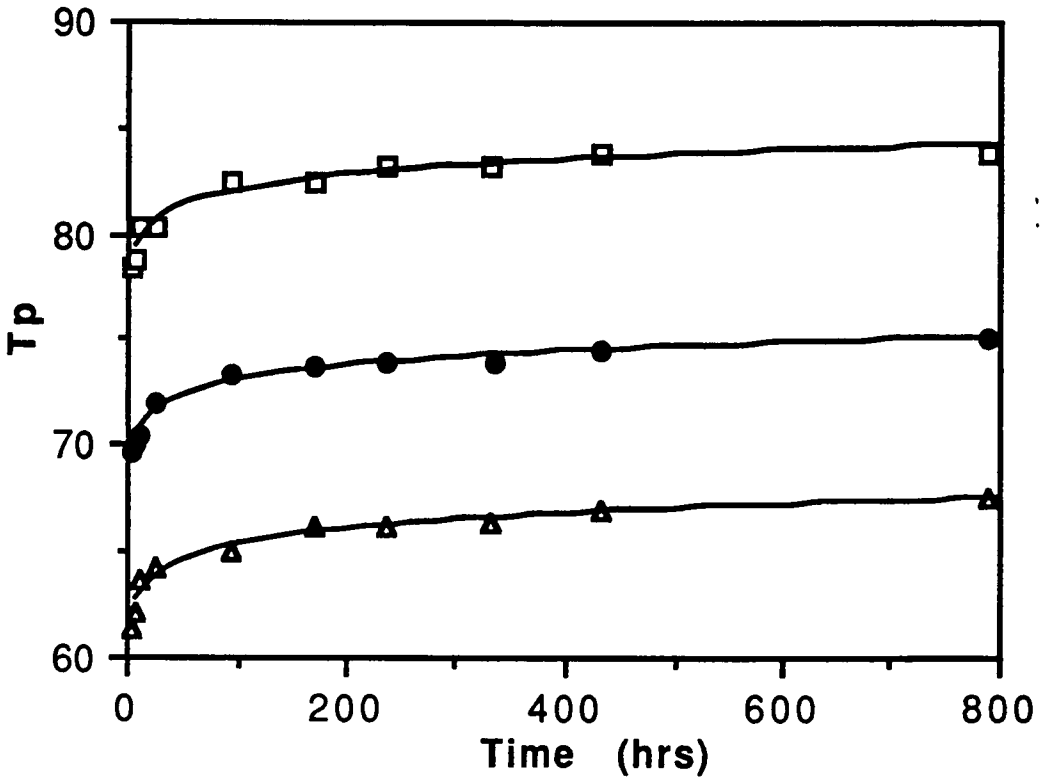


Figure 4.9: Tp versus time for EPR. ▲ 50 C annealing; ● 60 C annealing; □ 70 C annealing.

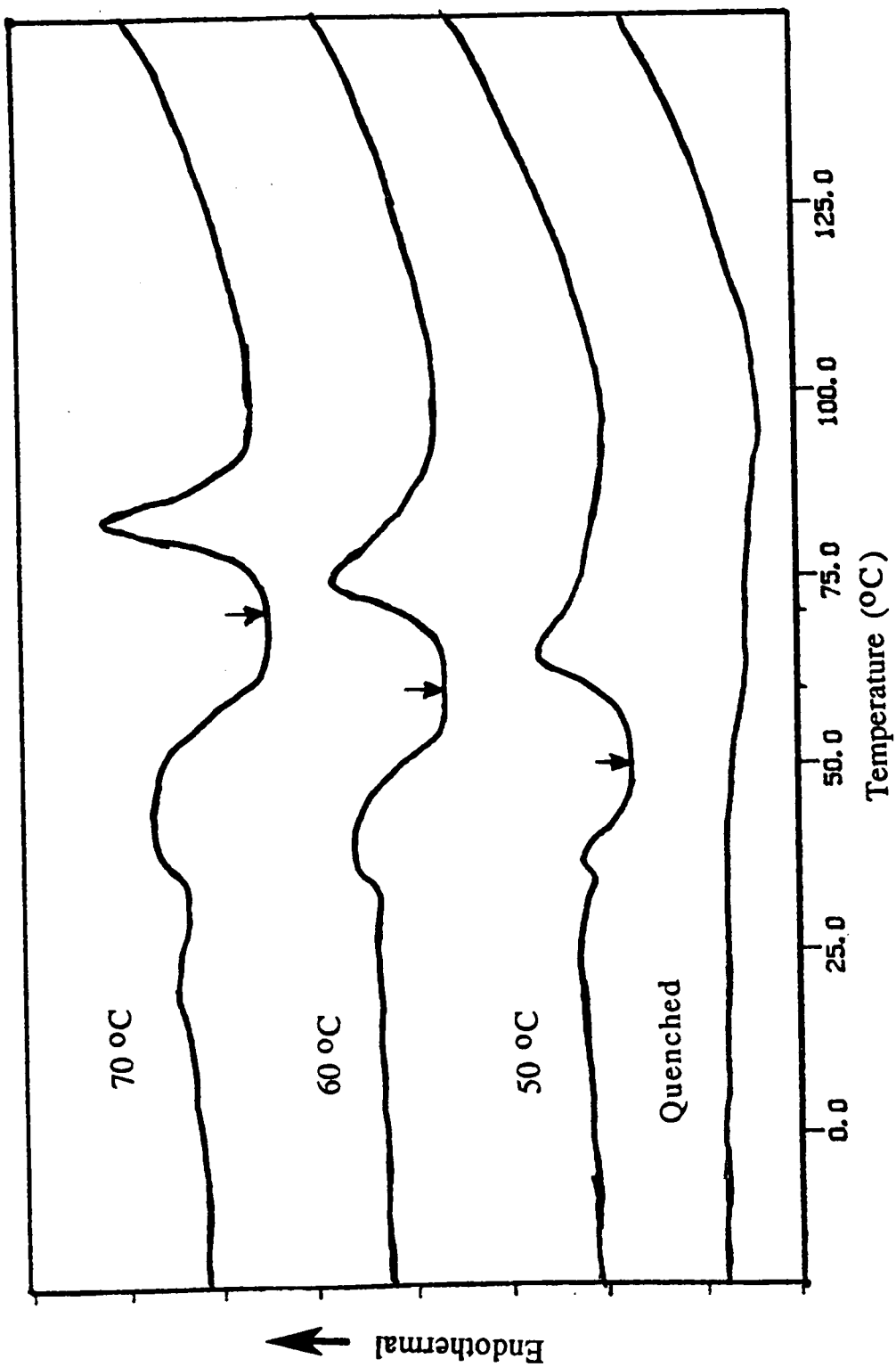


Figure 4.10: Annealing effects upon the endotherms of EPDM.

with EPR, the hump at 25 °C increases as the annealing temperature is raised. This phenomenon is most likely due to crystallization upon cooling of material which was unable to recrystallize during annealing. Room temperature annealing can also be observed at approximately 25 °C.

The subtraction curve for EPDM is also similar to that of EPR. Both room temperature and 60 °C annealing are manifest on the typical subtraction curve shown in Figure 4.11. The annealing data is tabulated in Table 4.4. The position of the loss peak is independent of annealing time and, as observed for EPR, is consistently about 3 to 4 °C below the annealing temperature for both 60 and 70 °C annealing. For 50 °C the value of Td is within about 1.5 °C of the actual annealing temperature. Tb can once again be observed to be far less consistent than Tp. The position of the gain peak, Tp, shows behavior similar to that of EPR, and is shown in Figure 4.12.

4.3.4 Crosslinked Ethylene Propylene Copolymer (XEPR)

Crosslinked EPR with 9 percent extractables (2 % DCP) was studied at annealing temperatures of 50, 60, and 70 C. The annealed endotherms are shown in Figure 4.13 and are identical to those of EPR. The quenched curve shows limited crystallinity and annealing can be seen to produce crystallity which is manifest as a peak about 10 °C above the annealing temperature. This is typical of what was previously observed for both EPR and EPDM.

A typical subtraction curve of XEPR is shown in Figure 4.14. The effects of room temperature annealing are not as drastic as seen previously on the subtraction curves of EPR and EPDM.

The subtraction data are shown in Table 4.5. The values of Td remain fairly constant with annealing time and generally seem to be within 2 °C of the actual annealing temperature for 50, 60, and 70 °C annealing. One may recall that for EPR the values for Td were consistently 4 to 5 °C lower than the annealing temperature for the upper two annealing temperatures. Tp shows the expected increase

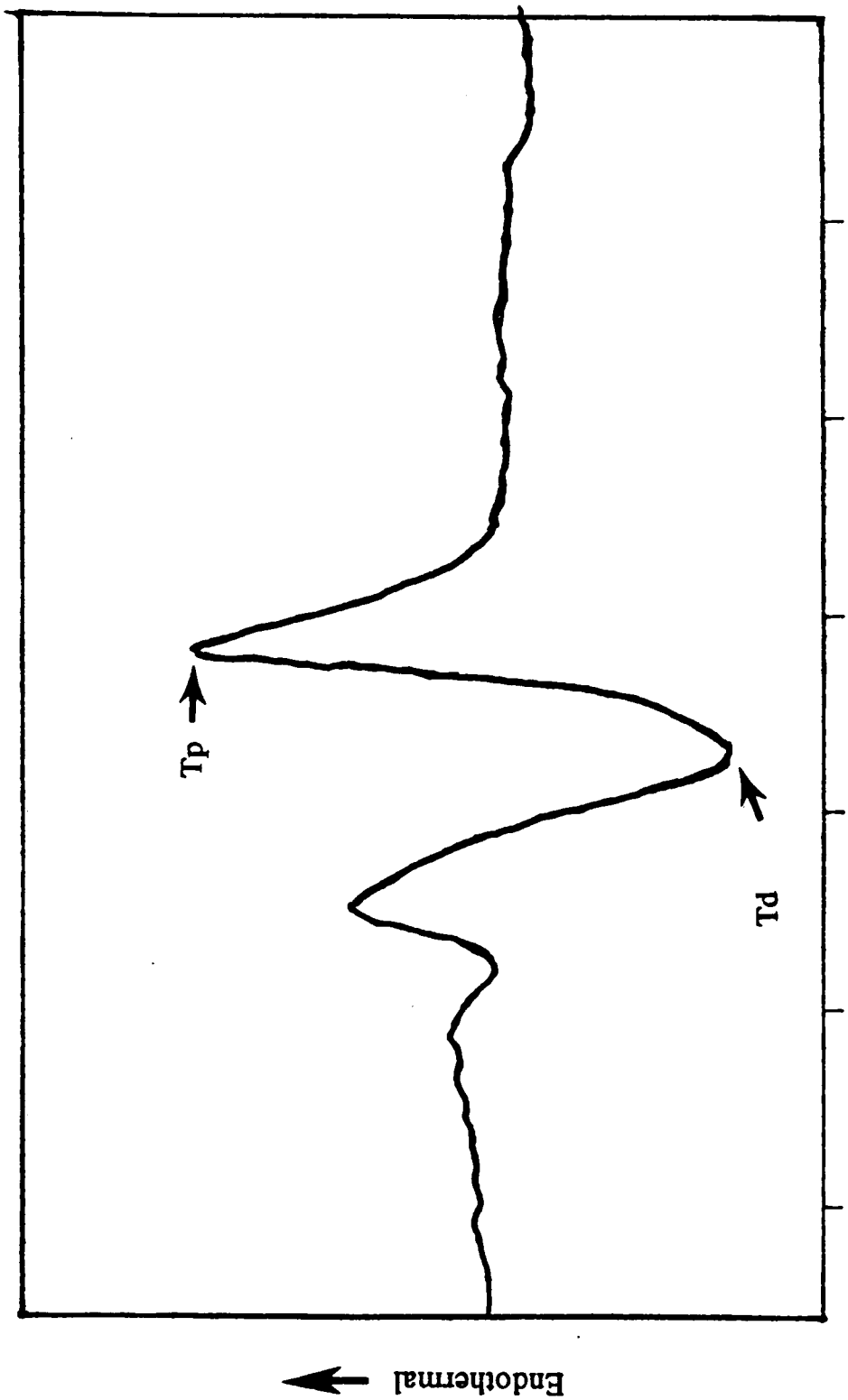


Figure 4.11: Typical subtraction curve of EPDM showing 60 C annealing.

Table 4.4: Annealing data for EPDM.

	50 °C annealing			60 °C annealing			70 °C annealing		
Time	Td	Tp	Tb	Td	Tp	Tb	Td	Tp	Tb
3	49.5	61.90	57.7	57.1	69.75	65.8	67.9	79.3	75.6
6	50.0	62.35	58.3	57.2	71.05	67.3	66.8	79.85	76.3
12	48.7	62.45	57.7	56.0	70.9	66.9	68.8	81.35	76.0
24	53.0	63.8	59.2	56.5	72.15	67.8	66.0	81.55	77.5
96	48.4	64.95	57.6	57.0	74.65	69.0	71.0	82.05	78.5
236	48.4	66.4	60.8	56.0	75.43	68.8	64.6	83.25	79.0
332	48.4	66.35	58.7	55.9	75.85	70.6	68.5	83.20	
433	47.6	66.85	61.0	55.5	75.95	70.3	66.0	83.90	79.3
790	48.0	66.90	60.0	55.0	76.08	70.5	65.0	84.30	79.0

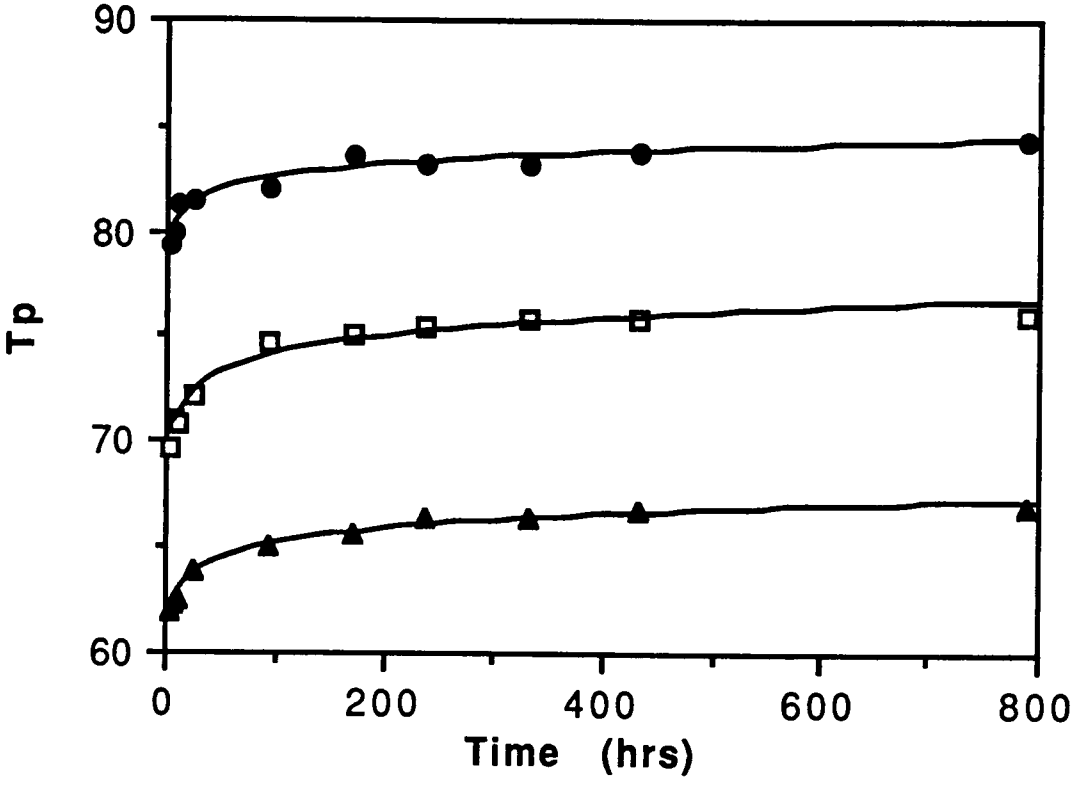


Figure 4.12: Tp versus time for EPDM. Δ 50 C annealing; □ 60 C annealing; ● 70 C annealing.

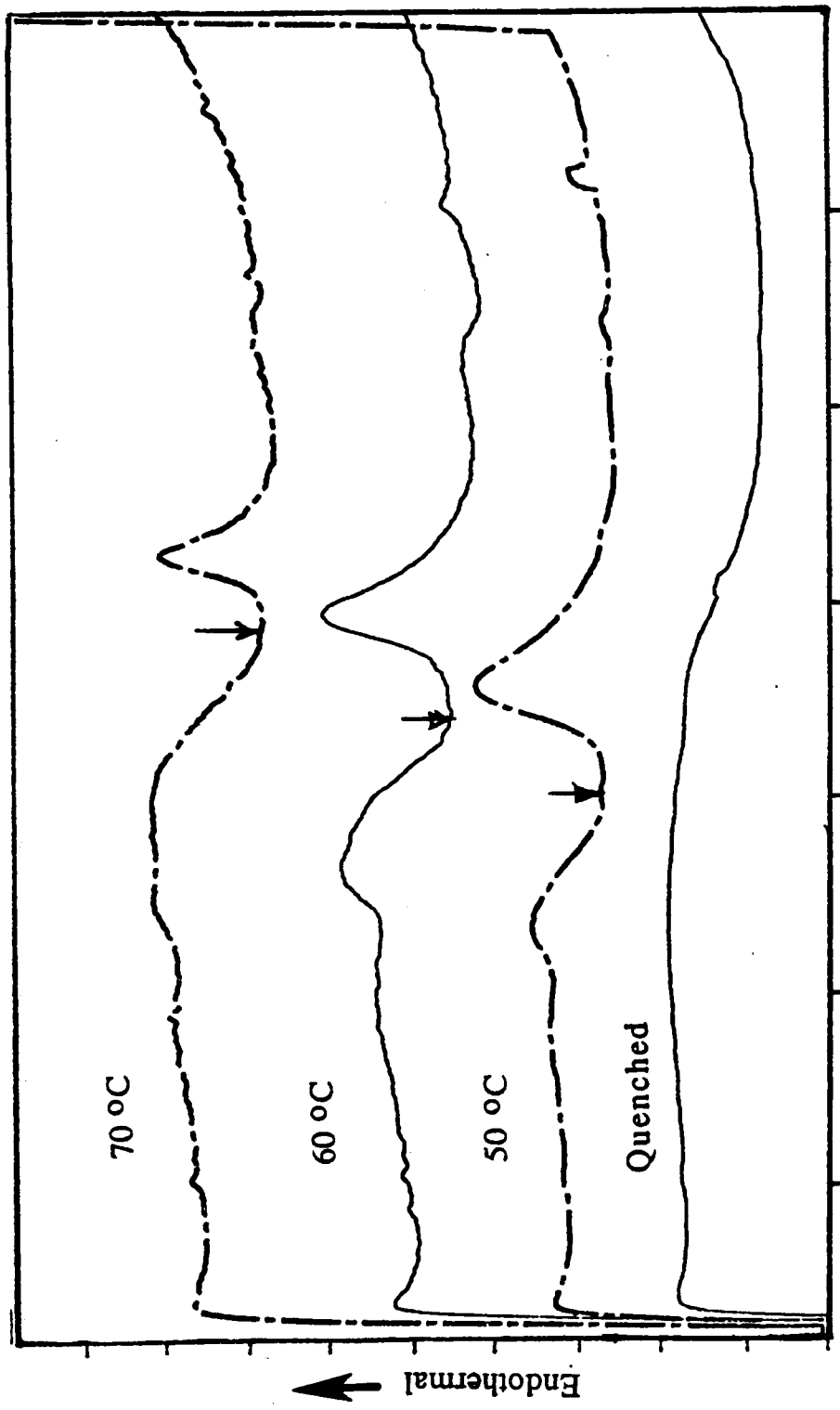


Figure 4.13: Annealing effects upon the endotherms of XEPR.

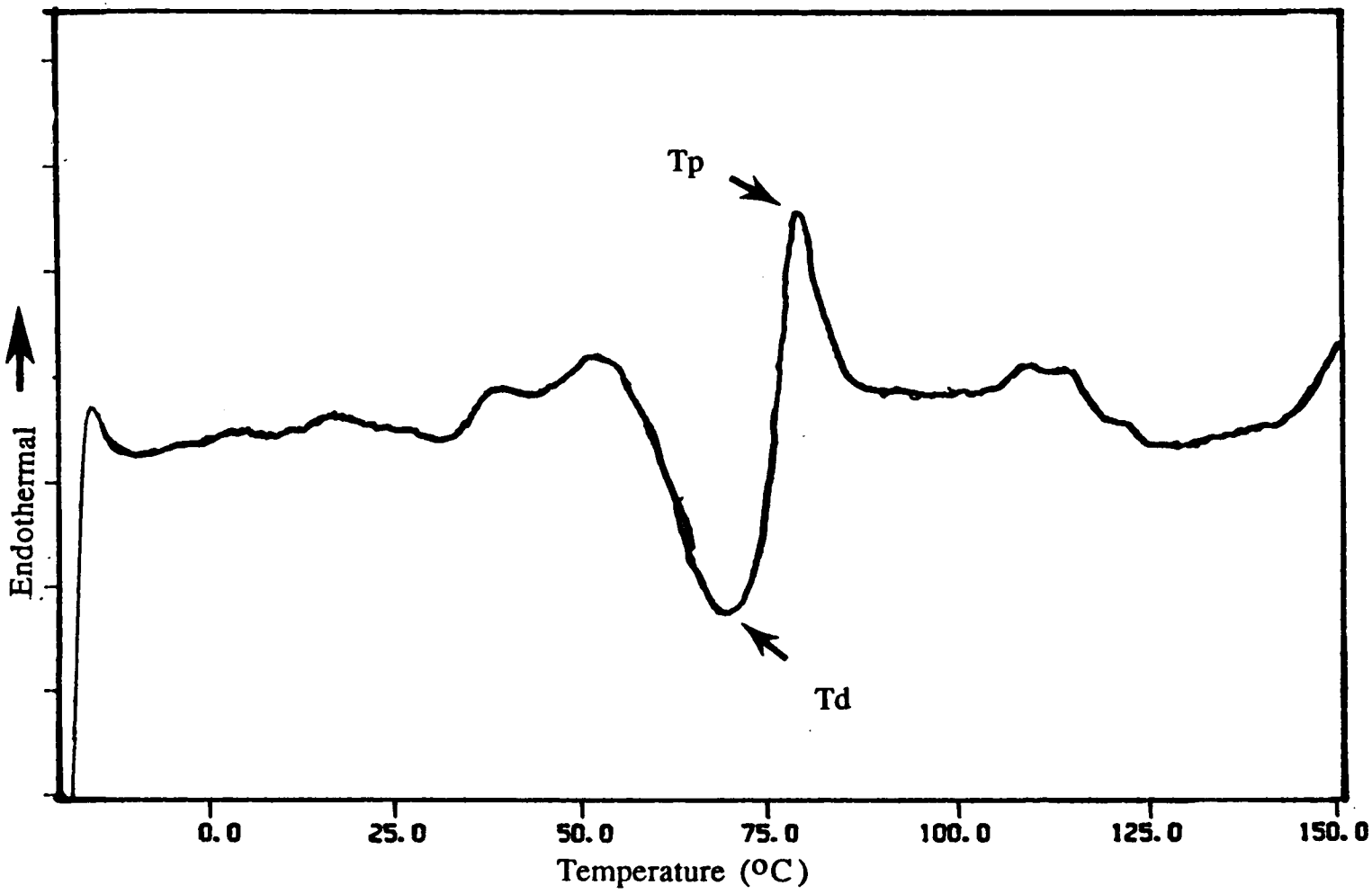


Figure 4.14: Typical subtraction curve of XEPR showing 70 C annealing.

Table 4.5: Annealing data for XEPR.

	50 °C annealing			60 °C annealing			70 °C annealing		
Time	Td	Tp	Tb	Td	Tp	Tb	Td	Tp	Tb
3	50.4	62.53		60.8	69.6		68.8	78.85	
6	51.0	63.20	59.0	58.9	71.07		69.1	80.53	
12	50.8	63.85	58.9	61.1	71.60	66.8	68.3	79.85	76.4
24	55.0	64.90		63.2	72.65	68.9			
50	48.0	64.93		59.0	72.67		69.2	80.75	
72	52.3	65.05	59.7	60.5	73.25		67.0	81.15	
180	50.2	65.80	60.4	59.5	73.75	69.5	68.2	82.10	78.2
300	50.0	66.40	61.1	59.4	73.90	68.7	67.6	82.15	79.0
470	49.0	66.60		59.4	74.6	70.0	69.0	82.6	

with annealing time. The gain peak position, Tp, is plotted against annealing time in Figure 4.15. The curves show the similar shape of those observed for EPR with increasing annealing temperature resulting in an upward shift of the curve.

4.3.5 Crosslinked Ethylene Propylene Terpolymer (XEPDM)

Crosslinking with two percent DCP yielded XEPDM with only 5 percent extractables. Annealing behavior was studied at temperatures of 50, 60, and 70 °C. The resulting endotherms from annealing are shown in Figure 4.16. The quenched endotherm shows a very broad melting range, as was observed for EPDM, with sharp peaks being generated for 50 and 60 °C annealing. Annealing at 70 °C resulted in generation of only a small peak. Room temperature annealing is also manifest on the endotherms at approximately 25 °C.

A typical subtraction curve for 50 °C annealing is shown in Figure 4.17. Room temperature annealing is not as evident as previously seen on the subtraction curves of EPDM and EPR. This is most likely due to the presence of crosslinks which act to slow the annealing of the material during transfer from the constant temperature bath to the DSC. The subtraction data are shown in Table 4.6. The position of the loss peak is within about 1 °C for 60 and 70 °C annealing and is consistently about 2 °C higher than the annealing temperature of 50 °C. The annealing behavior is shown in Figure 4.18 through the plot of Tp versus time.

4.4. Control Cables

The characteristics of cables which were supplied for this study can be found in Table 3.1. However, not all of these cables were examined in great detail. A selection of five cables which seemed to show the greatest variety in composition and melting behavior were chosen for extensive investigation. While no formulations were provided for these cables, one can infer the composition of the

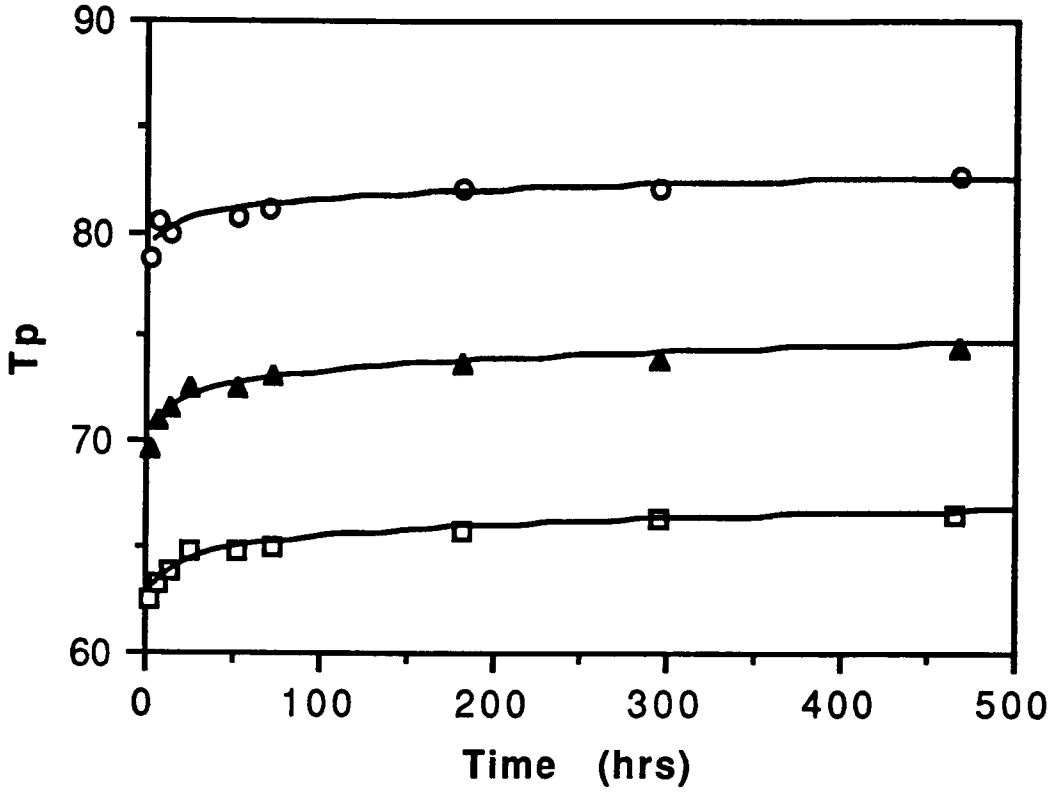


Figure 4.15: Tp versus time for XEPR. ◻ 50 C annealing; ▲ 60 C annealing; o 70 C annealing.

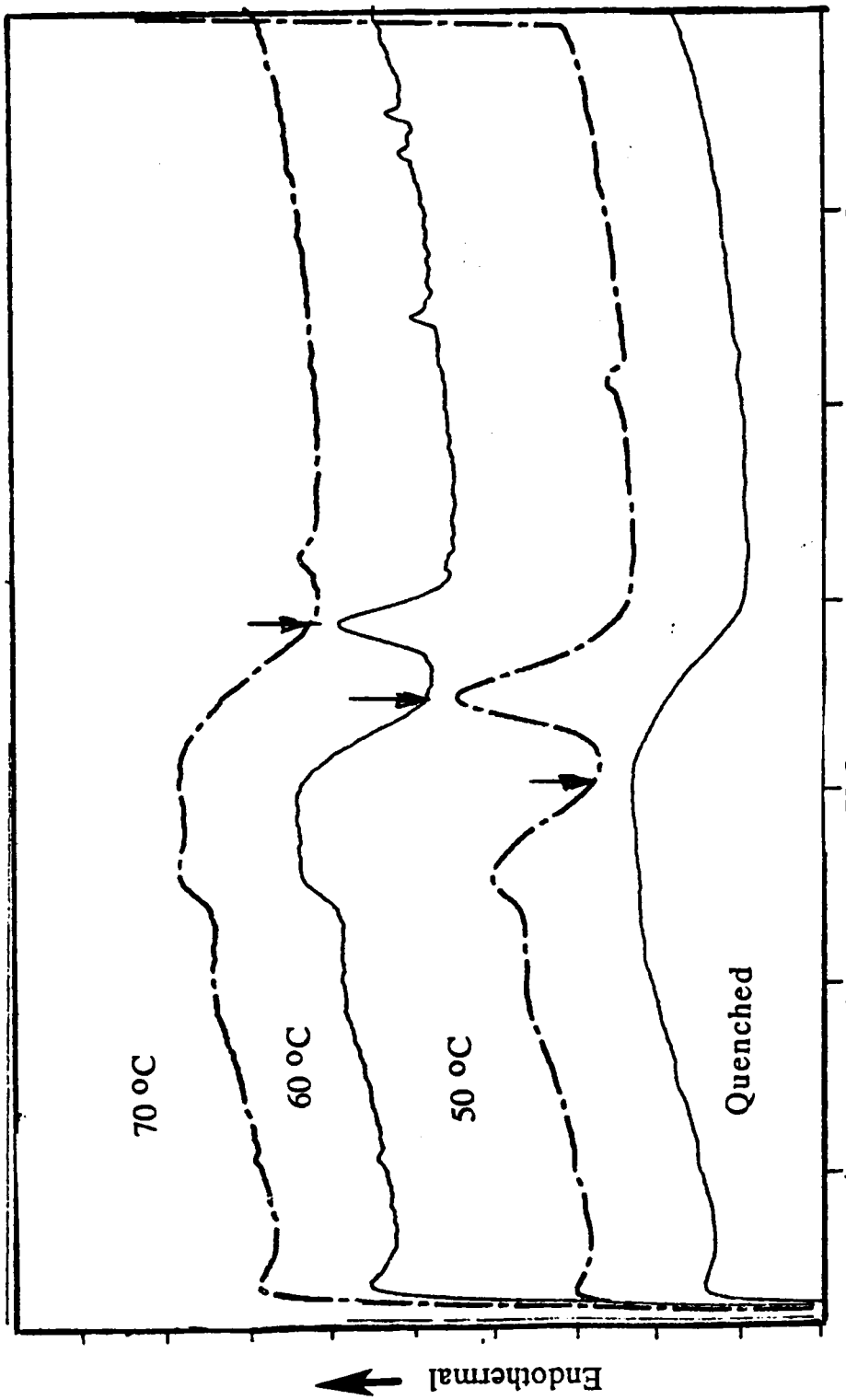


Figure 4.16: Annealing effects upon the endotherms of XEPDM.

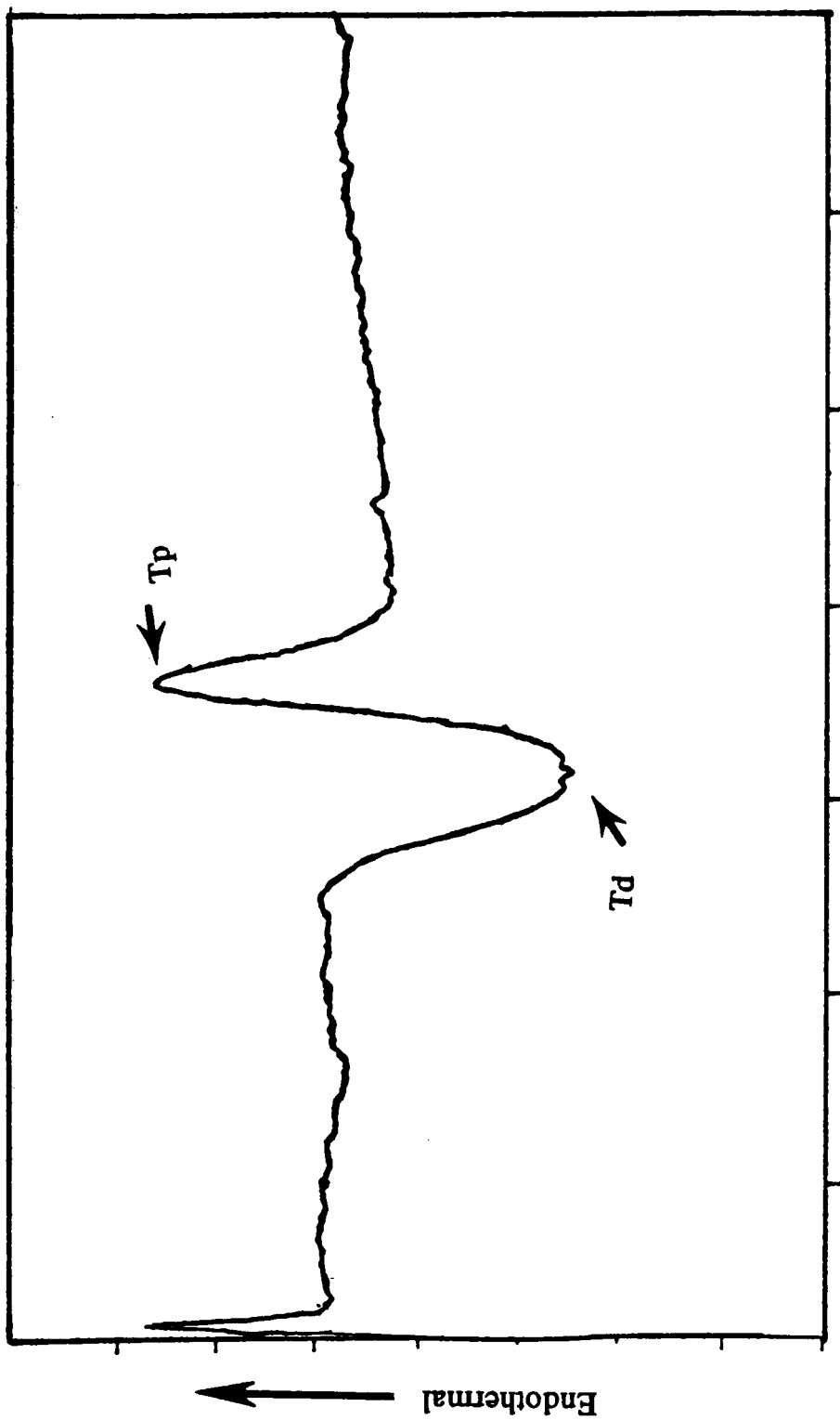


Figure 4.17: Typical subtraction curve for XEPDM showing 50 C annealing.

Table 4.6: Annealing data for XEPDM.

	50 °C annealing			60 °C annealing			70 °C annealing		
Time	Td	Tp	Tb	Td	Tp	Tb	Td	Tp	Tb
3	52.4	61.15	56.6	60.8	68.85		70.4	77.80	
6	53.4	61.40		60.5	69.95	66.8	69.8	78.20	75.8
12	52.3	60.85	57.1	60.4	69.30	66.0	70.0	78.40	
24	53.0	61.70	58.4				67.8	78.65	75.8
50	53.4	62.10		61.0	70.10		71.4	80.05	
72	52.9	62.95	58.9	60.7	71.00	67.2	70.2	79.73	
180	51.8	64.35		60.5	72.85	69.1	69.7	82.95	
300	52.0	64.30		61.0	72.90	68.8	68.8	84.40	76.3
470	53.2	64.67	58.7	60.8	72.95		69.7	83.0	

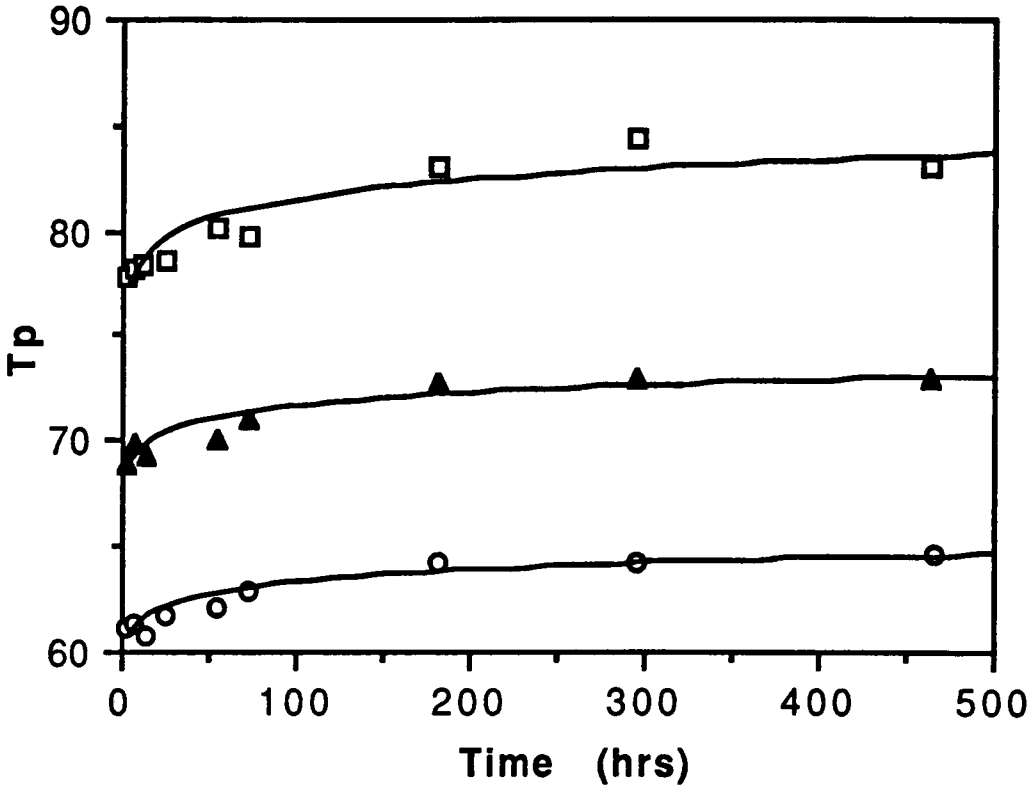


Figure 4.18: Tp versus time for XEPDM. ○ 50 C annealing; ▲ 60 C annealing; □ 70 C annealing.

semicrystalline insulating material from the melting behavior.

4.4.1 Cable A1 [Eaton (Samuel Moore)]

This cable was labelled as Dekoron Polyset P/N 015800-n and was triple stranded with an outside jacket. The original and quenched DSC endotherms for Cable A1 are shown in Figure 4.19. This cable appears to be composed of some type of XLPE blended with an EPR formulation. Comparing the original and quenched curves it also becomes apparent that there is already a fairly complicated thermal history inherent in the sample. The sample has one large melting peak located at 80 °C with a broader melting region extending down 5 °C or perhaps even lower. Figure 4.20 shows the subtraction curve for this cable. The sample has been exposed to temperatures of approximately 65 °C and perhaps 80 °C as well as room temperature, as shown by the position of the loss peak, Td.

The annealing behavior was explored for temperatures of 50, 55, 60, and 70 °C using "history erased" samples for annealing. The effects of annealing at each temperature upon the melting curves for a constant annealing time of 166 hours are shown in Figure 4.21. One can observe what can be considered as typical behavior for each annealing. The formation of a shoulder is apparent at 50 °C and it shifts to higher temperatures as the annealing temperature is increased. The 70 °C endotherm exhibits a smaller hump in the vicinity of 50 °C. This is a manifestation of material which was no longer able to recrystallize at 70 °C and therefore crystallizes upon cooling.

A typical subtraction curve for cable A1 is shown in Figure 4.22. The subtraction data are shown in Table 4.7. One can note that Td shows very little temperature dependence and is generally within 2 °C of the actual annealing temperature. For 70 °C annealing the value of Td is about 4 °C higher than the annealing temperature for annealing times longer than about 200 hours. The plot of Tp versus time is shown in Figure 4.23. The data appear to follow the same

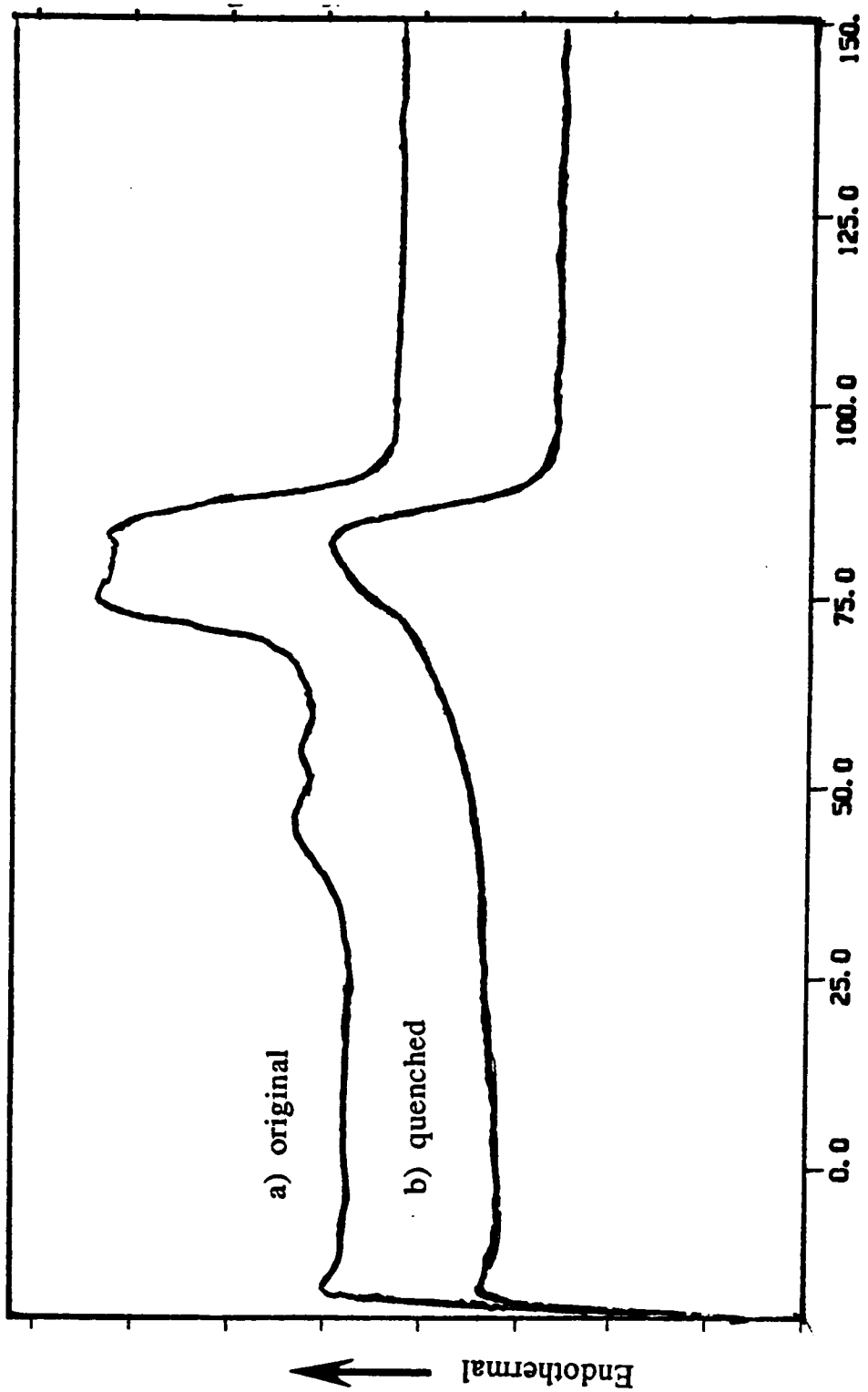


Figure 4.19: DSC endotherms for cable A1: a) original; b) quenched.

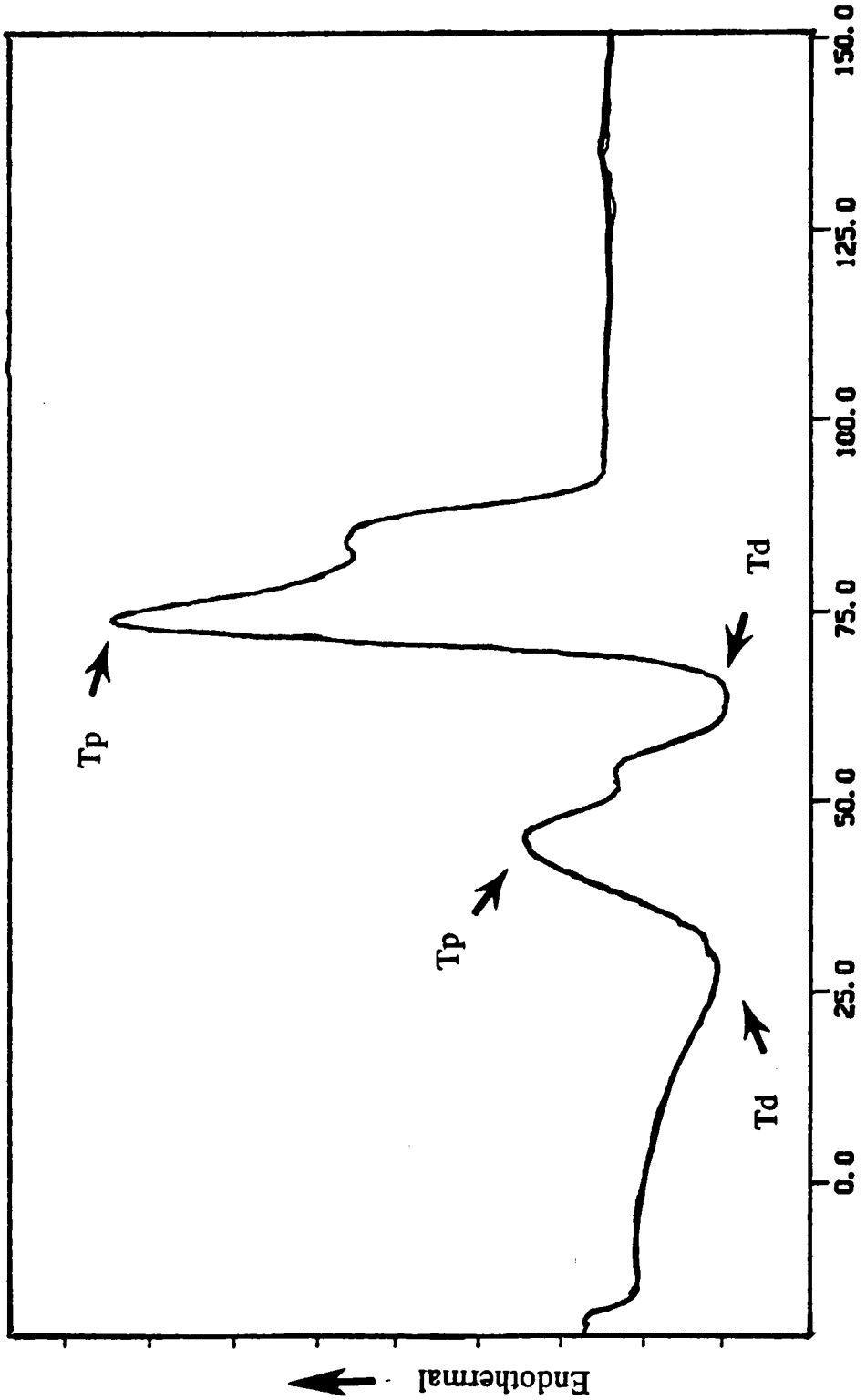


Figure 4.20: Original subtraction curve for cable A1.

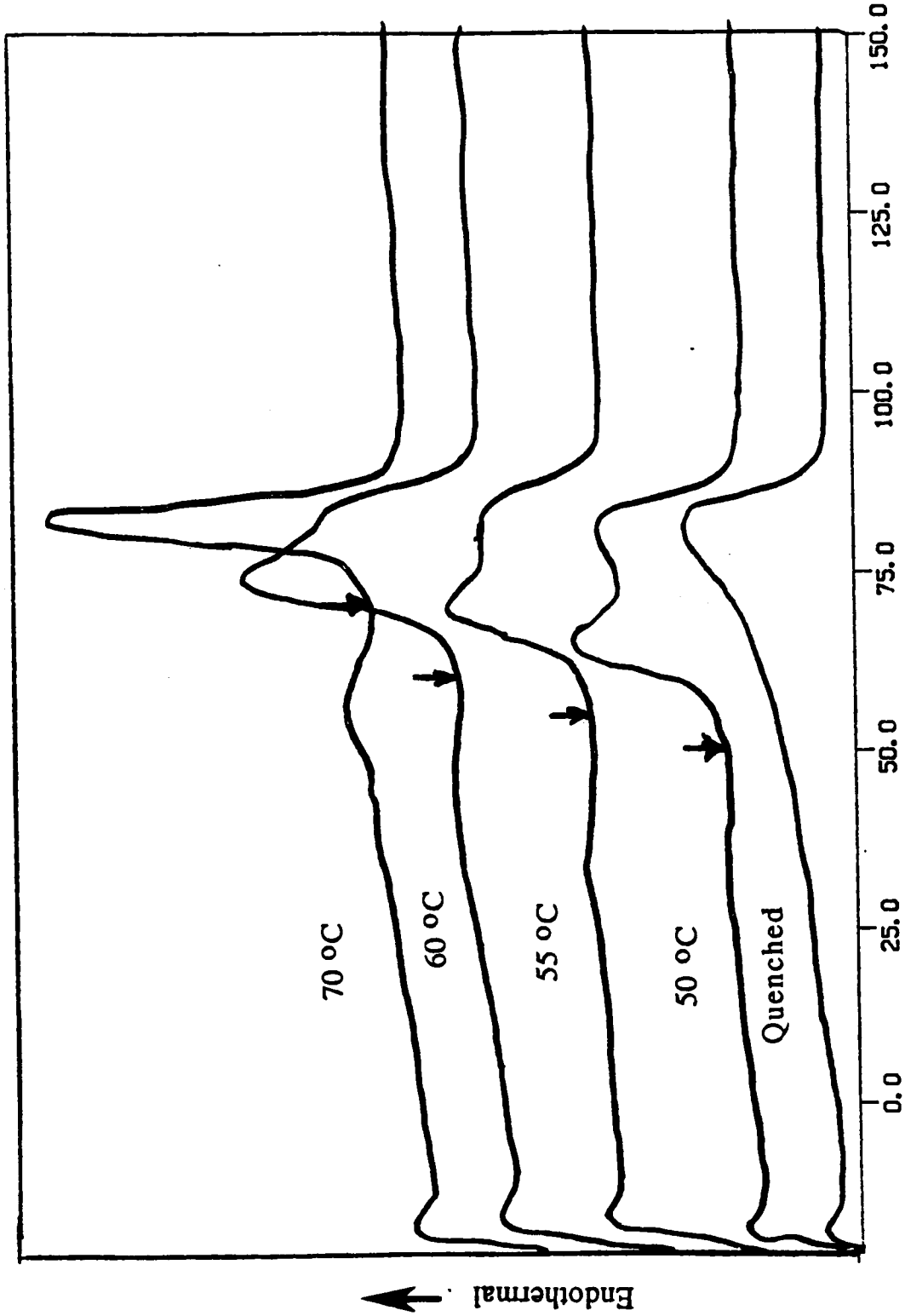


Figure 4.21: Annealing effects upon the "history erased" endotherms of cable A1.

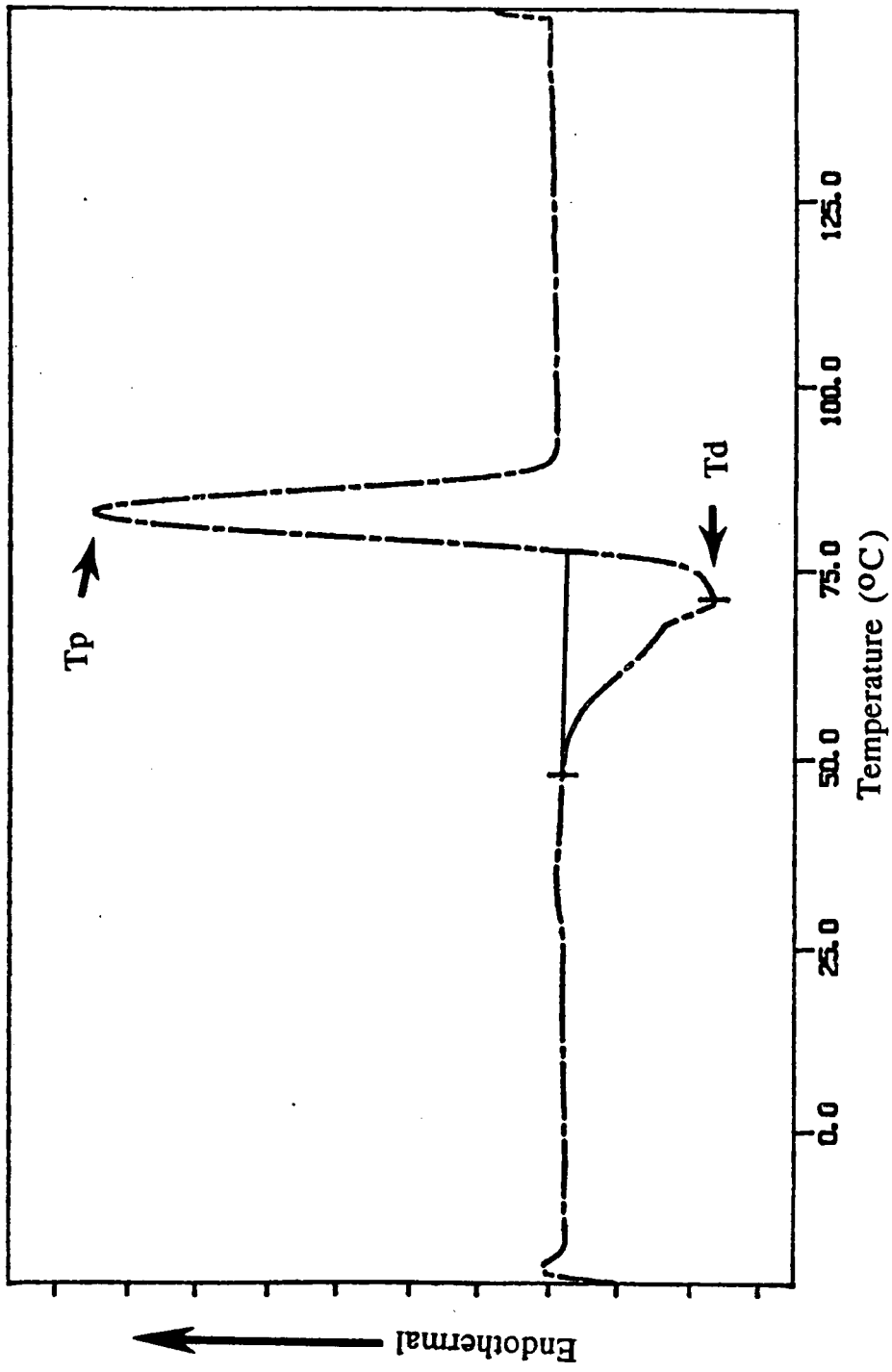


Figure 4.22: Typical subtraction curve of cable A1 showing 70 C annealing.

Table 4.7: Annealing data for cable A1.

	50 °C Annealing			55 °C Annealing			60 °C Annealing			70 °C Annealing		
Time	Tb	Tp	Td	Tb	Tp	Td	Tb	Tp	Td	Tb	Tp	Td
1	55.6	59.85	50.2	59.95	64.15	55.4	65.0	69.00	60.5	74.9	77.95	71.0
3	56.6	61.30	51.9	61.0	65.00	55.9	65.9	69.75	60.8	75.3	78.50	71.7
6	56.8	61.45	51.1	61.6	65.90	56.3	65.5	69.85	60.4	74.4	78.15	70.7
24	58.3	63.45	52.0	61.9	66.75	55.8	67.1	71.45	61.0	76.5	80.40	72.6
48	58.6	63.90	51.5	62.6	67.45	55.8	66.7	71.75	61.4	77.3	81.55	73.2
165	59.0	64.80	51.2	63.7	69.10	58.0	68.0	73.05	60.4	78.4	82.75	74.2
210	58.4	65.85	52.6	64.0	69.25	57.9	68.3	73.75	63.5	78.0	82.15	73.7
270	59.5	66.25	50.8	63.2	68.65	57.4	68.9	74.00	63.0	78.7	83.10	74.3
385	61.0	66.85	52.4	64.6	69.85	56.6	69.4	74.90	61.9	78.5	82.85	74.2
430	60.8	66.55	53.2	63.7	69.45	60.0	69.1	74.35	62.2	79.0	83.30	74.6
480	60.9	66.55	52.9	64.6	70.15	57.7						
860	60.1	66.8	52.3				70.0	76.65	63.2	78.5	82.95	74.0

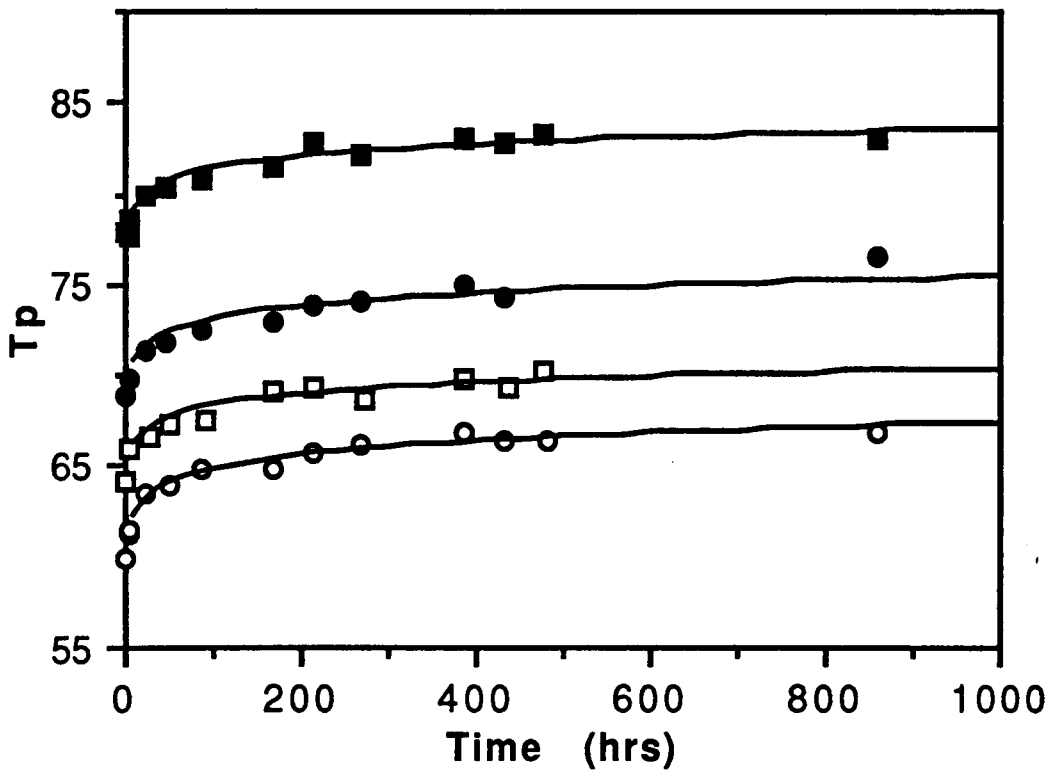


Figure 4.23: Tp versus time for cable A1.○ 50 C annealing;
□ 55 C annealing;● 60 C annealing;
■ 70 C annealing.

trend as observed for the "standard" materials.

Original samples were annealed at a temperature of 70 °C in order to determine if there were any differences between the annealing behavior of original samples and that of the history erased samples. Figure 4.24 shows the DSC endotherm of an original sample annealed at 70 °C for twelve hours. There are no major changes in the appearance of the melting curve shown in this figure and that of 70 °C annealing shown for a history erased sample in Figure 4.21. The subtraction curve appears identical as well (Figure 4.24 b). The position of the gain peak as a function of annealing time for 70 °C annealing of both the original and history erased samples is shown in Figure 4.25. One can observe that the curve produced from annealing the original samples lies slightly above the curve representing the annealing of "history erased" samples.

4.4.2 Cables A2 and A3 [Eaton (Samuel Moore)]

Both cable A2 and A3 show very similar melting behavior, as shown in Figure 4.26. From the appearance of the melting curves the insulating material seems to be either XLPE or XHPE blended with an EPDM or EPR rubber. The melting curves of both cables show a broad melting range with the high melting region being typical for the melting behavior of polyethylenes. From the endotherms, cable A2 shows what appears to be thermal treatment at temperatures of 30 and 50 °C while cable A3 shows only ambient annealing. It was assumed that they both would anneal in similar manners and only cable A3 was investigated in detail. Cable A2 was marked as Dekoron 2/C 600 V with serial number 0815182-8 and cable A3 as Dekoron 2/CD with serial number 015601-1. Both cables consisted of double strands of insulation with an outer jacket.

The subtraction curve for the original A3 is shown in Figure 4.27 and basically shows thermal treatment at roughly 95 °C and also ambient.

The changes in the melting curve of history erased cable A3 are

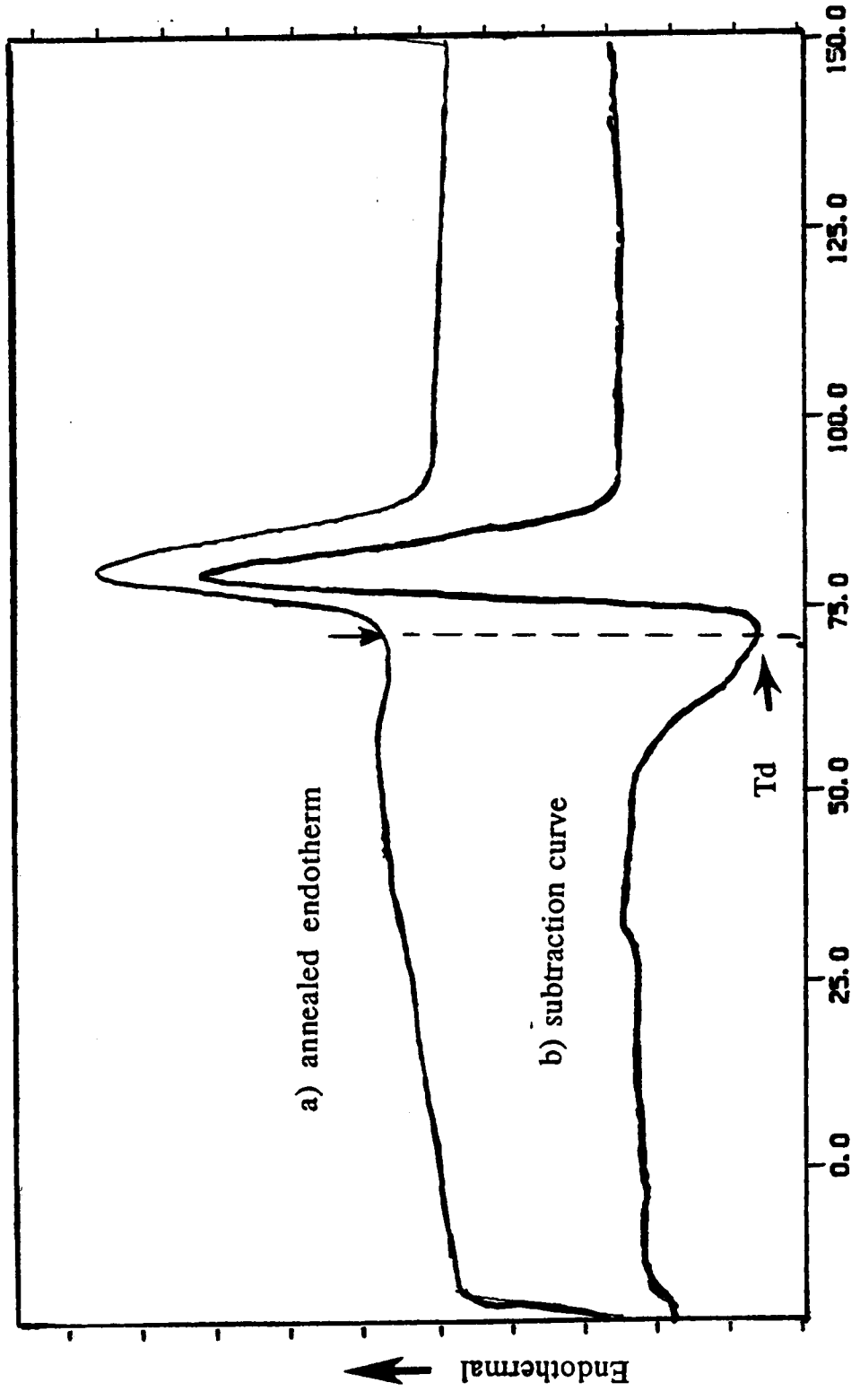


Figure 4.24: Original A1 cable annealed at 70 C: a) annealed endotherm;
b) subtraction curve.

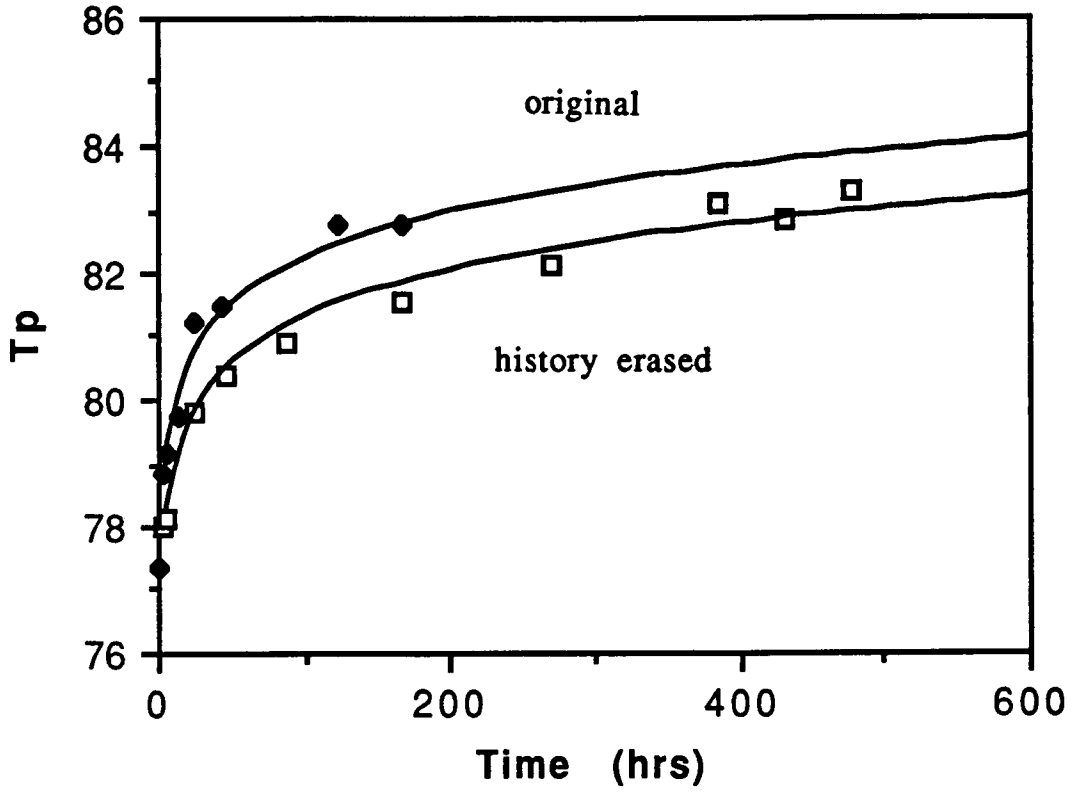


Figure 4.25: Tp versus time for original and history erased cable A1. ◆ original; □ history erased.

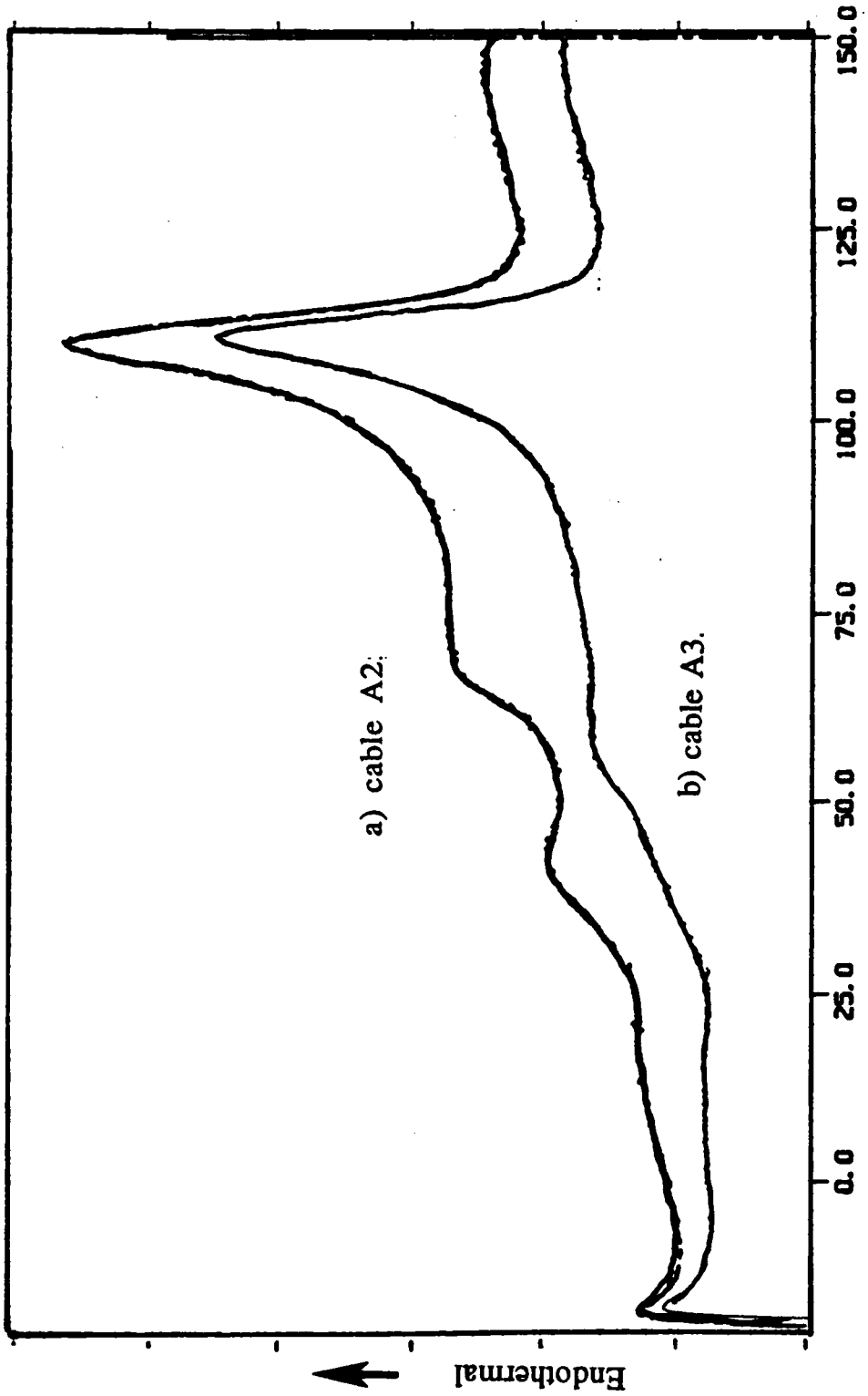


Figure 4.26: Original Endotherms for cables A2 and A3: a) cable A2; b) cable A3.

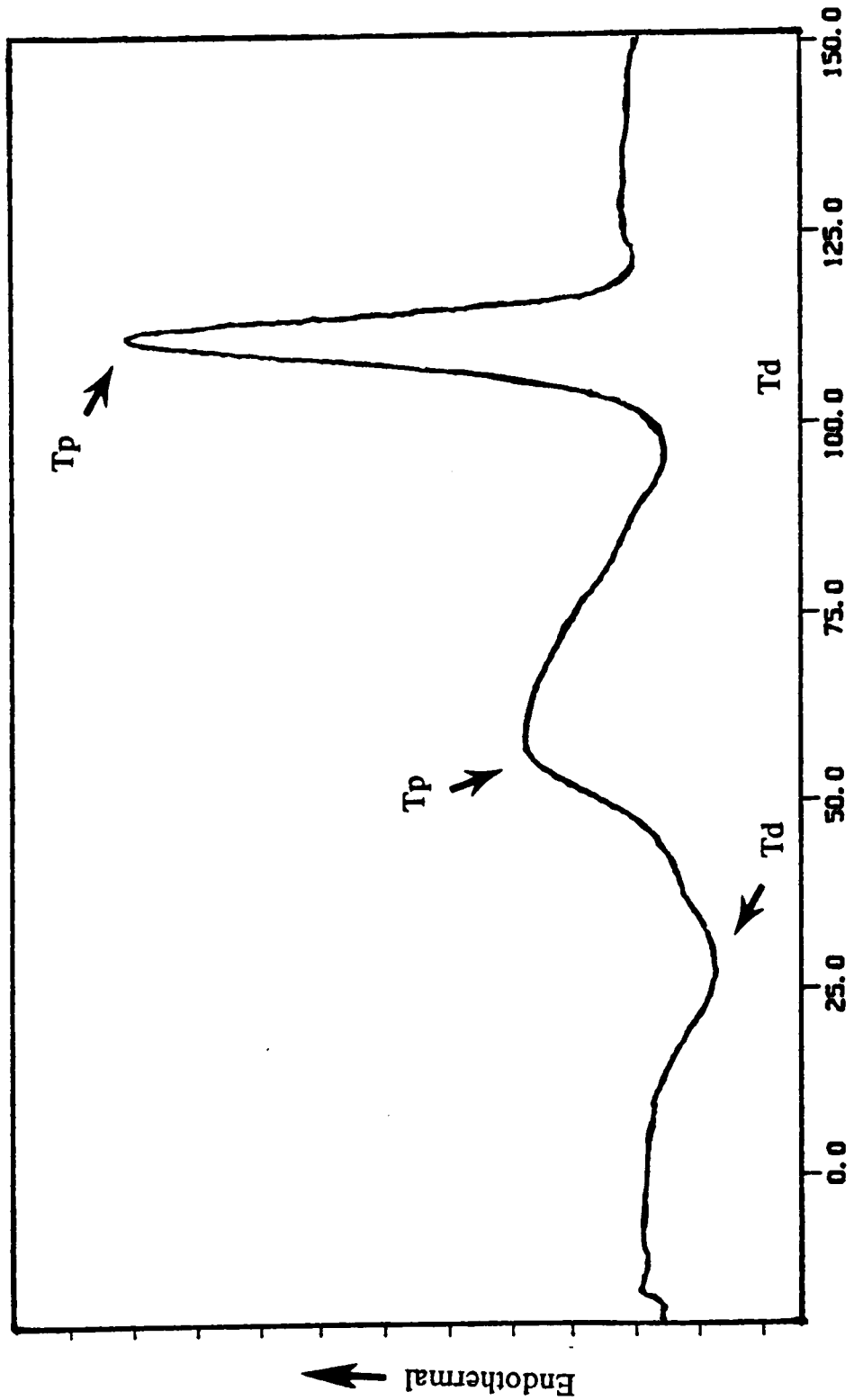


Figure 4.27: Subtraction curve for original cable A3.

shown in Figure 4.28 for 50, 55, 60, and 70 °C annealing. Once again annealing results in the generation of a shoulder on the DSC endotherm which shifts upward with increasing annealing temperature. One can also observe the lower transition which represents the melting of the EPR or EPDM material which was unable to recrystallize at the annealing temperatures.

Figure 4.29 shows a typical subtraction curve for a history erased sample of cable A3 annealed at 50 °C. The positions of the gain and loss peaks for the various annealing temperatures and times are shown in Table 4.8. Td can once again be shown to be independent of temperature with values within about 2 °C of the annealing temperature for all of the temperatures examined. The plot of Tp versus time is shown in Figure 4.30. The same basic trends observed for the standard material can also be observed for cable A3.

The effects of annealing upon the original A3 insulation were studied for a temperature of 70 °C. The DSC endotherm and the subtraction curve generated for an annealing time of 97 hours are shown in Figure 4.31. One can notice that there is a large difference in the general shape of the subtraction curve generated from the history erased sample and that of the original sample. Figure 4.32 shows the annealing behavior of both the original and history erased samples in the form of a plot of Tp versus time for each. One can observe a large difference between the behavior of the two sample types. This is most likely due to the thermal history inherent in the original cable at approximately 95 °C, as shown from Figure 4.27.

4.4.3 Cable C1 [BIW]

Cable C1 is marked as 600 V 2/C EPR/HYP 021866 and contains two strands of insulated conductors with an outside jacket. The original and quenched DSC endotherms are shown in Figure 4.33. This insulation appears from the melting behavior to be composed of EPR, as the marking suggests, blended with what appears to be a

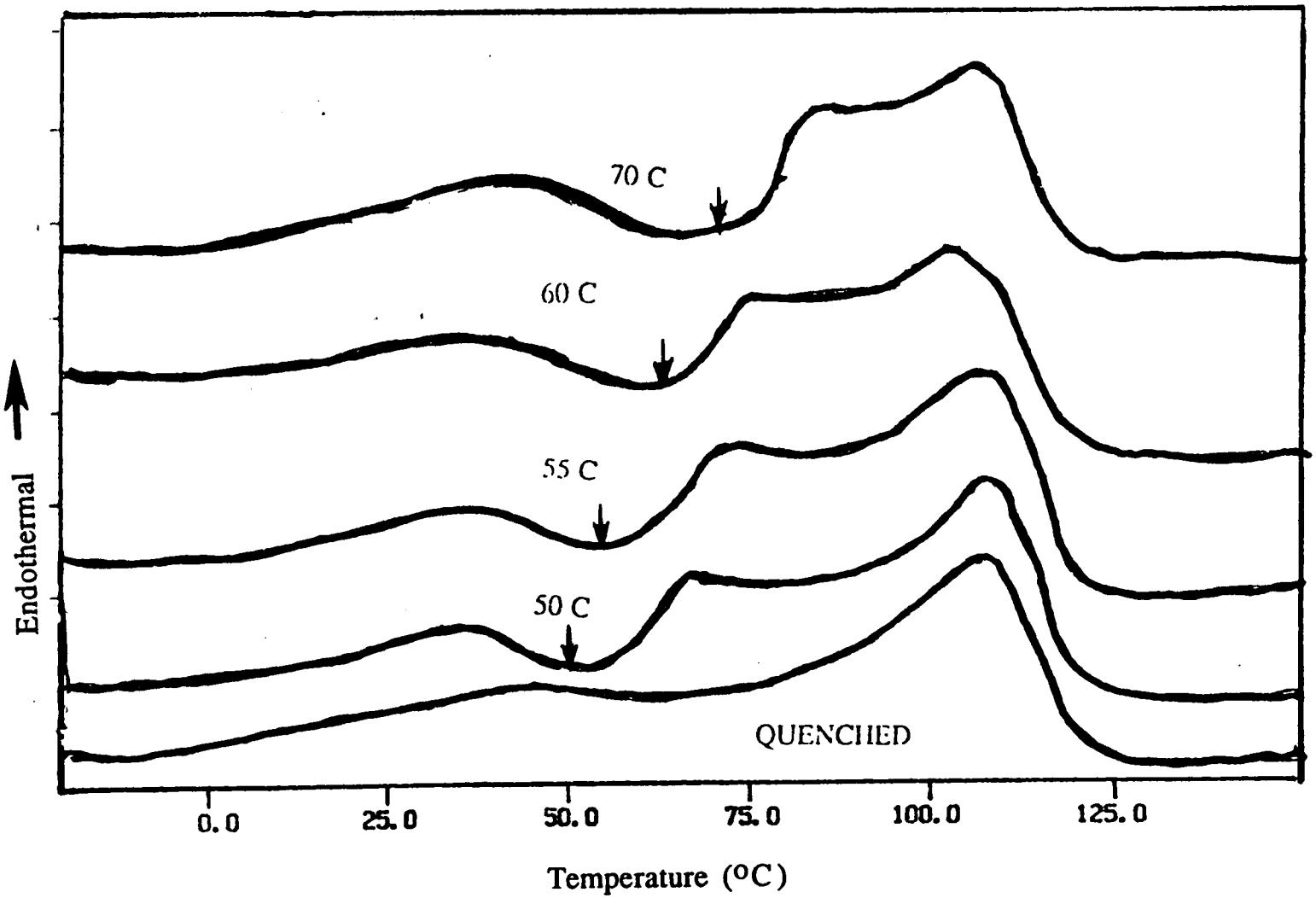


Figure 4.28: Annealing effects upon the "history erased" endotherms of cable A3.

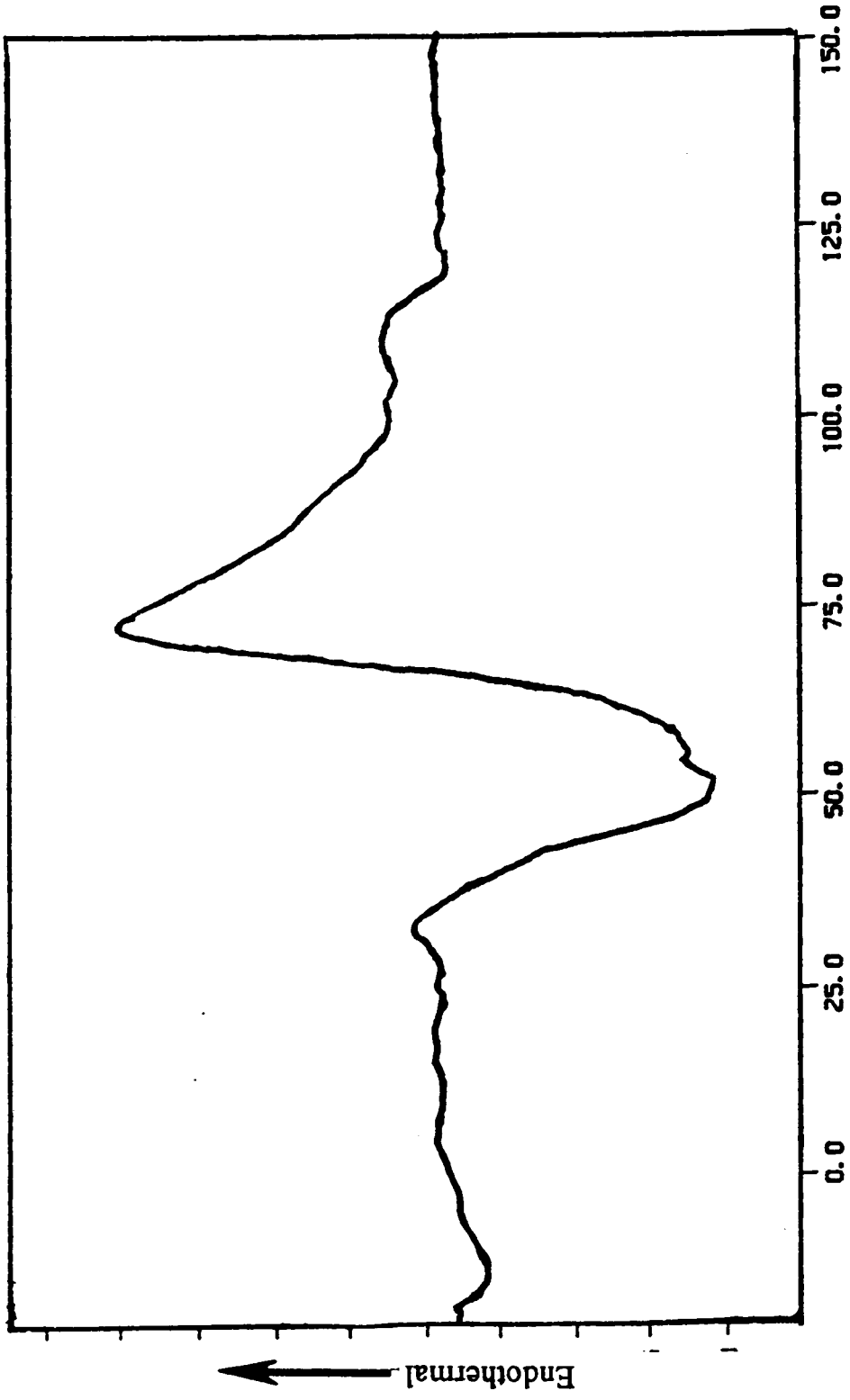


Figure 4.29: Typical subtraction curve for A3 showing 50 C annealing.

Table 4.8: Annealing data for cable A3.

	50 °C Annealing			55 °C Annealing			60 °C Annealing			70 °C Annealing		
Time	Tb	Tp	Td	Tb	Tp	Td	Tb	Tp	Td	Tb	Tp	Td
1	56.2	61.4	50.5	60.4	65.00	53.5	66.4	70.45	58.6	76.5	79.30	71.1
3	57.7	62.65	50.2	61.7	66.70	53.6	66.7	72.1	61.0	76.0	79.75	70.1
6				62.8	67.75	53.2	67.9	72.55	59.5	76.7	80.95	70.3
24	60.4	65.70	48.7	64.0	69.70	53.10	69.7	75.4	59.5	78.1	83.05	69.7
72	60.4	66.85	47.8	65.2	71.50	52.0	70.0	75.85	58.3	78.7	83.80	70.9
165	61.6	68.10	48.9	64.9	72.30	55.3	70.4	76.80	59.5	79.6	85.30	71.2
200	60.8	68.50	52.1									
225	61.1	68.10	47.10	65.6	74.35	55.6	70.0	77.35	55.3	80.2	85.80	70.6
325	62.5	69.80	49.3	66.4	73.30	52.1	71.3	78.5	63.7	80.2	86.50	72.4
430	61.2	70.40	52.3	67.6	74.05	52.0	72.4	79.30	55.3	81.1	87.30	71.2
480	62.2	70.00	47.5	66.7	74.30	56.2	71.8	79.30	56.0	81.1	87.50	70.6
500	62.8	70.10	48.7				71.8	79.10	62.5	80.2	87.40	70.3
720	63.7	70.90	52.0	68.2	75.40	52.0	72.1	80.90	55.0	80.9	88.12	72.47
1050										82.6	88.60	69.7

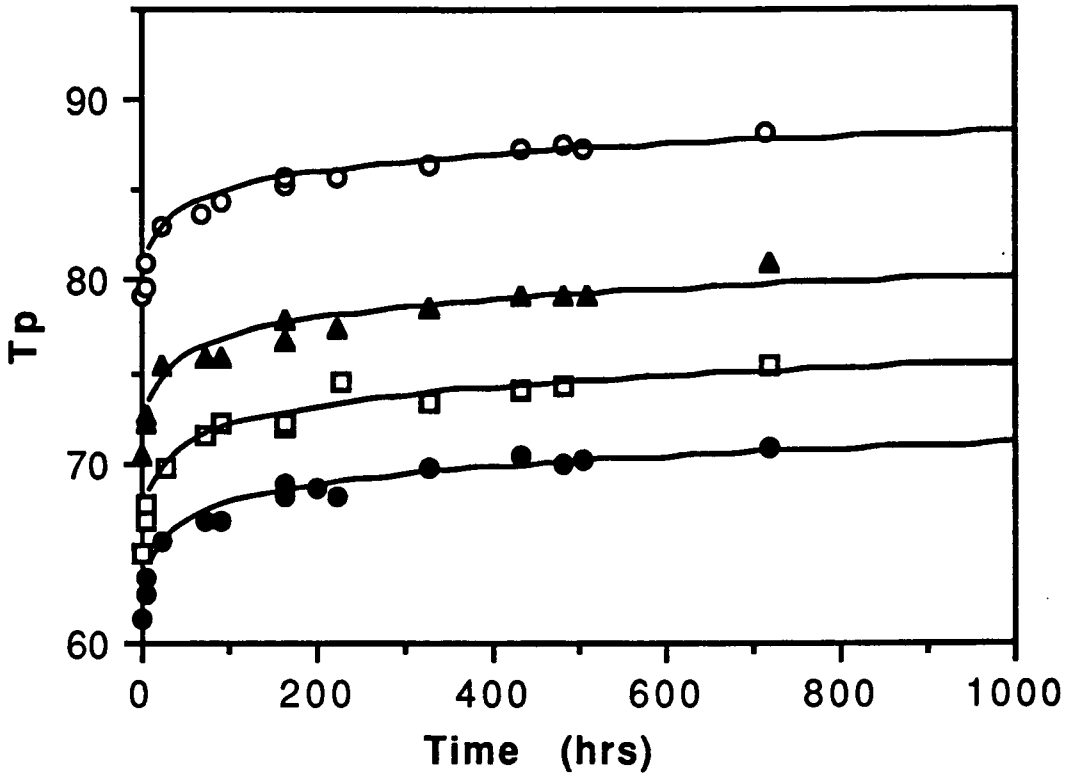


Figure 4.30: Tp versus time for cable A3. ● 50 C annealing;
□ 55 C annealing; ▲ 60 C annealing;
o 70 C annealing.

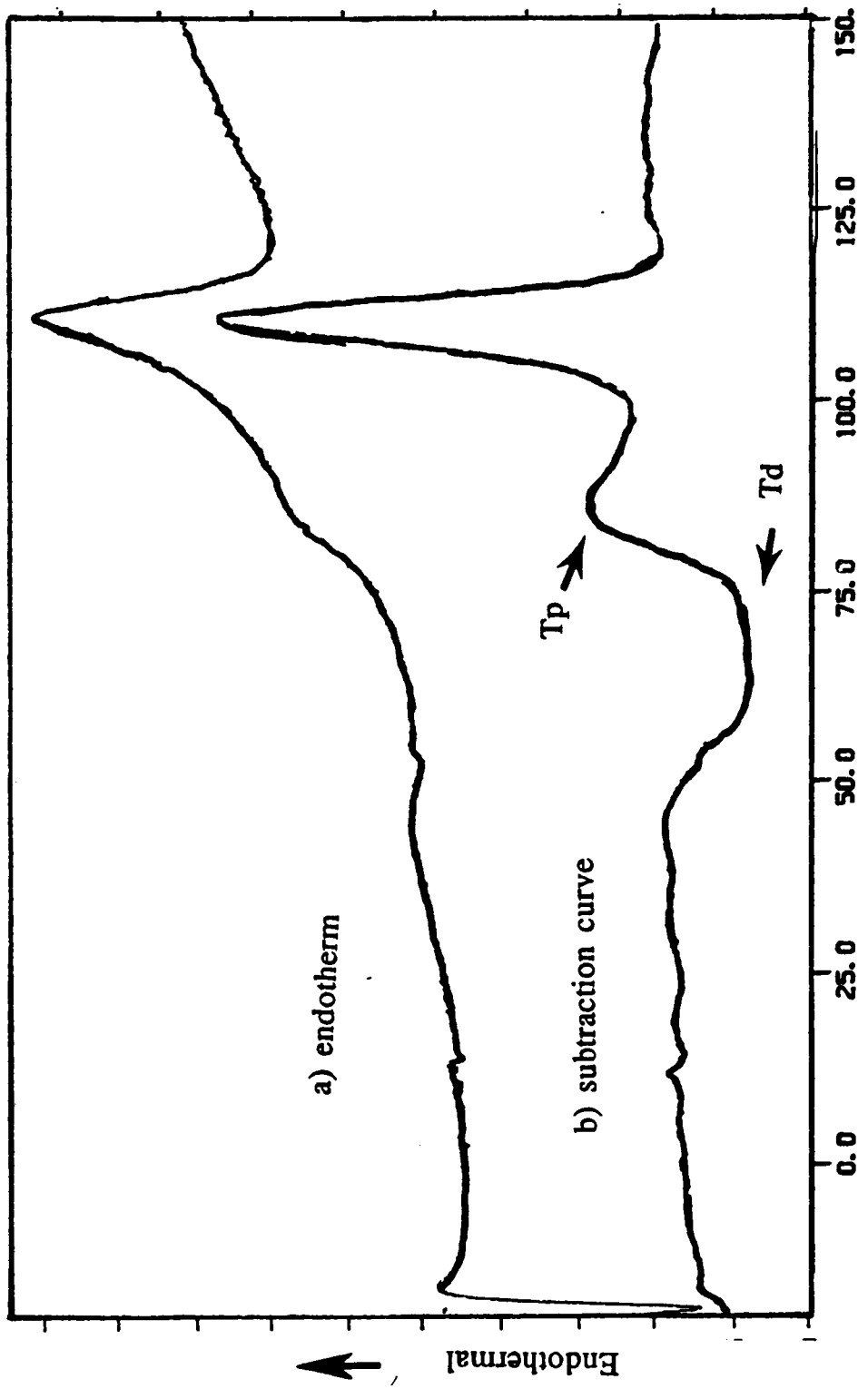


Figure 4.31: Original cable A3 annealed for 97 hours at 70 C:
a) endotherm; b) subtraction curve.

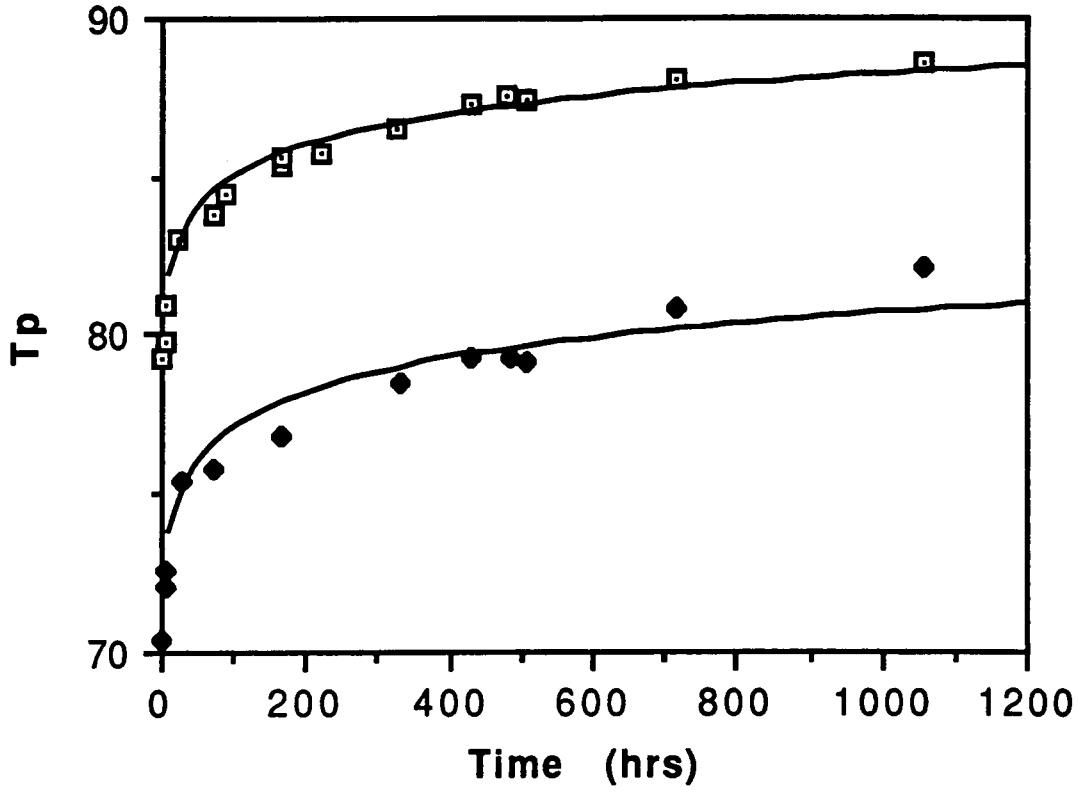


Figure 4.32: Tp versus time for original and "history erased" of cable A3 annealed at 70 C. ◆ original; ◘ history erased.

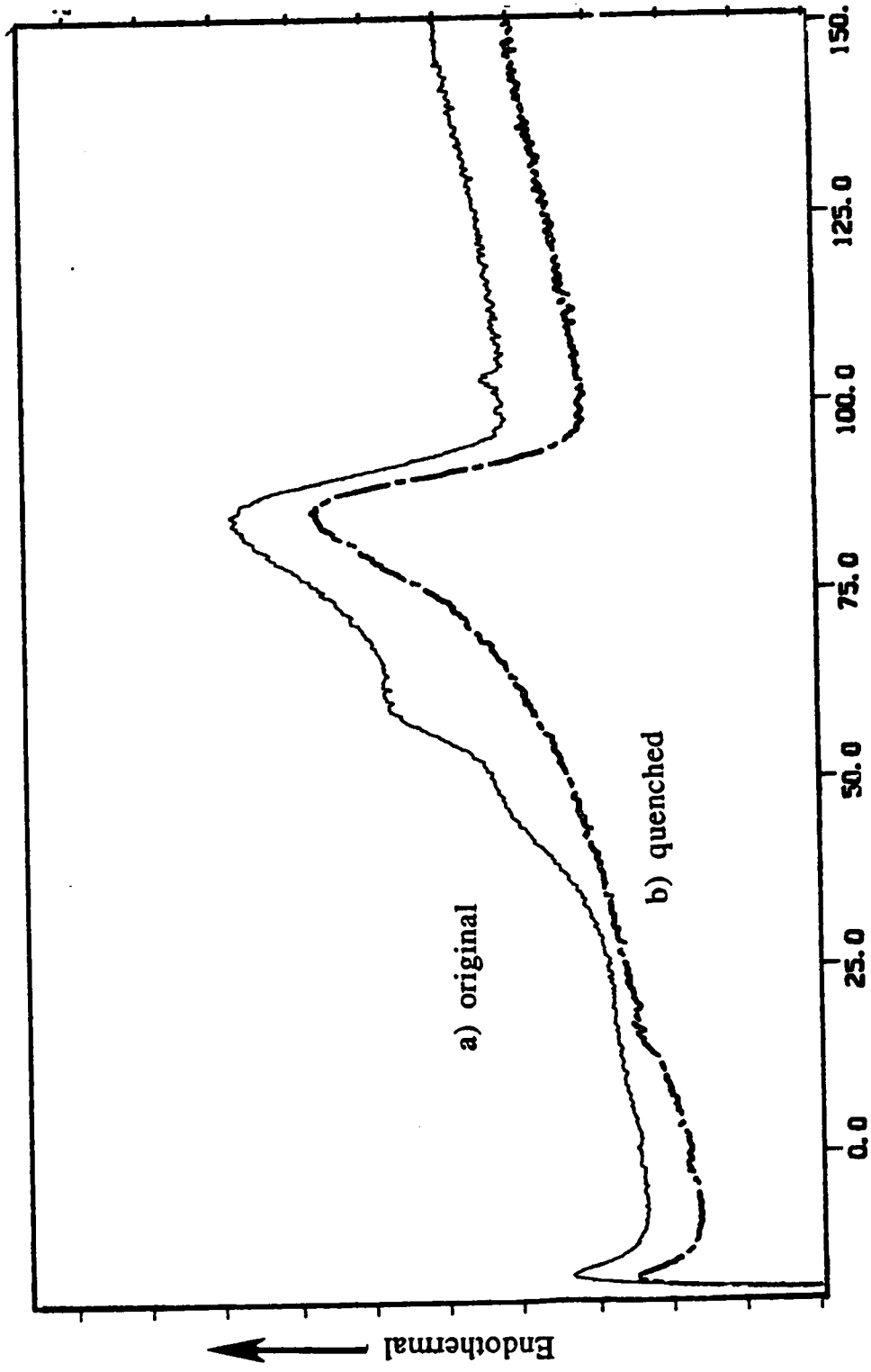


Figure 4.33: DSC endotherms for cable C1: a) original; b) quenched.

type of XLPE. The material has a fairly broad melting range which appears to begin around 10 °C with the major melting peak occurring at 80 °C. The presence of a shoulder at approximately 55 °C indicates some thermal treatment in the 40 to 50 °C range. The subtraction curve generated for the original insulation is shown in Figure 4.34 and indicates thermal treatments at temperatures of 45 °C and 30 °C. The 45 °C annealing is not as obvious on the subtraction curve as some of those examined previously. EPR is highly susceptible to ambient annealing such that the 30 °C annealing slightly masked that of 45 °C causing Td to be less apparent.

The annealing effects upon the melting curves of cable C1 are shown in Figure 4.35. Typical annealing behavior can be observed.

Figure 4.36 shows the subtraction curve corresponding to 50 °C annealing for 22 hours. The subtraction data are shown in Table 4.9. The annealing behavior for cable C1 is shown in Figure 4.37. The same general trends as found previously are observable in the data of cable C1.

4.4.4 Cable D1 [Anaconda]

Cable D1 is labelled as Flame Guard 1KV with triple strands of insulation and an outer jacket. The original and quenched endotherms are shown in Figure 4.38. There are two distinct melting regions located at approximately 20 °C and 80 °C. The original curve shows room temperature annealing at 25 °C manifest as separation of the lower peak into two distinct ones. The subtraction curve shown in Figure 4.39 confirms this and also shows heat treatment in the region of 60 °C.

The effects of annealing upon the DSC endotherms of cable D1 are shown in Figure 4.40. One can observe typical annealing behavior. This cable was studied extensively for annealing temperatures of 50, 60, and 70 °C. A typical subtraction curve obtained for 50 °C annealing is shown in Figure 4.41. The annealing data obtained from the subtraction curves are shown in Table 4.10.

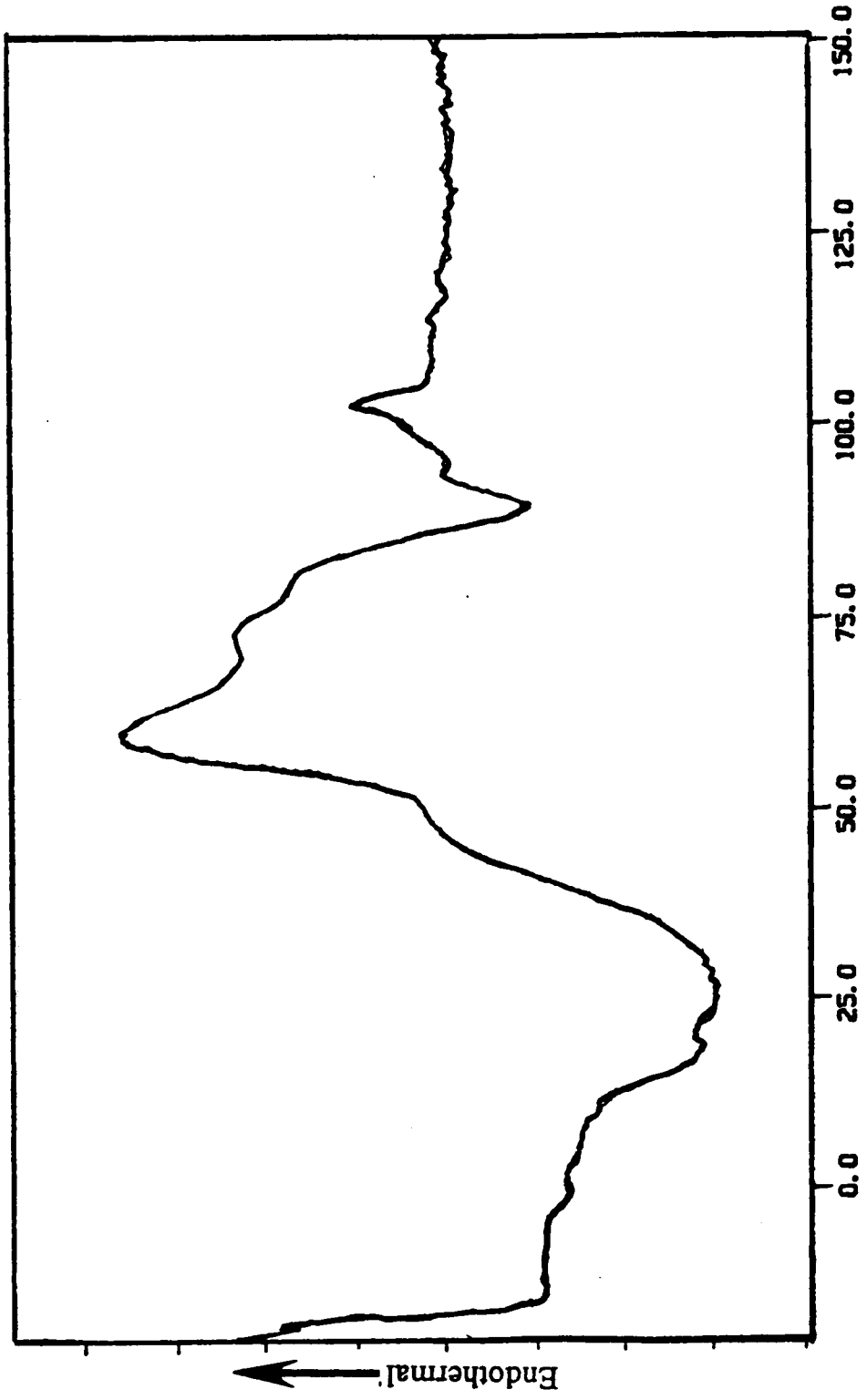


Figure 4.34: Original subtraction curve for cable C1.

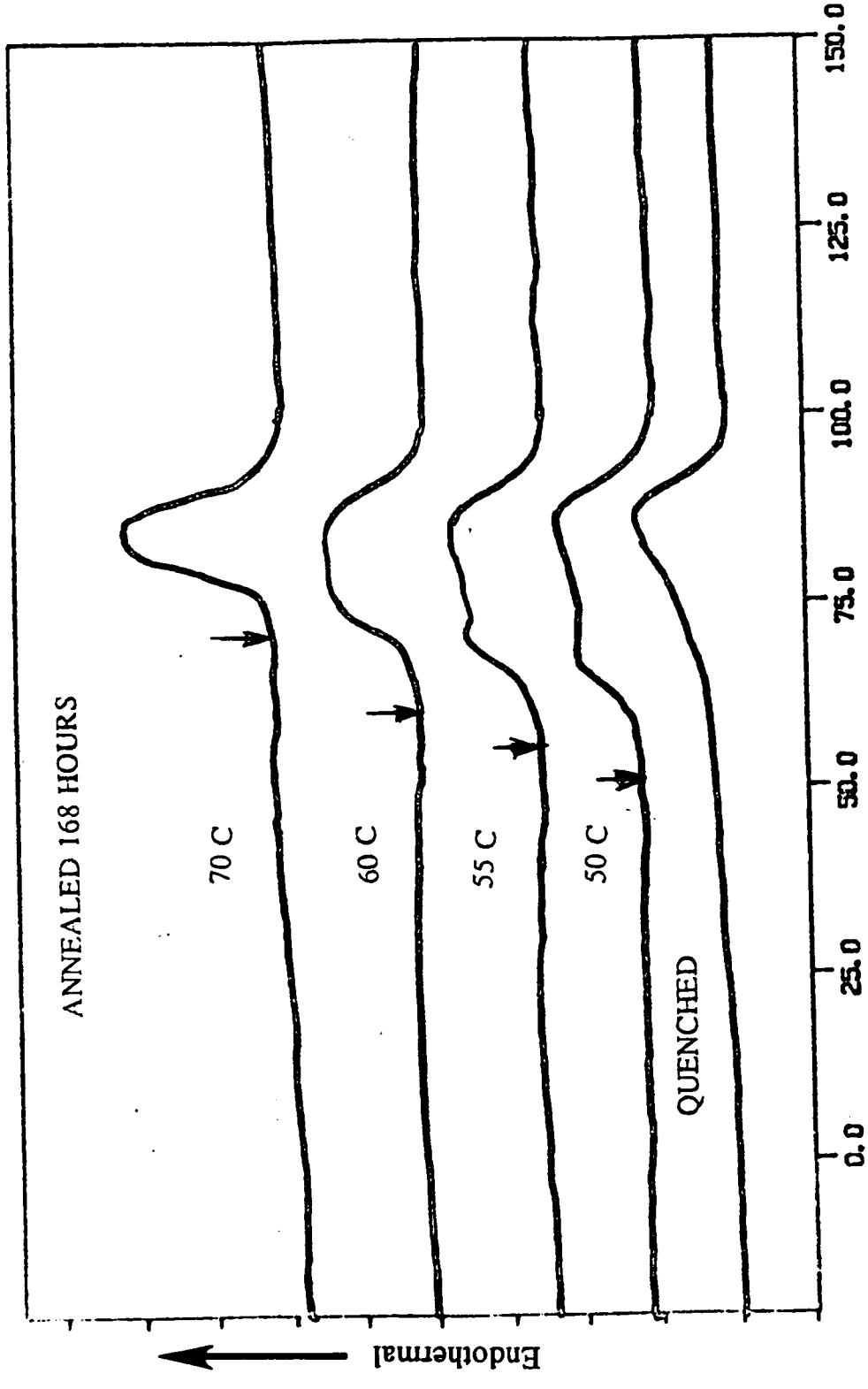


Figure 4.35: Annealing effects upon the "history erased" samples of cable C1.

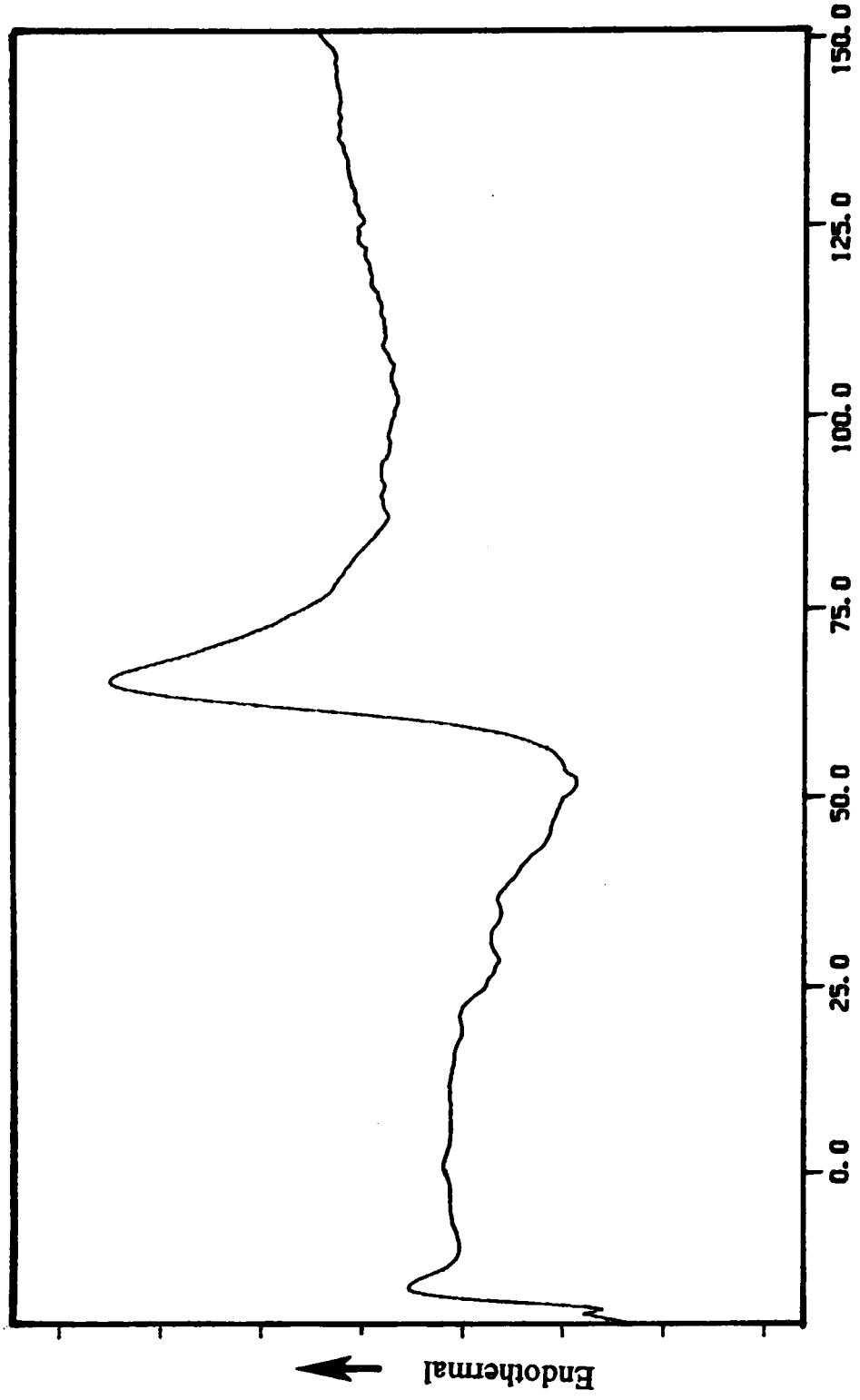


Figure 4.36: Typical subtraction curve for cable C1.

Table 4.9: Annealing data for cable C1.

	50 °C Annealing			55 °C Annealing			60 °C Annealing			70 °C Annealing		
Time	Td	Tp	Tb	Td	Tp	Tb	Td	Tp	Tb	Td	Tp	Tb
1	50.2	61.50	56.8	55.3	65.15	60.7	59.8	69.55	65.5	70.9	78.15	74.85
6	49.8	62.70	57.1	55.0	67.5	63.1	60.4	70.95	65.8	71.9	79.85	75.6
24	51.4	65.55	59.2	57.2	68.95	63.7	60.4	72.85	68.1	72.4	80.65	76.2
48	50.7	65.85	59.8	56.2	69.3	63.6	60.2	73.30	67.6	73.1	81.70	76.0
125	52.9	67.75	61.3	56.8	70.90	64..9	63.1	75.40	70.1	73.9	83.95	78.4
170	52.9	68.20	61.9	58.6	71.2	65.8	61.3	75.90	70.0	74.2	84.00	78.5
215	54.7	67.80	61.3				61.1	75.55	69.7	73.9	84.25	78.2
266	54.2	68.65	62.0	56.8	71.95	65.8	63.4	76.70	71.0	74.5	85.10	79.0
357	54.7	69.10	62.5	57.4	72.10	65.6	62.5	76.50	70.7	74.6	85.40	79.1
405	53.0	69.25	62.5	56.8	72.60	66.1	64.3	77.05	71.0	74.9	85.75	79.0
530	52.0	68.99	61.7	56.5	72.30	65.5	63.1	76.30	70.0	74.0	85.25	78.85

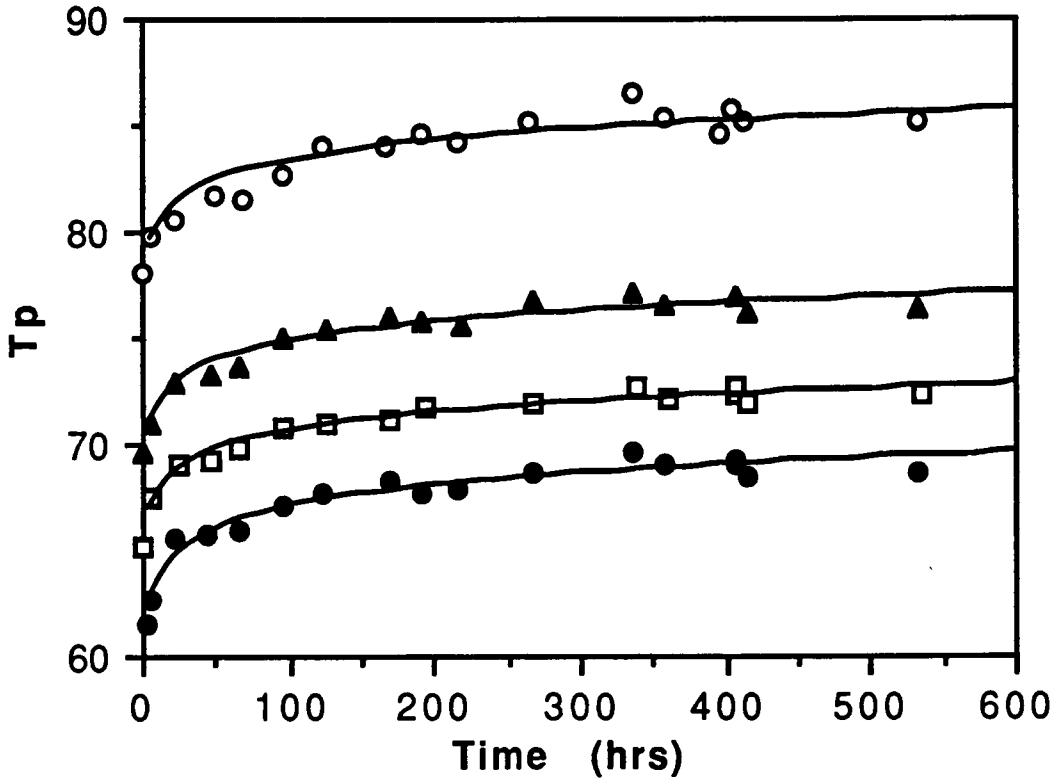


Figure 4.37: Tp versus time for cable C1. ● 50 C annealing;
□ 55 C annealing; ▲ 60 C annealing;
○ 70 C annealing.

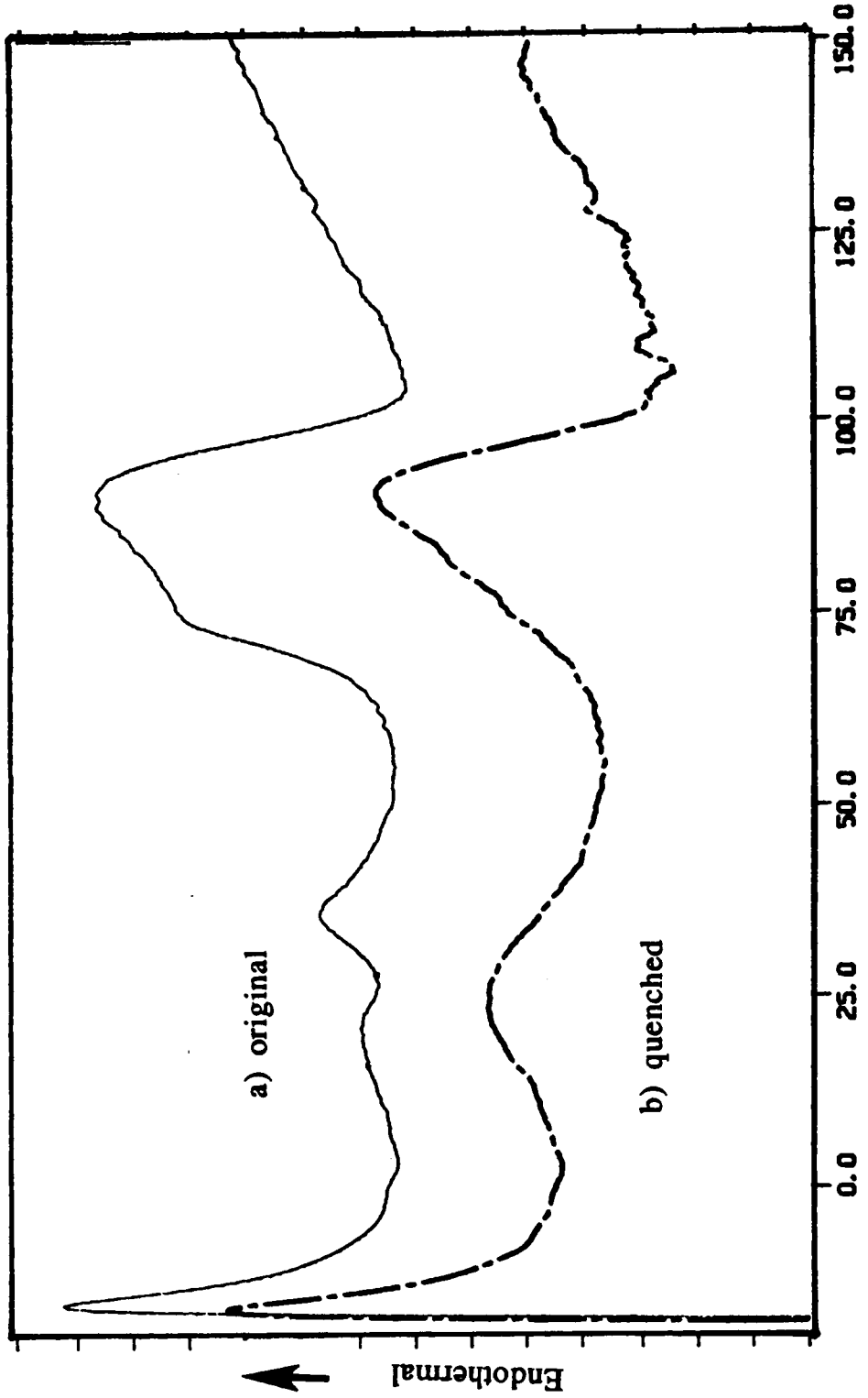


Figure 4.38: DSC endotherms for cable D1: a) original: b) quenched.

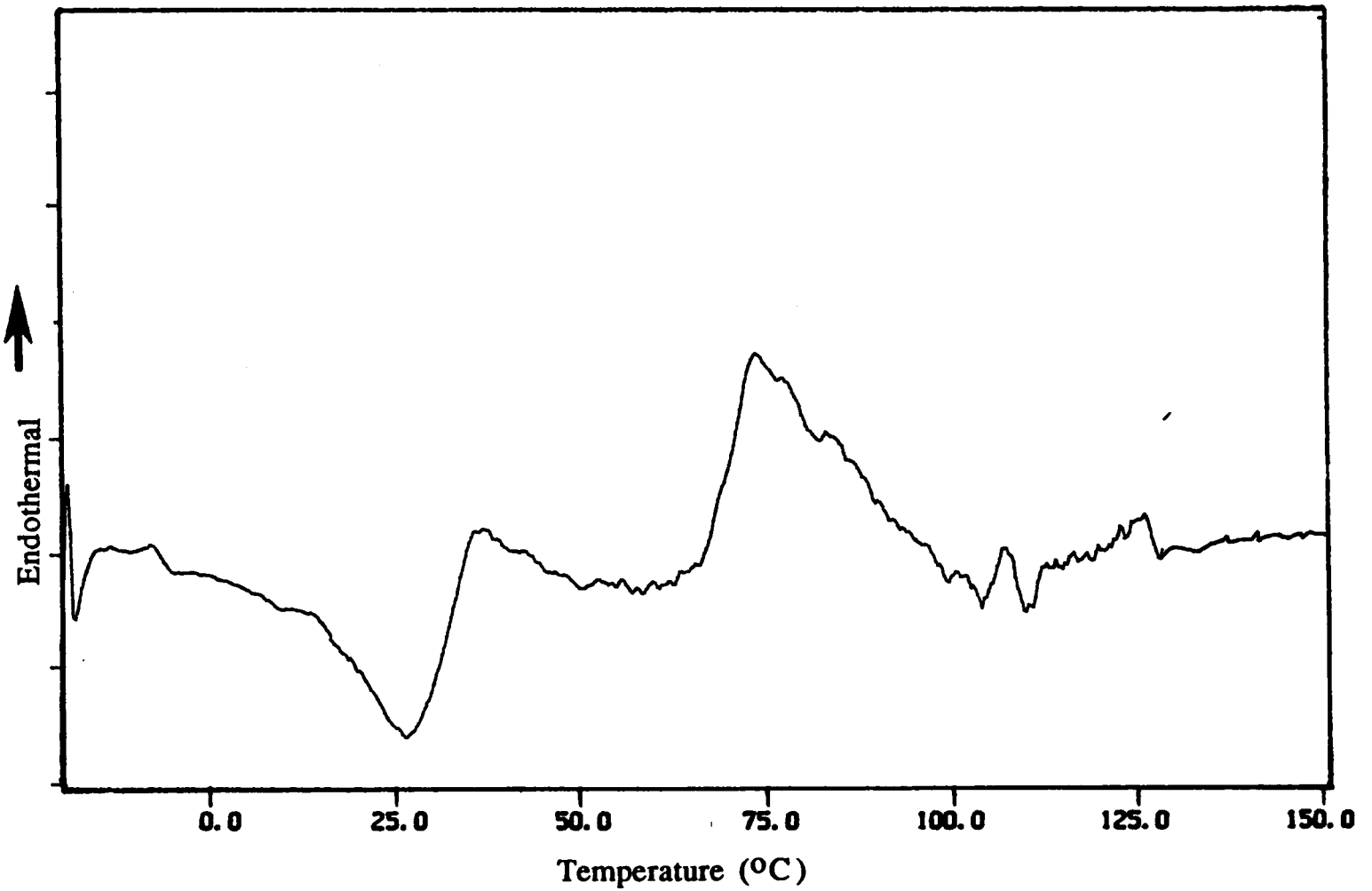


Figure 4.39: Subtraction curve for original cable D1.

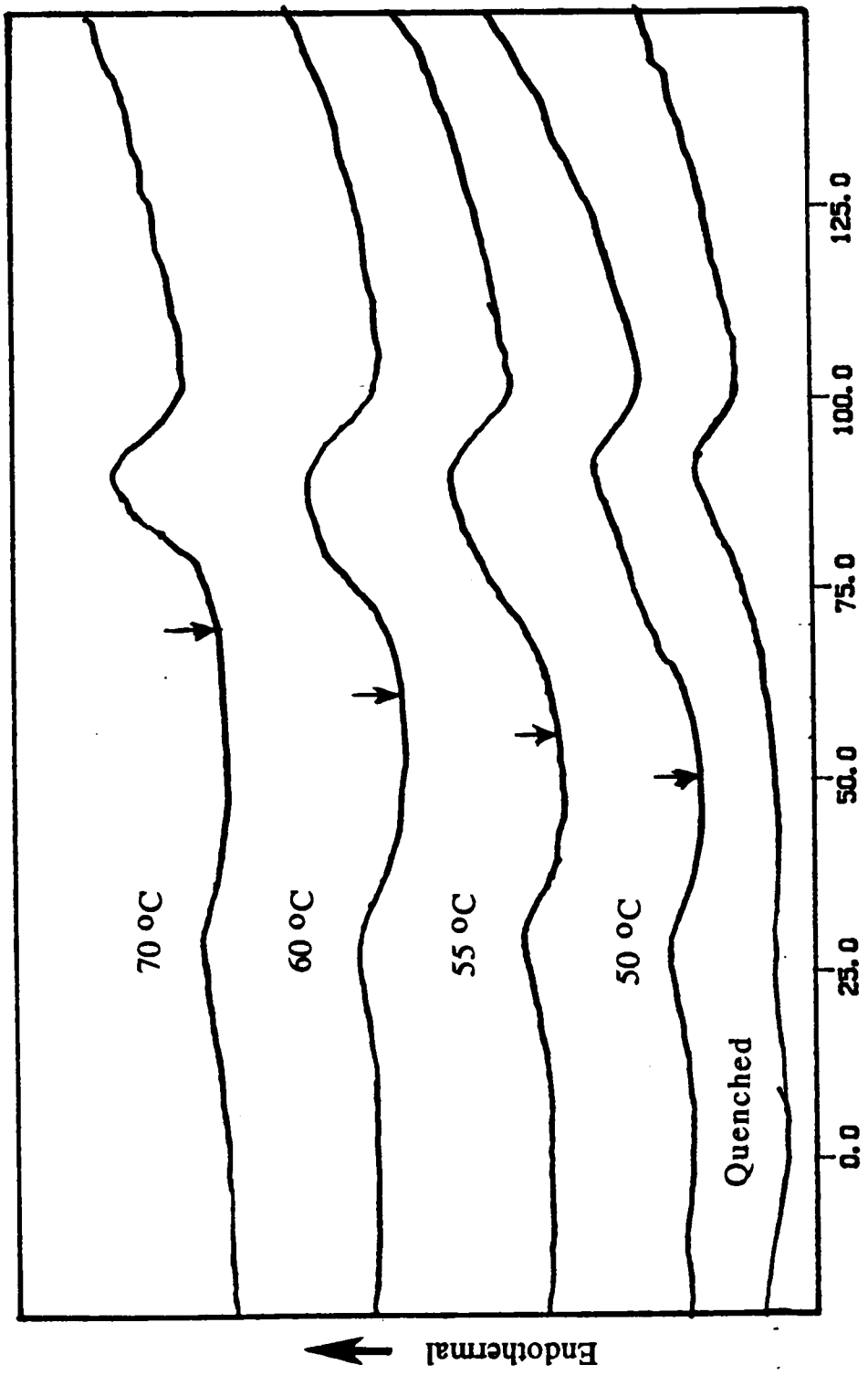


Figure 4.40: Annealing effects upon the history erased samples of cable D1.

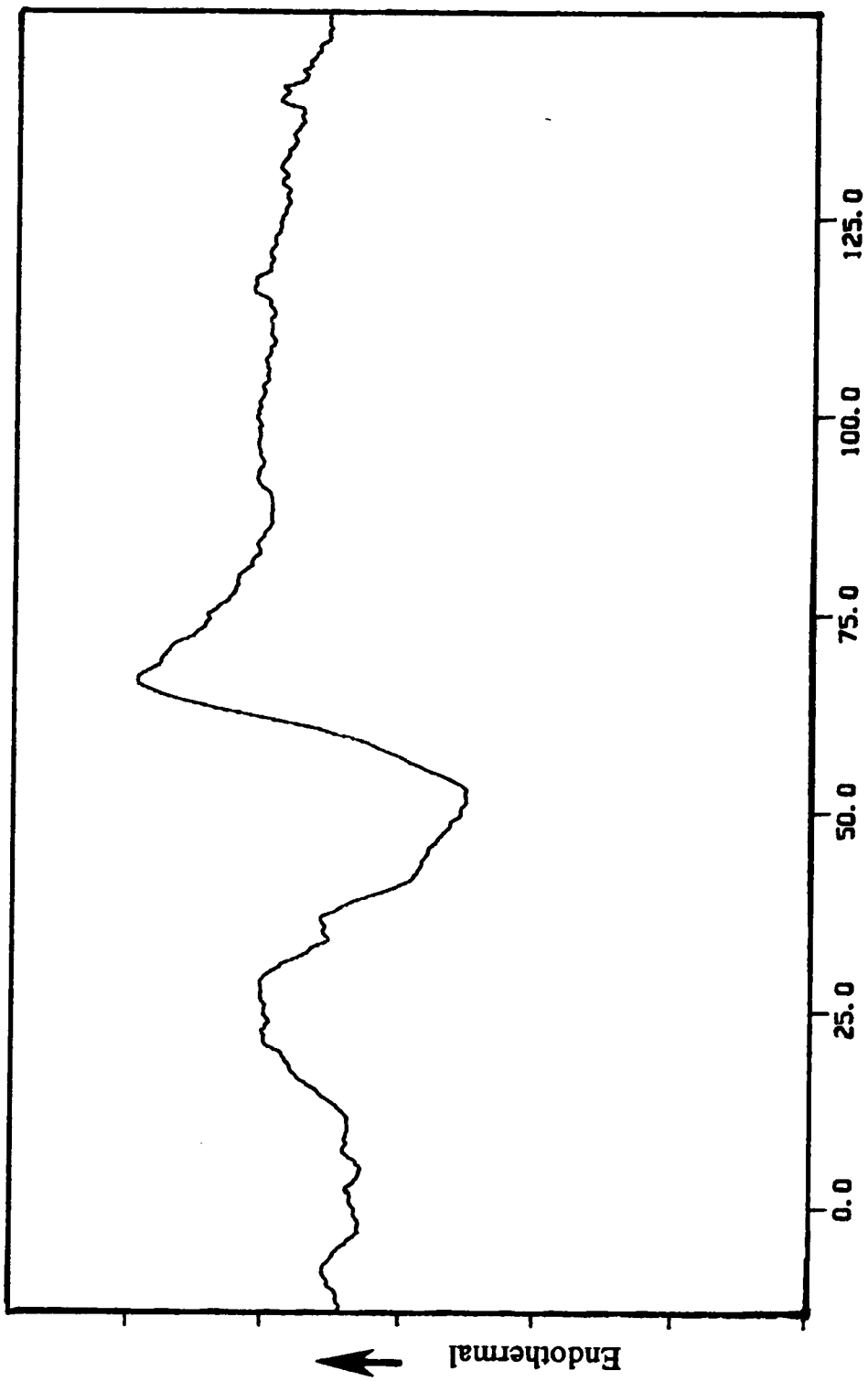


Figure 4.41: Typical subtraction curve for cable D1 showing 50 C annealing.

Table 4.10: Annealing data for cable D1.

	50 °C annealing			60 °C annealing			70 °C annealing		
Time	Tb	Tp	Td	Tb	Tp	Td	Tb	Tp	Td
3		64.00	52.0	66.7	72.10	61.0	76.0	79.75	70.1
12		67.73	51.6						
24		69.20	50.1	69.7	74.40	59.5	78.1	83.05	69.7
48	59.1	68.10	51.2	70.0	75.70	58.3	78.7	83.80	70.9
100	60.1	69.70	49.3	68.5	75.90	59.4	78.3	84.40	68.1
150	61.1	71.00	50.0	70.4	76.80	59.5	79.6	85.30	68.1
300	65.2	72.70	50.5	71.3	78.55	63.7	80.2	86.50	72.4
512		73.00	55.6	71.8	79.10	62.5	80.2	87.40	70.3
1060				74.2	84.10	61.0	82.6	88.6	69.7

The values for Td fluctuate about the actual annealing temperatures by about 2 °C. The plot of Tp versus time is shown in Figure 4.42 and is typical of what has been observed for the other cables and standard materials.

4.4.5 Cable B1 [Rockbestos]

This cable is labelled as 3/C 600V Firewall III, TC and contains three multi-colored strands of insulation with an outer jacket. This cable shows the most complex melting behavior in its original state. The endotherms for cable B1 are shown in Figure 4.43. One can observe three distinct melting peaks at 120 °C, 110 °C, and 100 °C. The lower temperature melting peak contains a shoulder which indicates thermal history around 60 °C. The original cable has also been exposed to temperatures of approximately 110 °C as well as 118 °C. The subtraction curve shown in Figure 4.44 shows three distinct loss peaks at 60, 110, and 115 °C.

The quenched endotherm in Figure 4.43 shows melting behavior typical of a blended material with two relatively distinct melting regions located at 100 o C and about 120 °C. The quenched curve also shows melting beginning below 40 °C. The lower melting curve is very typical of XLPE and the high temperature peak is most likely due to XHDPE. The two uncrosslinked polymers were probably blended and cross-linked together during manufacture.

In order to best characterize the annealing behavior of this insulation over a wide spectrum of annealing temperatures, annealing studies were carried out at temperatures of 100, 110, and 120 °C in addition to 50, 55, 60, and 70 °C. The effect of the lower annealing temperatures upon the general features of the history erased endotherms is shown in Figure 4.45. This figure shows typical behavior with the generation of a shoulder about 10 °C above the annealing temperature. As the annealing temperature is increased the shoulder is shifted upward and tends to sharpen

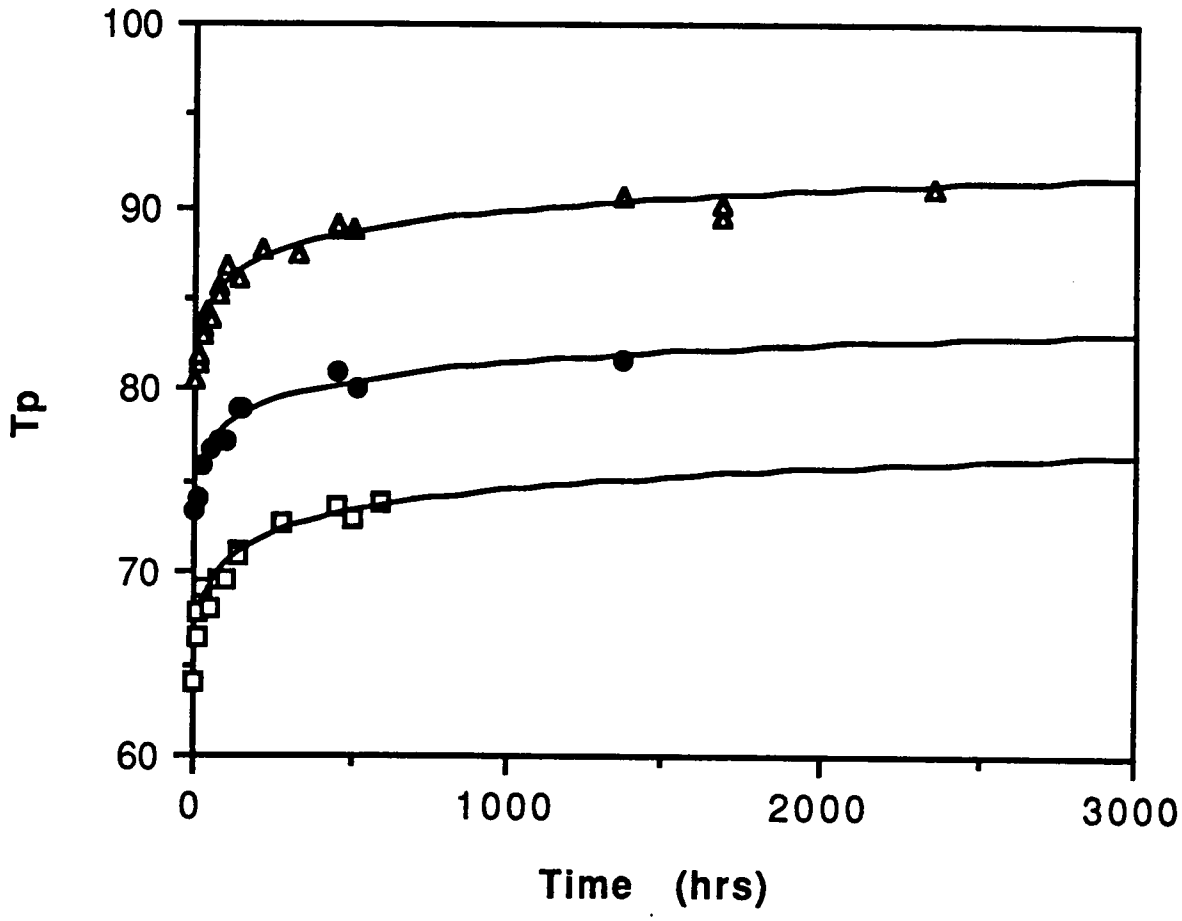


Figure 4.42: Tp versus time for cable D1. □ 50 C annealing; ● 60 C annealing; Δ 70 C annealing.

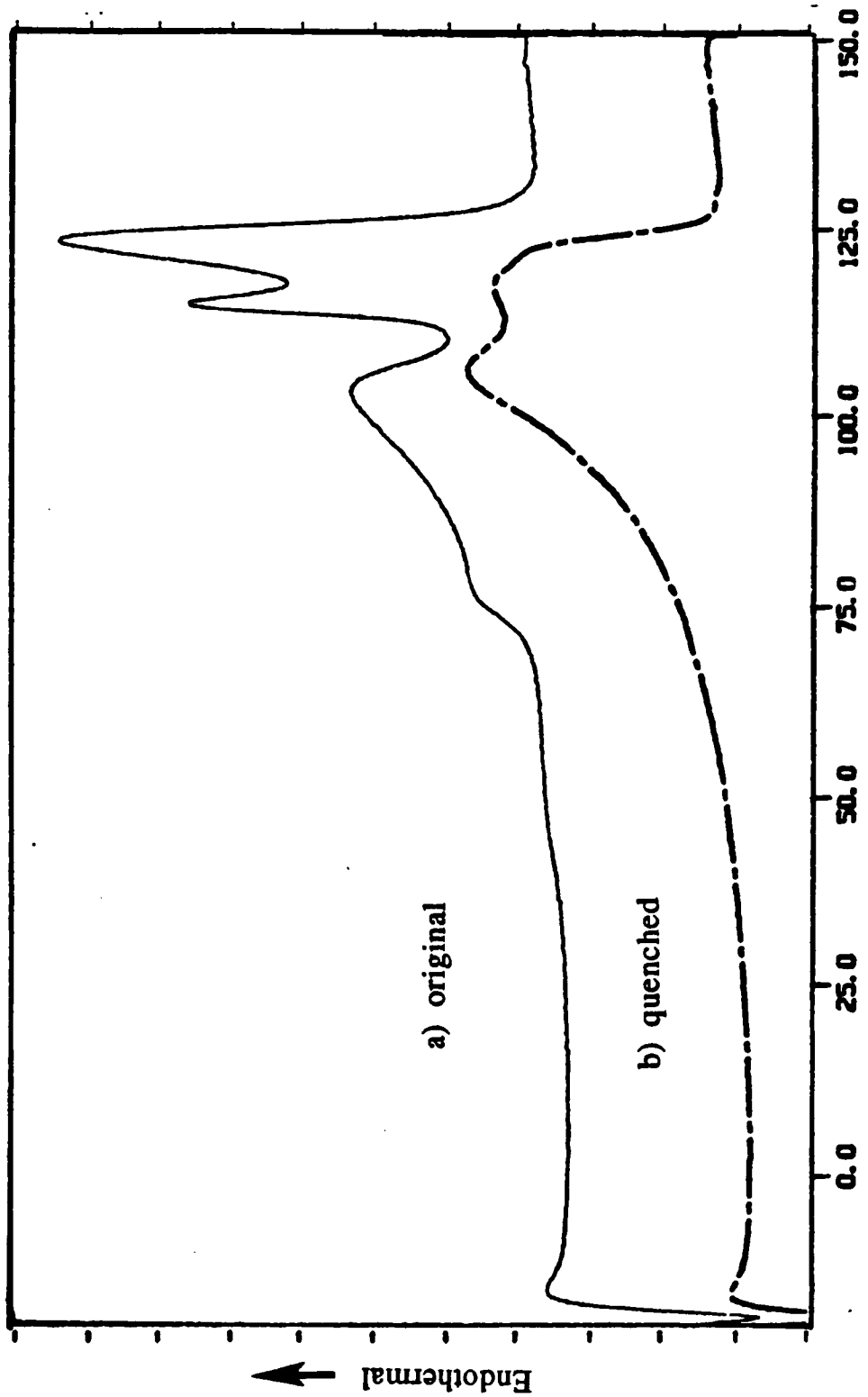


Figure 4.43: DSC endotherms for cable B1: a) original; b) quenched.

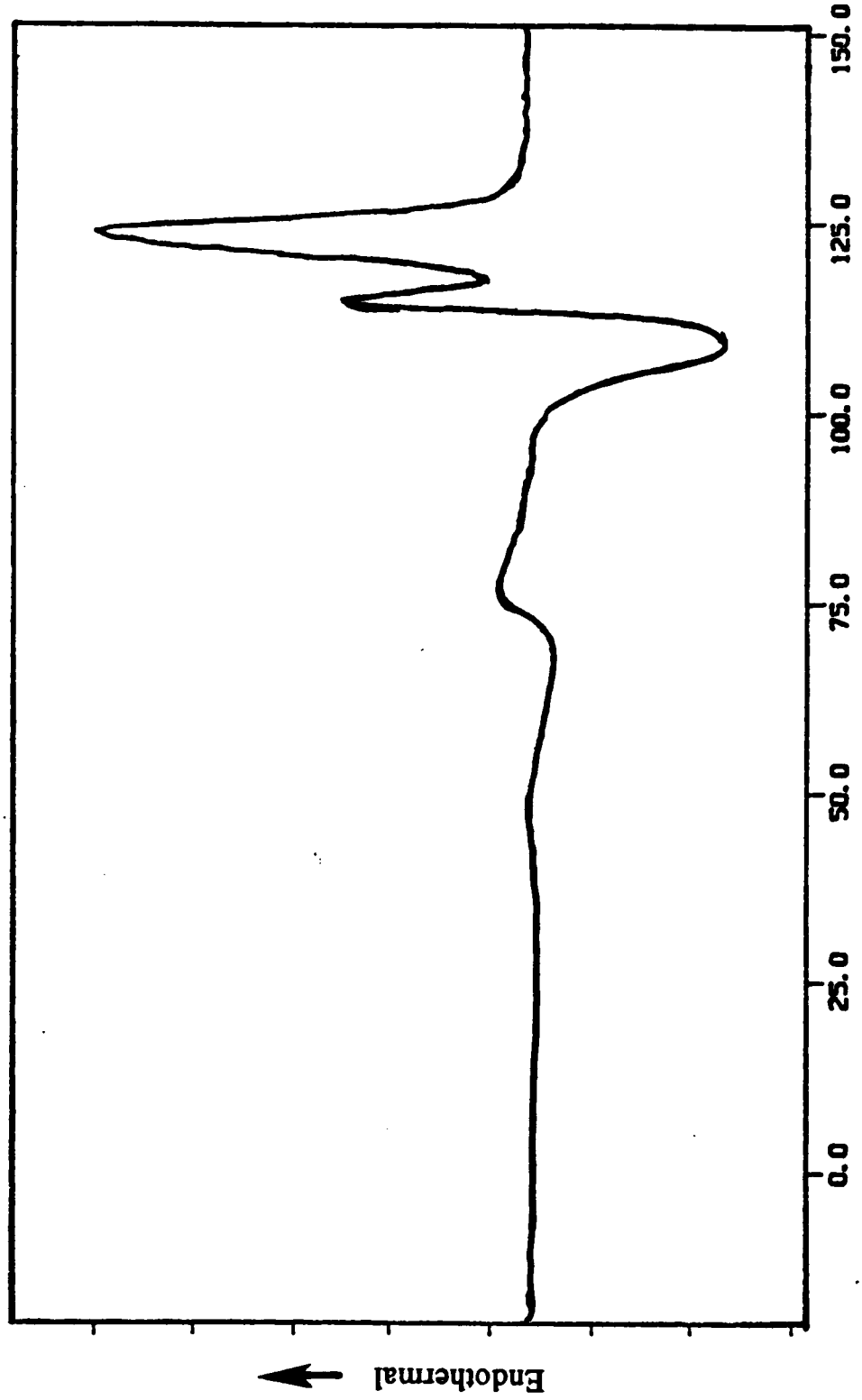


Figure 4.44: Original subtraction curve of cable B1.

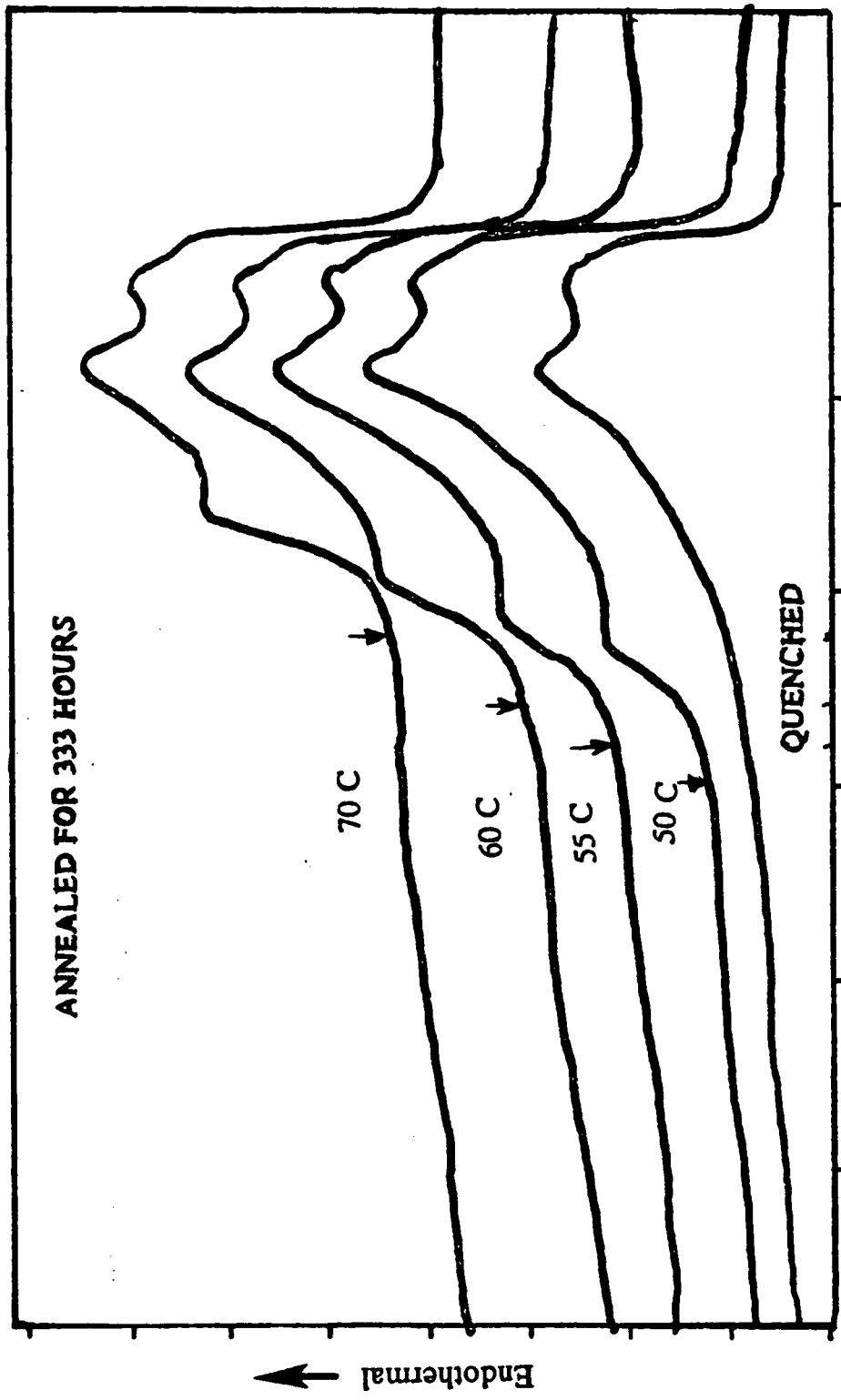


Figure 4.45: Low temperature annealing effects upon the melting behavior of cable B1.

slightly. The melting peak located at 100 °C also appears to sharpen with increasing annealing temperature but the high temperature melting peak remains essentially unchanged. The effect of high temperature annealing upon the melting curves is quite different and is shown in Figure 4.46. One can see that 100 °C annealing results in the generation of a sharp peak located about 105 °C. Only a slight hump is noticeable below the annealing temperature which implies that the majority of the XLPE portion of the insulation is able to recrystallize. The upper melting region (120 °C) still remains unchanged. As the annealing temperature is increased to 110 °C one can notice the appearance of a fairly sharp peak located at 90 °C which represents the XLPE which crystallized upon cooling from the annealing temperature. For 110 °C annealing, the upper curve shows the development of a very sharp peak located at 115 °C. Annealing at 120 °C results in an increase in the size of the peak at 90 °C which is an indication that more of the material is unable to recrystallize at the elevated annealing temperature. The peak generated by 110 °C annealing is shifted up to 125 °C and appears much sharper.

A subtraction curve typical of those generated for the lower annealing temperatures is shown in Figure 4.47. The subtraction curves generated by elevated annealing temperatures are shown in Figure 4.48. All the subtraction curves contain the same essential features for following the effects of annealing. The data obtained from the subtraction curves are shown in Table 4.11. The values obtained for the position of the loss peak for annealing between 50 and 70 °C show no major fluctuations and are generally within about 3 °C of the annealing temperature. For annealing at the higher temperatures one can see that the values are independent of annealing time as well. For 100 °C annealing the values of Td are all within 1 °C of the actual annealing temperature and for 110 and 120 °C annealing the values are about 2 to 3 °C lower. The position of the gain peak, Tp, for the various subtraction curves is plotted against time in Figure 4.49.

Samples of the original cable were annealed at 70 °C to

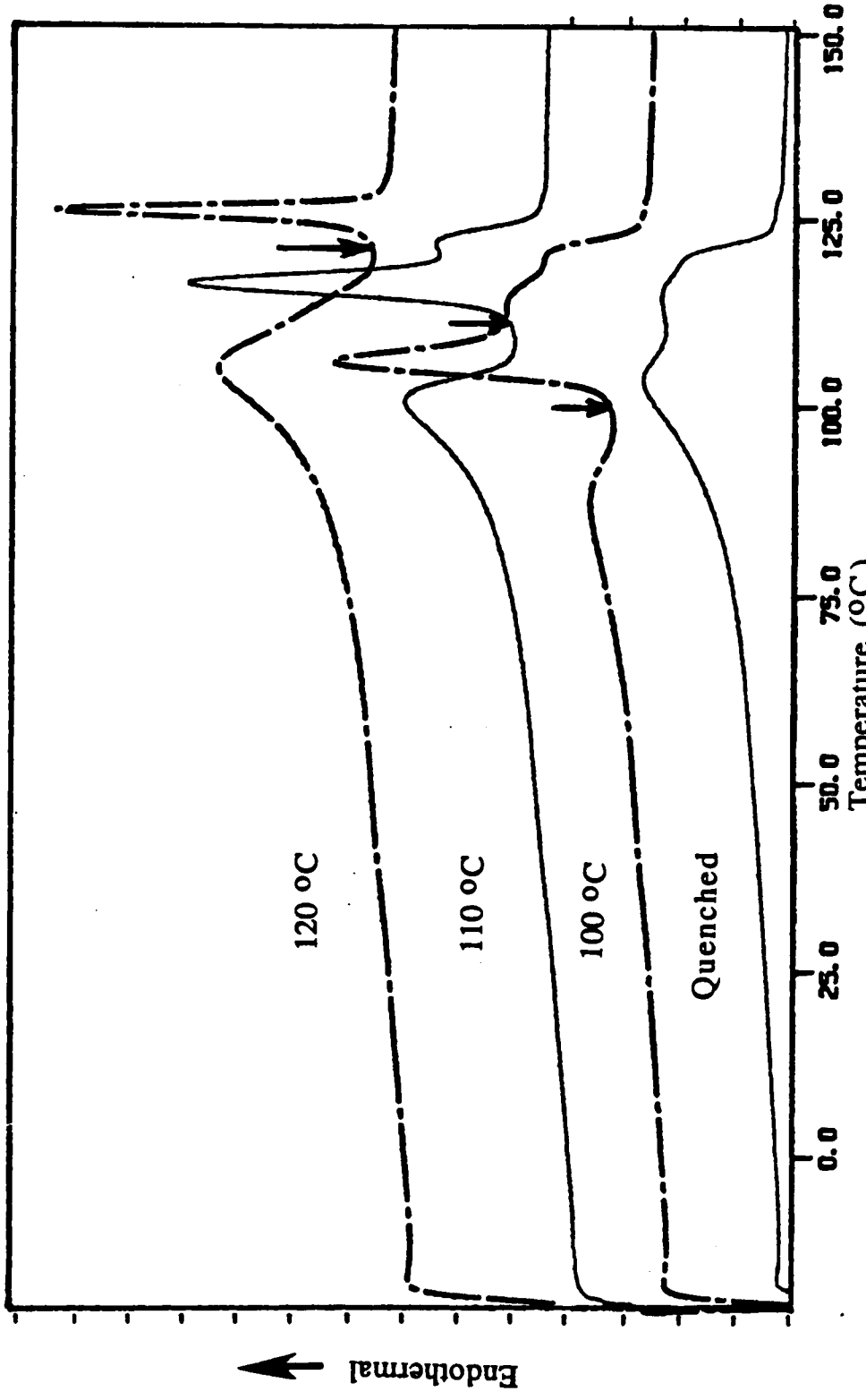


Figure 4.46: High temperature annealing effects upon the melting behavior of cable B1.

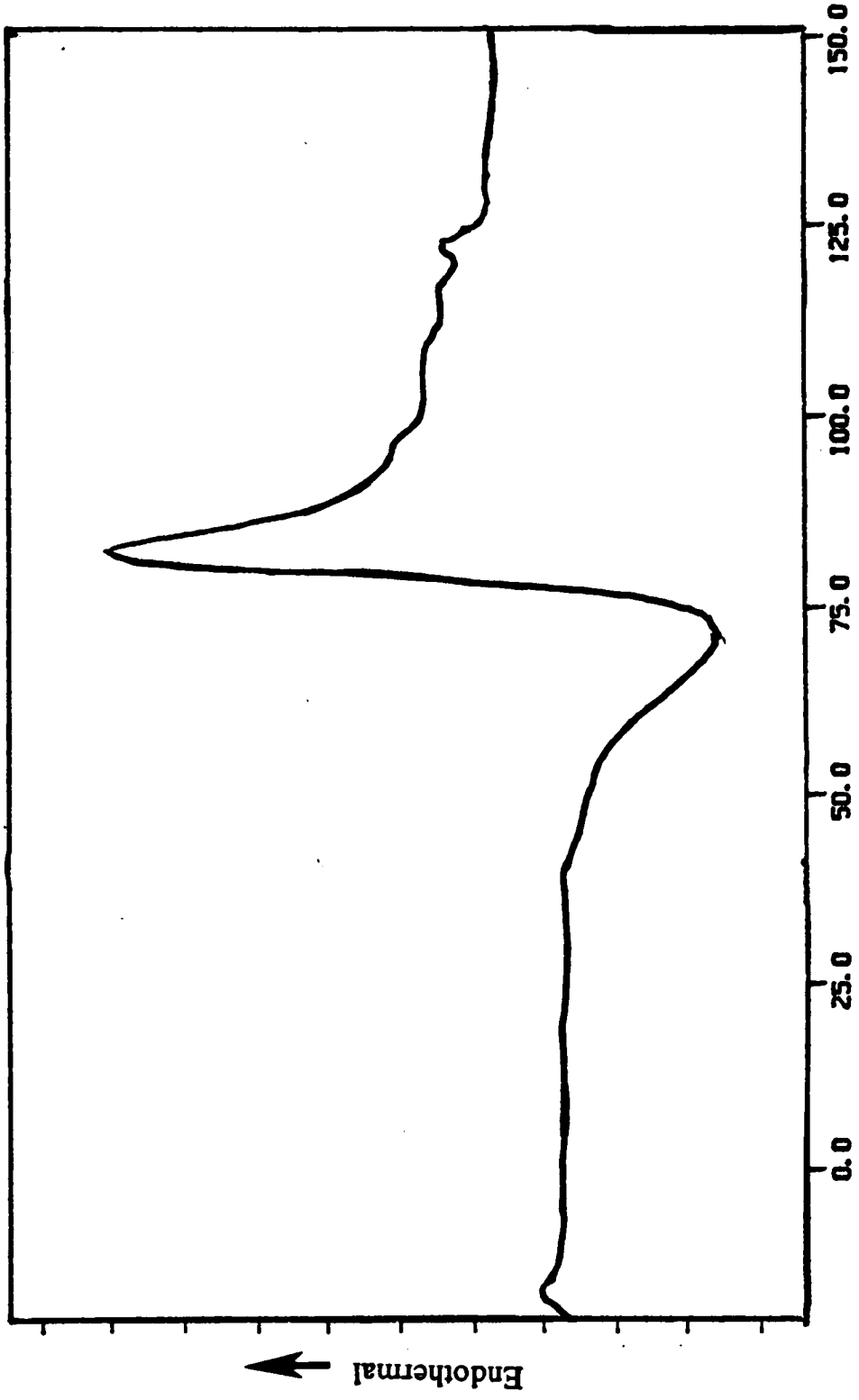


Figure 4.47: Typical subtraction curve for cable B1 showing 70 C annealing.

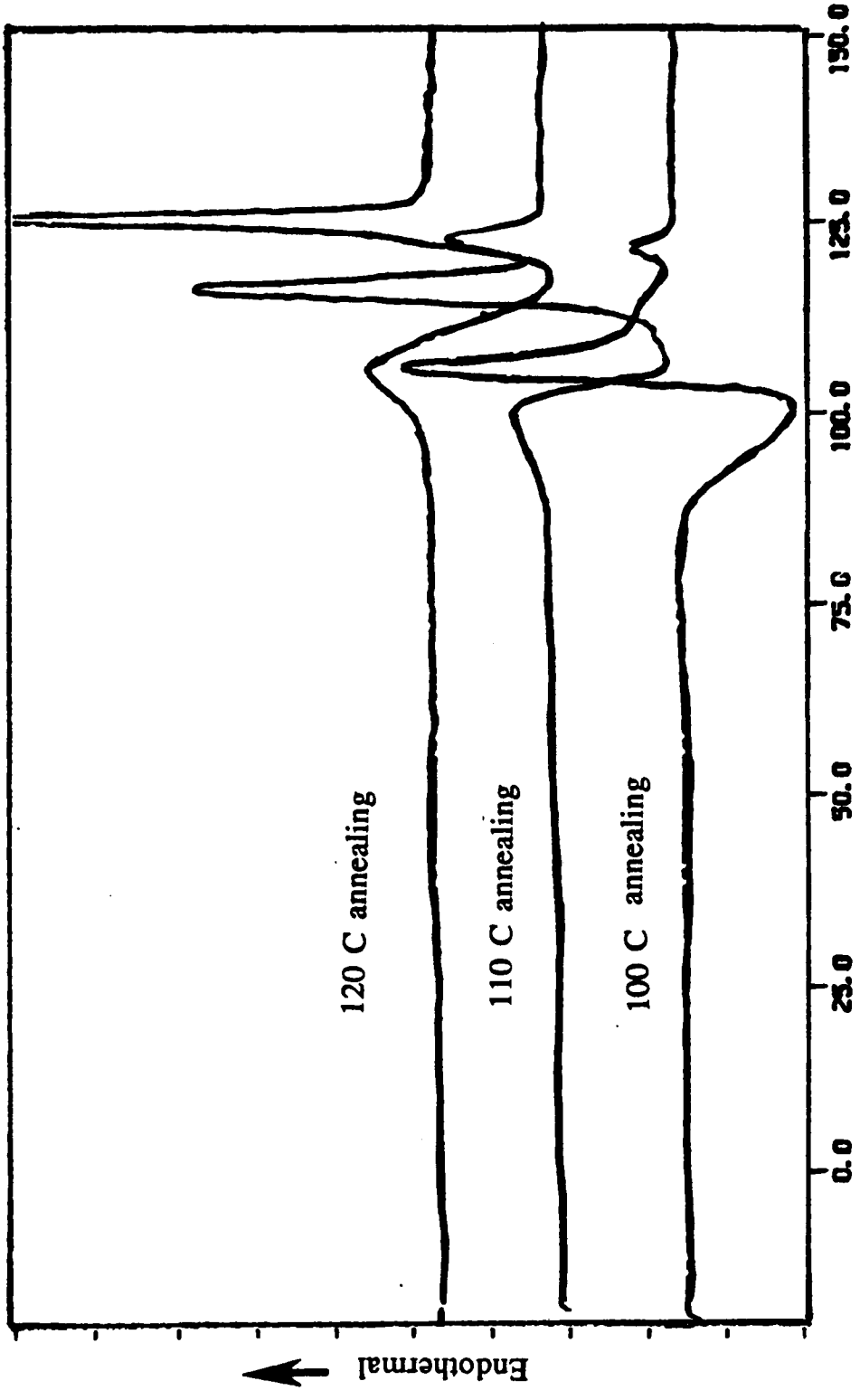


Figure 4.48: Subtraction curves for high temperature annealing of cable B1.

Table 4.11: Annealing data for cable B1.

	50 °C Annealing			55 °C Annealing			60 °C Annealing			70 °C Annealing		
Time	Td	Tp	Tb	Td	Tp	Tb	Td	Tp	Tb	Td	Tp	Tb
1	49.6	61.00	56.2	53.8	64.00	58.6	58.9	68.65	64.3	70.4	78.95	75.4
6	49.6	62.5	56.8	54.4	67.15	61.0	59.8	72.25	66.6	70.4	80.4	76.0
24	52.15	66.2	59.5				61.0	73.45	67.6	70.6	81.8	75.3
48	51.1	66.1	59.5	55.3	69.85	60.5	59.8	74.95	68.5	71.0	82.85	77.7
200				56.8	71.60	64.6	62.2	76.0	70.0	72.4	84.25	79.1
245	51.7	68.05	60.1	57.4	71.65	64.0	61.6	76.75	71.9	71.5	84.55	79.0
350	52.3	68.35	60.1	56.5	72.70	66.1	60.1	77.65	73.0	72.4	85.40	79.1
430	52.9	69.25	60.7	56.8	72.85	65.5	62.5	77.95	70.1	73.9	85.90	80.5
500	52.7	69.15	61.3	56.3	73.15	65.3	62.5	77.35	72.7	73.0	85.45	79.9

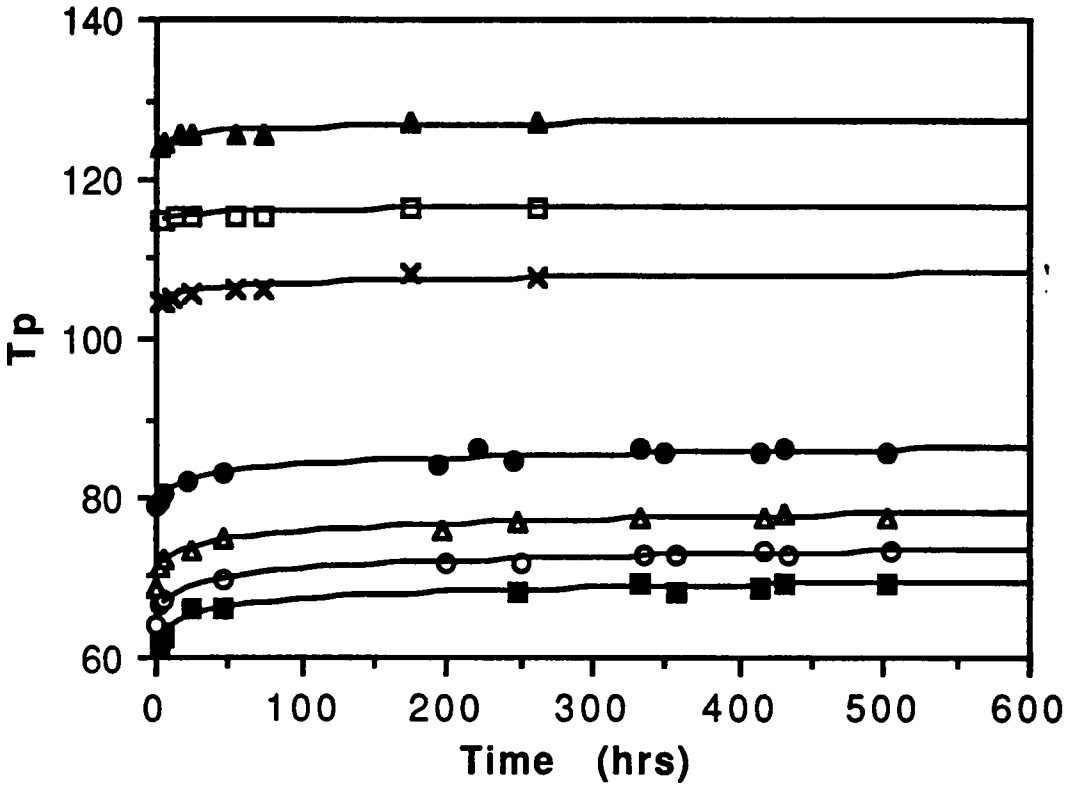


Figure 4.49: Tp versus time for cable B1. ■ 50 C annealing; o 55 C annealing; ▲ 60 C annealing; ● 70 C annealing; X 100 C annealing; □ 110 C annealing; ▲ 120 C annealing.

determine if these samples behaved similar to the history erased samples. An original endotherm and subtraction curve showing 70 °C annealing is shown in Figure 4.50 and the plot of Tp versus time for both original and history erased samples annealed at 70 °C is shown in Figure 4.51. One can observe that both samples appear to anneal in very similar fashions.

In order to attempt to characterize the multiple annealing behavior of this particular cable, original samples were annealed at a temperature of 98 °C for approximately 1.6 hours, allowed to cool, then annealed at temperatures of 70 and 80 °C. The resulting endotherms are shown in Figure 4.52. The position of the gain peak is shown to increase with annealing time in Figure 4.53.

4.5. Factors Effecting the Subtraction Curve

The subtraction technique which has been developed provides a means of estimating the thermal history of a semi-crystalline polymeric material. However, the annealing behavior of these materials presented has been studied under controlled laboratory conditions where most of the variables are known. In practice, a particular piece of insulation might experience cycling of temperatures, radiation exposure, degradation, multiple annealing, and annealing where fairly large temperature fluctuations are present. The effect that these types of factors have upon the results of the subtraction technique remain to be fully characterized. However, the effects of some of theses variable have been examined briefly.

4.5.1 Multiple Annealing

In order to determine if the thermal history can still be detected from the subtraction curve for multiple annealing temperatures samples of XLPE and EPDM were subjected to several consecutive temperature treatments.

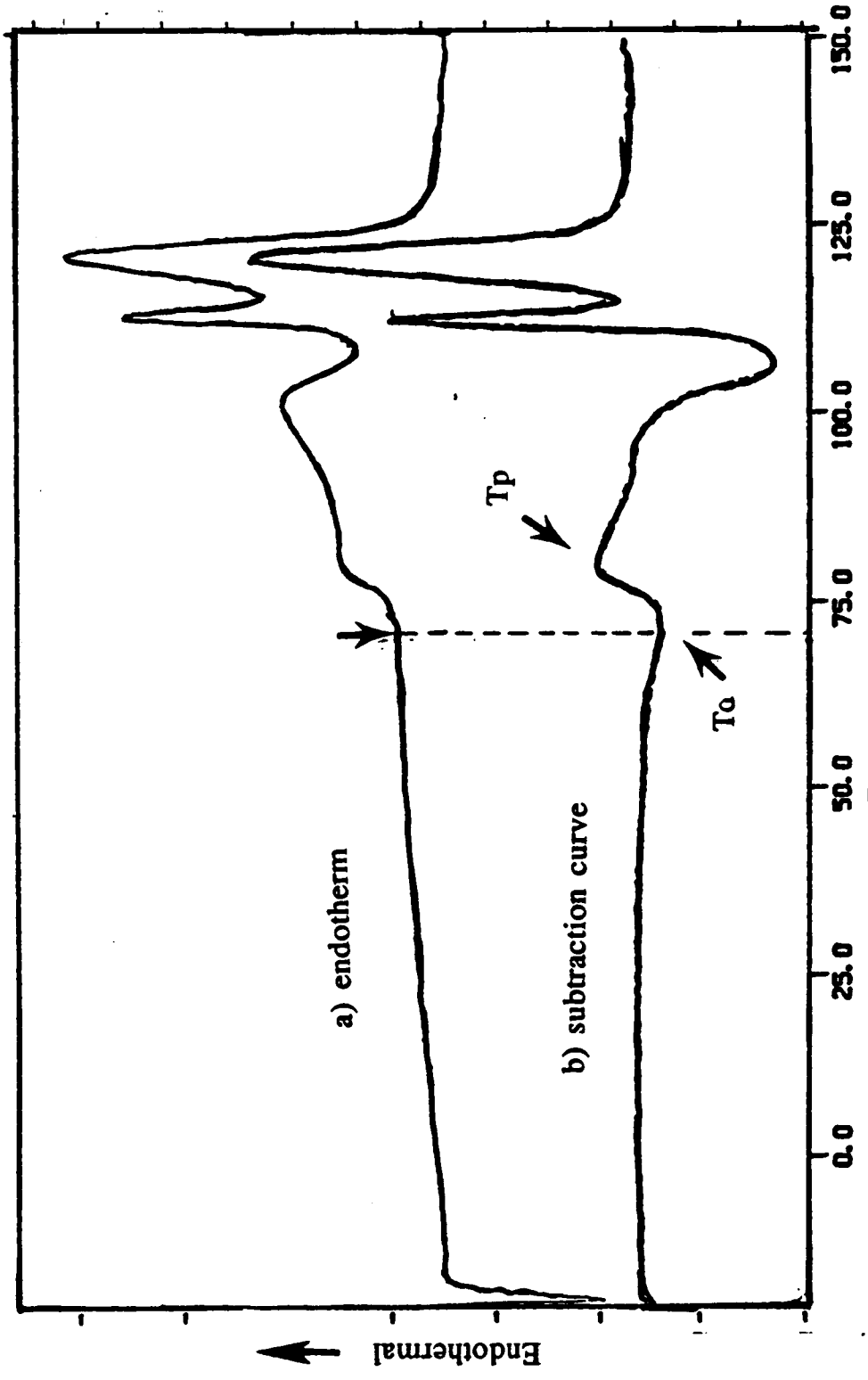


Figure 4.50: Original cable B1 annealed at 70 C: a) annealed endotherm; b) subtraction curve.

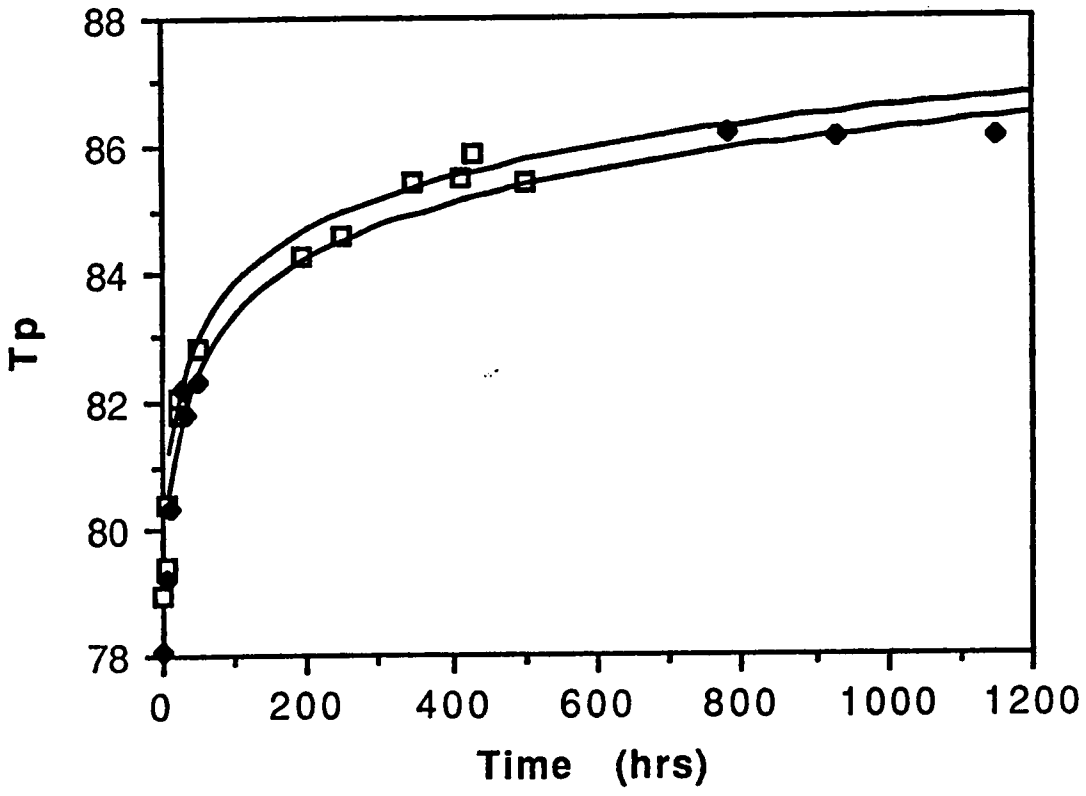


Figure 4.51: Tp versus time for 70 C annealing of original and "history erased" samples of cable B1. ● original; □ history erased.

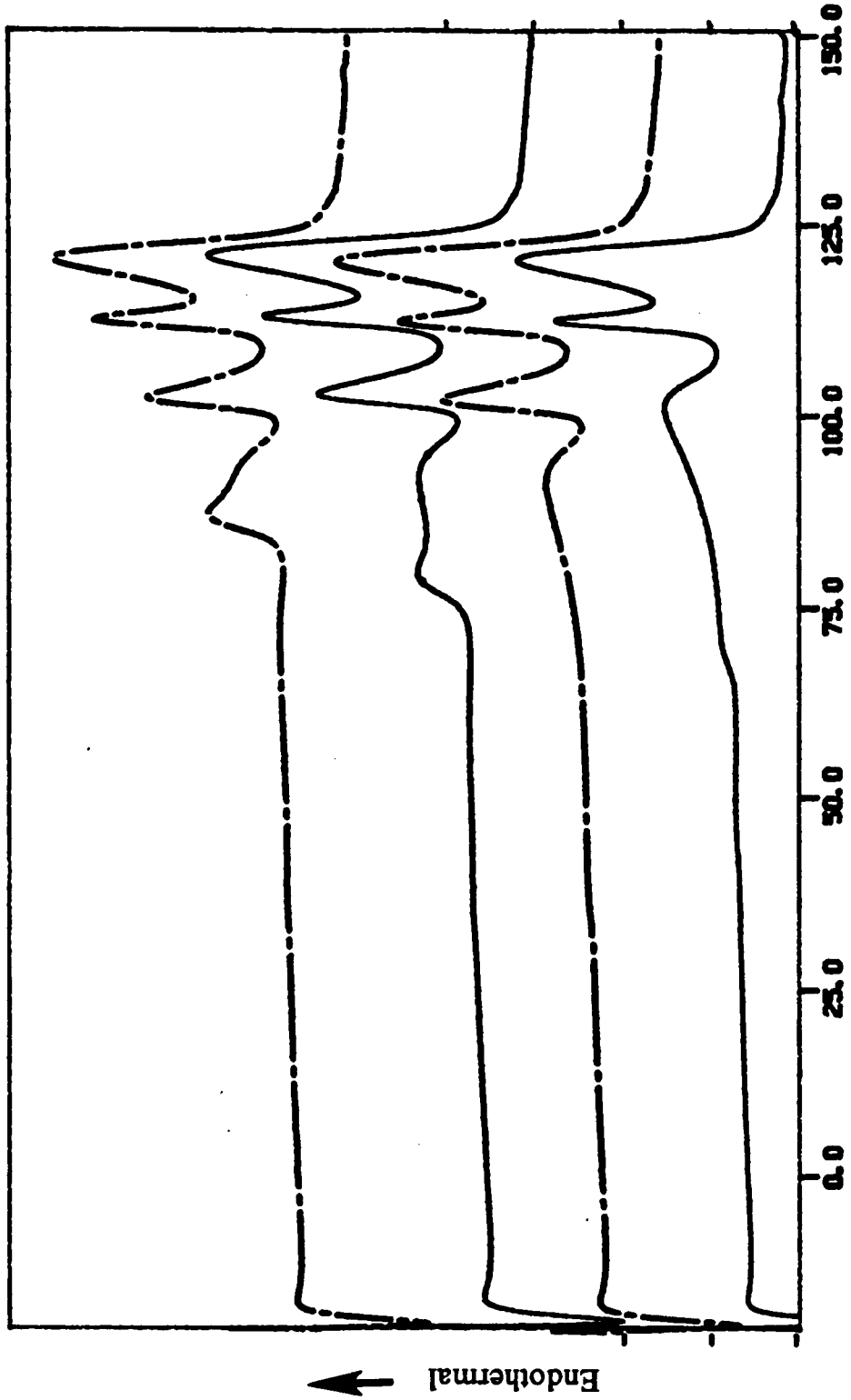


Figure 4.52: Effects of annealing at 98 C followed by 70 or 80 C annealing upon the original endotherms of cable B1.

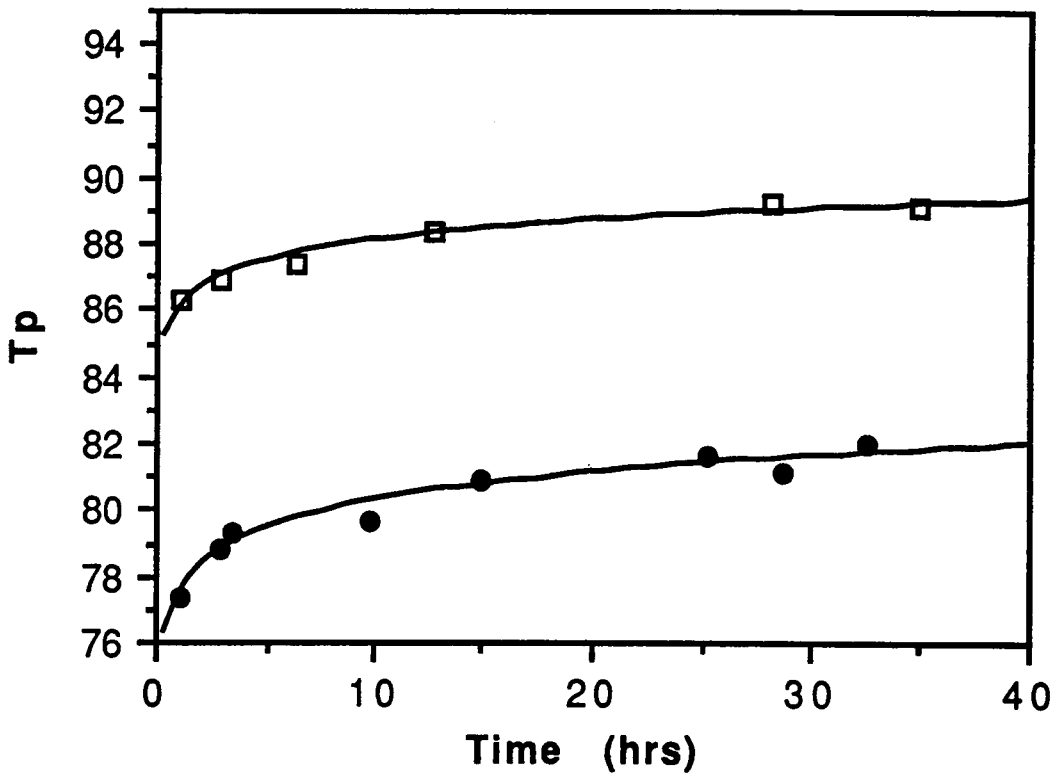


Figure 4.53: Tp versus time for original cable B1 annealed at 98 C followed by 70 or 80 C annealing. ●, 70 C annealing; □, 80 C annealing.

Figure 4.54 shows the DSC endotherm and resulting subtraction curve for a sample of XLPE annealed at temperatures of 70 °C for 10 hours, 60 °C for 40 hours, 50 °C for 233 hours, and 35 °C for 100 hours. The annealings below that of 70 °C are barely able to be discerned on both the endotherm and subtraction curve. The annealing at 35 °C is more detectable for those temperatures below 70 °C. The position of the loss peak for the 70 °C annealing is 73 °C and that for the 35 °C annealing is 41.2 °C. The position of the loss peak still predicts the 70 °C annealing but that of the 35 °C is about 6 °C higher than the actual annealing temperature. Referring back to Table 4.2, one can notice that values for the position of the loss peak show an elevated trend above 35 °C, but only by about 3 °C.

The position of the gain peak for the 70 °C annealing is approximately 81.65 and for the 35 °C annealing, 48.4 °C.

The effect of annealing at 70 °C for 50 hours and 50 °C for 240 hours upon the endotherm and subtraction curve for another sample of XLPE is shown in Figure 4.55. One can notice that the 70 °C annealing shows clearly upon both the endotherm and the subtraction curve, as expected and the 50 °C annealing is also more obvious than for annealing scheme of Figure 4.54. The position of the loss peaks for the 70 and 50 °C annealing are 73 and 54 °C, respectively. The corresponding gain peak positions are 83.7 and 63.7 °C, respectively.

The effects of multiple annealing were also explored for samples of EPDM. The effects of annealing at 70 °C for 24 hours, 50 °C for 24 hours, and 25 °C for 24 hours upon the endotherm and subtraction curve of EPDM is shown in Figure 4.56. The annealing produces discernable effects at all three temperatures with the peaks becoming more pronounced as the annealing temperature is lowered. The positions of the loss peaks on the subtraction curves are 30.2, 55.1, and 71.4 °C, corresponding to 25, 50, and 70 °C annealing, respectively. The positions of the gain peaks were found to be 42.25 °C, 64.0 °C, and 81.6 °C, respectively.

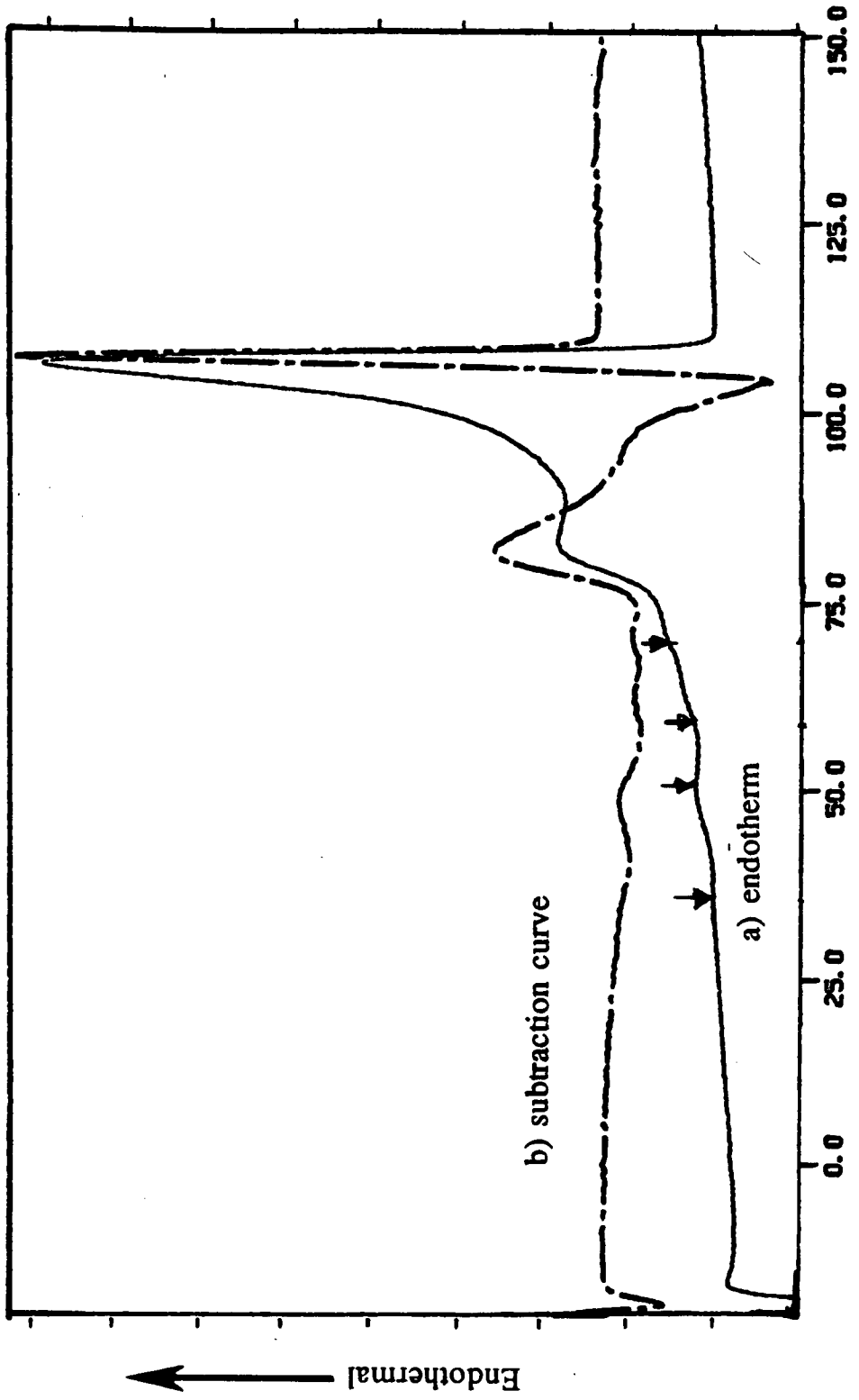


Figure 4.54: DSC endotherm and subtraction curve for multiple annealing of XLPE at 70, 60, 50, and 35 C; a) endotherm; b) subtraction curve.

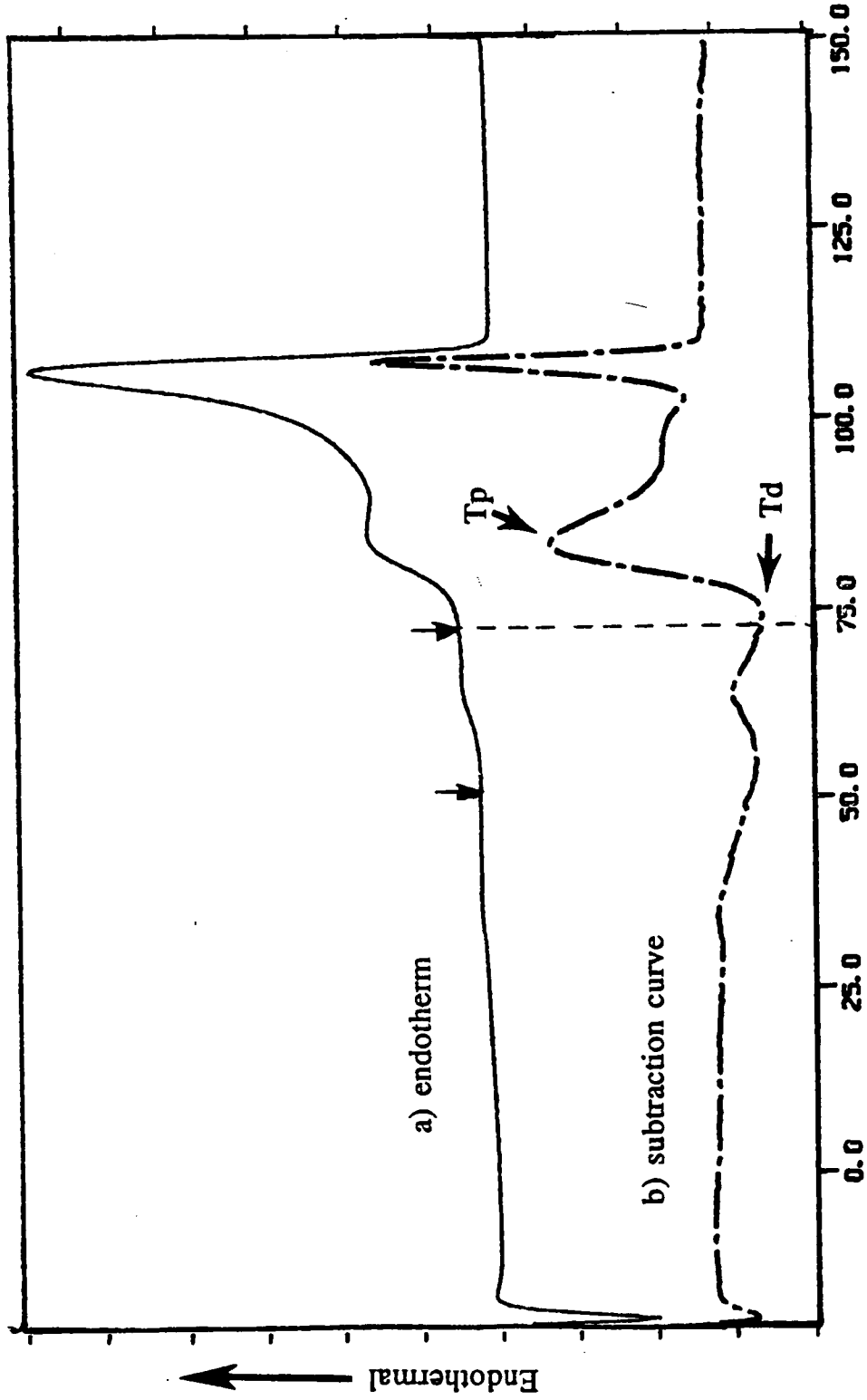


Figure 4.55: DSC endotherm and subtraction curve for multiple annealing of XLPE at 70 and 50 C; a) endotherm; b) subtraction curve.

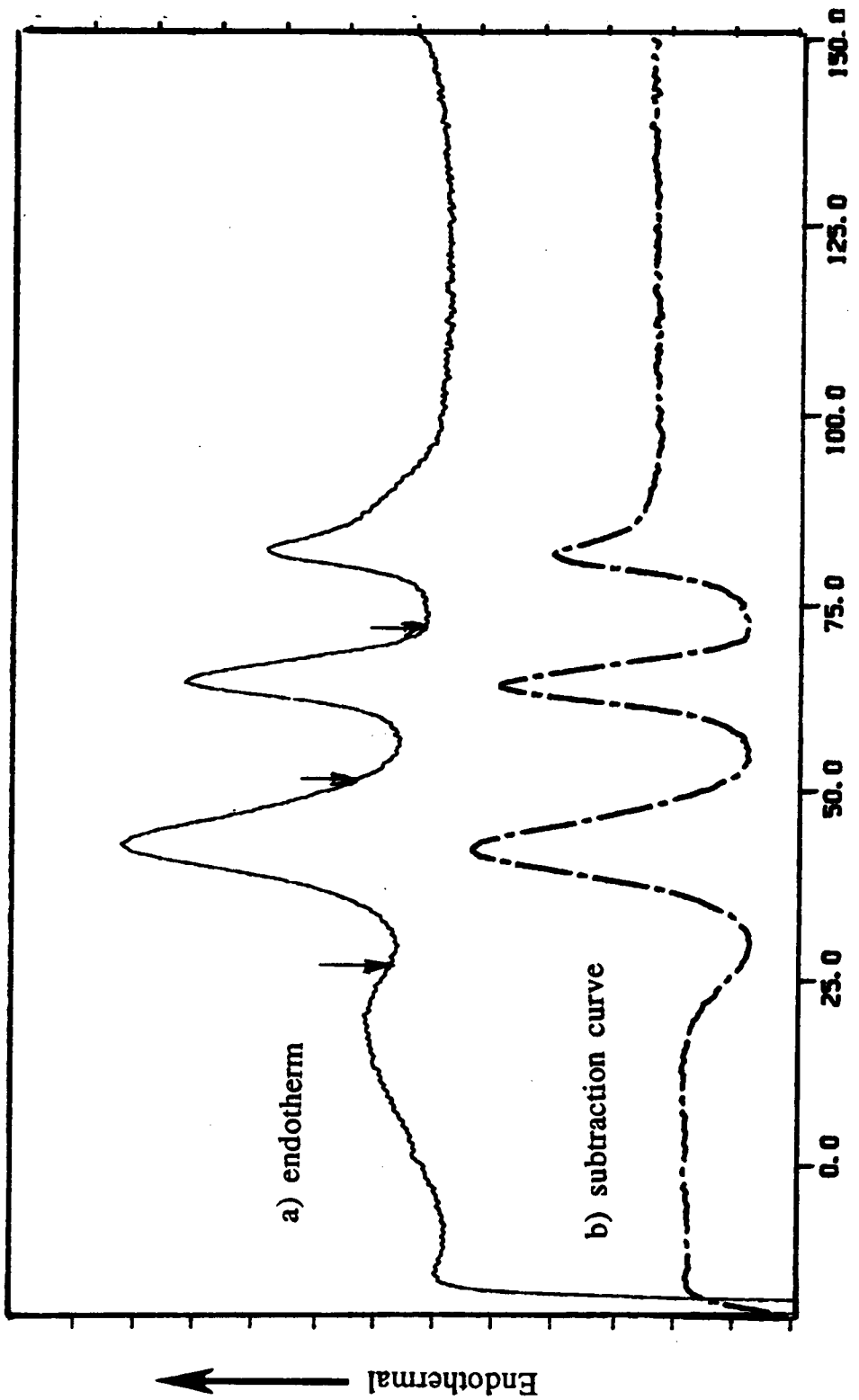


Figure 4.56: DSC endotherm and subtraction curve for multiple annealing of EPDM at 70, 50, and 25 C; a) endotherm; b) subtraction curve.

Figure 4.57 shows multiple annealing of EPDM at 70 °C for 24 hours and 35 °C for 35 hours. Once again both annealing temperatures produce easily discernable effects. The loss peak corresponding to the 70 °C annealing occurring at 71 °C and for the 35 °C annealing at 40 °C. The gain peaks representing the 35 and 70 °C annealing occurred at temperatures of 53.6 and 81.5 °C, respectively.

4.5.2 Cycling

In order to determine if cycling sample from the annealing temperature to ambient had any effects upon the position of the loss and gain peak two sample of XLPE were annealed at 70 °C for 12 hour intervals then allowed to annealed at room temperature for 12 hours. One sample was annealed for a cumulative time of 70 hours at 70 °C and the positions of the loss and gain peaks were determined to be 72.1 °C and 83.56, respectively. Another sample was annealed for a total of 120 hours at 70 °C and the loss and gain peak positions were found to occur at temperatures of 73.0 and 84.15 °C, respectively. The loss peaks for each sample gave representative values of the actual annealing temperature and by examining Table 4.2, the positions of the gain peaks correspond well with those determined for non-cycled 70 °C annealing. It therefore appears that cycling has no detrimental effects upon the prediction abilities of the technique.

4.5.3 Effects of Nonisothermal Crystallization upon the Subtraction Curve

The samples which have been examined thus far have primarily been those in which the previous thermal history has been erased before the annealing experiments were carried out. This procedure consists of holding the sample at 150 °C for five minutes then cooling

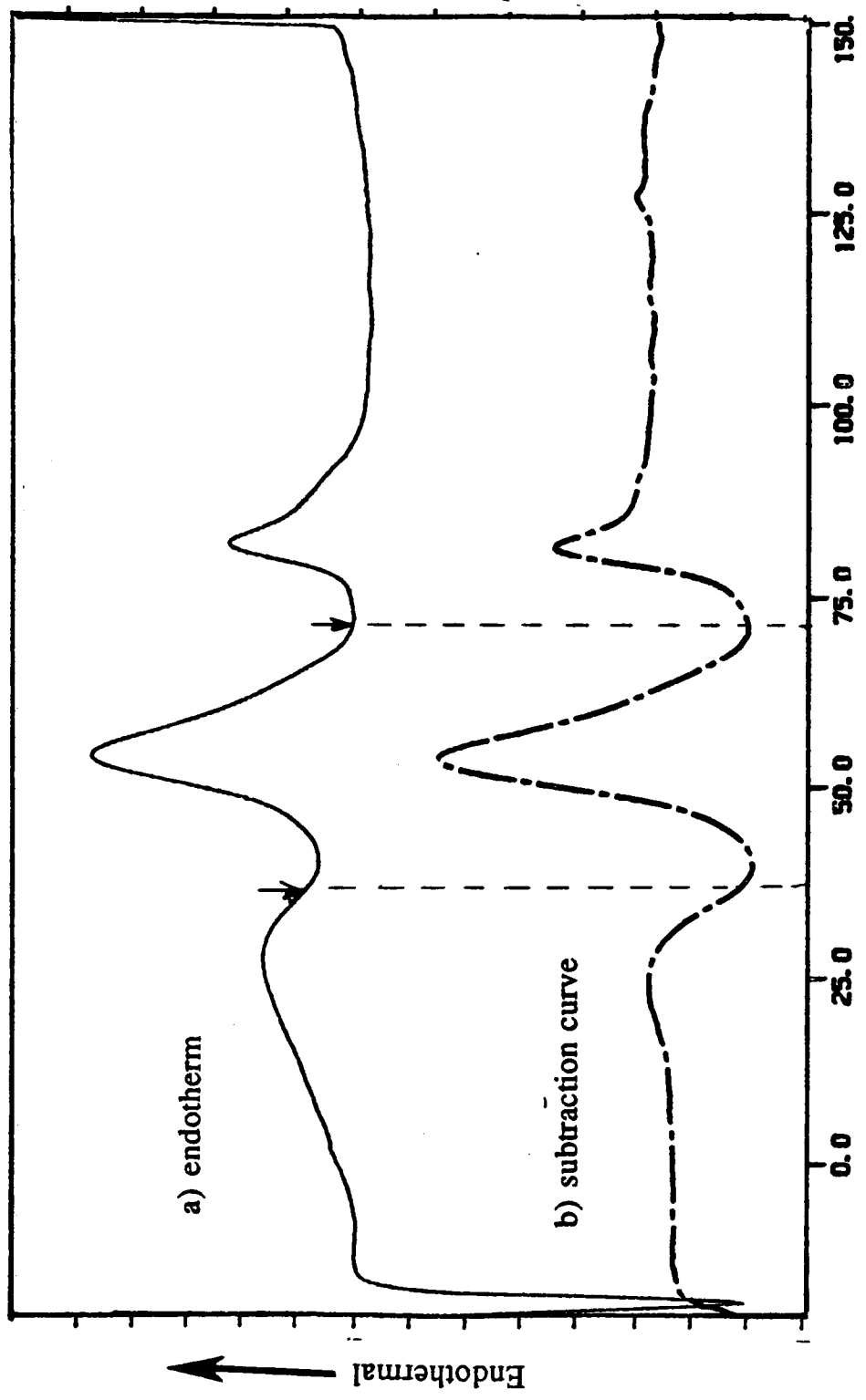


Figure 4.57: DSC endotherm and subtraction curve for multiple annealing of EPDM at 70 and 35 C; a) endotherm; b) subtraction curve.

the sample to -20 °C at a cooling rate of 40 °C/min. The quenched curve used for the subtraction technique was also cooled at 40 °C/min as well in order to eliminate any discrepancies which could result from the effects of isothermal crystallization. In practice, one would not know the exact rate at which the samples were cooled after processing. Some processes may involve slow cooling and others may involve quenching.

In order to see if such differences are detectable from the subtraction technique a sample of XLPE was quenched from the melt at various cooling rates of 2, 40 and 400 °C/min. The results of subtracting the endotherms produced from the various cooling rates are shown in Figure 4.58 (a-d). One can observe that such differences in the rates of nonisothermal crystallization produce noticeable effects on the subtraction curve close to the temperature at which the major melting peak occurs. The curves produced from subtracting the endotherms of the 40 and 400 °C/min cooling rates from that of the endotherm produced form 2°C/min cooling show identical effects with a gradual hump being produced before a sharp drop in the subtraction curve (Figure 4.58 c and d).

This is produced by a slight difference in the peak positions due to the different nonisothermal cooling rates. A slower cooling rate will allow the exclusion of branches and other defects from the crystals as well as allow the development of slightly thicker lamellae than would be produced in a quenched sample. This generates an increase in the overall crystallinity and shifts the peak position to a slightly higher temperature. This effect is shown in Figure 4.59 for the slow cooled and fast quenched samples of XLPE.

The curve generated from the subtraction of the endotherm produced from the 400 °C cooling rate from that of the 40 °C cooling rate shows less pronounced effects than were observed for the other subtraction curves and only shows a slight bump (Figure 4.58 b). This indicates that the major melting peak is occurring at essentially the same temperature for both samples with the presence of the hump indicating a slightly higher crystallinity for the 40

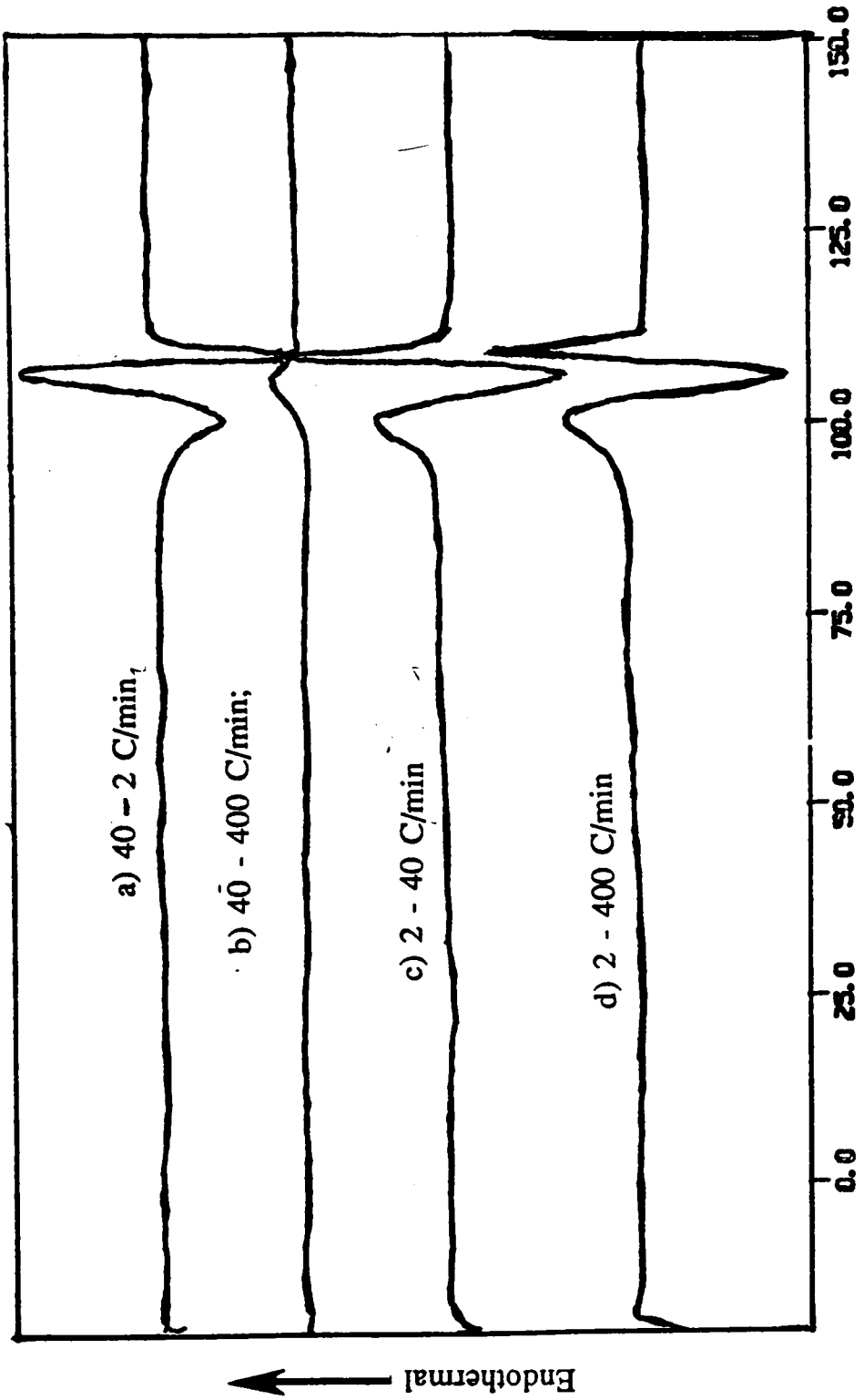


Figure 4.58: Non-isothermal cooling rate effects upon the subtraction curves for XLPE: a) 40 - 2 C/min; b) 40 - 400 C/min; c) 2 - 40 C/min; d) 2 - 400 C/min.

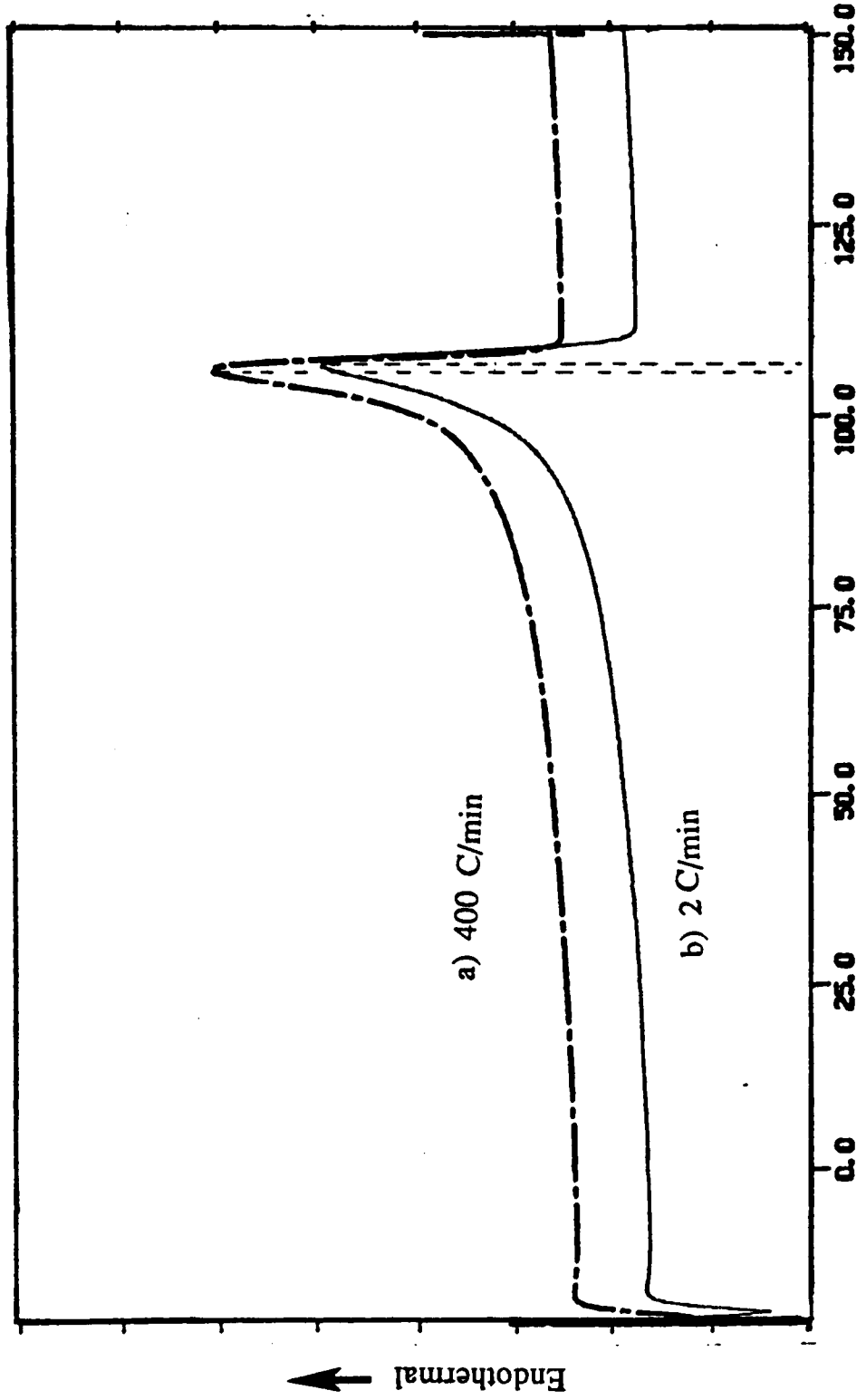


Figure 4.59: Endotherms of XLPE showing the effect of different non-isothermal cooling rates: a) 400 C/min b) 2C/min.

°C/min cooled sample.

Subtracting the 2 °C/min cooled sample from the 40 °C/min cooled sample results in a mirror image of the curve produced by subtracting the 40 °C/min from the 2 °C/min endotherms (Figure 4.58 a). This curve is similar to the form of those examined earlier in the annealing studies. The key to telling the difference between this phenomenon and that due to annealing is to notice the sharp loss peak which occurs after the gain peak. The curve generated from annealing does not exhibit a sharp loss peak above the gain peak.

4.6. Aged Samples

Several cable insulation samples which have been subjected to the realistic conditions of a power plant were kindly supplied by Montgomery Shaw of the University of Connecticut. These sample are part of an ongoing study at that university comparing natural and artificial aging of insulation.

The majority of the samples appeared to be composed of amorphous materials and were not examined in any detail. However, two of the cable types labelled as 246-155-RP and 246-155-RW showed melting curves similar to those observed for the Rockbestos cable (B1). Two samples of cable RP were supplied which had been subjected to different heat treatments, RP-3 and RP-5, along with a virgin sample (RP-Control). Three samples of the insulation RW representing different environments were supplied and labelled as RW-1, RW-2, and RW-4. A control sample was supplied as well.

4.6.1 Cable 246-155-RP

The melting behavior of the two aged samples, RP-3 and RP-5, are shown along with the endotherm for the control cable in Figure 4.60. One can notice that there are three melting regions. One starts at 50 °C and extends to about 100 °C, which appears typical of XLPE. Sharp melting peaks can be observed at 110 and 118 °C as well and are

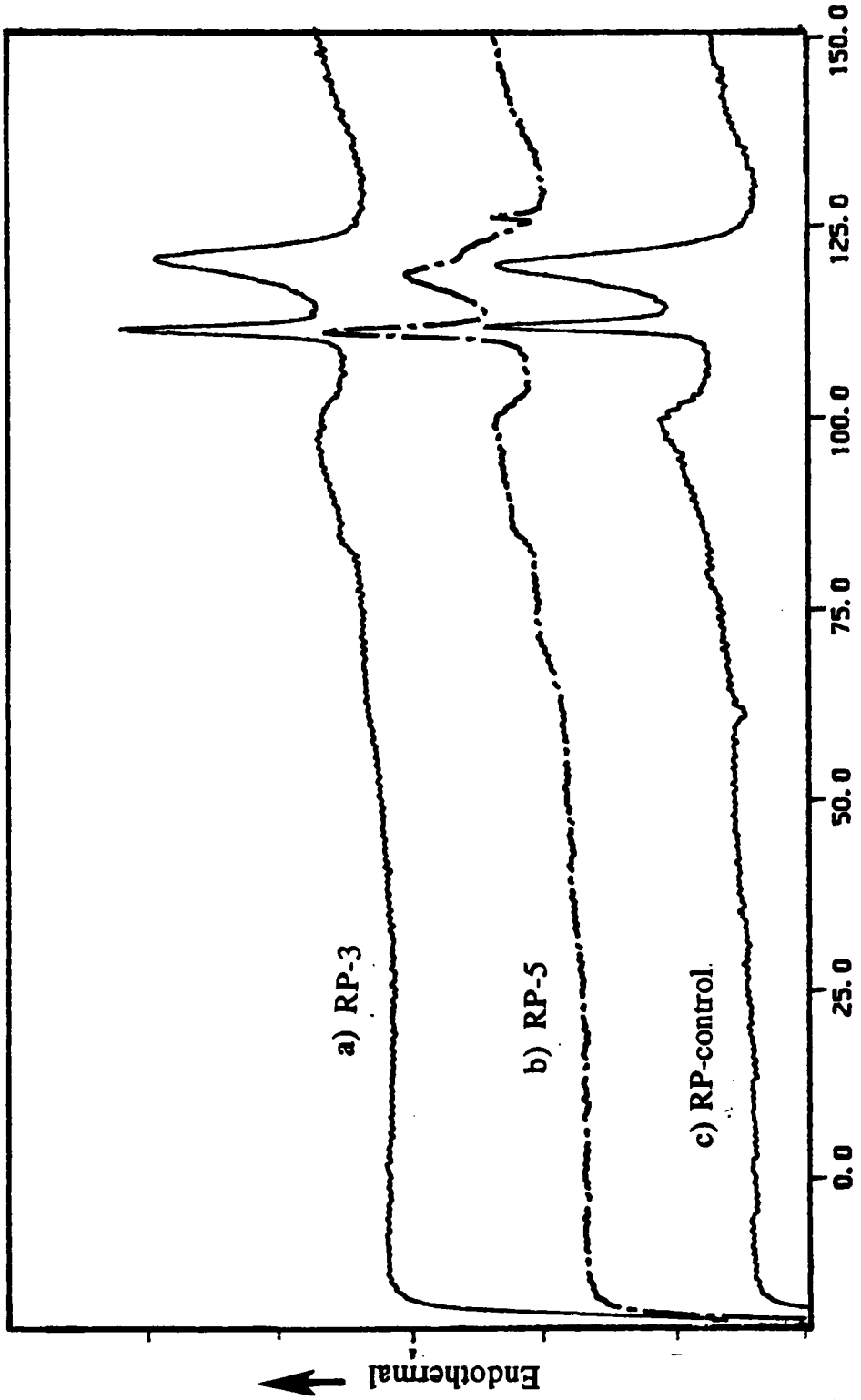


Figure 4.60: DSC endotherms for cable 246-155-RP; a) RP-3; b) RP-5; c) RP-control.

most likely due to crosslinked HDPE.

It is apparent from Figure 4.60 that the control sample contains a fairly complicated thermal history inherent from the manufacturing process. The melting behavior of RP-3 shows similar behavior in the high temperature region. The endotherm of RP-3 also shows a slight shoulder occurring at approximately 80 °C.

The endotherm of RP-5 shows a small peak occurring above 125 °C. This suggests that this sample may have been exposed to a temperature of roughly 126 °C and subsequently 115 and 104 °C to regenerate the sharp peaks. One can also notice that the transitions for the high temperature peaks of RP-5 are shifted slightly downward from those of both RP-3 and the control. In addition to this high temperature peak, RP-5 shows shoulders occurring at 70 and 80 °C.

In order to better quantify the inherent history within the control sample, the subtraction technique was performed upon the control cable by subtracting the quenched endotherm for the original endotherm. The resulting subtraction curve is shown in Figure 4.61 The subtraction curve shows what appears to be slight heat treatment at 40 °C and 70 °C with the major annealing temperatures occurring at 103 °C and 113 °C.

The subtraction technique was performed upon the aged samples using both the quenched and control endotherm as the second ramp. The results of subtracting the quenched endotherm from the original endotherm of RP-3 for three samples is shown in Figure 4.62. These subtraction curves show annealing history at temperatures of roughly 75, 103, and 113 °C and possibly 47 °C. The subtraction curve generated from subtracting the endotherm of the control sample from that of RP-3 is shown in Figure 4.63 and also shows annealing at temperatures of 47 and 75 °C. One can also notice a loss peak at a temperature of 98.8 °C as well. The sharp peak appearing at 110 °C is an indication that the melting peak present on the endotherm at that temperature is slightly higher for the aged sample than for the control.

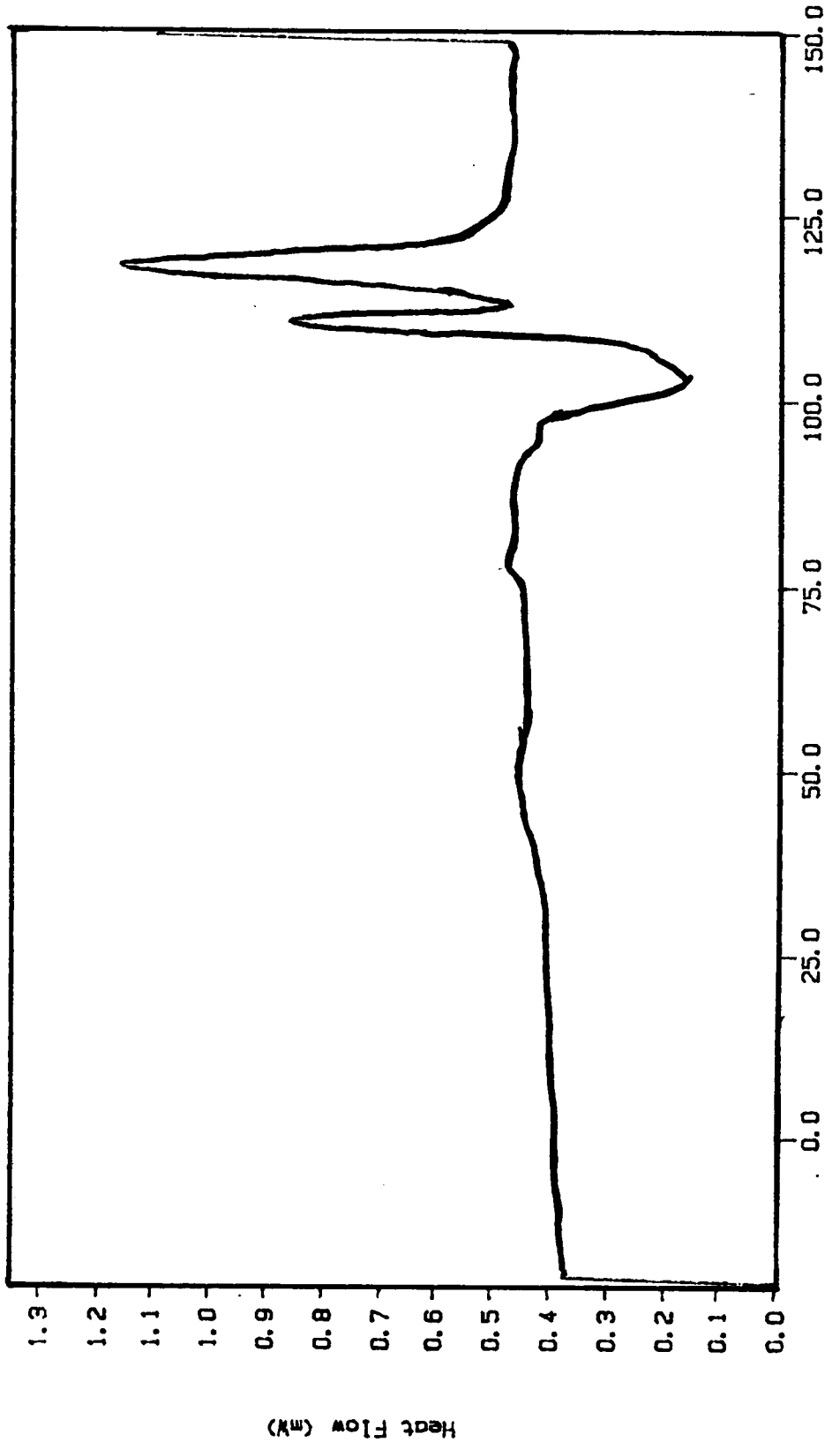


Figure 4.61: Subtraction curve for RP-Control.

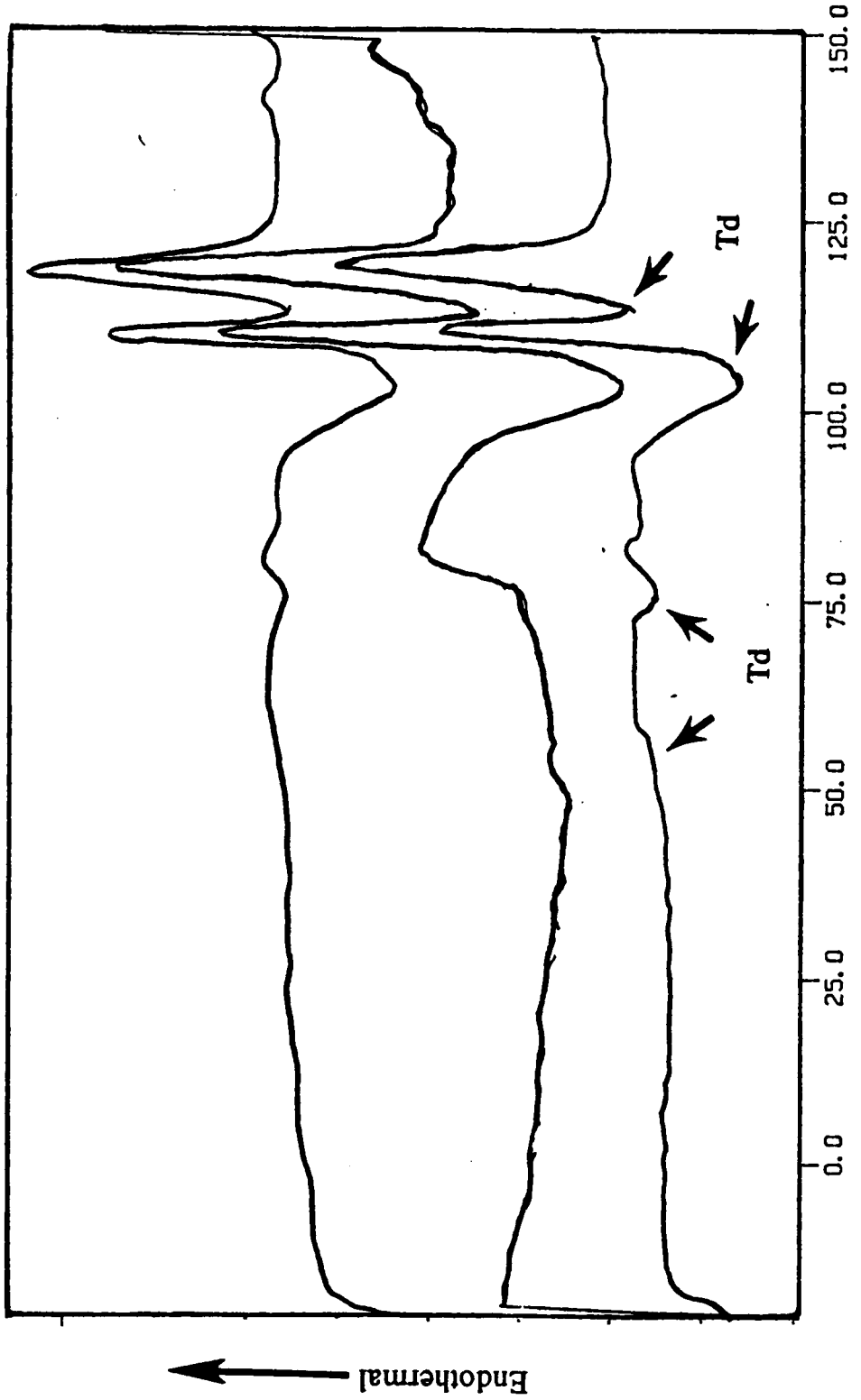


Figure 4.62: Subtraction curves for RP-3 generated from the subtraction of the quenched from the aged endotherms.

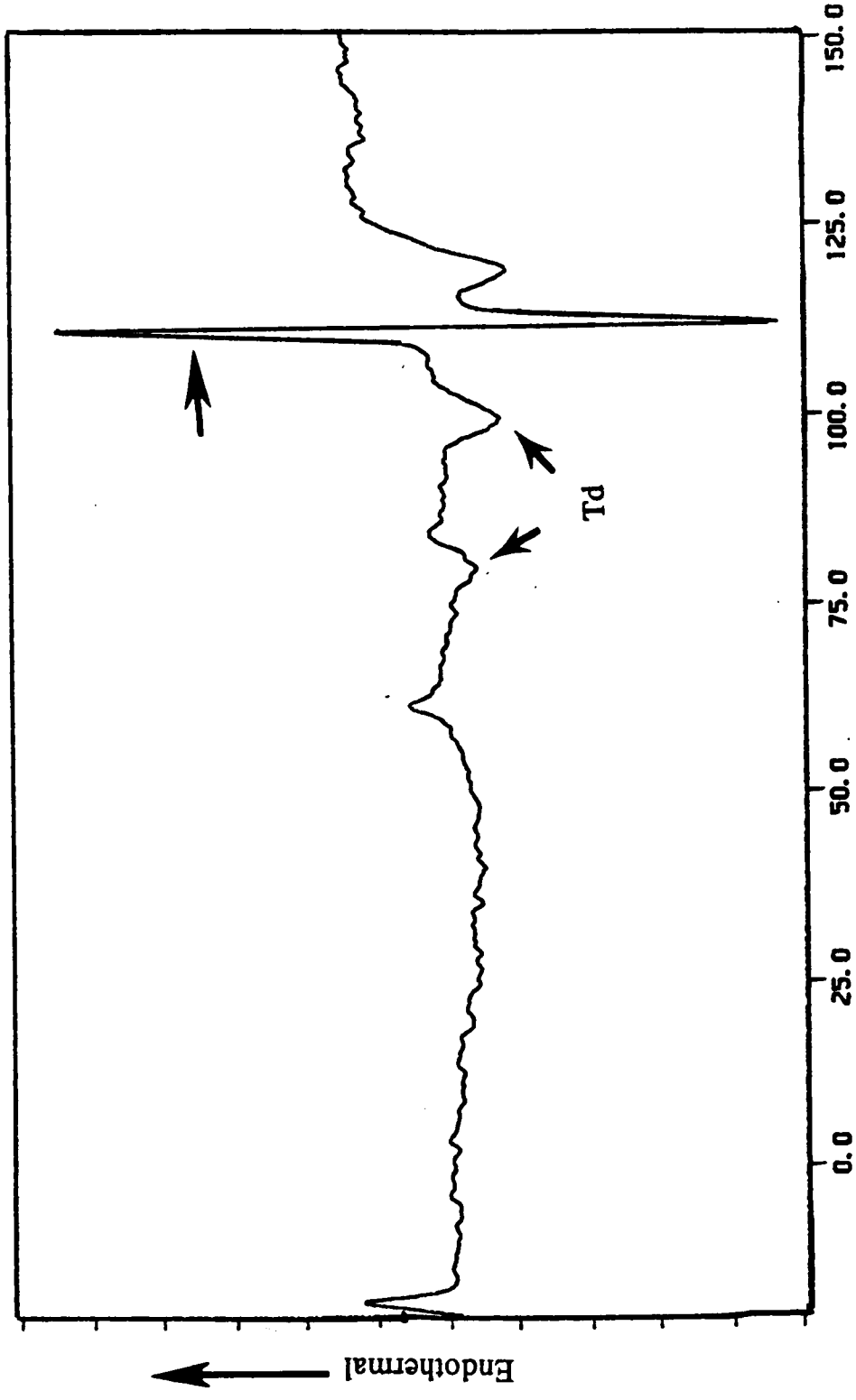


Figure 4.63: Subtraction curve for RP-3 generated from the subtraction of the control from the aged endotherm.

The subtraction curves generated for several samples of RP-5 using the quenched endotherm as the second ramp are shown in Figure 4.64. The position of the loss peaks indicate thermal history at 60 and perhaps 80 °C. The subtraction curves also show loss peaks at temperatures of 103 and 116 °C. Comparing some of the endotherms generated from RP-5 shown in Figure 4.65 one can observe inconsistencies in the high temperature melting peaks. This is suggestive of annealing in the 115 °C temperature region.

The subtraction curve generated by subtracting the control sample from that of the aged RP-5 sample is shown in Figure 4.66 and shows the 60 and 80 °C annealing that was observed from Figure 4.64. This subtraction curve also reveals annealing in the 98 °C region as well.

4.6.2 Cable 246-155-RW

The melting behavior of the three aged samples along with that of the control sample is shown in Figure 4.67. From the melting behavior we can see that cables RW and RP are identical in nature. One can observe the melting peak of XLPE occurring around 100 °C with the higher temperature peaks occurring at 110 °C and about 118 °C.

From the melting curves we can see that RW-1 exhibits what appears to be to slight shoulders, one occurring at about 78 °C and another in the region of 60 °C. No major differences can be observed between the control and aged sample above 100 °C. Several subtraction curves for RW-1 generated by subtracting the quenched endotherms from the aged endotherms are shown in Figure 4.68. Theses curves show loss peaks indicative of thermal treatment at temperatures of approximately 56 and 80 °C as well as 103 °C and 114 °C. The subtraction curve generated from using the control endotherm as the second ramp in the subtraction technique is shown in Figure 4.69. This subtraction curve also shows thermal treatment

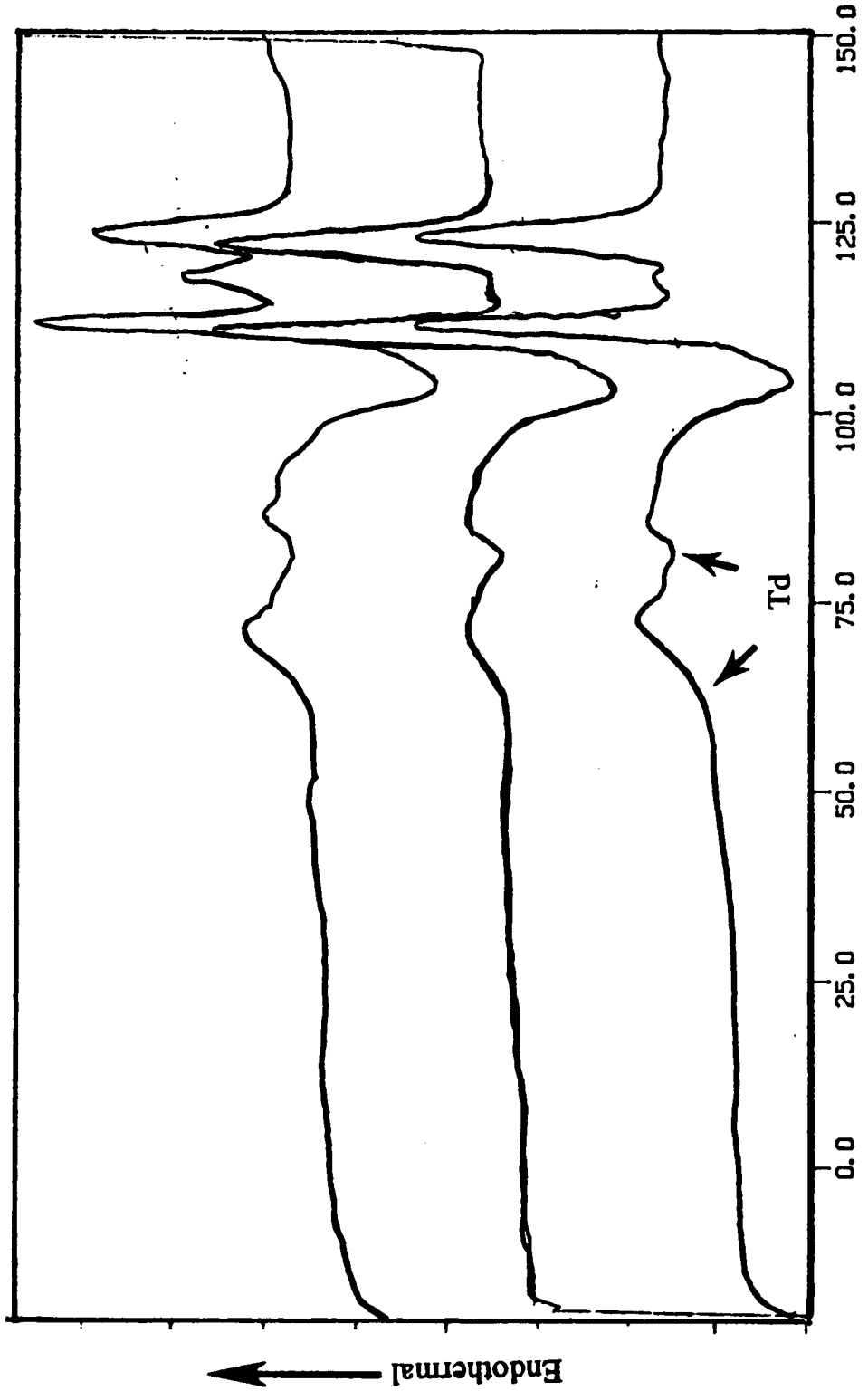


Figure 4.64: Subtraction curves for RP-5 generated from the subtraction of the quenched from the aged endotherms.

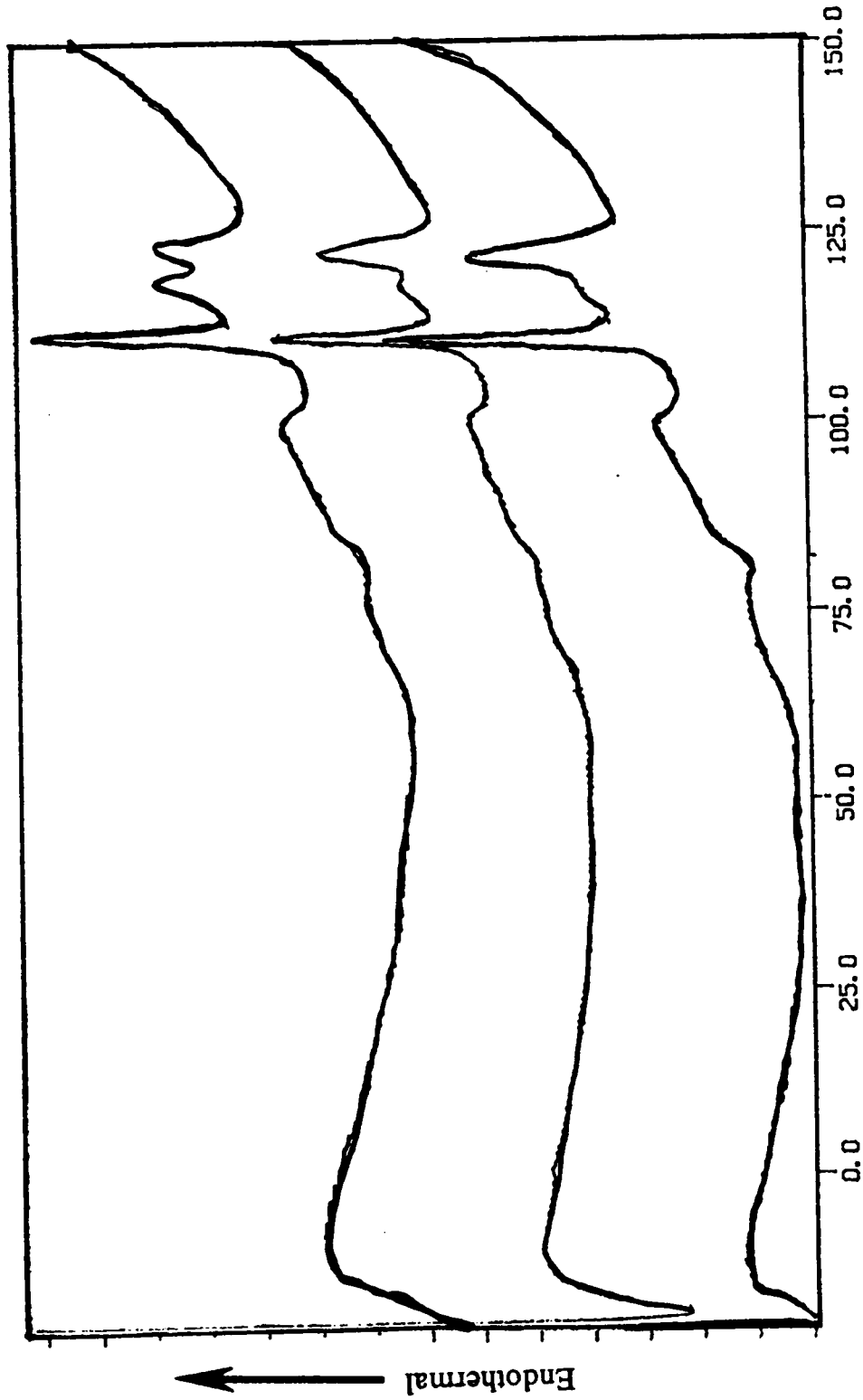


Figure 4.65: Inconsistencies in the high temperature melting behavior of RP-5.

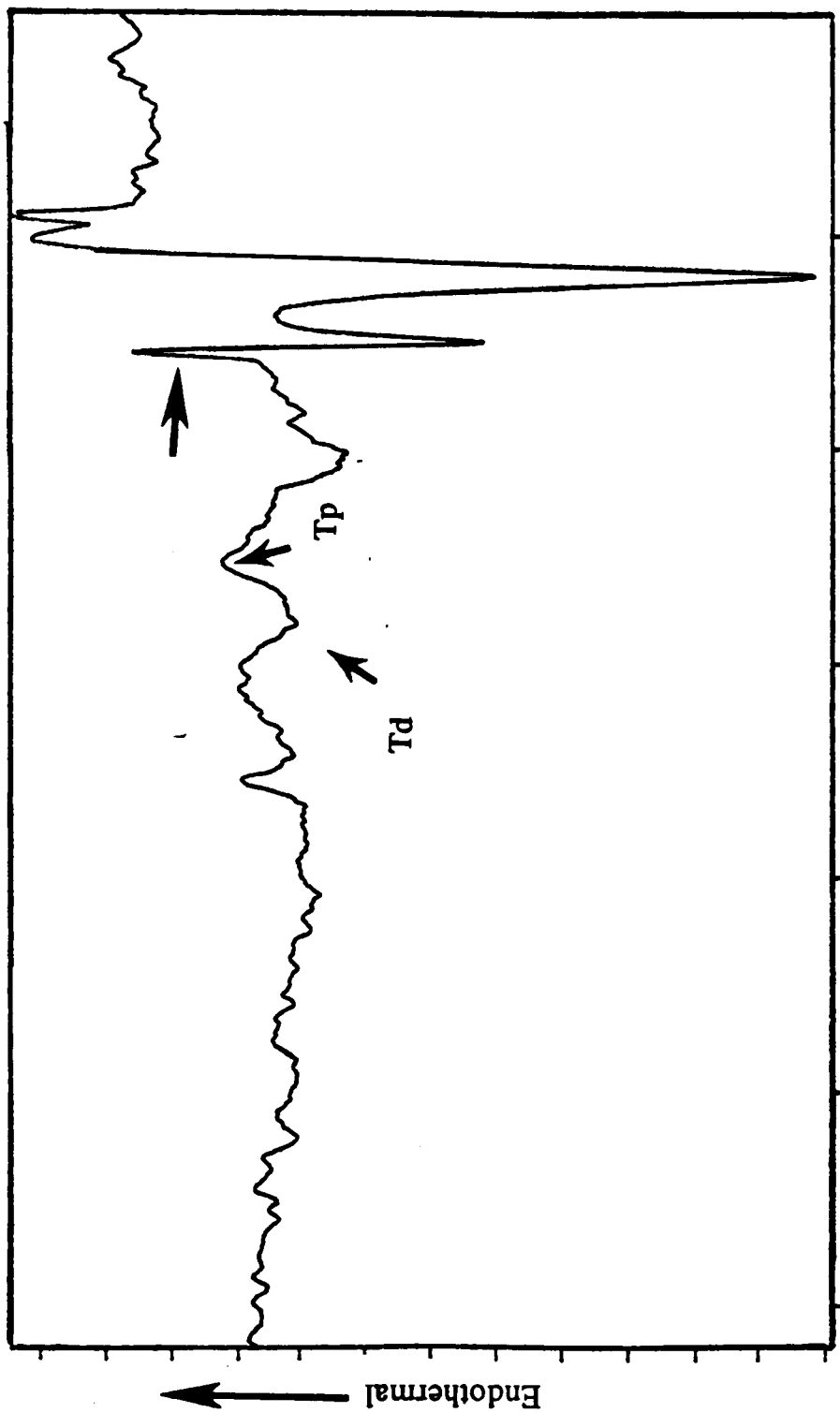


Figure 4.66: Subtraction curve for RP-5 generated from the subtraction of the control from the aged endotherm.

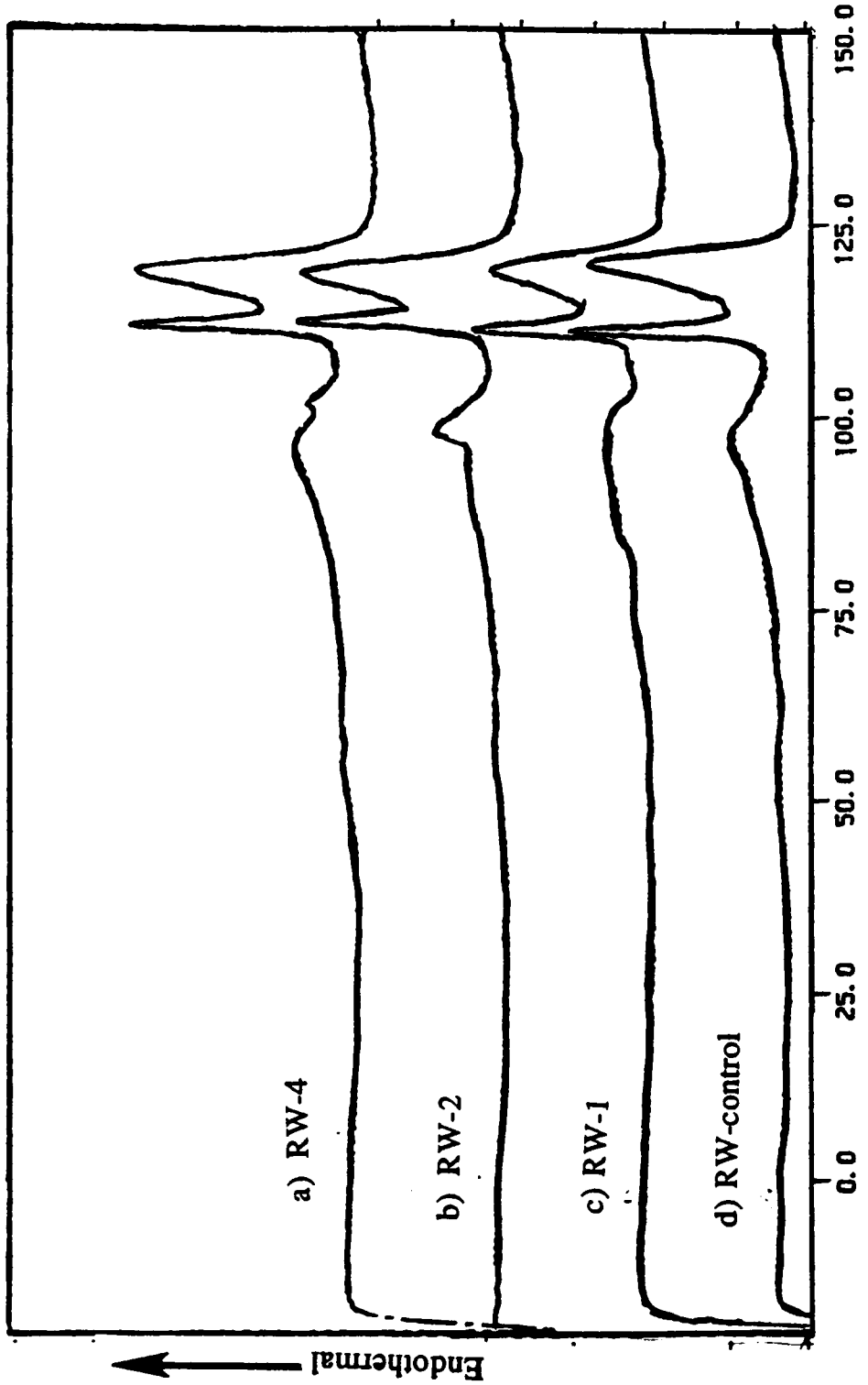


Figure 4.67: DSC endotherms for cable 246-155-RW: a) RW-4; b) RW-2; c) RW-1; d) RW-control.

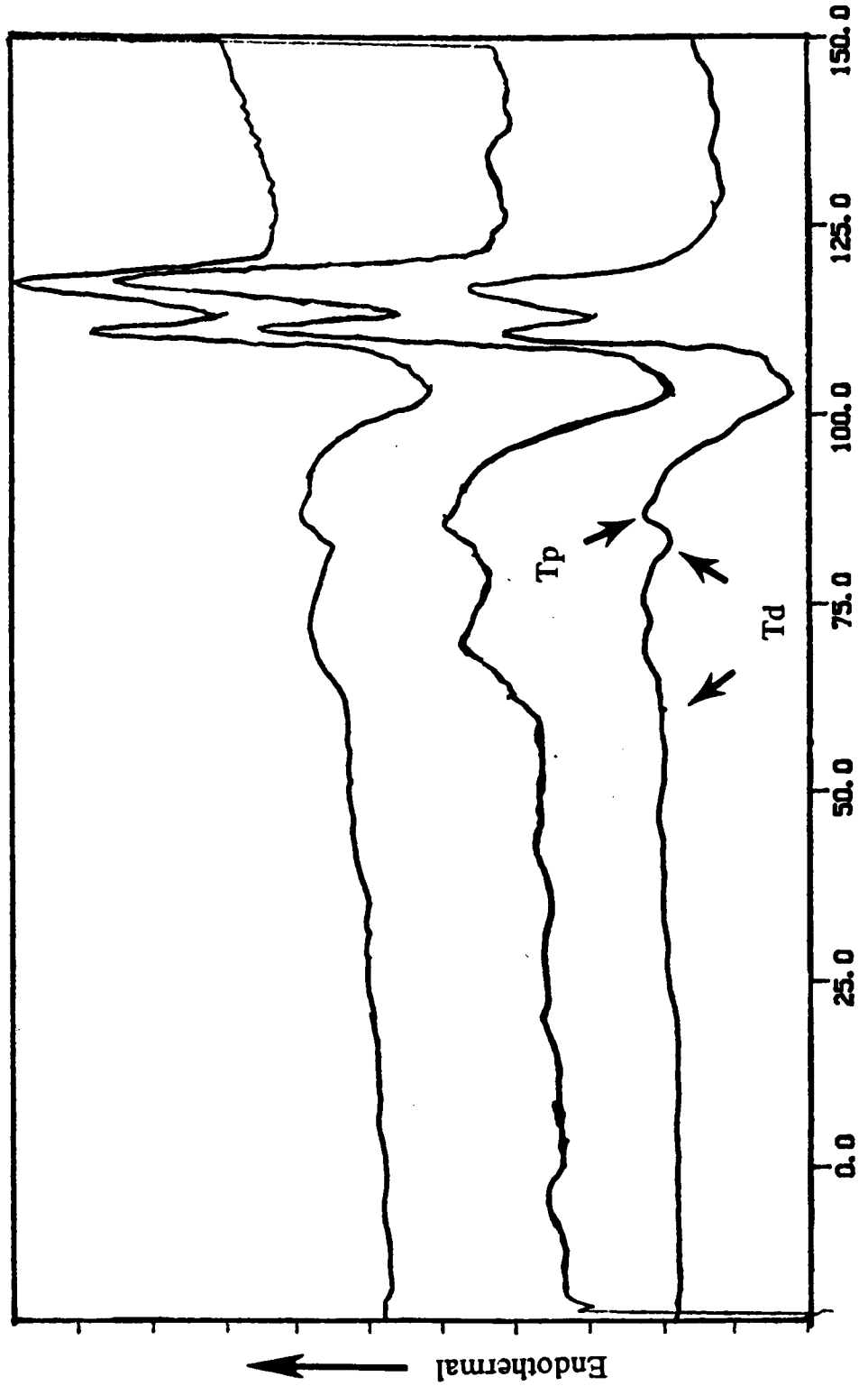


Figure 4.68: Subtraction curves for RW-1 generated from the subtraction of the quenched from the aged endotherms.

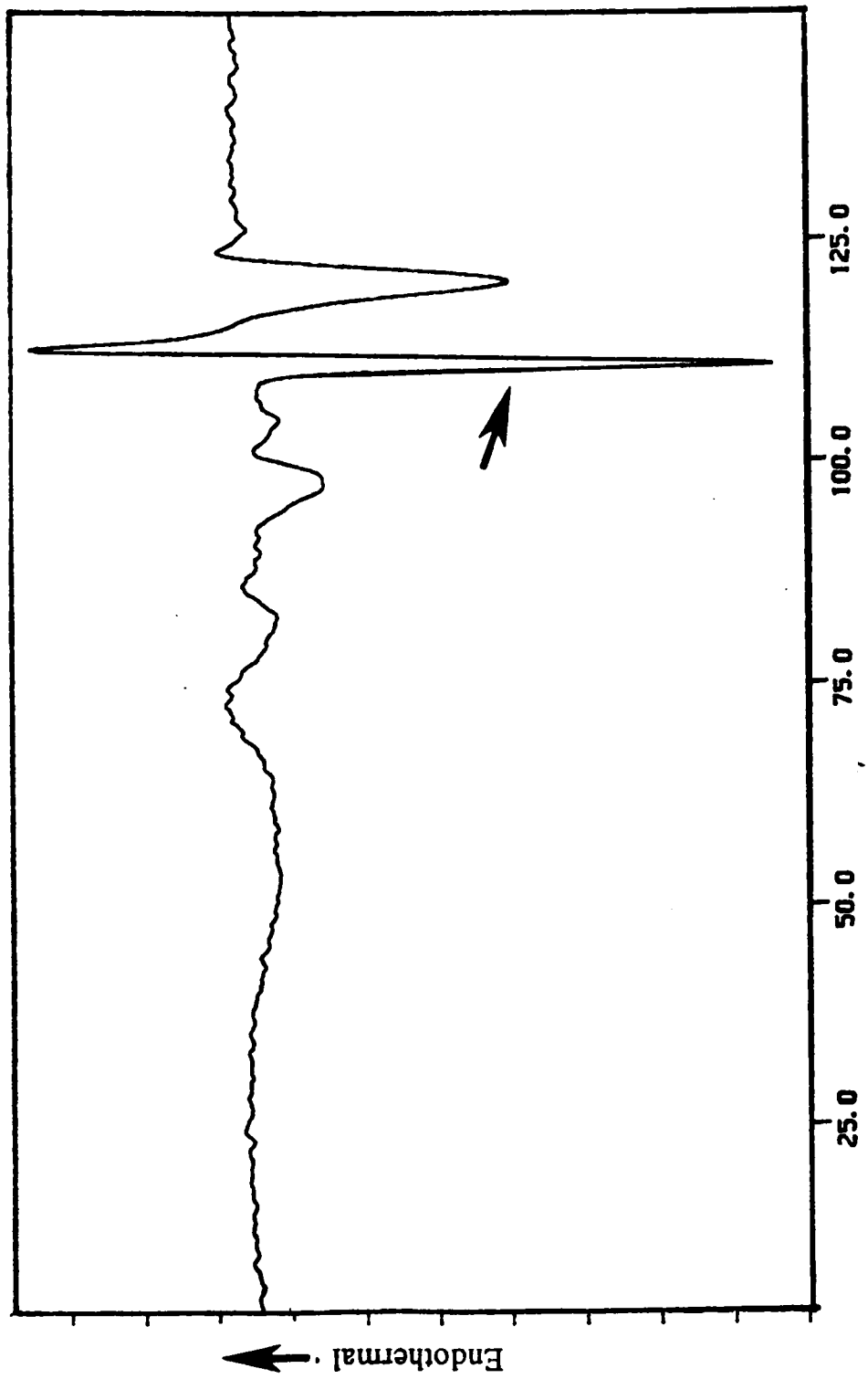


Figure 4.69: Subtraction curve for RW-1 generated from the subtraction of the control from the aged endotherm.

at temperatures of roughly 60 and 81 °C. An additional loss peak occurs at 96 °C as well.

The aged sample designated as RW-2 shows an additional peak located at approximately 95 °C which suggests that this sample has been exposed temperatures slightly below 95 °C. No other history is apparent from the endotherm below 95 °C. The peak which occurs at 110 °C appears to be shifted upward when compared to the control cable and this could be expected if the sample had been annealed at 95 °C. The subtraction curves produced using the quenched and the control endotherms are shown in Figures 4.70 and 4.71, respectively. Both types of subtraction curves indicate thermal history at a temperature of 92 °C.

Sample RW-4 shows the development of a peak at about 98 °C, but no gross changes in the overall melting behavior are observable in that region as one might expect for 98 °C annealing. There appears to be a slight shoulder at about 50 °C as well. The subtraction curves obtained using the quenched endotherms are shown in Figure 4.72. Only the middle subtraction curve in Figure 4.72 shows the presence of a loss peak at 90 °C. The other curves show what could possibly be the result of annealing at 78 and 64 °C, but the loss peaks are very subtle for these temperatures. The subtraction curve generated from subtracting the control endotherm from that of RW-4 reveals a loss peak located at 99 °C and a very slight dip at 86 °C. This is shown in Figure 4.73. The sharp peak present at 110 °C indicates that the melting peak located at 110 °C on the endotherm for the control sample occurs at a slightly lower temperature than the same transition on the endotherm of RW-4. This behavior is expected if the sample had been exposed to heat treatment at 99 °C.

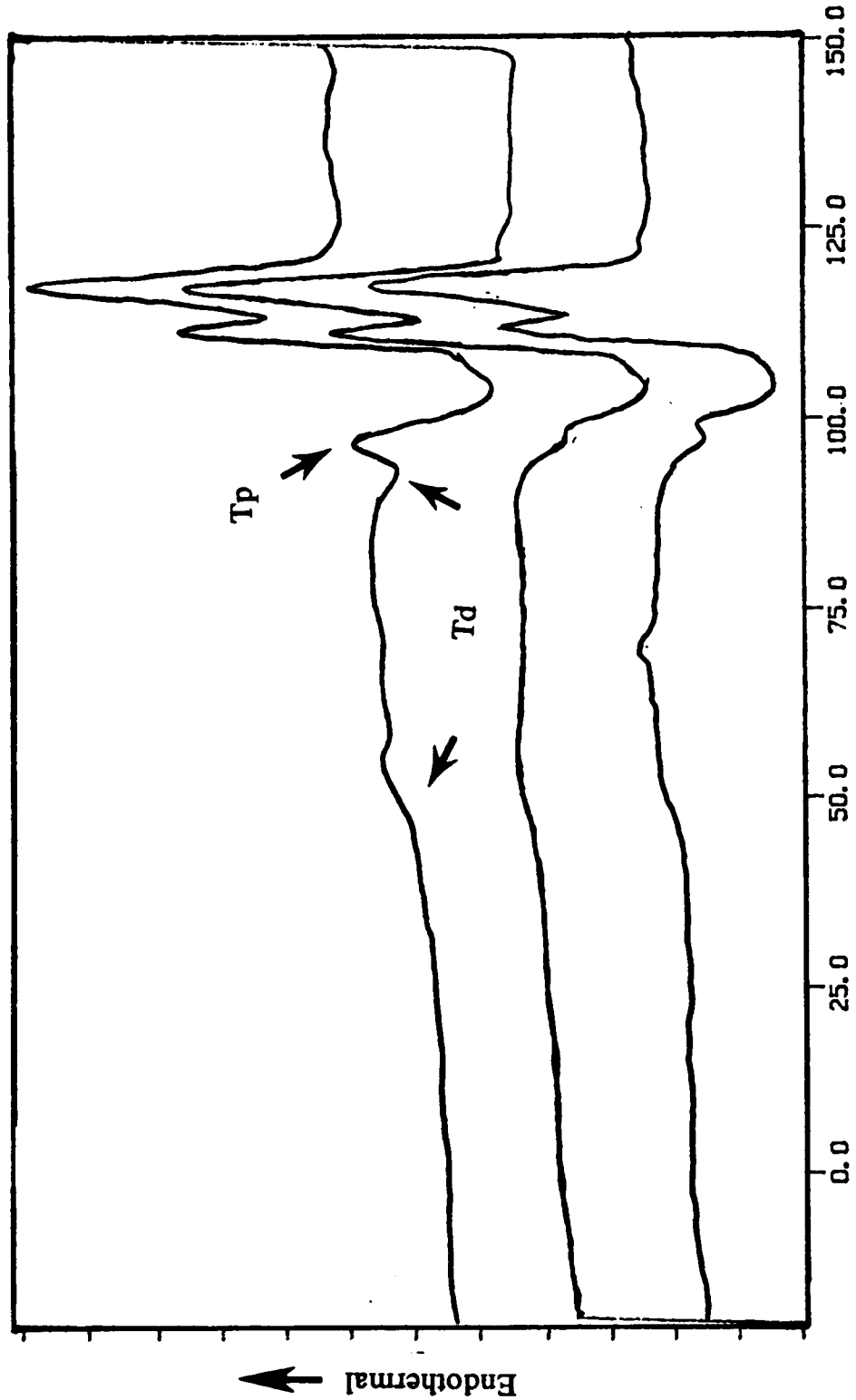


Figure 4.70: Subtraction curves for RW-2 generated from the subtraction of the quenched from the aged endotherms.

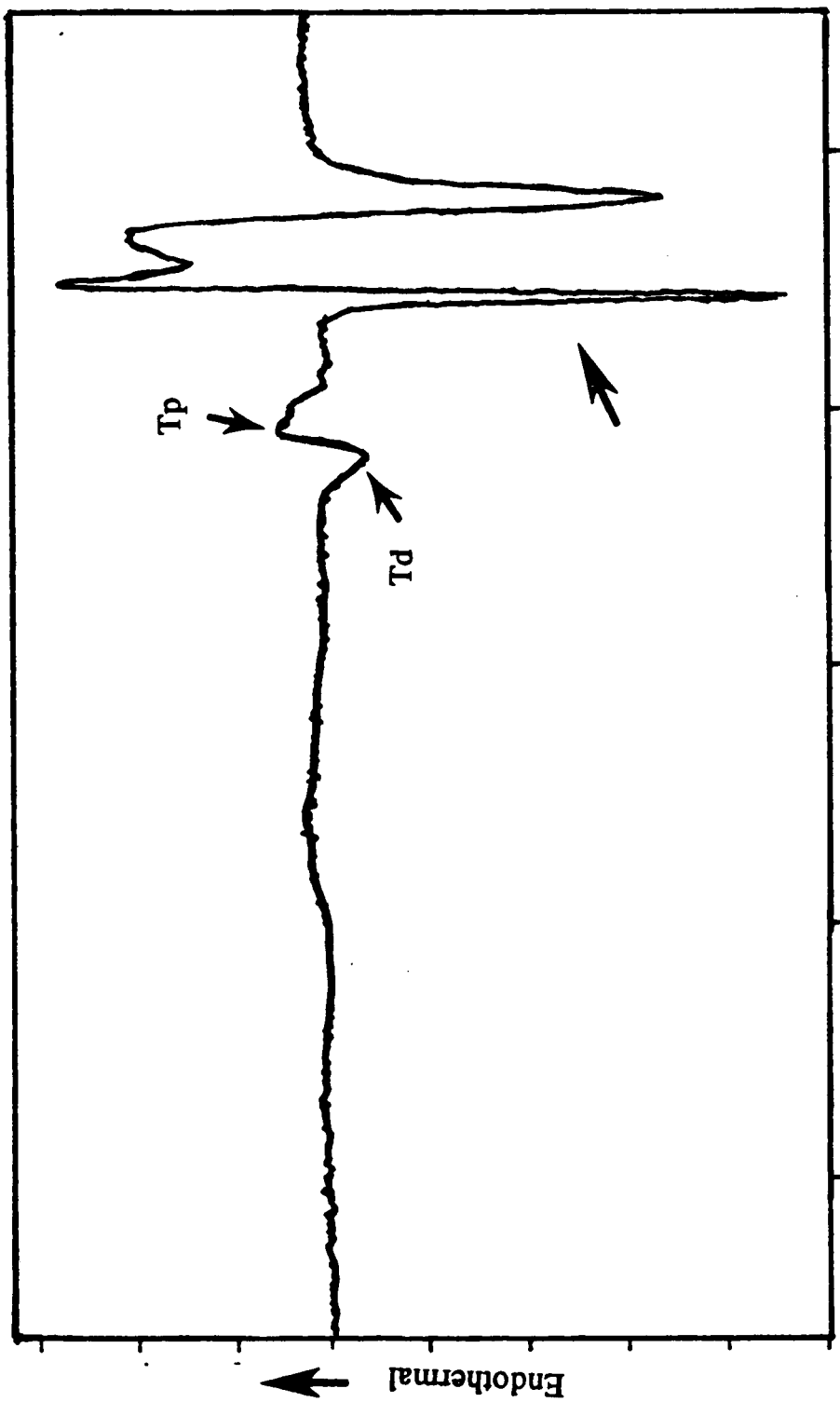


Figure 4.71: Subtraction curve for RW-2 generated from the subtraction of the control from the aged endotherm.

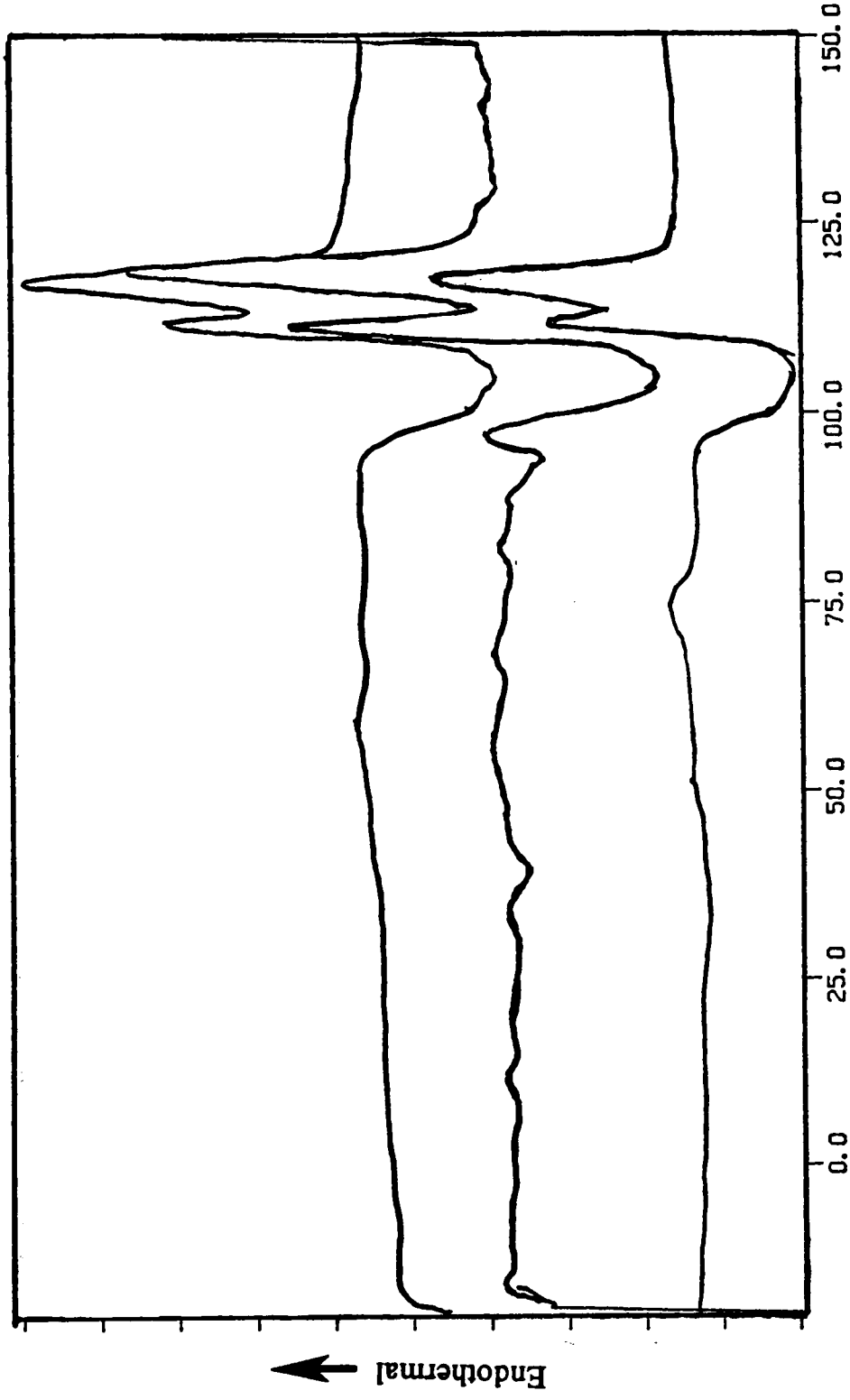


Figure 4.72: Subtraction curves for RW-4 generated from the subtraction of the quenched from the aged endotherms.

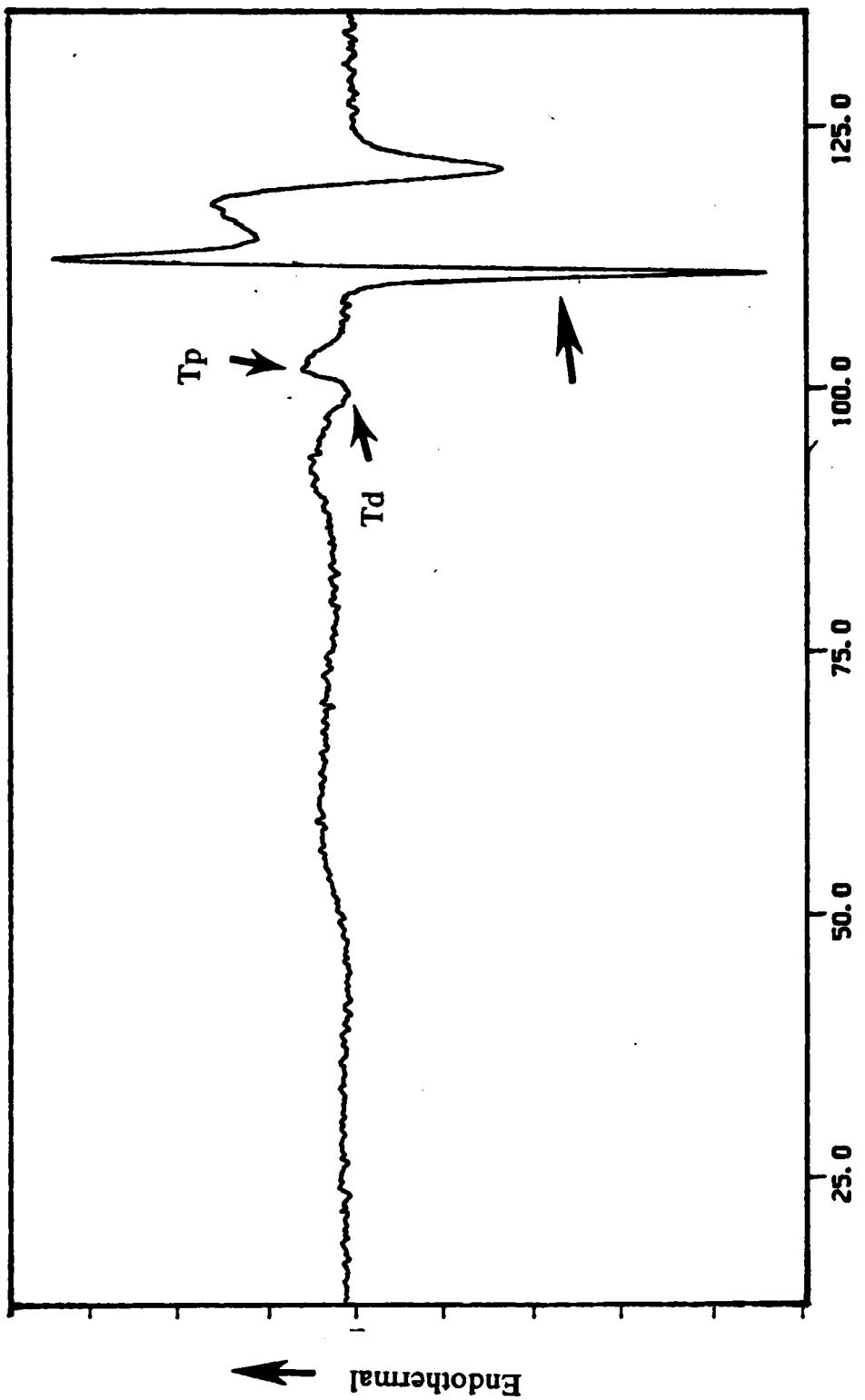


Figure 4.73: Subtraction curve for RW-4 generated from the subtraction of the control from the aged endotherm.

5. DISCUSSION

Information obtained from the subtraction technique in the form of the position of the gain peak, Tp, and the position of the loss peak, Td, yield the needed values to estimate thermal history in semicrystalline polymeric systems. It has been demonstrated that for the standard materials as well as for the control cables the value obtained for Td remains essentially constant with annealing time and is usually within about 2 to 3 °C of the actual annealing temperature. The value of Tp has been shown to increase with annealing time over fairly large time scales (over two months). All that needs to be determined for a particular sample in order to predict the thermal history is the rate of change of Tp with annealing time for a particular annealing temperature.

5.1. Reference Materials

5.1.1 Crosslinked Low Density Polyethylene (XLPE)

In order to assist in the interpretation of the annealing behavior and the kinetics of the gain peak shift, Tp can be plotted against logarithmic time to yield straight lines with equations of the form:

$$Tp(T,t)= A(T)+B\log(t)$$

The position of the gain peak and the y-intercept (A) both show a temperature dependence but the slope B shows a very small temperature dependence between about 45 and 70 °C and can be considered a material parameter. Such a plot is shown for the annealing data obtained for XLPE in Figure 5.1. The slopes of the

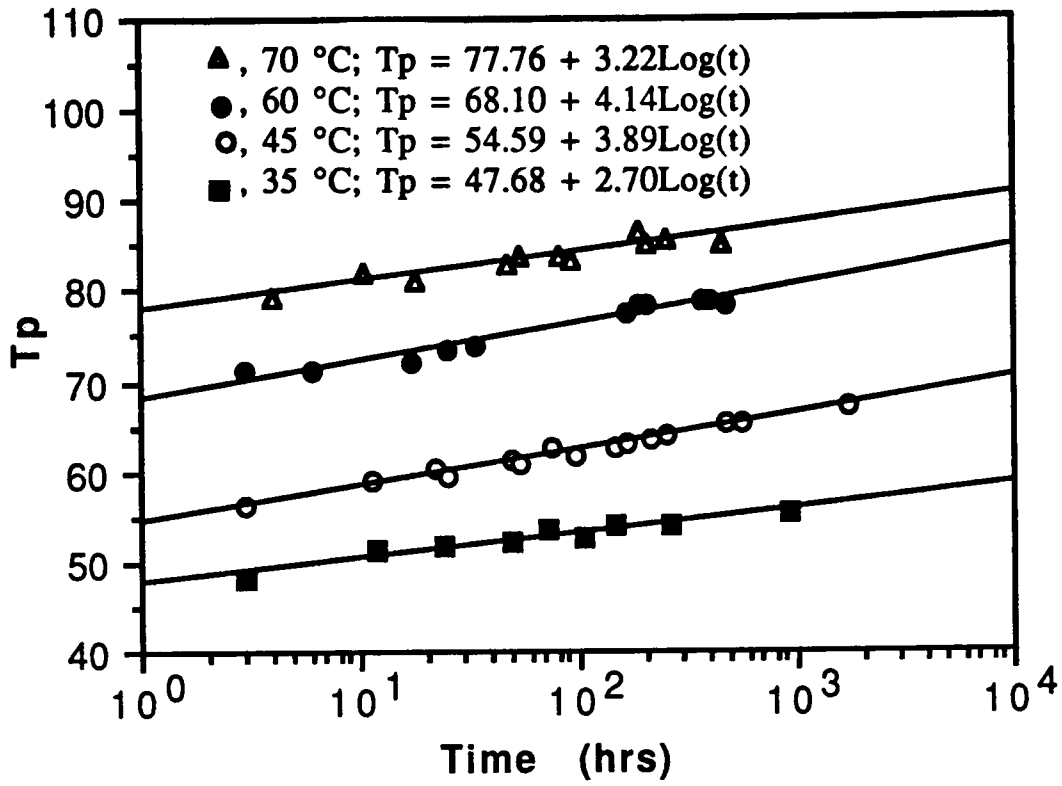


Figure 5.1: Tp versus logarithmic time for XLPE.

corresponding lines are given on the graph.

One can notice that the lines are shifted upward with increasing annealing temperature, as one might expect. However, the slopes of the equations show slightly different behavior. It is the slopes which give an indication of the ability of a sample to anneal at a particular temperature. A large value for the slope of the equation generated for a particular temperature indicates that the sample is highly susceptible to annealing at that temperature. A smaller value indicates that the sample anneals slower and thus is less susceptible to annealing. With this in mind, one can observe that the slope of the 35 ^{o}C annealing line is the smallest (2.12 ^{o}C/hr), with an increase to 3.89 and 4.42 ^{o}C/hr for 45 and 60 ^{o}C, respectively. However, for 70 ^{o}C annealing one can observe a sharp decrease in the slope to a value of 2.9 ^{o}C/hr. This indicates that as one increases the annealing temperature from 35 up to 60 oC, the ability of the thinner lamellae to melt and recrystallize is increased. At a temperature of 60 ^{o}C more of the material is melted and perhaps much of the material which was able to recrystallize at 35 °C is also able to recrystallize at 60 °C as well. However, at 70 °C, a portion of the "fast annealing" material has reached its thermodynamic barrier for recrystallization and remains in the molten state and the annealing begins to effect the thicker and higher melting lamellae. These thicker lamellae are already closer to their "equilibrium state", and thus anneal at a slower rate.

Another important feature of Figure 5.1 is the linear relationship which exists over the whole spectrum of annealing times for a particular annealing temperature. Knowing the annealing temperature, one can obtain the characteristic annealing parameters from the subtraction data for two or three short annealing times at the annealing temperature. One can then use the equation generated to estimate the thermal history for longer times.

5.1.2 Ethylene Propylene Copolymer (EPR)

Given the vast difference in the basic melting behavior of XLPE and EPR, it is surprising that the same basic relationship between the position of the gain peak and time exists for both materials. The plot of Tp versus logarithmic time is shown in Figure 5.2 with the equations for each annealing temperature given on the graph. The points generated from shorter annealing times fit well with those generated from longer annealing times. This feature, as with XLPE, will allow one to extrapolate to longer times by simply obtaining an equation from shorter times.

The annealing parameters for the standard materials are presented in Table 5.1. Unlike XLPE, the slopes of the annealing curves do not show as pronounced a change with annealing temperature as was observed for XLPE. They remain essentially constant (avg. 2.37 °C/hr) with increasing annealing temperature. The slopes of the XLPE annealing equations also tend to be larger than those of EPR which indicates that the melting point of the lamellae produced by annealing increases at a greater rate than those of EPR.

One can notice another interesting feature in the values of the y-intercept for XLPE and EPR. For the comparable annealing temperatures of 60 and 70 °C the values of the y-intercept of XLPE are 68.1 and 77.76 °C, respectively. For EPR the y-intercepts are 68.5 and 77.26, respectively. This is surprising considering the large difference in the basic melting behavior of the two materials and suggests that the y-intercept is dependent upon the annealing temperature alone and is independent of the material.

5.1.3 Ethylene Propylene Terpolymer (EPDM)

The plot of Tp versus logarithmic time for EPDM is shown in Figure 5.3 along with the corresponding annealing equations. Once again there seems top be a good correlation between the short and

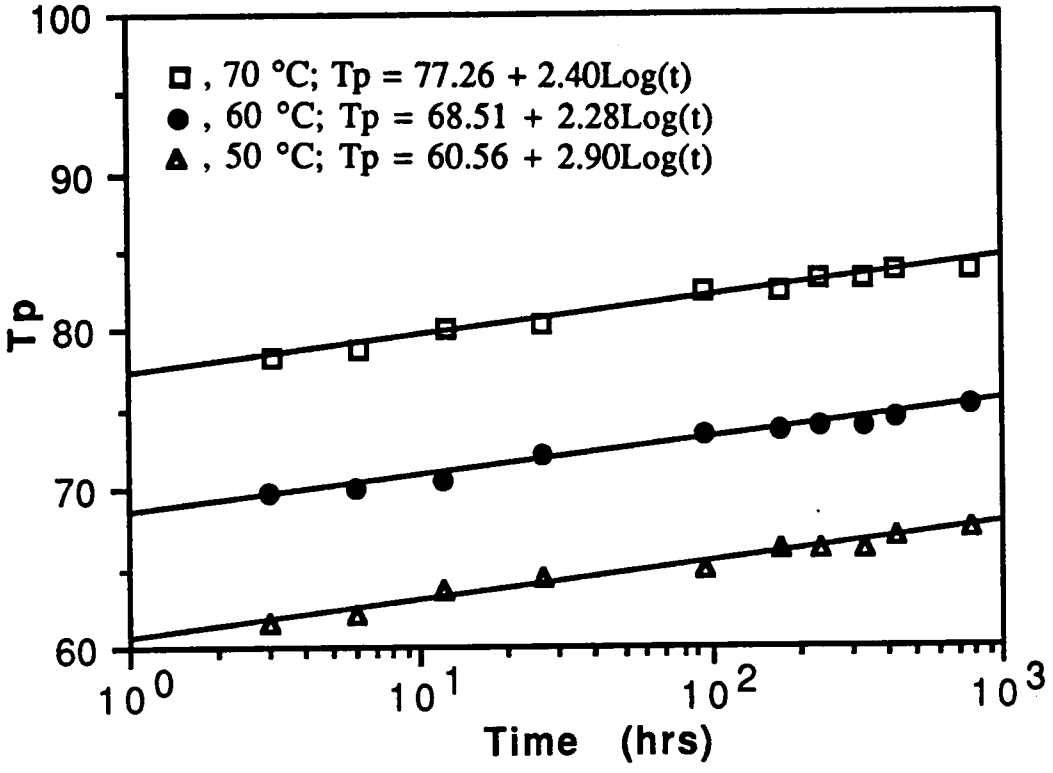


Figure 5.2: Tp versus logarithmic time for EPR.

Table 5.1 Annealing parameters.

Material / Ta	Y-int. A	Slope B
XLPE 70 C	77.76	3.22 °C/h
XLPE 60 C	68.10	4.14
XLPE 45 C	54.59	3.89
XLPE 35 C	47.68	2.70
EPR 70 C	77.26	2.40
EPR 60 C	68.51	2.28
EPR 50 C	60.56	2.39
EPDM 70 C	78.56	1.99
EPDM 60 C	68.42	2.85
EPDM 50 C	60.50	2.32
XEPR 70 C	78.47	1.51
XEPR 60 C	69.24	2.02
XEPR 50 C	61.82	1.82
XEPDM 70 C	75.43	3.00
XEPDM 60 C	67.67	1.98
XEPDM 50 C	59.54	1.86
A1 70 C	76.99	2.17
A1 60 C	68.36	2.33
A1 55 C	64.24	2.03
A1 50 C	59.82	2.52
A3 70 C	78.58	3.20
A3 60 C	70.10	3.37
A3 55 C	65.01	3.48
A3 50 C	61.10	3.29
C1 70 C	77.29	3.04
C1 60 C	69.03	2.91
C1 55 C	65.09	2.77
C1 50 C	60.56	3.25
B1 70 C	78.29	2.81
B1 60 C	69.28	3.15
B1 55 C	64.47	3.20
B1 50 C	61.00	3.05
D1 70 C	78.35	3.79
D1 60 C	71.35	3.33
D1 50 C	62.45	4.01

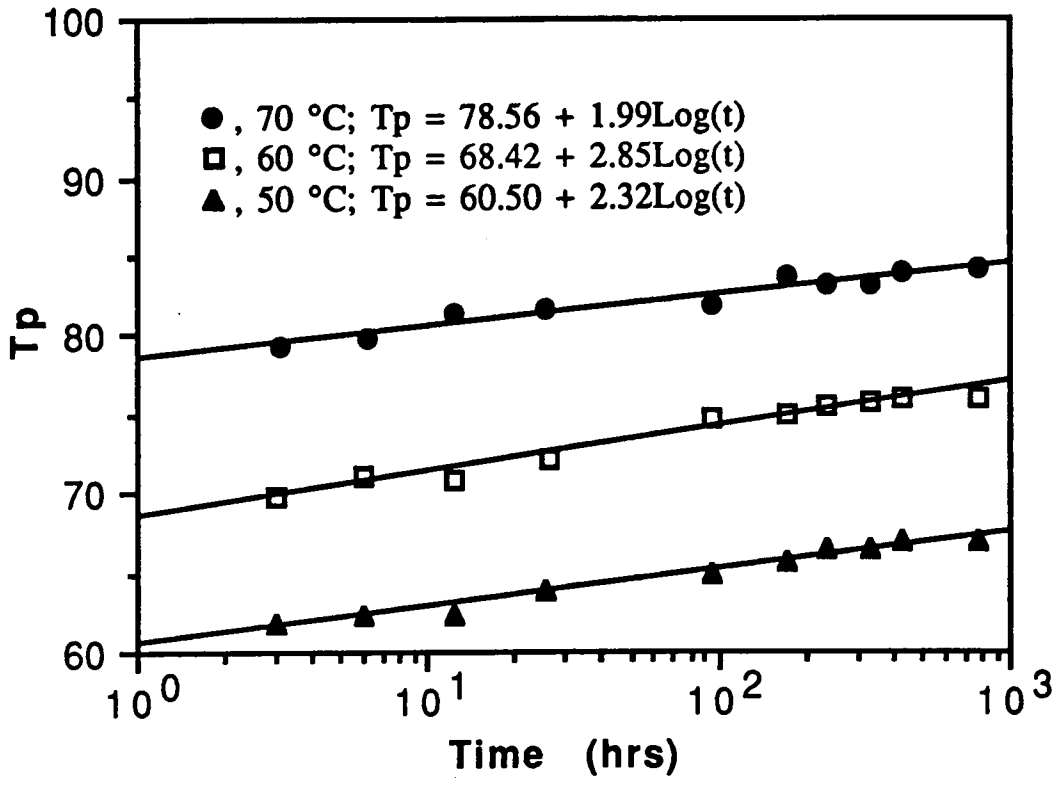


Figure 5.3: Tp versus logarithmic time for EPDM.

long term annealing points.

The annealing behavior of EPDM is virtually the same as that of EPR. For 50 °C annealing the values of both the slopes and the y-intercepts of the annealing equations are within 0.08 of one another. The 60 °C and 70 °C annealing equations of EPR and EPDM are also quite similar with the y-intercepts being within 1 °C of one another. The y-intercepts for the EPDM equations of 70 and 60 °C annealing also match those obtained for the corresponding annealing equations of XLPE.

The slopes of the annealing equations for EPDM show slightly more variation than those of EPR with a decrease occurring for the 70 °C annealing equation. However, it appears that both EPR and EPDM anneal in similar fashions.

5.1.4 Crosslinked EPR (XEPR)

The annealing kinetics for XEPR are shown in Figure 5.4 with the equations given on the graph. It becomes apparent from the lower values of the slopes of the annealing equations that XEPR anneals more slowly than EPR. The slopes are constant with time and on the average about 0.5 °C/hrs lower than those obtained for EPR (Table 5.1). One can also notice that the y-intercepts have values very close to those found for EPR, EPDM, and XLPE, which gives increasing evidence that this parameter is a function of annealing temperature alone

5.1.5 Crosslinked EPDM (XEPDM)

The annealing equations and plot of Tp versus time for XEPDM are shown in Figure 5.5. There is an overall decrease in the slopes of the 50 and 60 °C annealing equations compared with those of EPDM, but one can observe a major increase for the 70 °C annealing equation of XEPDM. There is also a large amount of scatter present in the data for this temperature as well. Looking back to Figure 4.16

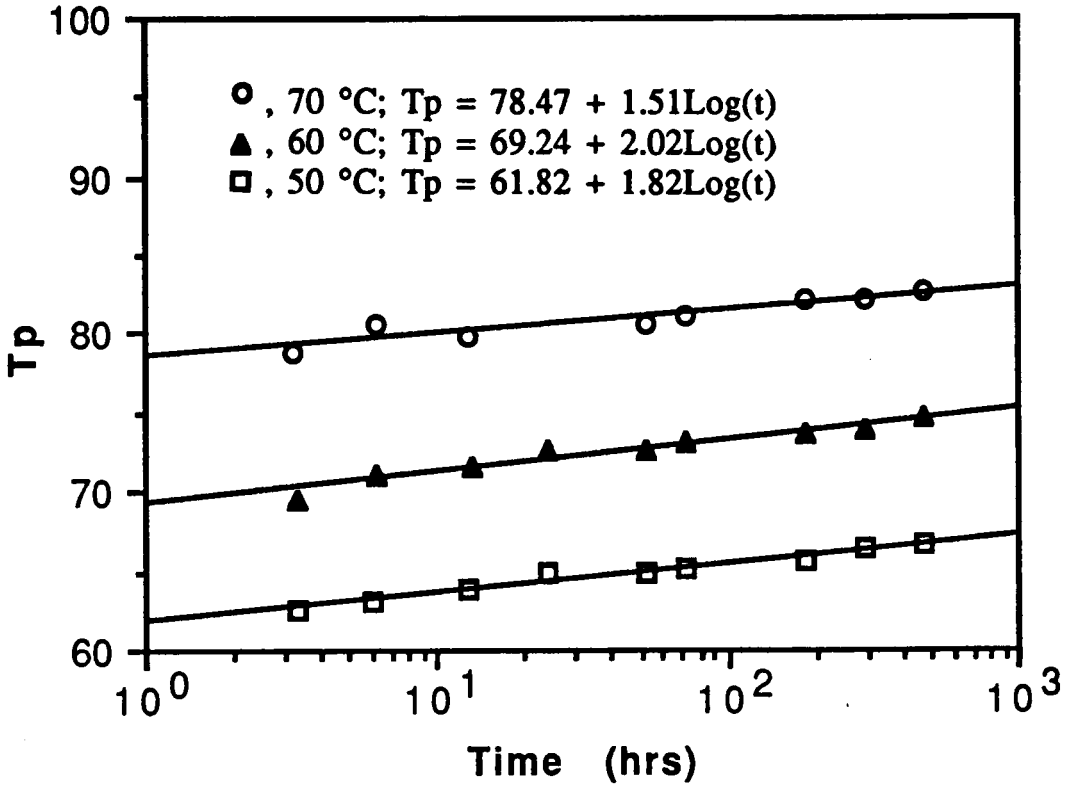


Figure 5.4: Tp versus logarithmic time for XEPR.

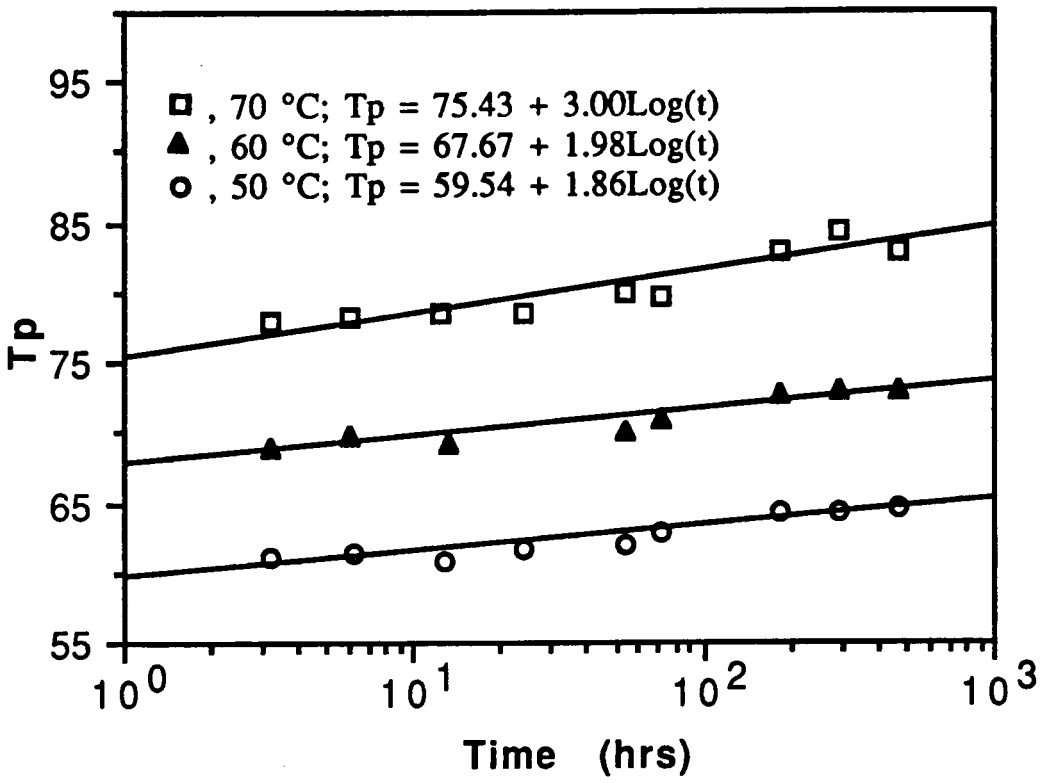


Figure 5.5: Tp versus logarithmic time for XEPDM.

which shows the effects of the various annealing temperatures upon the DSC endotherms one can observe that 70 °C annealing does not generate a very well defined peak and essentially the majority of the material is unable to recrystallize and remains molten during annealing. The annealing at 70 °C is perhaps affecting part of the soluble phase which was not incorporated into the gel. Since peroxide crosslinking favors areas with tertiary carbons (i.e. branch points) as well as double bonds, then the material which constitutes the soluble phase could very well contain longer sequences between branches and unsaturated carbon bonds on average than found in the bulk EPDM. Branch points act as defects and hinder crystallization, thus one might expect this soluble phase to recrystallize faster than the bulk EPDM, as observed. Also, one could expect the molecular weight of the soluble portion to be lower than that of the bulk EPDM as well, which would also cause and increase in the recrystallization rate for the soluble phase of XEPDM. The same effects were not observed for the XEPR because most of the gel phase is able to recrystallize at 70 °C as shown in Figure 4.13, and therefore dominates the kinetics, However, no studies have been done upon the soluble phase of XEPDM to support this hypotheses.

We can now take a brief moment to consider the effect that crosslinking a system has upon the rate of annealing. From the data obtained for EPR and XEPR and the 50 and 60 °C annealing data of EPDM and XEPDM, we can see that crosslinking appears to slow the rate of annealing, as shown through a decrease in the slopes of the annealing equations with crosslinking. The introduction of crosslinks acts to hinder the mobility of molecule thus slowing the rate of annealing and crystal thickening.

5.2. Control Cables

5.2.1 Cable A1 [Eaton Corp. (Samuel Moore)]

The plot of Tp versus logarithmic time for this cable is shown in Figure 5.6. The slopes of the equations appear to be independent of the annealing temperature with an average value of 2.25 °C/hrs. This value is in the range of those determined for EPR and EPDM and is only slightly above those of the crosslinked samples (Table 5.1). The melting curves for this cable (Figures 4.34 and 4.35) indicated the presence of some type of lower melting material in the form of either EPR or EPDM. One can also notice that the y-intercepts are consistent with those determined for the other materials as well.

The position of the gain peak as a function of annealing time for 70 °C annealing of both the original and history erased samples is shown in Figure 5.7. One can observe that the line produced from the original samples is shifted upward and the slope is about .2 °C/hr steeper. This indicates that Tp shifts upward at a slightly faster rate than for the history erased samples, but for all practical purposes behaves the same.

5.2.2 Cable A3 [Eaton Corp. (Samuel Moore)]

This insulation appeared from its melting behavior to consist of either XLPE or XHDPE (Figure 4.26). Therefore one might expect the annealing parameters to be similar to those already obtained for XLPE. One can see in Figure 5.8 that this is actually the case. For 70 °C annealing the slope of the equation for cable A3 is identical to that obtained for XLPE. The other slopes are also similar in values. Also, the y-intercepts follow the same trends as previously observed, their values being governed by annealing temperature alone.

The differences in the annealing behavior of the original and history erased samples of cable A3 can be seen in Figure 5.9. One

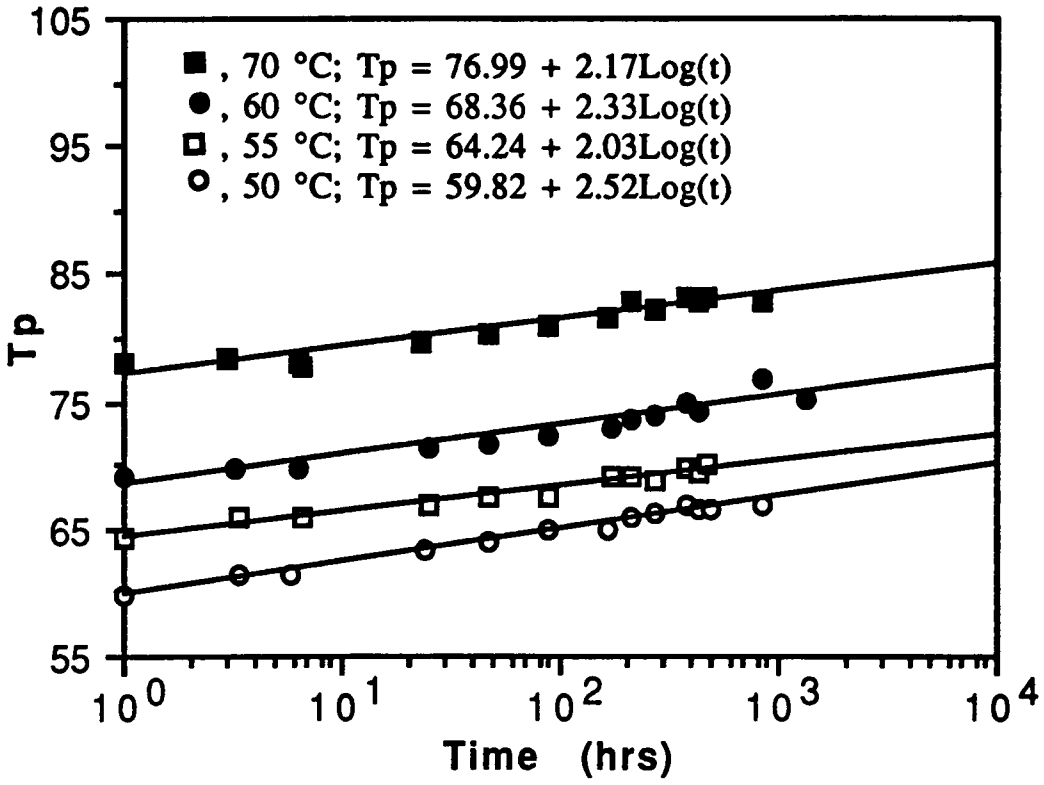


Figure 5.6: Tp versus logarithmic time for cable A1.

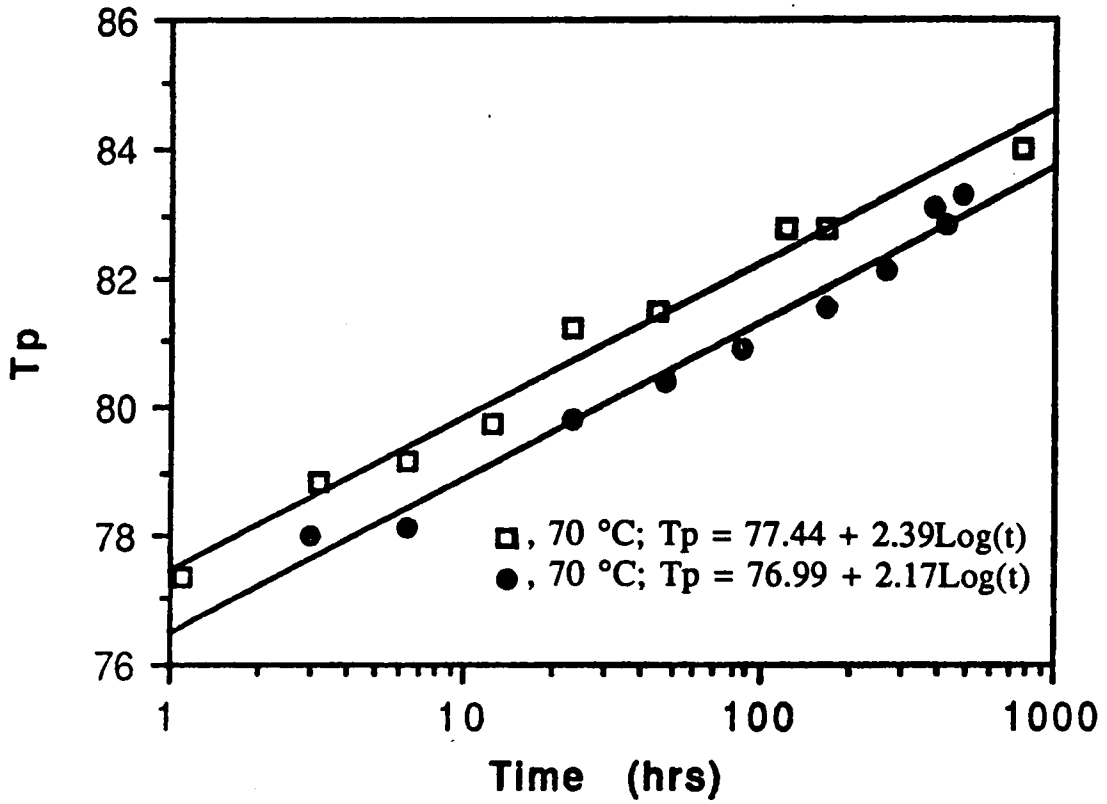


Figure 5.7: Tp versus logarithmic time for original and history erased samples of cable A1.

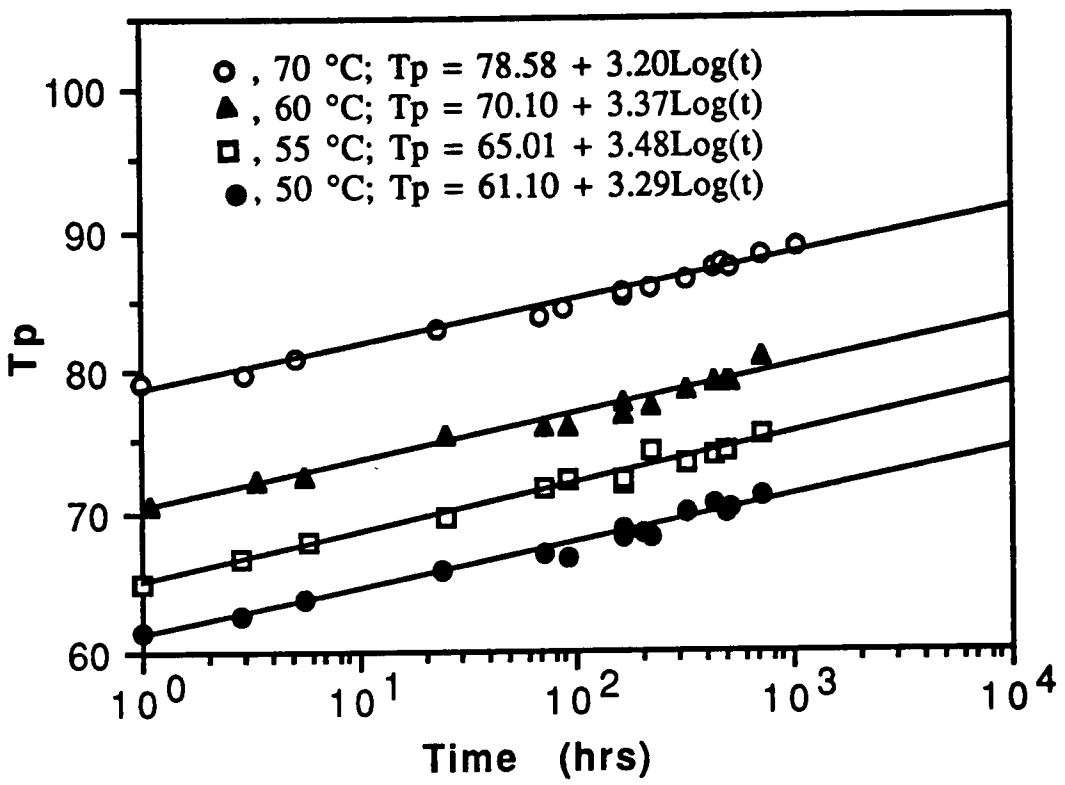


Figure 5.8: Tp versus logarithmic time for cable A3.

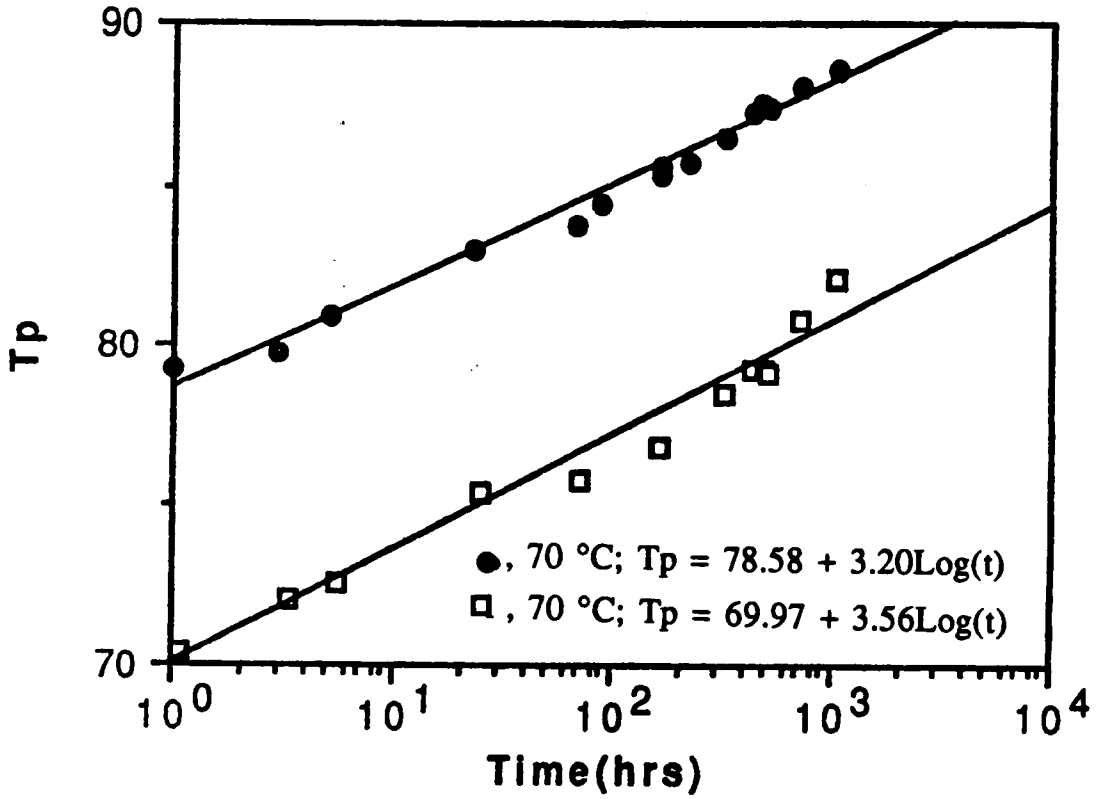


Figure 5.9: Tp versus logarithmic time for original and history erased samples of cable A3.

can see that the line generated from annealing the original sample at 70 °C is shifted downward by about 9 °C from that produced by annealing history erased samples. However, the values obtained for the slopes appear to remain constant.

This is easily explained by considering that the original cable had been previously exposed to a temperature of approximately 95 °C, shown by the subtraction curve in Figure 4.27. Therefore, a portion of the material which might ordinarily melt and recrystallize during 70 °C annealing has already done so during the 95 °C treatment. When the original sample is annealed at 70 °C, there is not as much material present that will melt and recrystallize at the temperature and therefore the upward shift of the gain peak is slower.

5.2.3 Cable C1 [BIW]

The annealing kinetics of cable C1 are shown in Figure 5.10 through the plot of Tp versus logarithmic time. The y-intercepts are consistent with those obtained for other materials and the values for the slopes show very little temperature dependence. The material composing this insulation appeared from its melting behavior (Figure 4.33) to be XLPE blended with an EPR or EPDM. The average value of the slopes obtained from annealing lines is 3.0 °C/hrs, which is in the range of those determined for XLPE.

5.2.4 Cable D1 [Anaconda]

The plot of Tp versus time is shown for cable D1 in Figure 5.11 and yields the same basic form as obtained previously for the other materials. The intercepts are equivalent to those obtained from the annealing equations of the other materials and the slopes are generally temperature independent and typical of those obtained for XLPE (Table 5.1).

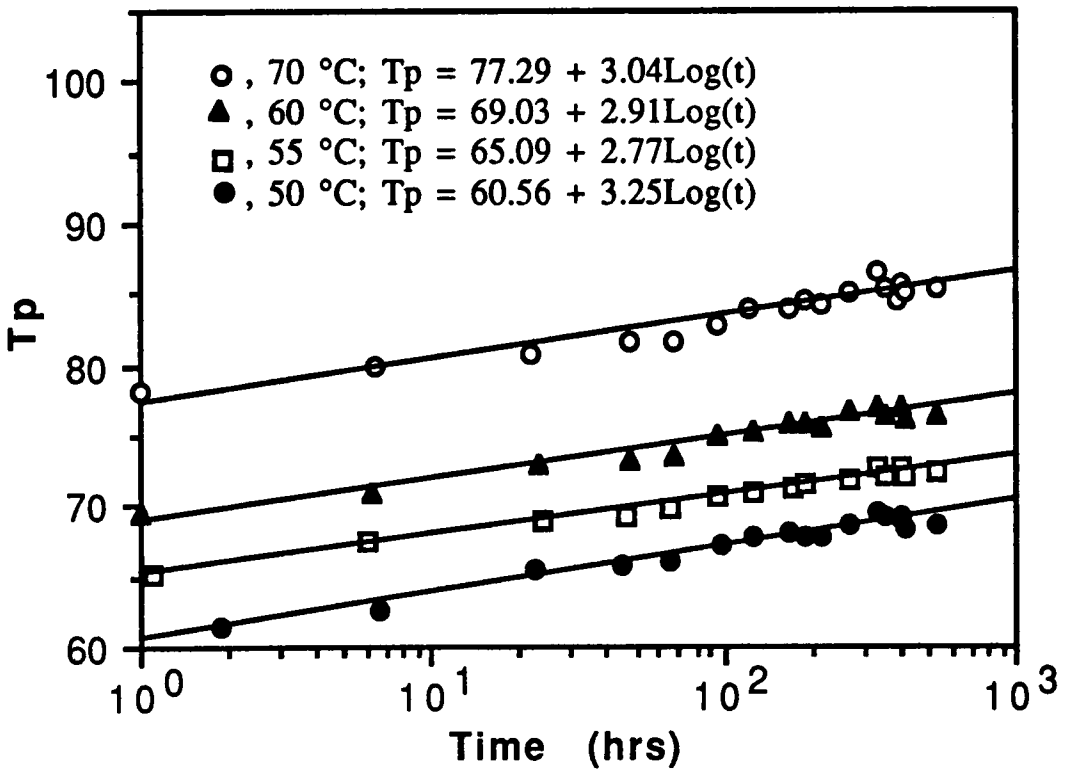


Figure 5.10: Tp versus logarithmic time for cable C1.

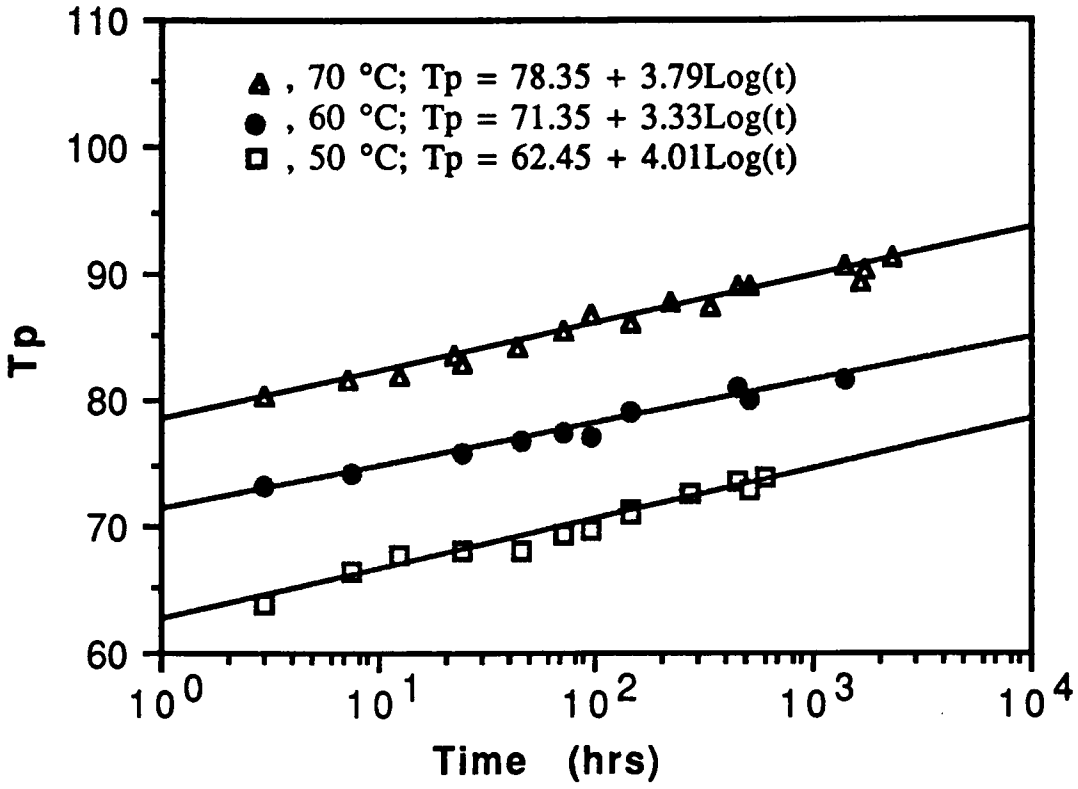


Figure 5.11: Tp versus logarithmic time for cable D1.

5.2.5 Cable B1 [Rockbestos]

The lines generated for the Tp versus time plot of the low temperature annealing data is shown in Figure 5.12. Recalling that this cable was most likely composed of blended LPE and HPE cross-linked together, one would expect the slopes to be in the vicinity of those obtained for XLPE in the low temperature annealing region. The equations are shown both in Figure 5.12 and Table 5.1, and the slopes do indeed match fairly closely those of XLPE and the other XLPE blended cables (A3, C1, and D1). The slopes show very little temperature dependence and yield an average value of 3.1 °C/hrs.

The high temperature annealing results also yield lines with equations of similar nature to the lower annealing temperature ones, as shown in Figure 5.13. The slopes of the lines are much lower than those obtained for annealing temperatures between 50 and 70 °C. The values of the 100 °C and the 120 °C annealing lines are 1.6 and 1.3 °C/hrs, respectively. That of the 110 °C annealing shows a surprisingly low value of .8 °C/hrs. This strongly suggests that the values of the slopes can change if the annealing temperature is close to the major melting peak. Referring back to Figure 4.46 we can observe that the high temperatures are within the regions where both of the melting points of the quenched material exist. Further studies are necessary at these elevated temperatures to quantify their behavior.

The subtraction data were analyzed for both the original and history erased 70 °C annealing experiments and the results are shown in Figure 5.14. There is very little difference between the two sets of data. Thus the original and history erased samples appear to anneal identically at a temperature of 70 °C.

The plot of Tp versus time for the samples annealed at 98 °C then subsequently annealed at temperatures of 70 and 80 °C is shown in Figure 5.15. The data for the history erased annealing at 70 °C are

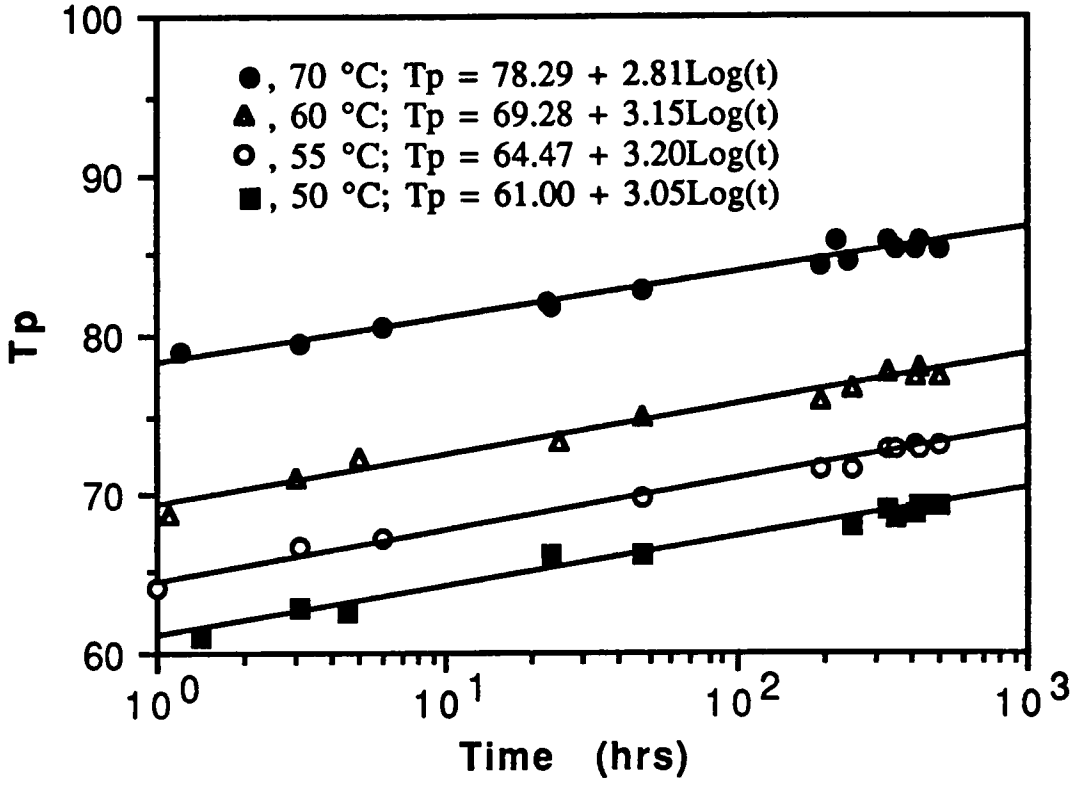


Figure 5.12: Tp versus logarithmic time for low temperature annealing of cable B1.

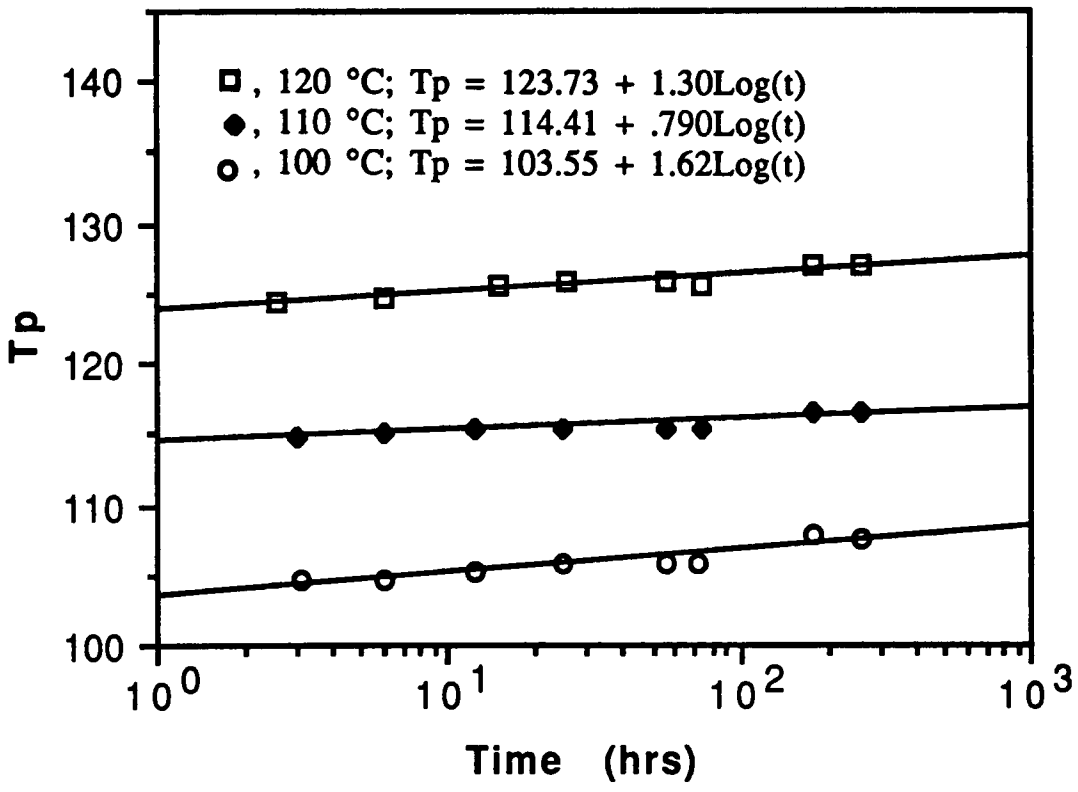


Figure 5.13: Tp versus logarithmic time for high temperature annealing of cable B1.

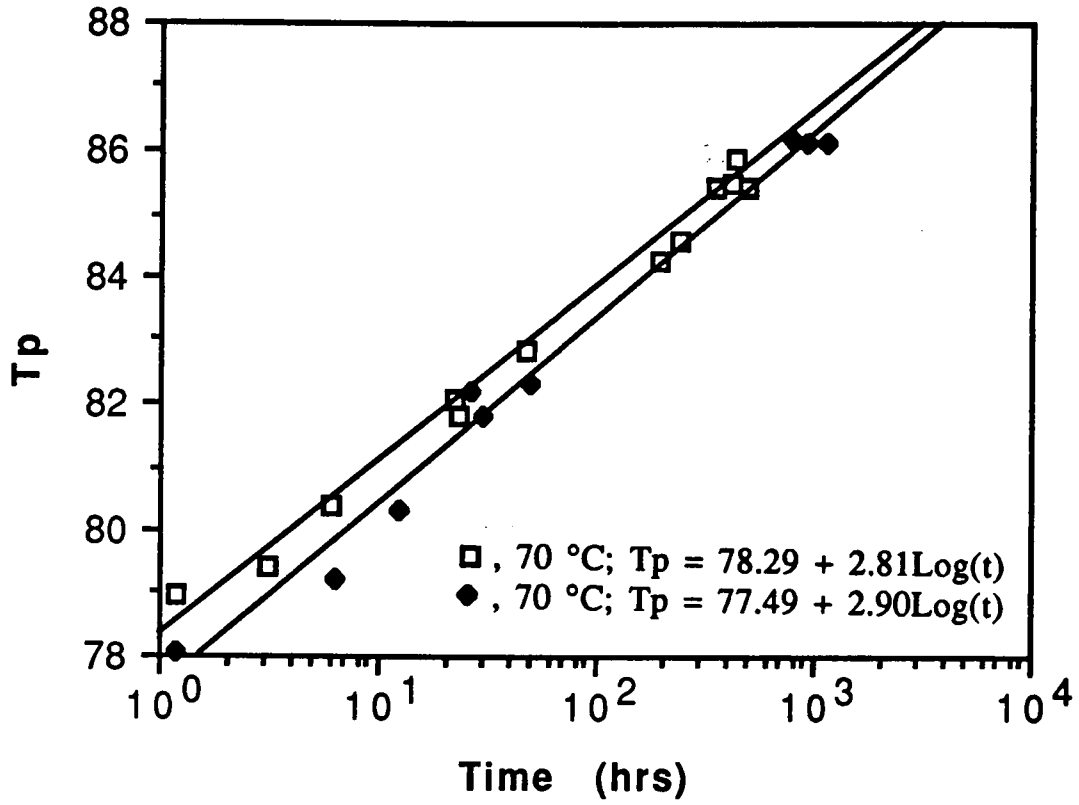


Figure 5.14: Tp versus logarithmic time for original and history erased samples of cable B1.

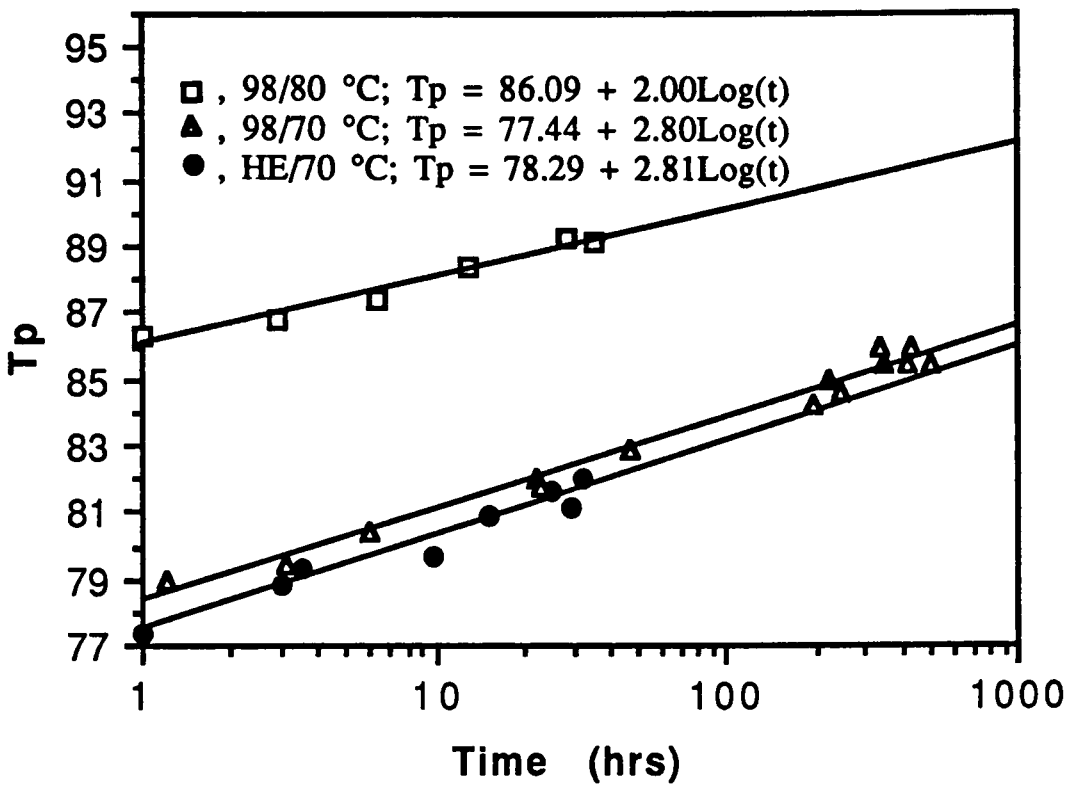


Figure 5.15: Tp versus time for 98 C annealing followed by 70 or 80 C annealing of original cable B1.

also plotted in the figure as well. One can observe that annealing of the original cable at 70 °C after annealing at 98 °C produces similar results to those obtained from annealing history erased samples at a single temperature of 70 °C.

5.3 Data Analysis

In order to test the validity and accuracy of the equations developed an error analysis was performed upon selected sets of data using simple linear regression. The results are shown in Table 5.2. Most of the equations developed show reasonably good fits with correlation coefficients greater than 0.97. Errors in the slopes of the fitted lines ranged from plus or minus 0.1 to approximately 0.3 ^{o}C/hr and for the intercepts errors of plus or minus 0.3 ^{o}C could be expected.

While multiple points were not obtained for particular annealing times, confidence limits of 95 percent were calculated for the dependent variable Tp in order to obtain an estimation of the scatter present for a particular annealing time. This calculation was performed using Statgraphics software. The results are also shown in Table 5.2. In general for all the materials, Tp was calculated to have on average an accuracy of roughly plus or minus 0.36 ^{o}C with less scatter expected for shorter and intermediate annealing times. For the maximum error in Tp of 0.72 ^{o}C, an error of approximately 60 percent of the actual time could be obtained in the estimation of the annealing time. However, even with an error of this magnitude possible, the technique will still allow the distinction between short and long periods of annealing. Table 5.3 shows some of the time estimation errors possible using the limits given in Table 5.2.

5.4. Estimating Thermal History

It has been shown for both the control cable insulation and the standard materials that the position of the gain peak, Tp, on the

Table 5.2 : Data from statistical analysis of annealing results.

Material	Temp. (°C)	Standard Error slope	y-intcpt.	Corr. Coef.	Short 1-48 hrs	Intermd. 150-350	Long 500-
Cable A1	50	.10	.20	.990	± .25 °C	± .18 °C	± .25 °C
	55	.13	.27	.978	.30	.29	.42
	60	.17	.37	.969	.42	.45	.68
	70	.17	.34	.964	.43	.36	.54
Cable A3	50	.13	.27	.990	.27	.18	.22
	55	.16	.33	.988	.26	.27	.36
	60	.32	.70	.953	.39	.36	.54
	70	.12	.25	.990	.22	.17	.29
Cable B1	50	.16	.33	.980	.36	.27	.41
	55	.10	.22	.995	.22	.20	.27
	60	.16	.32	.988	.36	.27	.40
	70	.14	.30	.984	.36	.27	.30
Cable C1	50	.17	.36	.980	.32	.18	.25
	55	.17	.36	.969	.36	.27	.38
	70	.30	.82	.900	.60	.45	.60
XLPE	35	.38	.34	.960	.54	.54	.72
	45	.10	.24	.996	.14	.11	.22
	70	.24	.45	.969	.40	.27	.54
EPDM	50	.12	.25	.989	.32	.36	.39
	60	.17	.34	.986	.40	.36	.47
	70	.16	.33	.975	.50	.36	.64
EPR	50	.13	.54	.988	.32	.27	.36
	60	.12	.24	.988	.36	.25	.36
	70	.11	.23	.991	.29	.32	.36

Table 5.3: Examples of Typical Time Estimation Errors.

Cable	Temp. (°C)	Tp(24 hrs) (°C)	Range (hrs)	Tp(200 hr) (°C)	Range (hrs)	Tp(500 hr) (°C)	Range (hrs)
A 1	50	63.29	16-30	65.61	160-251	66.62	397-630
	55	67.04	17-33	68.91	144-278	69.72	310-805
	60	71.57	16-36	73.72	128-312	74.64	255-980
	70	80.00	15-38	81.98	112-354	82.84	282-886
B1	50	65.20	18-31	68.02	163-245	69.23	366-681
	55	68.88	20-28	71.83	173-231	73.1	412-607
	60	73.63	18-31	76.52	164-243	77.78	373-670
	70	82.16	17-32	84.75	160-250	85.87	391-640
EPDM	50	63.70	17-33	63.83	140-286	66.76	339-736
	60	72.35	17-33	74.97	149-267	76.11	342-730
	70	81.30	13-42	83.13	132-303	83.90	238-1048

subtraction curve follows a logarithmic time dependence over the whole spectrum of annealing times. The annealing temperature has also been shown to correspond approximately to the position of the loss peak, Td, which remains essentially constant with annealing time.

Thus, if one wishes to extract the thermal history from a particular sample and has access to a DSC to generate the subtraction curve, all that needs to be known is the annealing equation for that particular sample. Of course, if the particular material is a cable insulation which has been previously characterized either in this or other studies yet to come, one simply would use the pre-determined equation for the annealing temperature of interest. However, if such an equation is not available one has to develop their own. This can be done in one of several ways.

5.4.1 Development of a Calibration Curve

The first method consists of carrying out a number of annealing experiments in order to generate the Tp versus logarithmic time plot. One would first perform the subtraction technique on the sample and determine the temperature of interest from the position of the loss peak, Td. Since the points generated from the shorter annealing times appear to correspond well with those of longer times, one simply has to anneal the sample at the temperature, Td for short periods of time (1, 3, 6, 12, and 24 hours) and perform the subtraction technique on these samples. From these points an annealing equation can be generated to predict the length of the temperature exposure.

The question now arises as to what sample to anneal in order to develop this calibration curve. There are two choices; either one can use a virgin sample or a history erased sample. If a virgin sample is not available one essentially has no choice but to use history erased samples for the development of the calibration curve. It has been shown for the 70 °C annealing of cables A1 and B1 that there is little

difference between the annealing equation generated for history erased samples and that for the original samples. Cable A3 showed considerable differences between the two only because the original samples had been previously exposed to 95 °C.

Basically if the original cable had been exposed to a temperature which resulted in large scale annealing during processing, and then is annealed at a lower temperature one may obtain erroneous results from developing the calibration curve from history erased samples. One may recall that this was the case for cable B1, which showed annealing at temperatures of 110 and 115 °C, as well as 60 °C. The equations generated from annealing the history erased samples still matched well with those generated from the original samples. However, the majority of the XLPE was molten at 110 °C and thus crystallized upon cooling. The 60 °C history did not effect the results because annealing at 70 °C erased that history. A difference between the annealing behavior of the history erased and original samples most likely would have been observed for 50 or 60 °C annealing. So the inherent thermal history from processing creates discrepancies between equations developed from history erased and virgin samples only if material has been melted and recrystallized such that a shoulder is observable on the DSC endotherm above the temperature at which one wishes to characterize the material. The catch is that if you do not have the virgin sample there is no way to tell the difference between history generated from processing and history generated during use.

The use of virgin samples also has its limitations as well. One has to remember that most of the polymeric insulation is sensitive to room temperature annealing. While extended room temperature annealing is not going to effect the results above about 40 °C, annealing produced by storage where the material can be exposed to hot summer temperatures in an enclosed shed will. Thus one has to be careful of the storage of virgin samples for future analysis.

Therefore, the best method of developing the calibration curve is to anneal virgin samples if available. It is also instructive to anneal

history erased samples as well determine if there is a major difference. If virgin samples are not available then the limitations discussed earlier should be kept in mind during data analysis.

5.4.2 Development of the General Annealing Equation

The plots of Tp versus logarithmic time have yielded equations of the form:

$$Tp = A + B\text{Log}(t)$$

The parameter B appears to be independent of the annealing temperature for EPRs and EPDMs. For XLPEs the value of B is constant only if the annealing temperature is roughly 20 °C below the temperature of the major melting peak. For XLPE this is about 80 °C. Above this temperature the slope appears to change from that obtained from the lower temperatures, but may assume another constant value. So the slope of the annealing equation appears to be primarily a material variable over a fairly broad range of temperatures (35 to 80 °C). The characteristic slopes for the various materials are given in Table 5.4. They were determined by simply taking the average of the slopes generated from the annealing temperatures examined. For insulation containing typical XLPE (melting temperature of 100 °C) the characteristic slope is 3.16 °C/hrs. For material composed primarily of an EPR or EPDM cross-linked blend the characteristic is slope 2.36 °C/hrs (determined from the standards). For the cable insulation examined which contain crosslinked blends of LPE with EPR or EPDM the slopes appear to match those more typical for XLPE (cables D1, C1 and A3, Table 5.4). It appears that the faster annealing XLPE portion of the blend masks the annealing effects of the EPR or EPDM portion. Thus if one wishes to characterize the annealing behavior of a blended insulation without developing a calibration curve the characteristic value for

Table 5.4: Characteristic parameters for the various materials.

Material	Characteristic Parameter
XLPE	3.48 °C/hrs
EPR	2.36
EPDM	2.38
XEPR	1.78
XEPDM	1.92
Cable A1 (EPR)	2.26
Cable A3 (XLPE)	3.34
Cable C1 (Blend)	3.00
Cable B1 (XPEs)	3.10
Cable D1 (XPE/EPR)	3.71

XLPE should be used in the annealing equation.
The value of the y-intercept, A, appears to have a strong temperature dependence and varies slightly between materials. If one plots the y-intercepts of the annealing equations against the annealing temperatures one obtains a relation which effectively describes the annealing temperature dependence of the y-intercept (A). Such a plot is shown for the EPRs and EPDMs in Figure 5.16 and for XLPE and cables composed primarily of XLPE (B1 and A3) in Figure 5.17. The equations are essentially identical for the EPR materials and the XLPE materials.

By taking the average of the values obtained for the slopes and intercepts of the equations shown in Figure 5.16 a characteristic equation which describes the shift in the y-intercepts of the annealing equations with annealing temperature for EPRs and EPDMs can be obtained:

$$A = 18.4 + .84(Ta) \qquad 5.1$$

And likewise for XLPE:

$$A = 16.7 + .874(Ta) \qquad 5.2$$

Substituting into the form of the annealing equation we have the following general expression describing the annealing behavior of EPRs and EPDMs at any temperature between approximately 50 and 70 °C:

$$Tp = 18.4 + .84\ (Ta) + BLog(t) \qquad 5.3$$

where Ta is the annealing temperature and B is the characteristic annealing parameter for EPRs and EPDMs determined earlier to be 2.36 °C/hr. Thus the final form of the general annealing equation for these materials is:

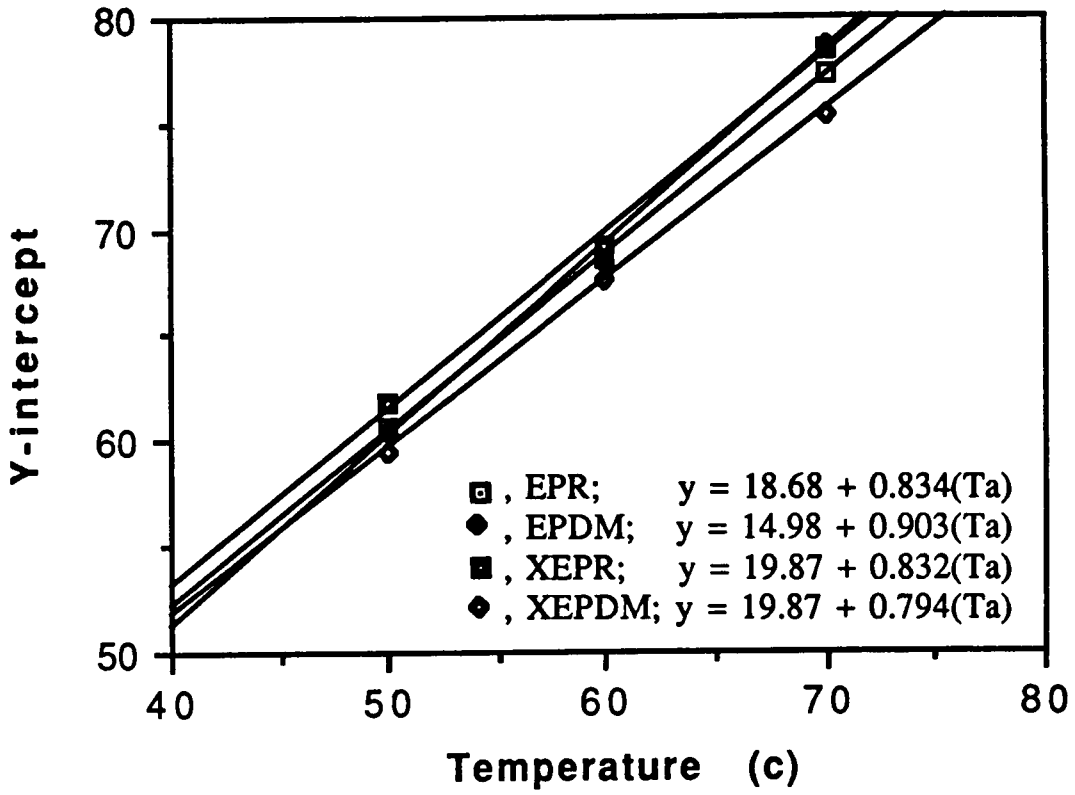


Figure 5.16: Y-intercepts of annealing equations plotted against annealing temperatures for EPRs and EPDMs.

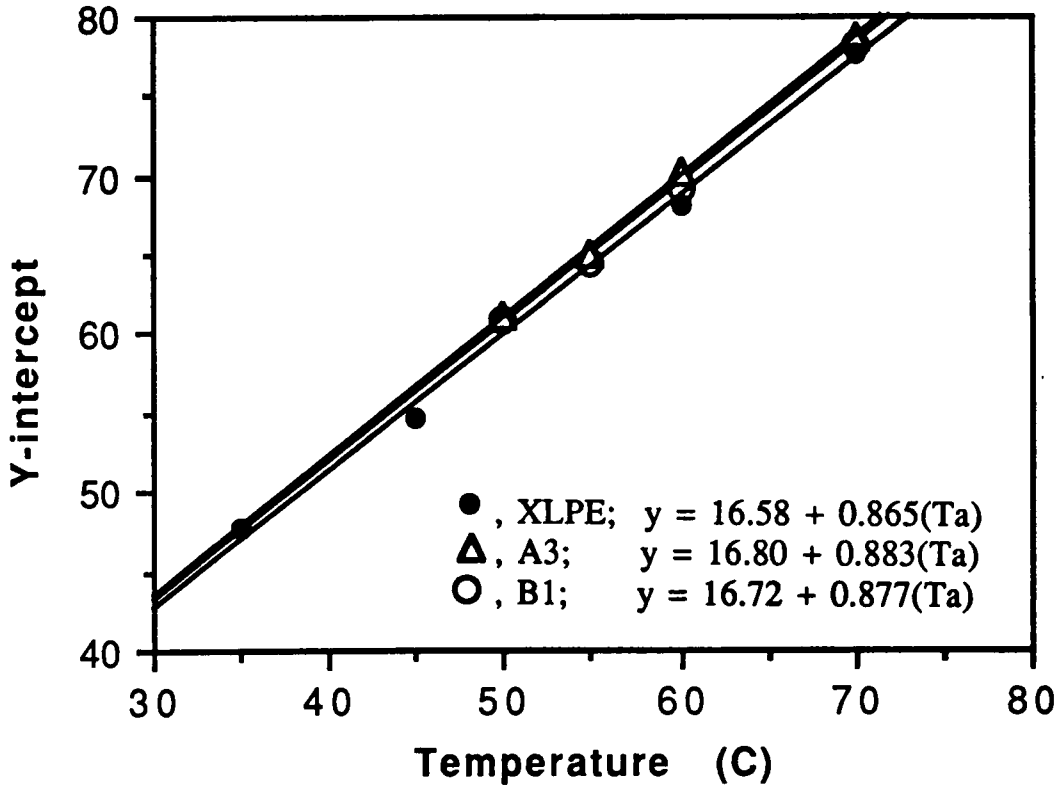


Figure 5.17: Y-intercepts of annealing equations plotted against annealing temperatures for XLPE, B1, and A3.

$$Tp = 18.4 + .84(Ta) + 2.36Log(t) \qquad 5.4$$

The same simple manipulation can be performed for XLPEs to yield the general annealing equation:

$$Tp = 16.7 + .87(Ta) + 3.16Log(t) \qquad 5.5$$

5.5. Multiple Annealing and Cycling Studies

Now that the general annealing equations have been developed we can test the effect of multiple annealing upon the prediction of the amount of time that a sample has been exposed to a particular temperature. Using equations 5.4 for EPDM and 5.5 for XLPE and the values obtained for Tp and Td from the multiple annealing and cycling experiments, estimations of the time of annealing were obtained. These are summarized in Table 5.5. Time estimations were also obtained by using the actual annealing temperature as well, and are also shown in Table 5.5. From the table it becomes apparent that for multiple annealings only the highest annealing temperature can be predicted with any accuracy. In general, better time estimations were obtained using the actual annealing temperature as opposed to Td in the equations, but in practice one will have no choice but to use the annealing temperature value obtained from the subtraction curve. However, the estimations obtained using the Td values for the highest annealing temperature were all reasonably close. In other words, this technique may not give extremely accurate predictions, but it should allow one to distinguish between annealing for short (under a day), intermediate (1 to 2 weeks), and long (over a month) periods of time.

Cycling of temperatures appears to have little effect upon the estimation of annealing time or temperature.

Table 5.5: Summary of multiple annealing and cycling experiments.

Material	Ta (°C)	Td (°C)	Tp (°C)	Time (hrs)	Predicted Time (Td)	Predicted Time (Ta)
XLPE	70	73.0	81.70	10	3	18 hrs
	35	41.2	48.4	100	----------	----------
XLPE	70	73.0	83.70	50	16	85
	50	54.0	63.70	240	1	13
EPDM	70	71.4	81.60	24	23	72
	50	55.1	64.00	24	----------	34
	25	30.2	42.25	24	----------	----------
EPDM	70	71.0	81.50	24	29	66
	35	40.0	53.60	35	5	288
XLPE	70	72.1	83.56	70	20	77
XLPE	70	73.0	84.15	120	20	118

5.6. Aged Samples

This subtraction technique has been developed under controlled laboratory conditions where all of the variables are known. While the effects of changing the annealing temperature, annealing time, and the preannealed history of the sample have been studied to some degree, there is still a large number of different conditions which may be encountered in practice and which may adversely effect the ability of this technique to discern thermal history. Some of these will be encountered in examining the thermal history of the aged samples.

5.6.1 Cable 246-155-RW

The positions of the loss and gain peaks as determined from the subtraction curves are shown in Table 5.6 for cable RW. Values given in bold were obtained from the subtraction of the control endotherm from the aged endotherm. The y-intercept and slope of the annealing equation as well as the estimations of annealing time are also given.

Since the Rockbestos cable B1 appears to be of the same nature as cables RW and RP, the equations developed describing its annealing behavior can be used in helping to determine that of the aged samples. The control cable RW appears to have history at temperatures of 103.8 and 113 ^{o}C which is inherent from the manufacturing process. By plotting the y-intercepts of the high temperature equations developed for cable B1 against annealing temperature a plot similar to those in Figures 5.16 and 5.17 can be developed which describes the position of the y-intercept of the annealing equation as a function of the annealing temperature for the elevated temperatures. This plot is show in Figure 5.18. From Table 4.12 one could observe that in the high temperature regions Td tends to run slightly lower than the actual annealing temperature.

Table 5.6: Predictions for cable 246-155-RW

Cable	Td (°C)	Tp (°C)	Ta (°C)	y-intcpt. (°C)	Slope (°C/hr)	Time (hrs)
RW-Con.	113.0	125.00	116.0	123.0	1.3	33
	103.3	110.30	104.0	108.6	1.6	11
RW-1	113.3	124.20	116.0	123.0	1.3	8
	112.8	123.60	116.0	123.0	1.3	3
	103.3	114.16	104.0	108.6	1.6	3,000
	103.2	115.34	104.0	108.6	1.6	16,000
	96.93	**100.4**	**95.0**	**96.4**	**2.0**	**93**
	83.7	91.70	80.0	86.1	2.0	630
	82.0	91.28	80.0	86.1	2.0	389
	81.87	85.33	80.0	86.1	2.0	Short
	79.00	85.60	75.0	81.95	2.6	Short
	62.67	71.73	60.0	67.1	3.1	27
	56.80	69.70	60.0	64.47	3.1	48
RW-2	113.3	121.2	116.0	123.0	1.3	24
	113.0	123.6	116.0	123.0	1.3	3
	104.7	115.35	104.0	104.0	1.6	25,000
	103.7	116.52	104.0	108.6	1.6	90,000
	92.3	94..8	92.0	92.9	2.0	9
	94.8	**97.6**	**93.0**	**94.24**	**2.0**	**48**
RW-4	114.3	125.96	116	123.0	1.3	189
	113.15	123.6	116	123.0	1.3	Short
	104.2	113.35	104	108.6	1.6	930
	93.3	95.87	92	92.90	2.0	30
	99.07	104.47	98	100.7	2.0	69

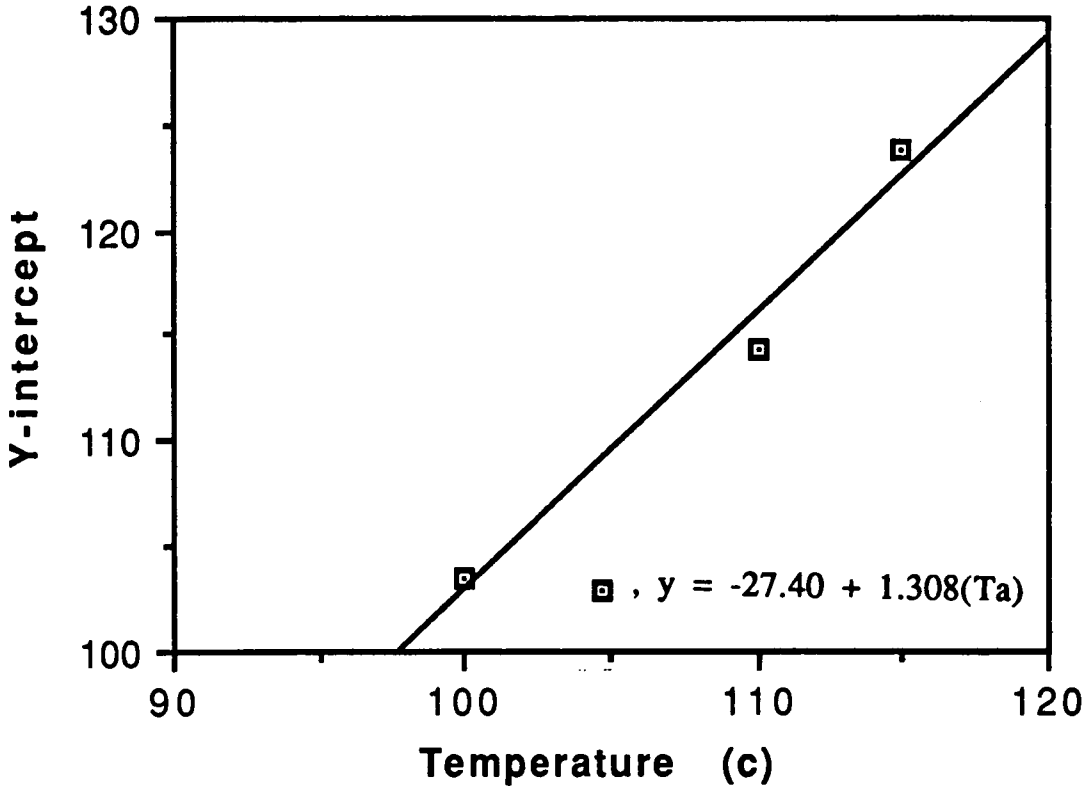


Figure 5.18: Y-intercepts of annealing equations plotted against annealing temperature for high temperature annealing of cable B1.

Therefore an annealing temperature of roughly 115 °C was used to obtain the y-intercept. Using the rough equation developed from this plot and the annealing temperature of 115 °C, a value of 123.0 °C is obtained for the y-intercept. The slope which is used is that corresponding to 120 °C annealing of B1, which yields a value of 1.3 °C/hr. Using these parameters, an annealing time of approximately 33 hours is obtained for the history at 115 °C. An estimation of the 103 °C annealing time using the same approached outlined above yields annealing parameters of 108.6 °C and 1.6 °C/hr for the y-intercept and slope, respectively. This equation gives an estimation of the annealing time at approximately 104 °C as 11 hours.

Cable RW-1 appears to have had thermal history at temperatures of 80 and 60 °C in addition to those present in the control cable at temperatures of 104 and 115 oC. Estimations for the 115 °C annealing shown in cable RW-1 are similar to those obtained for the control with values of 9 and 3 hour annealing times being obtained for the two points examined. However, for the 104 annealing, the position of the gain peak has been shifted upward by about 5 °C which gives estimations corresponding to over 3,000 hours. While such an extended annealing time for 104 °C is highly unlikely, and also would have generated more drastic changes in the overall appearance of the original DSC endotherms, the cable has probably been exposed to an additional temperature in the range of 100 to 104 °C. Another possibility is that the additional annealing at 80 °C also was able to shift the peak generated by the 104 °C annealing inherent in the sample upward. While subsequent annealing below a higher annealing temperature was shown to produce no major error in the estimation of annealing time for temperatures below 70 °C, it is likely that the same immunity may not be observed for higher temperature annealing. This can be confirmed by the data show in Table 5.6 for dual annealing of cable B1 at 98 °C and subsequently 80 °C. The position of the gain peak generated by the 98 °C annealing is shifted slightly upward with increasing annealing time at 80 °C.

Table 5.7: Annealing data for cable B1 annealed at 98 °C for 1.6 hours and subsequently 80 °C.

Time at 80 °C (hrs)	Td (98 °C) (°C)	Tp (98 °C) (°C)
0.0	99.25	102.20
1.0	99.12	102.33
2.9	99.25	102.35
6.4	99.00	102.40
12.8	100.00	102.50
17.8	99.40	103.25
28.1	99.40	102.60
35.0	99.15	102.00

The annealing equation developed for dual annealing at 98 °C and subsequently 80 °C for cable B1 was used to estimate the annealing time at 80 °C for cable RW-1. The values obtained for Td and Tp from the subtraction curves generated by using quenched endotherms as the second ramp yield annealing times of 630 and 389 hours. The values obtained from the subtraction of the control from the RW-1 endotherm yields an estimation of a very short period of time at that temperature.

The annealing in the 60 °C region was estimated using the equations for 55 and 60 °C annealing of cable B1. There were two points obtained from the various subtraction curves and both yielded estimates in the area of one to two days. However, the annealing at 80 °C most likely resulted in low annealing time estimations for the 60 °C region, as occurred under laboratory conditions for multiple annealing with XLPE.

An additional annealing temperature of 96.93 °C was observed for the subtraction curve generated using the control sample as the second ramp. The annealing equation was developed using the rough correlation given in Figure 5.18, which yielded a y-intercept of 96.4 °C and a slope of 2.0 °C/hr. This equation gave an estimation of 93 hours for the annealing time.

For cable RW-2, thermal history was observed at a temperature of roughly 92 °C. The additional annealing temperatures of 104 and 115 °C were also observed. Estimations for the high temperature annealings at 115 and 104 °C yielded results similar to those obtained for RW-1, with the annealing time for 115 °C estimated to be between 3 and 24 hours. The annealing at 104 °C gave an estimation of an extended period of annealing time.

The values corresponding to the 92 °C annealing yielded a range of 9 to 48 hours.

Cable RW-4 also showed history at temperature of roughly 94 to 99 °C, as well as 104 and 115 °C. The 115 °C annealing data yielded one time of 189 hours and another corresponding to a short time.

The 104 °C data gave an estimated time of over 900 hours. This extended time is more than likely an anomaly generated created by annealing in the 94 to 99 °C temperature region. Annealing times of 36 and 69 hours were obtained for the annealing at 92 and 98 °C, respectively.

5.6.2 Cable 246-155-RP

The loss and gain peak positions obtained from the subtraction curves of the aged RP samples are shown in Table 5.8. The control sample shows similar annealing temperatures of 104 and 116 °C which are inherent in the material from the manufacturing process. The annealing time estimations were determined to be much longer than those of cable RW. The 116 °C annealing time was found to be roughly 189 hours and the 104 °C annealing time was found to be extremely long (16,000 hours). These values are most assuredly in error.

The aged cable RP-3 yields annealing times of 3 and 24 hours for the 115 °C annealing points and times of 5 and 5,870 for two points representing 104 °C. The same equation developed for the RW samples was used in the calculation. Such large inconsistencies between points representing the same annealing temperature are yet to be explained.

RP-3 also shows annealing at a temperature in the vicinity of 70 to 75 °C. The annealing times were calculated using the 70 °C annealing equation developed from the dual annealing of cable B1. Annealing times ranged from 5 to 26 hours, as shown in table 5.7. This cable also showed a slight depression at a temperature of approximately 47 °C but the gain peak was not developed enough to extract a value from it.

Another subtle observation which needs to be considered for this cable, as well as for RP-5, is the form of the subtraction curve generated by subtracting the control from the aged sample. Looking at Figure 4.63 one can observe the sharp upward deflection of the

Table 5.8: Predictions for cable 246-155-RP

Cable	Td (°C)	Tp (°C)	Ta (°C)	y-intcpt. (°C)	Slope (°C/hr)	Time (hrs)
RP-Cont.	114.0	125.96	116.0	123.00	1.3	189
	103.7	115.34	104.0	108.60	1.6	16,000
RP-3	112.7	123.60	116.0	123.00	1.3	3
	113.5	124.78	116.0	123.00	1.3	23
	103.5	114.63	104.0	108.60	1.6	5,800
	102.7	109.75	104.0	108.60	1.6	5
	74.8	80.20	70.0	77.44	2.8	9.8
	76.0	81.40	70.0	77.44	2.8	26
	78.9	**83.73**	**75.0**	**81.95**	**2.4**	**5**
	47.8	--------	-------	-------	--------	-------
RP-5	103.3	111.20	104.0	108.60	1.6	48
	103.9	110.55	104.0	108.60	1.6	16
	104.0	115.30	104.0	108.60	1.6	15,400
	81.1	71.20	80.0	86.09	2.0	Short
	81.4	86.20	80.0	86.09	2.0	Short
	80.8	**89.4**	**80.0**	**86.09**	**2.0**	**50**
	59.2	71.20	57.0	66.29	3.16	38
	58.9	72.30	57.0	66.29	3.16	16
	59.8	71.20	57.0	66.29	3.16	38

peak located at roughly 114 °C on the subtraction curve. This is an indication that the sharp peak present on the endotherm for the aged RP-3 sample at 114 °C occurs at a lower temperature than that of the corresponding peak on the endotherm of the control sample. This phenomenon may be due to radiation exposure during ageing. Ordinarily when a polymer is melted at moderate to slow heating rates, the lamellae tend to thicken slightly before completely melting. This results in an increase in the observed melting point. Radiation acts to create crosslinks in the amorphous regions which limit the ability of the molecules to thicken during melting. Thus a slight depression of the melting point is observed for a sample which has been exposed to radiation in the solid state, which is exactly what is being observed for this sample. Radiation exposure would also limit the ability of the sample to anneal since crosslinks inhibit the thickening mechanisms. Therefore, one could not expect to accurately predict annealing times using equations developed from non irradiated samples.

Cable RP-5 was shown earlier to contain gross inconsistencies in the higher melting region. Thus the subtraction data for the 115 °C loss peak will not be considered. The positions obtained for the 104 °C annealing yielded annealing times of 48 and 16 hours, which are slightly more realistic than those obtained for the control sample. The sample also shows annealing at temperatures of approximately 57 and 80 °C. Using the general annealing equation developed earlier (eq. 5.5) with an annealing temperature of 57 °C, annealing times of approximately 38, 86, and 38 hours were obtained from points representing this annealing temperature.

For the 80 °C annealing, short annealing times were predicted (under an hour) from two of the values for the position of the gain peak and a value of 50 was obtained for another. The calculations were made using the equation obtained from dual annealing at 98 and 80 °C for cable B1.

This cable also shows the same depression of the melting point as observed for RP-3, as shown in Figure 4.66 through the sharp

upward peak occurring on the subtraction curve at 114 °C. This may be indicative of radiation exposure inducing crosslinking in the amorphous regions which suppresses the melting peak. The inconsistent behavior between samples could also be explained by irradiation as well. The samples were supplied in the form of several thin (less than 1 mm) slivers of insulation. If the samples were obtained from different regions where one sliver may have come from a region exposed to the radiation source and another slice from a region which was not as assessable to the source, different melting behaviors could be expected. Also, if the slivers represented layers obtained from the same area, then a top layer sample would contain more crosslinks than a sample from a lower layer.

5.7. Sources of Error

As we have seen through applying this technique toward actual aged samples, there are several deficiencies which remain to be worked out. First of all, in developing this technique, the materials were for the most part examined at single annealing temperatures under constant temperature conditions. The majority of the samples, save cable B1, were examined in the lower temperature regions below 70 °C and multiple annealing calibration curves were not developed for extended periods of time. Another factor which apparently is involved in a number of the samples is exposure to radiation and how it effects the overall prediction of thermal history.

5.7.1 Constant Versus Fluctuating Temperatures

In practice, the temperature conditions which a control cable is likely to be exposed to within a power plant will involve a relatively broad range. Even ambient temperatures will tend to fluctuate several degrees over the course of a day, and in areas where elevated temperatures are a factor, fluctuations of 5 to 10 °C may even be experienced. This creates perhaps the major source of error

using this technique. If, for example, one has a piece of insulation which has been exposed for several weeks at a temperature of say 50 °C, and has experienced an upward fluctuation of about 5 °C for a small amount of time. The position of the gain peak will be indicative of the highest annealing temperature, which in our case is 55 °C for a short period of time, instead of the temperature with the longest annealing time. So when the estimation is made, one obtains short time period estimations for a temperature roughly five degrees greater than normal operating conditions. This is likely to be the source of the low annealing time estimations for most of the annealing temperatures detected in the aged samples examined. This is a shortcoming dictated by the physics of the annealing process itself more so than lack of development of the technique.

5.7.2 Multiple and High Temperature Annealing

The multiple annealing behavior over extended periods of time has not been studied for any of the materials. It is safe to assume that the ability to predict an annealing temperature and exposure time will be greatly effected by the history present in the sample above that temperature. It is also conceivable that as the difference in annealing temperatures is decreased, the lower annealing temperature will begin to effect the position of the shoulder generated by the higher annealing temperature. While this was examined for XLPE at a temperature difference of 10 °C (70 and 60 °C annealing) and no major effects were observed in the position of the gain peak indicative of the higher annealing, such experiments have not been carried out higher annealing temperatures. This was a problem present in estimating the length of time of the 104 °C annealing of the control samples. One may recall that extremely long times were predicted for this annealing temperature and that in most of the cases annealing at either 70, 80, or 98 °C was detectable in the sample as well.

In the development of a general annealing equation, it was

assumed that the slope of the annealing equation was a function of the material alone. While this assumption is valid over a fairly broad range of temperatures below the major melting peak, we have seen evidence that the slope does indeed change at temperatures above 80 °C for cable B1. However, the material is a blend of XLPE and XHDPE, representing two essentially different materials, which could explain the observed decrease in slope with increasing temperature. At lower annealing temperatures the XLPE dominates the kinetics and at the higher temperatures, above about 80 °C, XHDPE dominates. The general trend observed for blended EPR and LPE crosslinked systems was that XLPE tended to dominate, with annealing equations being produced with characteristic annealing parameters closer to those obtained for XLPE. Such considerations are important when using a general annealing equation for blended materials over a wide range of annealing temperatures and further research is needed to better quantify the behavior of such blends.

5.7.3 Radiation Exposure

The extraction of thermal history from samples of cable insulation which have been exposed to radiation is another area which remains to be explored. Crosslinking in the solid state, which occurs upon irradiation, will change the melting behavior of the insulation as well as limit the ability of the lamellae to thicken, thus distorting its annealing behavior from that of a control sample. This phenomena has not been investigated in this research and much work remains to be done to better understand the effects of radiation upon thermal history determination.

6. CONCLUSIONS

This thesis has presented a new method of characterizing annealing behavior in semicrystalline polymer systems through the use of differential scanning calorimetry. The technique also allows one to obtain an estimate of the thermal history of a semicrystalline polymer system as well. From the research conducted using this technique several conclusions can be drawn upon the general annealing behavior of semicrystalline polymeric systems as well as the capabilities of the technique as a means of estimating thermal history.

6.1. Annealing Behavior of "Reference" Polyolefins

The annealing behavior of several reference materials was studied to gain a basic understanding of annealing behavior and how it is reflected in the subtraction technique. These materials included XLPE, EPR, EPDM, XEPDM, and XEPR.

The position of the gain peak, Tp, obtained from the subtraction curve follows a logarithmic time dependence for annealing times up to 1000 hours. This temperature can be considered as representative of the melting point of the new crystals formed by melting and recrystallization.

The equation which describes the annealing behavior is in the following form:

$$Tp = A + B\text{Log}(t)$$

This same equation was obtained for the annealing behavior of all of the materials investigated. The parameter A, in general, exhibits only annealing temperature dependence and the characteristic slope, B, is largely a function of the material over fairly broad temperature ranges. General annealing equations were developed which describe the annealing behavior of XLPEs and EPRs.

6.2. Control Cables

All of the control cables examined in this research exhibited similar behavior to the reference materials studied regardless of the complexity of the composition and melting behavior. In general, the characteristic slope obtained for a particular blend will correspond to the slope of the "fastest" (i.e. largest slope) annealing reference material present in the blend. Cable insulations composed of blends of XLPE tend to follow similar annealing behavior to that of the reference XLPE. Likewise, cable materials which yeilded slopes similar to those obtained for ERRs were comprised of what appeared to be low melting EPR material.

6.3. Determination of Thermal History

This technique can be used as a means of estimating the thermal history of polyolefin samples if one is aware of its limitations.

The position of what is termed as the loss peak, Td, corresponds to the annealing temperature, and the position of the gain peak, Tp, can be used to obtain an estimation of the annealing time. Once the annealing parameters are obtained for a particular sample, either by generating a calibration curve or from predetermined values, the annealing equation corresponding to the temperature of interest can be used to estimate the annealing time.

However, the following limitations must be kept in mind:

1) If a particular sample has history present at a temperature above that of another, parameters corresponding to the lower annealing temperature obtained from single temperature annealing may result in an incorrect estimation of the annealing time.

2) If a sample has been irradiated, the subtraction technique may not yield accurate time estimations unless annealing

parameters are used which were obtained from studies of irradiated samples.

3) The accuracy of this technique will only allow distinctions between relatively short and long annealing times.

7. FUTURE WORK

7.1. Multiple Annealing

The technique developed for studying annealing behavior can be used to obtain estimations of the thermal history of polyolefins. However, multiple annealing has been shown to effect the kinetics of the annealing process. New calibration curves need to be developed for dual temperatures.

7.2. High Temperature Annealing

The annealing studies performed in this research dealt mainly with annealing temperatures 20 to 30 °C below the major melting peak of the polymer. Since many cables may actually be exposed to elevated temperatures closer to the major melting peak of the insulation, further work needs to be done to better quantify the annealing behavior at these elevated temperatures.

7.3. Radiation Effects

The effects of radiation would most certainly change the annealing behavior from that of an unirradiated sample. It would be very interesting as well as useful to compare the differences obtained by annealing irradiated samples.

7.4. Temperature Fluctuations

The effects of non-constant temperature control upon the features of the subtraction curve which allow thermal history estimation need to be further examined.

7.5. General Annealing Studies

The merit of this technique is not so much in its ability to discern thermal history, but that it is a new method to study and quantify annealing behavior of different materials or materials processed under different conditions. It would be interesting to study the effects of orientation and mechanical stress upon the annealing behavior of polymeric systems. One could also easily study the effects of crystallization in different regimes upon the annealing behavior of certain polymers as well.

While the crystallization of several polymers at elevated pressures has been studied, no work has been done to examine the annealing behavior at higher pressures.

Molecular weight is known to effect the crystallization behavior of polymers. It would thus be interesting to see if molecular weight influences the kinetics of annealing as well by studying the annealing behavior at a certain reference temperature difference from the onset of melting for different molecular weight samples. The effect of crosslink density could be followed in a similar fashion.

LIST OF REFERENCES

LIST OF REFERENCES

Bassett, D.C. and A. Keller (1962), Phil. Mag., 7, 1553.

Cheam, T.C. and S. Krimm (1981), J. Polym. Sci., Polym. Phys., 19, 423.

DeGennes, P.G. (1971), J. Chem. Phys., 55, 572.

DeGennes, P.G., (1976), Macromolecules, 9, 591.

DiMarzio, E.A., C.M. Guttman, and J.D. Hoffman (1979), Faraday Discuss. Chem. Soc., 68, 210.

Eichhorn, R.M. (1983) in "Engineering Dielectrics," Vol IIA, STP 783, (Bartnikas and Eichhorn ED.), ASTM, Philadelphia, 355-444.

Fishcher, E.W. (1957), Z. Naturforsch, 12a, 753.

Fishcher, E.W., and G.F. Schmidt (1962), Angew. Chem. Intern. Ed., 1, 488.

Fishcher, E.W. (1969), Kolloid Z.Z. Polymere, 231, 458.

Flory, P.J. (1955), Trans. Faraday Soc., 51, 848.

Flory, P.J. (1962), J. Am. Chem. Soc., 84, 2857.

Flory, P.J. (1978), Nature, 272, 226.

Fujisawa, V., T. Yasui, Y. Kawasaki, and H. Matsumura (1968), IEEE Pas-87, 1899.

Herman, K., O. Gerngross, and W. Abitz (1930), Z. Phys. Chem., 10, 371.

Hoffman, J.D., G.T. Davis, and J.I. Lauritzen Jr. (1976), in "Treatise on Solid State Chemistry" (N.B. Hannay Ed.), Plenum Press, New York, vol. 3, p. 497.

Hoffman, J.D. (1979), Faraday Discuss. Chem. Soc., 68, 378.

Holland, V. F. (1964), J. Appl. Phys., 35, 59.

Jaccodine, R. (1955), Nature, 176, 305.

Kapur, S. and C.E. Rogers (1972), J. Polym. Sci., Polym. Phys., 10, 2107.

Kelen, T (1983), "Polymer Degradation", Van Nostrand Reinhold Co., New York, 173-201.

Keller, A. (1957), Phil. Mag., 2, 1171.

Keller, A. and A. Oconnor (1958), Disc. Faraday Soc., 25, 114.

Killian, H.G. (1969), Kolloid Z.Z. Polymere, 231, 534.

Kiss, K.D., H.C. Doepken, Jr., N. Srinivas, ans B.S. Bernstein (1979), in "Durability of Macromolecular Materials" (R.K. Eby Ed.), ACS Symposium Series, Washington D.C., 433-466.

Lauritzen, J.I. Jr., and J.D. Hoffman, (1973), J. Appl. Phys., 44, 4430.

Lee, Y.D. and P.J. Phillips (1990), J. Appl. Polm. Sci., Polym. Phys.,40, 263.

Mandelkern, L. (1975), J. Polym. Sci., Symp., 50, 457.

Mark, H.F., S.M. Atlas, S.W. Shalaby, and E.M. Pierce (1975), in "Flame Retardent Polymeric Materials", (M. Lewin, S. Atlas, and E. Pierce, Ed.), Plenum Press, New York, pp. 1-17.

Markezich, R.L. (1989), Dech Plus Digest, 2, 1.

Mason, J.H. (1959), "Progress in Dielectrics", Vol. 1, (J.S. Birks and J.H Schulman, Ed.), Heywood and Co., London, 1-58.

Niegisch, W.D. (1959), J. Polym. Sci., 40, 263.

Nitta, Y. (1974), I.E.E.E. EI-9, 109.

Peterman, J., M. Miles, and H. Gleiter (1976), J. Macrom. Sci., Phys. B12, 393.

Peterman, J., and R.M. Gohil (1979), J. Macrom. Sci., B16, 177.

Phillips, P.J. (1979), Polym. Prep. (Am. Chem. Soc., Div. Polym. Chem.) 20, 438.

Phillips, P.J. (1988) "Morphology of Extruded Dielectric Cable Insulation," EPRI EL-5921 Final Report, EPRI, July 1988.

Phillips, P.J. and G.J. Rensch (1989), J. Polym. Sci., B, 27, 155.

Phillips, P.J. and W.S. Lambert (1990), Macromolecules, 23, 2075.

Pope, D.P. (1976), J. Polym. Sci., Polym. Phys., 14, 811.

Pope, D.P. and A. Keller (1976), J. Polym. Sci., Polym. Phys., 14, 821.

Rabek, J.F. (1980), "Experimental Methods in Polymer Chemistry", John Wiley and Sons, New York.

Reneker, D.H. (1962), J. of Polym. Sci., 59, 539.

Sanchez I.C., J.P. Colson, and R.K. Eby (1973), J. Appl. Phys., 44, 4332.

Sanchez, I.C., A. Peterson, R.K. Rby, and F.L. McCrackin (1974), J. of Appl. Phys., 45, 4216.

Spells, S.J., D.M. Saddler, and A Keller (1980), J. Polym. Sci., Polym. Phys., 18, 1421.

Statton, W.O. and P.H. Geil (1962), J. Appl. Polym. Sci., 3, 357.

Strobl, G.R., M.J. Schneider, and I.G. Voight-Martin (1980), J. of Polym. Sci., Polym. Phys., 18, 1361.

Tanaka, T. and T. Fukada (1974), !974 Annual Report, Conf. on Electrical Insulation and Dielectric Phenomena, National Academy of Sciences, National Research Council, pp. 239-249.

Tanaka, T, T. Fukada, and S. Suzuki (1976), I.E.E.E. Transaction on Power Apparatus and Systems, Vol. Pas-95, pp. 1892-1900.

Tanaka, T., and A. Greenwood (1983), "Advanced Power Cable Technology", Vol. II, CRC Press, Inc. Boca Raton, FL.

Till, P.H. Jr. (1957), J. Polym. Sci., 24, 301.

Vatansever, A. (1987), Ph.D. Dissertation, The University of Tennessee.

Yoon, D.Y. and P.J. Flory (1979), Discuss. Chem. Soc., 68, 288.

Zachmann, H.G. (1967), Kolloid Z.Z. Polymere, 216, 180.

VITA

F. Scott Dibrell was born on April 15, 1965 in Nashville, Tennessee. He attended McGavock High School where he graduated in May of 1983. He attended the University of Tennessee that fall and obtained a Bachelor of Science degree in Chemical Engineering in December of 1987. Upon graduating he decided to avoid work at all costs and entered the Department of Polymer Engineering as a research assistant under the supervision and guidance of Dr. Paul "The Pope" Phillips (whom he is greatly indebted to). He defended this thesis in August of 1990 and miraculously managed to pass his orals. He will officially obtain his Master of Science degree in December of 1990. Upon graduation he will continue with his tradition of avoiding work and is currently in search of a wealthy older woman in need of a traveling companion.